

DESIGN GUIDE FOR STABLE H_2/O_2 COMBUSTORS

Volume 1: Design Application

Contract NAS 8-20672

STABILITY CHARACTERIZATION OF ADVANCED INJECTORS

George C. Marshall Space Flight Center
National Aeronautics and Space Administration

Report 20672-P2D

May 1970

CASE FILE

COPY



AEROJET LIQUID ROCKET COMPANY

A DIVISION OF AEROJET-GENERAL 

SACRAMENTO, CALIFORNIA

Report 20672-P2D

DESIGN GUIDE FOR STABLE H_2/O_2 COMBUSTORS

Volume 1: Design Application

Prepared under

Contract NAS 8-20672

STABILITY CHARACTERIZATION OF ADVANCED INJECTORS

for

George C. Marshall Space Flight Center
National Aeronautics and Space Administration
Huntsville, Alabama

A E R O J E T L I Q U I D R O C K E T C O M P A N Y

Engineering Operations

Sacramento, California

FOREWORD

This Design Guide is submitted in partial fulfillment of Contract NAS 8-20672, Stability Characterization of Advanced Injectors, Phase II.

The purpose of the Design Guide is to provide an orderly procedure for designing a dynamically stable injector for an advanced cryogenic engine. Since 1962, a series of research programs, principally funded by NASA but also involving other agencies, has produced a wealth of data on the design and operating characteristics of specific cryogenic systems. It is the intent of this Guide to present comprehensively the accomplishments of this research in a manner useful to the designer, emphasizing application. The theoretical discussion is limited to that necessary to understand the proper usage of the tools provided. The work presented represents a culmination of seven years of effort in investigating the problem of combustion stability in high-pressure liquid oxygen/hydrogen engines with the principal emphasis placed on what was felt to be future injector designs for such an engine. Initially, efforts were concentrated on a variety of injector types and engine systems. Later emphasis, because of monetary as well as technological considerations, was placed on the coaxial and impinging triplet injectors. The initial phases of the program demonstrated that the nature of the stability problem was no different with high-pressure from that with low-pressure engines.

The later phases of the program led to refinement of the stability parameters which had been identified in the early phases of the program as being significant. The results indicate that, in general, some form of stabilizing device is required to produce a dynamically stable system. It is possible, however, to design a dynamically stable system capable of withstanding some small bomb-induced pressure perturbations.

This report is arranged in a manner which is consistent with engine design procedures such that consideration may be given to the design of a stable engine in the early phases of the program. The general practice for

FOREWORD (cont.)

engine design used as an outline for this report is the identification of the engine system through feasibility studies followed by design refinements and identification of operating requirements. Finally, there is discussion of development hardware design and formulation of testing requirements to demonstrate the design.

Section 1 introduces the subject of instability as a process that can be described by measurable phenomena. It eschews speculation as to mechanisms but is consistent with the proposals of most prominent theoreticians. It also contains a critique of the available design data and indicates the areas where new test data are required. A short section is devoted to the methods of calculation that are proposed.

Section 2 reviews present design procedures for chambers and injectors and introduces new parameters that have been found useful in characterizing the stability of specific configurations.

Section 3 describes the application of stability criteria to the three principal situations facing the designer. It is presented in the form of design alternatives together with descriptions of the necessary calculations to be made in order to reach a decision. Simple manual procedures are offered with recommendations as to the particular occasions when it may be necessary to resort to the computer.

Attention is directed toward early determination of the existence of a potential instability problem. Precise calculation of parameters is subordinated to simplified formulations to enable evaluation of the stability of the proposed system. This approach is justified in that it identifies for the designer what types of corrections may be required to stabilize the proposed engine system. The designer may then give consideration to tradeoffs between stabilization devices and requirements for performance, structural integrity, durability, maintenance, and pressure schedules.

FOREWORD (cont.)

Section 4 provides a description of the computerized model discussed in Volume II and its application to injector and chamber design. The purpose of this subsection is to provide the user the option of performing rigorous analyses of the effect of nozzle contour on the system. The model also includes a subroutine for treating the effect on stability of altering injection distribution.

Section 5 discusses the various stabilization devices that may be used if required to meet engine stability specifications. The section includes design criteria for baffles and a simplified analysis for acoustic liners. The section on acoustic liners is limited because design information on this subject is available in the several references listed. Consideration is given to tradeoffs required to secure optimum design.

Section 6 describes the subscale testing tools which may be used to characterize the stability of an injector pattern. Methods of reducing high-frequency stability data and descriptions of the instrumentation necessary to obtain these data are included. Development testing of prototype injectors is described, together with discussion of the locations of transducers and the interpretation of the test data, including identification of instability modes.

Volume II describes the operation of the various computer programs referenced in Sections 3, 4, 5 and 6 of Volume I. Input requirements and output format are discussed with special attention to selecting cases that will most clearly bracket the required answers. A discussion of the rationale employed and of the limiting assumptions is provided for each program. Programmers' handbooks are referenced.

Appendix A contains short discussions of the principal theories that have been advanced to explain combustion instability. They are included

FOREWORD (cont.)

only to give the designer a feeling for the principles involved. For rigorous treatment of each, a reference list is appended.

The data presented in the Design Guide are derived principally from the following contracts: NAS 8-4008, NAS 8-11741, F04611-67-C-0019, and NAS 8-20672.

This work was sponsored by the NASA Marshall Space Flight Center, Huntsville, Mr. R. J. Richmond, project engineer.

The combustion model which provided the basis for this analytical technique is the Sensitive Time Lag theory first developed by Dr. L. H. Crocco and later extended by Dr. F. H. Reardon.

The work was conducted by the Engine Components Department, Thrust Chamber Engineering Section, of the Aerojet Liquid Rocket Company under Dr. N. E. Van Huff, manager; Mr. J. M. McBride, project manager; and Mr. W. W. Howard, project engineer.

Special acknowledgement is given to Mr. R. C. Waugh for his contribution in the development of analytical models, Mr. D. P. Dudley for programming and conversion of the computer program, Mr. R. K. Turner for the reduction of combustion stability theory into design criteria and analysis and correlations of test data, and Mr. W. J. Nord for organizing and editing the material contained in these reports.

Report 20672-P2D

CONTENTS

	<u>Page</u>
1. Introduction	1
1.1 Scope and Limitations	1
1.2 Nature of Combustion Instability	3
2. Initial Design	11
2.1 Injector Variables	11
2.2 Chamber Variables	15
3. Stability Evaluation	17
3.1 Determining Stability	17
3.2 Manipulating Initial Design	35
3.3 Illustrative Design Problems	51
4. Use of Computer Programs	77
4.1 Description of Computer Program	77
4.2 Operating the Program	83
4.3 Illustrative Design Problems	119
5. Stabilization Devices	159
5.1 Baffles	161
5.2 Acoustic Liners	186
Bibliography	192
6. Test Programs	195
6.1 Subscale and Model Testing	195
6.2 Development Testing	203
6.3 Data Analysis	225
Nomenclature	230
General References	233

APPENDICES

	<u>Page</u>
A. Analytical Approaches to Combustion Stability	237
B. Test Program for Contract NAS 8-20672, Phase II	245

TABLES

<u>No.</u>		<u>Page</u>
1	Chamber Response as Function of Chamber Type	23
2	Annular Chamber Nozzle Admittance Study	25
3	Transverse Bessel Function Arguments	28
4	A_{vn} as Function of Injector Zone	48
5	Generalized Injector Response Tabulation	56
6	Primary Response Frequency as Function of Chamber Design	61
7	Sensitive Frequency as Function of Oxidizer Orifice Diameter	70
8	Program Combinations for Design Criteria	90
9	Input Data for Mode Example Problems	118
10	Output of Longitudinal Mode Example Problem	120
11	Output of Transverse Mode Example Problem	126
12	Output of Nonlinear Mode Example Problem	148
13	Effect of Baffles on Engine Performance	180
14	Results of Analog Transducer Resonance on Input Frequencies	213

ILLUSTRATIONS

<u>No.</u>		<u>Page</u>
1	Combustion Chamber Schematic	7
2	Injector Orifice Patterns	12
3	Various Chamber Contours	14
4	Response Curve for Crocco Sensitive Time Lag Model	18

ILLUSTRATIONS (cont.)

<u>No.</u>		<u>Page</u>
5	F(VR sin ϕ) as Function of Impingement Velocity Ratio	22
6	Chamber Response as Function of Nozzle Orientation	26
7	Comparing Injector and Chamber Responses	30
8	Effect of Displacing Sensitive Frequency	38
9	Varying Injector Distribution	45
10	A_{vn} as Function of Chamber Radius	46
11	Decision Diagram -- Evaluating Stability	50
12	Decision Diagram -- Selecting Chamber Design	58
13	Predicted Stability Characteristics -- 1.5 Contraction Ratio	62
14	Predicted Stability Characteristics -- 3.0 Contraction Ratio	63
15	Decision Diagram -- Designing Stable Injector	64
16	Annular Combustor	66
17	Effect of F(VR sin ϕ) on Combustion Response	75
18	General Flow Diagram of the Computer Program	79
19	Overall Schematic of the Computer Program	80
20	Input Load Sequence Required by the Computer Program	82
21	Real Part of Pressure Admittance Coefficient versus Axial Distance	99
22	Imaginary Part of Radial Velocity Admittance Coefficient versus Axial Distance	100
23	Baffle Shapes and Blade Arrangement	160
24	Transverse Mode Characteristics	162
25	Possible Mode Orientations for Various Baffles	166
26	Effect of Number of Baffle Blades	168
27	Effect of Baffle Spacing vs Baffle Length	168
28	Effect of Baffle Spacing on First Tangential Mode	169
29	Damping versus Baffle Length and Number of Blades	170
30	Frequency Depression versus Baffle Length	170
31	Attenuation in Closed-Open Tube	172

ILLUSTRATIONS (cont.)

<u>No.</u>		<u>Page</u>
32	Pocket Spacing versus Damping	172
33	Combustion Response	175
34	Decay Rate versus Baffle Height (effect of flame zone)	176
35	Calorimetric Heat Flux	182
36	Gas-Side Film Coefficient Profile	183
37	Helmholtz Resonator	186
38	Transverse Excitation Chamber (exploded view)	196
39	Oscillograms of Various Types of Instability	197
40	Decay of Fundamental Mode and Regrowth of Second Mode	198
41	Growth of Second Mode and Decay into Fundamental	199
42	Amplitude Plots Showing Growth and Decay Rates	200
43	Longitudinal Excitation Chamber (sectional view)	202
44	Recommended Locations for Transducers in Order to Identify Modes of Instability	204
45	Axial Pressure Profiles of Longitudinal Modes in an Enclosed Cylinder	208
46	Analog Run No. 1	214
47	Analog Run No. 2	216
48	Analog Run No. 23	218
49	Analog Run No. 18	220
50	Tangential Pulse Gun	223
51	Nondirected Pulse Charge	224
52	Identification of a 1T-2L Mode of Instability	226
53	Power Spectral Density Plot	228

1. INTRODUCTION

1.1 SCOPE AND LIMITATIONS

This design guide is intended to aid in the design of advanced cryogenic engines using oxygen and hydrogen. The method of analysis is based on the sensitive time lag model first developed by Crocco. The application of the model discussed in Section 3 consists of two approaches. The first approach is a simplification of the second for the purpose of making preliminary estimates of the system's stability without resorting to computerized models. The basic assumption on restriction of the first approach is that losses associated with the nozzle geometry are constant for all modes in the chamber. By doing this, the gains of the system define the range of frequencies at which instability is likely to occur. Methods for calculating acoustic modes in the chamber are given so that the stability of a specific system may be obtained. The fully characterized system may identify problems concerning unstable modes requiring the use of the devices described in Section 5 for corrective action in the design.

The second approach discussed in Section 3 allows for a more rigorous and, consequently, more accurate determination of the stability of the system by using the computer model.

The basic approach for analyzing the stability characteristics of such an engine discussed herein is limited only by the amount of empirical data available on the various injector element types. Included in the design guide are empirical correlations for the commonly used impinging coaxial injector and the conventional impinging orifice injectors. If the design to be analyzed is other than these types of elements, Section 6.1 describes an experimental method whereby using a subscale tool, termed the Excitation Chamber, the necessary data can be obtained.

1.1, Scope and Limitations (cont.)

The empirical parameters required for a given injector are best described as being equivalent to a gain parameter (interaction index, n) and a phase parameter (the sensitive time lag, τ). These two parameters coupled with an assumed combustion response function, $\frac{Q'}{P'}$, which is itself a function of these parameters and given by:

$$\frac{Q'}{P'} = \frac{\bar{Q}}{\bar{P}} n (1 - e^{S\tau}) \quad \text{Eq 1}$$

constitute the major assumption in the model first proposed by Crocco.*

Justification for the assumed response function can be found in several references** as well as the experimental results of Contract NAS 8-20672. In addition, the more popular mechanistic stability model which is based on such physical processes as heat transfer to the droplet or pressure dependent vaporization show in general that such a response curve is realistic. A brief discussion of the various stability models can be found in Appendix A.

The work conducted to date indicates that the interaction index can be determined within +15% of its nominal value and the sensitive time lag parameter, when determined from the excitation chamber discussed in Section 5, within +5% of its nominal value. Correlation for the sensitive time lag based on data from conventional engine tests is somewhat less accurate and gives a nominal value in the order of +25% of the sensitive time lag.

*Crocco, L. and Cheng, S. I., "Theory of Combustion Instability in Liquid Propellant Rocket Motors," AGARDograph No. 8, Butterworths Scientific Pub., Ltd., London, 1956.

**1. Crocco, L., "Theoretical Studies on Liquid Propellant Rocket Instability," Tenth Symposium (International) on Combustion, The Combustion Institute, 1965.

**2. Crocco, L., Grey, J., and Harrje, D. T., "Theory of Liquid Propellant Rocket Combustion Instability and Its Experimental Verification," ARS Journal, Vol. 30, No. 2, February 1960.

1, Introduction (cont.)

1.2 NATURE OF COMBUSTION INSTABILITY

The subject of combustion instability may be divided into two categories. Phenomena of the first type are the results of coupling between the feed system and the combustion process. The feed system contribution is generally considered analogous to that of a resonant system with constant passive resistance, while the combustion process provides the driving force to maintain the oscillation both in the feed system and in the combustion process. The classic treatment of one such sample rocket engine system was first described by Summerfield*. With an increase in engine scale and system complexity the analytical formulation of feed system-coupled low frequency has become more complex. In the case of large systems, the frequencies of the feed system modes approach the order of the frequencies of the acoustic modes of the combustion chamber, necessitating a more rigorous treatment of the combustion chamber. In the case of the staged-combustion cycles the complexity has been increased by the need to consider coupling between the primary and secondary combustors as well as coupling between the combustors and their respective feed systems. A treatment of feed system-coupled instability is provided in the references**. The application to the staged combustion cycle is currently being treated analytically under Phase II of NAS-8-20672 and will be discussed in the subsequent final report.

The second category of instability is termed high frequency or "intrinsic" combustion instability. Other terms that have been used to describe this effect are "resonant burning", "acoustic mode instability", "tangential instability", "radial instability", "longitudinal instability",

*Summerfield, Martin, "A Theory of Unstable Combustion in Liquid Propellant Rocket Systems," ARS Journal, Vol. 21, No. 5, September 1951, pp 108-114.
**Report 20672-PIF, Stability Characterization of Advanced Injectors, Final Report on Phase I, Contract NAS 8-20672, Aerojet-General Corporation, 25 October 1968.

1.2, Nature of Combustion Instability (cont.)

"combined modes instability" (referring to combinations of tangential, radial, and longitudinal modes), "screeching", and "detonation-like modes of instability".

Basically, all these descriptions indicate modes of instability associated with the geometry of the combustion chamber and the properties of the combustion gases. The frequencies observed correspond closely to the values obtained using the speed of sound in combustion gases and the characteristic dimensions of the chamber.

1.2.1 Physical Effects

Low frequency instability is usually reflected by significant periodic variations in the propellant system pressures as well as in the chamber pressure. These oscillations produce acceleration loads on the components of the engine system which on occasion result in failure from overstress or fatigue.

High frequency or "intrinsic" instability is observed as oscillations of large pressure amplitudes in the combustion chamber, regardless of the response in the feed system. Besides mechanical vibrations that may be damaging to the structure, there are locally intense increases in the heat flux resulting in melting and erosion of the interior surfaces.

The onset of instability is often very sudden and violent. Even when system procedures permit shutdown and restart, this cannot be effected in time to prevent serious damage. System safety is therefore dependent upon avoiding instability or upon its suppression.

1.2, Nature of Combustion Instability (cont.)

1.2.2 Combustion Response

Combustion response is generally used to describe the ratio of the volumetric burning rate to the local pressure, or what is sometimes referred to as the combustion admittance. To date two basic approaches have been taken to describe combustion response. The first is referred to as the "heuristic approach" where the combustion response is assumed to have a certain shape such as trigometric function which varies with frequency, thus allowing it to be described in two parameters (phase and gain). These parameters are considered to be characteristic of the injector design and propellants used. Justification for this approach can be found in the cited references*. The second approach, generally referred to as the "mechanistic approach," requires that specific processes such as vaporization, mixing or kinetics be identified as the rate-controlling process. Typical of this type of approach are the models discussed briefly in Appendix A and in the references**.

The former approach is the one which forms the basis for the design methods described in this report. It is worth noting that to the first order the shape of the combustion response resulting from the two approaches is generally the same when either mixing or vaporization is assumed to be the rate-controlling processes in the mechanistic approach.

The assumption of a combustion response, which can be characterized by injector and propellant parameters, allows the theoretician to describe implicitly the energy input to the system and how it varies with frequency.

*1. Crocco and Cheng, op cit.

2. Crocco, L., op cit.

3. Crocco, Grey, and Harrje, op cit.

**1. Dykema, O. W., "An Engineering Approach to Combustion Instability," 2nd Combustion Conference, ICRPG, CPIA Publication No. 105, May 1966.

2. Heidman, M. F., and Weiber, P. R., "Analysis of Frequency Response Characteristics of Propellant Vaporization," NASA TN D-3749, December 1966.

1.2, Nature of Combustion Instability (cont.)

To demonstrate physically the significance of the combustion response, if it is assumed the combustion is concentrated at one of the boundaries of the system and if the mean or steady flow effects are ignored, the local energy input to the system is given by the product of the local perturbation pressure and velocity, or since the admittance is the ratio of these parameters, the local energy input can be expressed as the product of the combustion response (G) and the square of the local pressure (P) or:

$$\tilde{E} = G \tilde{P}^2 \quad \text{Eq 2}$$

This is, in general, an oversimplification; however, it does give a feeling for the significance of combustion response. This simplification also points to one other observation which can be made: that the energy input is dependent on the local pressure so that sources in regions of low acoustic pressure do not contribute much to the combustion response. This concept, then, leads to treatment of injection distribution effects which are quantized in Section 4. Knowing the combustion response gives one of the two major ingredients--the energy input in determining the stability of a system.

The indicated references* give justification for the assumed response function used in the heuristic approach as based on the physical processes which occur in a rocket engine during combustion; therefore, it is not too surprising that agreement exists between the mechanistic and heuristic approach. Consider for example the mechanistic model proposed by Dykema**, keeping in mind that the heuristic approach results in the combustion response being described by a magnitude (gain) and a phase parameter. This model considers a fuel or oxidizer droplet, spherical in shape, in either an oxidizing

*1. Crocco and Cheng, op cit.

2. Crocco, L., op cit.

3. Crocco, Grey, and Harrje, op cit.

**Dykema, O. W., op cit.

1.2, Nature of Combustion Instability (cont.)

or reducing atmosphere. The mechanism or process which is rate-controlling is the diffusion process, the rate of diffusion being analogous to a magnitude parameter and the time required to diffuse to the flame surface from the droplet surface being analogous to a phase or time-lag parameter. In general, it can be said that both the heuristic and mechanistic response curves* can be described as having a maximum at a given frequency and the response decreasing on either side of the sensitive or preferred frequency. This description generally also applies to the heuristic model response function and the response function approaches differ only in the shape of the curve.

1.2.3 Acoustic Modes

The most common modes of instability observed in a rocket engine are generally referred to as either longitudinal or transverse. In the case of the longitudinal modes the frequency can be estimated by considering the combustion chamber as a closed tube with the injector at one end and the nozzle at the other. As a first approximation of the effective length (see Figure 1),

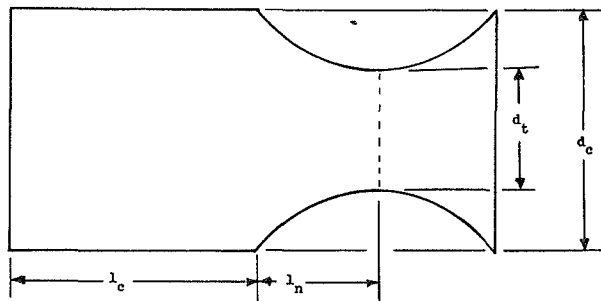


Figure 1 -- Combustion Chamber Schematic

*1. Dykema, O. W., op cit.

2. Heidman and Wieher, op cit.

1.2, Nature of Combustion Instability (cont.)

taking the entire length of the cylindrical section ℓ , plus 2/3 the nozzle conical section length gives for the longitudinal mode frequencies:

$$\text{nth longitudinal mode } (f_n) = n/2 \frac{c}{\ell_1 + 2/3 \ell_2}, \quad n = 1, 2, 3 \quad \text{Eq 3}$$

If the chamber Mach number becomes excessively large, the travel time of the wave toward the nozzle increases and that toward the injector is reduced. A correction factor has been derived for approximating the shift in frequency due to the presence of mean flow* which is given by:

$$\frac{f_{\text{mean}}}{f_{\text{flow}}} = \frac{f_{\text{no}}}{f_{\text{flow}}} (1 - M_c^2) \quad \text{Eq 4}$$

As a first approximation for the transverse mode the chamber is treated as a cylinder of radius r_c and the transverse mode frequencies are given by

$$f_n = \frac{c S_{v\eta}}{2\pi r_c} \quad \text{Eq 5}$$

where the value of $S_{v\eta}$ is unique for each transverse mode. A list of this $S_{v\eta}$ coefficient is given in Table 3, Section 3.1 for the various types of transverse modes (i.e., radial or longitudinal). A physical description of each of these modes is found in Section 6.

Mathematically the constant $S_{v\eta}$ is derived in the following fashion. Starting with the wave equation in cylindrical coordinates

$$\nabla^2 P = \frac{1}{c^2} \frac{\partial^2 P}{\partial t^2}, \quad \text{Eq 6}$$

*Handbook of Astronautical Engineering, Heinz Hermann Koelle, Editor, "Combustion Parameters and Interior Flow" by R. S. Levine, pp 20-57 through 20-68. McGraw Hill Book Co., 1961.

1.2, Nature of Combustion Instability (cont.)

where

$$\nabla^2 P = \frac{\partial^2 P}{\partial r^2} + \frac{1}{r} \frac{\partial P}{\partial r} + \frac{1}{r^2} \frac{\partial^2 P}{\partial \theta^2}.$$

The separation of variables technique discussed in detail in Reference * is used to solve the above wave equation. The resulting solution is of the form

$$P = J_{\nu} (S_{\nu\eta} r/r_c) \cos \nu \theta \quad \text{Eq 7}$$

for the standing modes described in Section 6.

The value of $S_{\nu\eta}$ is dictated by the fact that at the chamber wall the velocity normal to the solid wall must be zero. From the momentum equation for a system with no mean flow this boundary condition requires that

$$\frac{\partial P}{\partial r} = -\rho \frac{\partial v}{\partial t} = 0 \text{ at } r = r_c. \quad \text{Eq 8}$$

The values of $S_{\nu\eta}$ given in Table 3 satisfy the condition that at $r/r_c = 1$

$$J'_{\nu} (S_{\nu\eta}) = 0 \quad \text{Eq 9}$$

The value of $S_{\nu\eta}$ used depends on the mode for which the frequency is desired as indicated in the table.

Physically the nozzle represents a "hole" in the acoustic cavity (chamber) from which energy can be radiated. The degree to which this energy can be radiated is measured by the nozzle admittance which is discussed in the

*C. R. Wylie, Advanced Engineering Mathematics, Second Edition, McGraw-Hill Book Co., 1960.

1.2, Nature of Combustion Instability (cont.)

body of the text. Suffice it to say that the larger the real part of the nozzle admittance the greater the nozzle losses. Based on studies of the parameters that affect nozzle admittance the variation is of the order shown in Table 1, Section 3.1.

2. INITIAL DESIGN

The purpose of this section is to acquaint the designer with the terminology and parameters associated with combustion stability.

The stability of a rocket engine system, as treated in this guide, is dependent upon three factors:

- a The thermodynamic properties of the propellants,
- b The combustion response as the result of the type of injection and mixing employed,
- c The acoustic properties of the combustion chamber, including its capacity for damping.

It may be presumed that the designer has no option in the choice of operating system and propellants; these are determined by the original mission requirements and may be treated as initial design constraints. Moreover, the basic design of the chamber and injector is usually dictated by considerations of combustion efficiency, available space envelope, structural necessity, cooling requirements, and propellant system feed pressures. By the time attention can be directed to matters of stability, most of the important design parameters have been established and the engineer is limited to compromises, mostly affecting the injector pattern and the nozzle contour.

2.1 INJECTOR VARIABLES

In actual design practice the primary injector parameters -- chamber pressure, mixture ratio, propellant inlet pressures, injector-chamber diameter -- are set within certain limits by mission considerations. In addition, the choice of injection pattern is limited by the requirement to maintain combustion efficiency above a certain percentage of the theoretical maximum. A portion of the propellant flow may also be diverted for cooling the more sensitive surface of the chamber and injector.

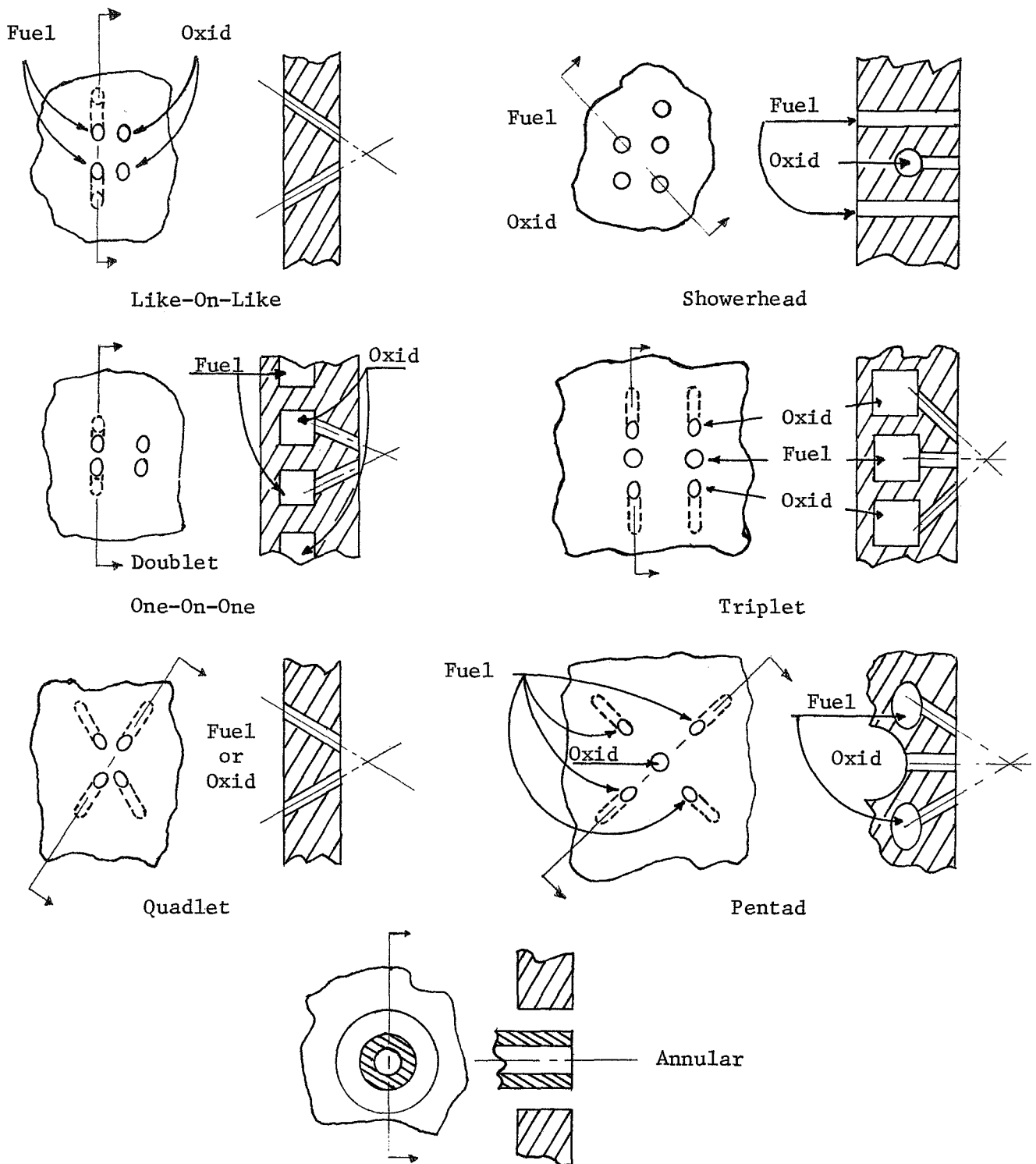


Figure 2 -- Injector Orifice Patterns

2.1, Injector Variables (cont.)

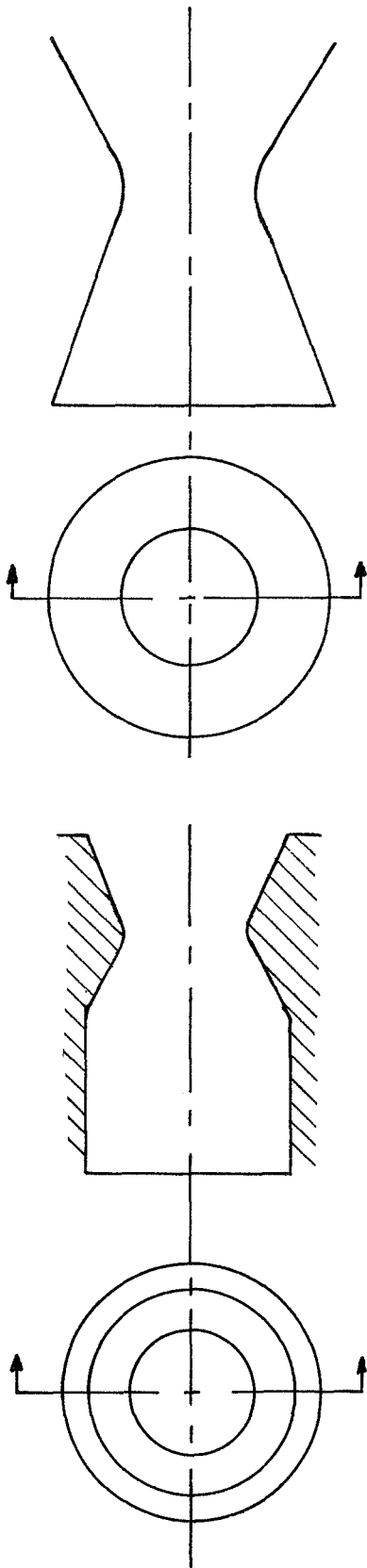
The duration of the combustion time-lag may be modified considerably by the method employed for injecting the propellants. Basically, the injection systems may be divided into parallel-injecting and impinging types. Examples of the most common injection elements are diagrammed in Figure 2.

The parallel-injecting, or "showerhead" type is simplest. Oxidizer orifices are interspersed with fuel orifices in either a symmetrical or axisymmetrical distribution with the axes of the orifices parallel to each other. This leads to relatively slow vaporization and mixing, and a long total time-lag. However, the last, or sensitive, portion of the lag may be very short, depending on the velocity of injection and the spacing between orifices.

Impinging types may be classified as "like" or "unlike". In the former, each element is produced by two or more streams of the same propellant impinging to form a spray. Fuel and oxidizer sprays diffuse and react. The rate of reaction will be affected by factors that govern the size and dispersion of the spray droplets -- namely, the velocity of injection, angle of impingement, and the size and distribution of the orifices.

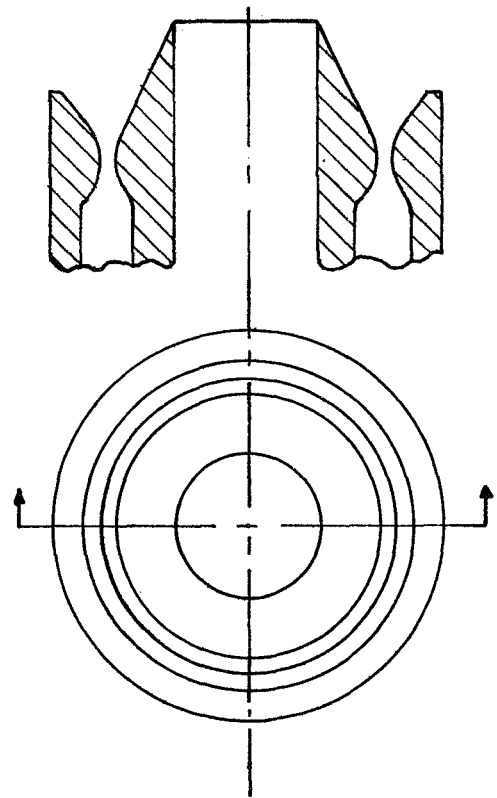
The "unlike" impinging types combine the fuel and oxidizer streams immediately upon injection. The various combinations are designed "one-on-one," triplet, quadlet, pentad, etc., as two, three, four, five, or more streams compose each element. In general, the reaction time of the "unlike" impinging types is less than for the others discussed, but the important variables are still velocity of injection, angle of impingement, and the orifice size and distribution.

The "coaxial" injection element is formed by the intersection of two conical streams having a common axis.

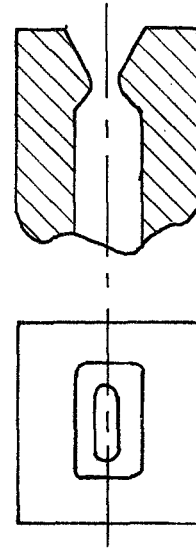


a. Cylindrical Chamber

b. Conical Chamber



d. Annular Chamber



d. Rectangular Chamber

Figure 3 -- Various Chamber Contours

2, Initial Design (cont.)

2.2 CHAMBER VARIABLES

The contribution of the combustion chamber to stability is largely determined by its acoustic properties -- that is, the orientation and frequency of the modes of resonance and the capacity for damping. The only factor that requires consideration in respect to stability, therefore, is the geometry of the chamber interior.

The orientation of the resonant frequencies is determined by the free paths for wave travel. Since most combustors generally have symmetry in a cylindrical sense with the axial direction passing through the throat of the combustion chamber, the following nomenclature compatible with a cylindrical coordinate system has been adapted to identify modes of instability: longitudinal modes for pressure oscillations in the axial direction and in the direction of flow; radial modes for pressure oscillations transverse to the direction of flow in the radial direction of the cylindrical coordinate system; and tangential modes in the direction of changing angular position and transverse to flow. These modes may appear singularly or combined depending on the geometry of the system. A pictorial presentation of these models are found in Figure 3.

The most commonly employed chamber type is the cylindrical, Figure 3a, which is subject to all the modes described above. The frequency of the longitudinal modes is inversely proportional to the length of the chamber up to the nozzle, that of the transverse modes inversely to the chamber diameter.

The conical chamber, shown in Figure 3b, is a variation of the cylindrical chamber. The converging angle modifies the frequencies of the natural chamber resonances, but the same acoustic modes are present.

2.2, Chamber Variables (cont.)

The annular chamber, Figure 3c, is simply a cylindrical chamber with a large center body. This latter inhibits the development of radial modes and permits additional variations in nozzle contour that affect the damping capacity.

The rectangular chamber may be treated as a small segment of an annular chamber of very large radius. The frequencies of longitudinal oscillations are the same as for the cylindrical chamber. The transverse oscillations vary inversely with the distance between the opposite walls.

The length and diameter of the chamber and the chamber pressure are set within fairly close limits by performance requirements. The principal area open to modification for purposes of stabilizing combustion is the configuration of the nozzle. The effects of damping are subsumed under the term nozzle admittance. The principal factors affecting the admittance are Mach number, the length and angle of the convergent section, and the radii at the approach and at the throat. Additional effects are produced by viscous drag at the chamber walls and changes in the gas constituents as they are transported along the chamber. The techniques by which the nozzle damping may be increased are discussed in Section 3.2.

3. STABILITY EVALUATION

It is the intent of this section to provide the designer with a procedure for evaluating the stability of the system with which he is concerned, to discuss the influence of certain parameters that are known to affect stability, and to present some guidelines that have been found helpful in stabilizing an unstable design.

3.1 DETERMINING STABILITY

The approach used in evaluating the stability of a system is to compare the rate at which the volumetric burning rate is increased for a unit change in chamber pressure (combustion response) with the rate at which gases are expelled from the chamber for a given unit change in pressure (nozzle response).

It is not possible with the linear model, which is the basis of this design guide, to treat induced perturbations quantitatively. This is a non-linear phenomena (i.e., combustion response is dependent on the magnitude of the pressure amplitude) and as such requires a non-linear analysis. However, experience shows that a qualitative treatment of the problem is possible with the data provided. That is to say, the most likely modes of instability can be identified, and by referring to Section 5 the designer can then consider what sort of damping device would be required and the physical characteristics it should have.

Figure 4 is a plot showing the assumed shape of the combustion response curve. This curve is defined by the relationship

$$N_{\text{injector}} = n_o \left(1 - \cos \pi \frac{f}{f_s}\right) \quad \text{Eq. 10}$$

3.1, Determining Stability (cont.)

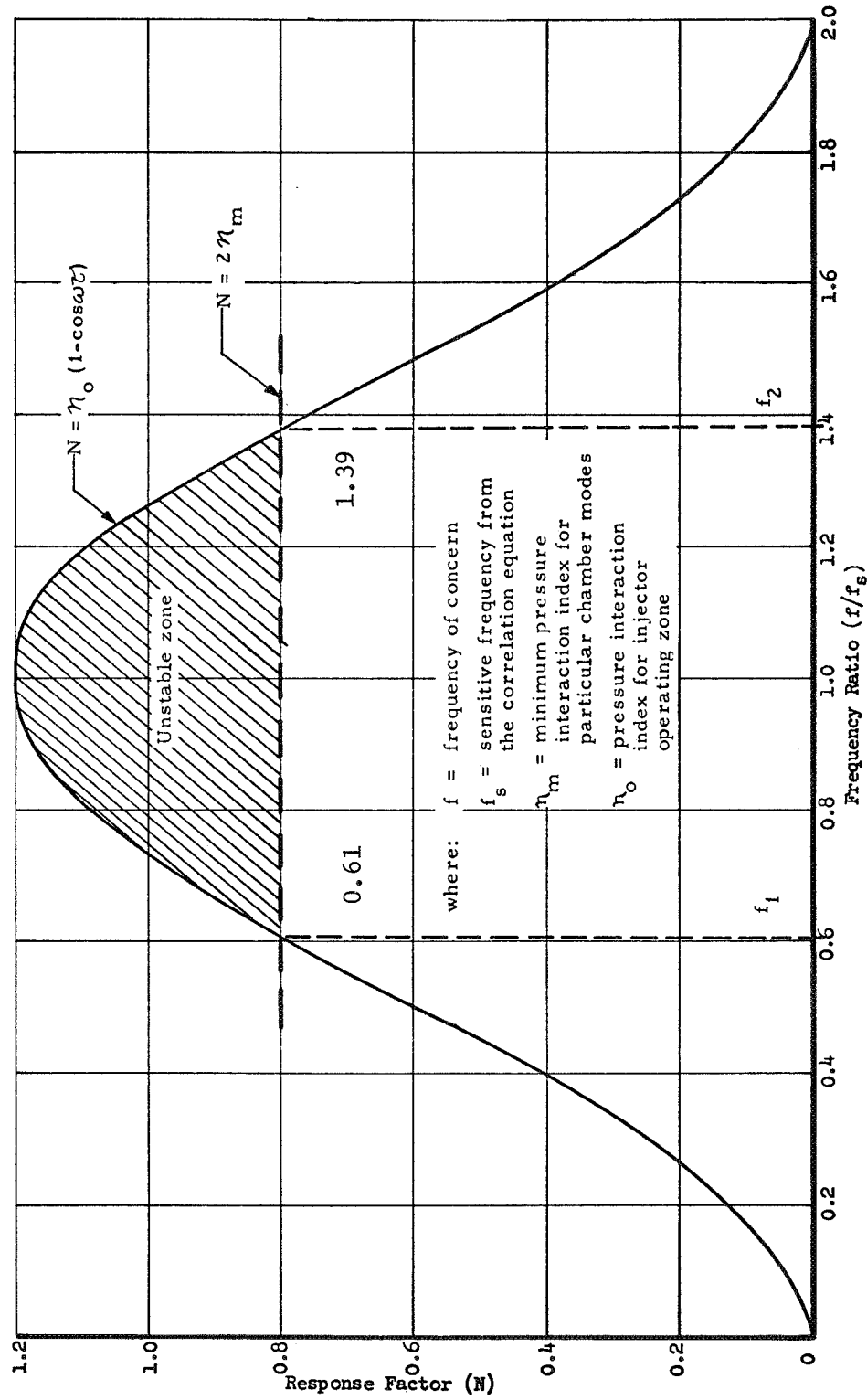


Figure 4 -- Response Curve for Crocco Sensitive Time Lag Model

3.1, Determining Stability (cont.)

where n_o is an experimentally determined parameter used to describe the magnitude of the injector response at the most sensitive frequency, f_g . The sensitive frequency is also experimentally determined and represents the frequency at which a given injector exhibits its maximum gain (i.e., N_{injector} is at a maximum).

Correlations for f_g are given in the following sections as a function of injector design and operating parameters. As determined experimentally, n_o was found to be insensitive to injector design and operating conditions evaluated during this program and also to range in magnitude from 0.40 to 0.60. For the purpose of any design examples presented, the value 0.60 is used since this is the most conservative (i.e., most unstable condition) from the standpoint of anticipating an instability problem. The parameter f represents the frequency of interest.

Also indicated in Figure 4 is the magnitude of the chamber response, N_{chamber} . In the design examples which follow, this parameter, which is a measure of the chamber's ability to expel the additional gas volume generated by an unstable combustion process, is assumed to be independent of frequency over a given frequency range. In Section 4, Use of the Computer, the model allows this parameter to vary. The function is held constant in this section to permit a preliminary determination of stability without resorting to the complex computer program. Different constant values for N_{chamber} are supplied, however, depending on the type of chamber considered (i.e., cylindrical, annular, rectangular, etc.). The values for the various types of chambers can be found in Table 1, page 23.

The procedure for evaluating system stability is outlined below and involves three basic steps: (1) determining the injector response curve, (2) determination of the chamber response based on the type of chamber, and

3.1, Determining Stability (cont.)

(3) determination of the acoustic modes of the chamber in the vicinity of the frequency range where the injector shows a high response.

Step 1. Determination of the Injector Response Curve

From Equation 10 it can be seen that two parameters are required to identify the injector response curve--the sensitive frequency (f_s) and the injector response magnitude parameter (n_o).

From experimental results to date, the injector response has been found to be nearly constant and ranging from 0.40 to 0.60. The recommended value for use is 0.60. The value of f_s is dependent on the type of injector orifice element being used and operating conditions. Empirical relationships for two types of injector elements investigated in this program, the impinging coaxial element and the conventional impinging elements, are

for the impinging coaxial element

$$f_s = \frac{4550 (\bar{M}_c)^{0.15} (P_r)^{1/3}}{d_o^{0.15} F(VR \sin \phi)}, \quad \text{Eq. 11}$$

and for a conventional impinging element

$$f_s = 1750 \frac{(M_c P_r)^{1/3}}{(d_o)^{1/2}} \quad \text{Eq. 11a}$$

3.1, Determining Stability (cont.)

where

M_c = chamber Mach number at the injector face.
 P_r = ratio of chamber pressure (P_c) to the critical pressure of oxygen (P_{crit}) for $P_c \leq P_{crit}$

($P_r = 1.0$ for $P_c > P_{crit}$).

d_o = diameter of oxidizer orifice (inches)

$F (VR \sin \theta)$ is defined by Figure 5.

VR = Injection velocity ratio (fuel/oxidizer)

ϕ = included angle between fuel and oxidizer stream

Example 1: Assume LO_2/LH_2 propellants with coaxial injection.

A. Mach Number (M_c) = 0.182

(Assume $A_c/A_t = 3.33$, $\gamma = 1.2$)

B. $P_r = 1.0$ (since $P_c > P_{crit}$)

C. Oxidizer injection velocity = 50 ft/sec

Fuel injection velocity = 500 ft/sec

$VR = 10.0$

D. Oxidizer orifice diameter (d_o) = 0.100 in.

E. $\phi = 7.5$ degrees

$\therefore F (VR \sin \phi) = 1.30$ (see Figure 5)

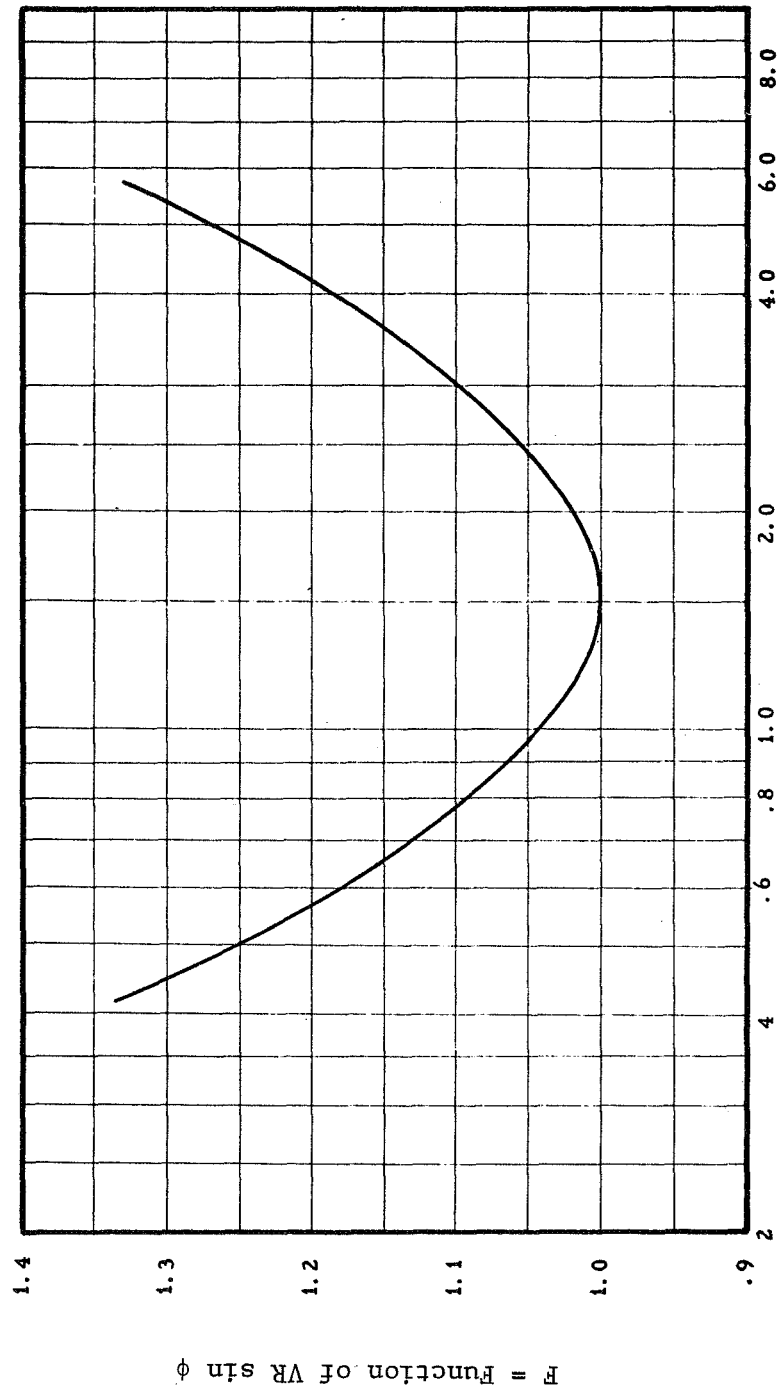


Figure 5 -- F (VR sin ϕ) as Function of Impingement Velocity Ratio

3.1, Determining Stability (cont.)

$$\begin{aligned}
 \text{Then } f_s &= \frac{4550 \bar{M}_c^{0.15} \times (P_r)^{1/3}}{d_{ox}^{0.15} F (VR \sin \phi)}, \\
 &= \frac{4550 (0.180)^{0.15} (1.0)}{(0.100)^{0.15} \times 1.01} = 4930 \text{ Hz.}
 \end{aligned}$$

Step 2. Determine Chamber Response (N_{chamber})

The term N_{chamber} defines the minimum chamber response required to establish an acoustic instability within the chamber. This term is strongly dependent upon the characteristics of the nozzle. Table 1 lists the interaction indices obtained for a variety of chamber shapes with uniform injection.

Table 1 -- Chamber Response as Function of Chamber Type

<u>Type</u>	<u>(N_{chambers}) (Fundamental and Higher Order Modes)</u>
Cylindrical	0.35 to 0.75
Annular	0.90 to 1.30
Conical	0.45 to 0.75
Rectangular	1.00 to 1.40

Because of the complexity of the equations (see Volume 2) and the number of data points required to define a plot of N_{chamber} it is recommended that this parameter be evaluated by running the appropriate subprograms of the Combustion Stability Computer Program whenever possible. (See Section 4, Table 8, for the required input). The output of the computer program in terms of n_{min} which can be converted to N_{chamber} by the relationship $N_{\text{chamber}} = 2 \times n_{\text{min}}$.

3.1, Determining Stability (cont.)

Certain guidelines can be established for selection of N_{chamber} when it is not possible to use the computer program.

1. For the most conservative estimate of system stability (i.e., most likely to be unstable) pick the lowest value of N_{chamber}).
2. Low values of N_{chamber} are generally associated with high contraction ratio chambers or low Mach numbers (i.e., $M_c \leq 0.20$).
3. High values of N_{chamber} are generally associated with high contraction ratios or high Mach numbers (i.e., $M_c \geq 0.30$).
4. For annular nozzles, parametric studies indicate a greater than 20% increase in N_{chamber} can be obtained by forming the nozzle as shown in Table 2 and Figure 6, Case 5 as contrasted with Case 8.

Step 3. Calculate the Frequencies of the Acoustic Modes of the Chamber

Chamber mode frequency, f_c , is the final parameter needed to construct the response graph and represents the various resonant frequencies which can exist in a particular chamber in the transverse and longitudinal directions. These frequencies may be determined from the acoustic equation:

$$\text{Frequency} = \frac{\text{speed of sound}}{\text{wave length}} \quad \text{Eq. 12}$$

Table 2 -- Annular Chamber Nozzle Admittance Study

* CASE	CHAMBER NOZZLE RADIUS, IN.	CHAMBER RADIUS, IN.	CHAMBER NOZZLE CONVERGENCE RADIUS, "F CHAMBER, IN.	CHAMBER THROAT RADIUS OF CURVATURE, IN.	CHAMBER ANGLE OF CONVERGENCE (°)	CENTERBODY NOZZLE RADIUS, IN.	CENTERBODY THROAT RADIUS OF CHAMBER, IN.	CENTERBODY RADIUS, IN.	CENTERBODY NOZZLE ENTRANCE RADIUS OF CHAMBER, IN.	CENTERBODY ANGLE OF CONVERGENCE (°)	MEAN THROAT RADIUS, IN.
1	4.645	5.25	.50	1.25	20	3.545	1.25	3.07	.50	20	4.12
2	5.25	5.25	.001	.001	.001	4.285	3.438	3.07	.375	40	4.78
3	4.30	5.25	.375	.3438	40	3.07	.001	3.07	.001	.001	3.73
4	4.325	5.25	.625	.406	32	3.105	6.0	3.07	6.0	3	3.76
5	4.80	5.25	.75	.600	17	3.71	.75	3.07	.531	25	4.29
6	4.95	5.25	1.70	.500	11	3.92	.6875	3.07	.281	30	4.46
7	5.10	5.25	5.0	3.0	5	4.105	.5625	3.07	.250	35	4.63
8	4.650	5.25	.50	1.25	40	4.315	1.25	3.07	.50	40	4.48

Reference Figure 6

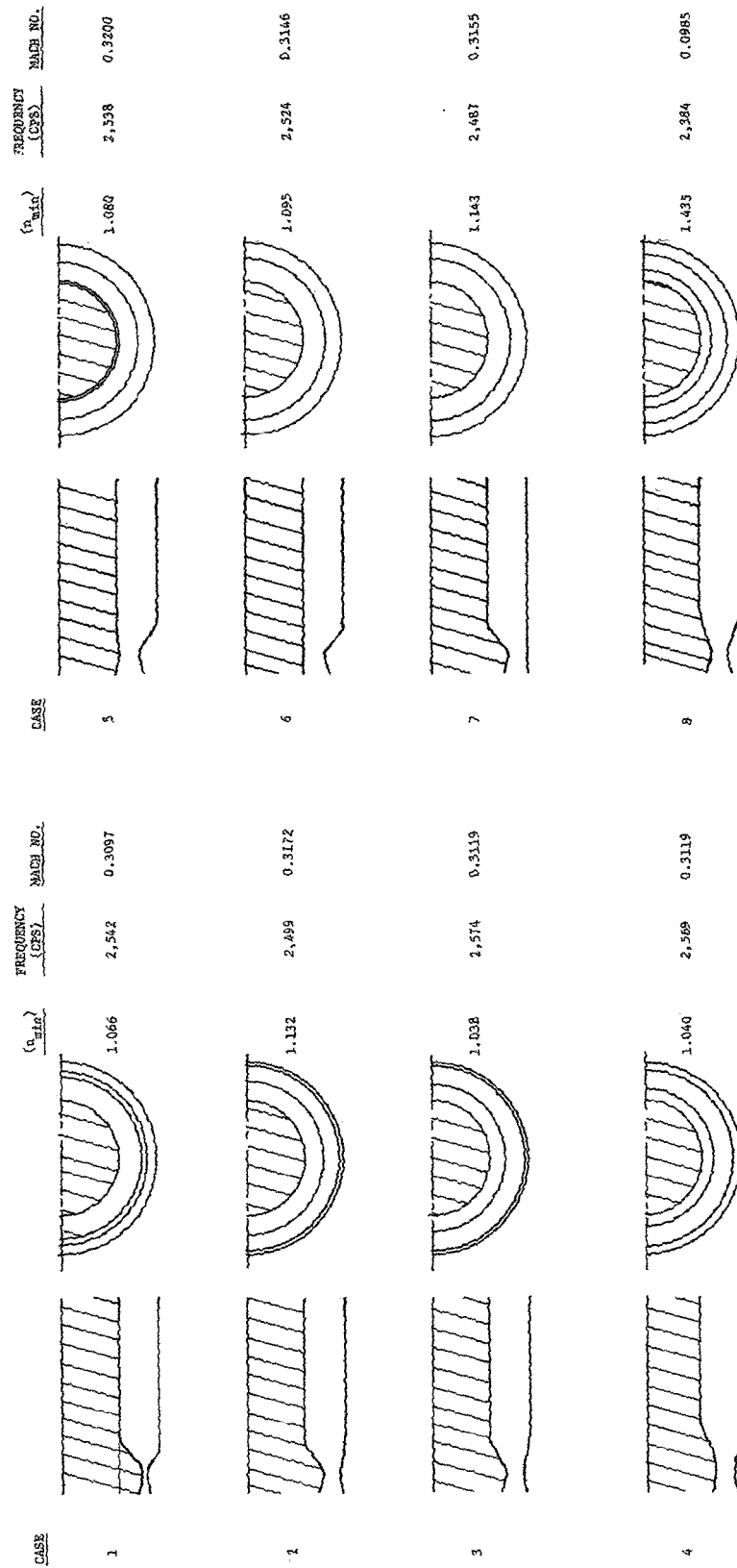


Figure 6 -- Chamber Response as Function of Nozzle Orientation

3.1, Determining Stability (cont.)

For longitudinal modes, the characteristic length is the distance from the injector face to the nozzle throat. For the convergent section of the nozzle, a factor of 2/3 (based on the geometry of cones) is applied. Thus, for a cylindrical chamber

$$\ell_{\text{eff}} = \ell_c + 2/3 \ell_n,$$

where the subscripts c and n refer to the cylindrical and nozzle portions, respectively.

For transverse modes, the characteristic length is the chamber diameter. For transverse modes, Equation 12 becomes:

$$f_{\text{mode}} = \frac{c}{2\pi r} \times S_{v\eta} \quad \text{Eq 5 (ref)}$$

where c is the acoustic velocity, r is the radius, and $S_{v\eta}$ is the argument of the Bessel function as given by Table 3. A separate Bessel function applies for combinations of radial and tangential oscillations. The frequency for combinations of longitudinal and transverse modes is the vectoral sum of the individual modes, thus

$$f_{1L, 1T} = \sqrt{(f_{1L})^2 + (f_{1R})^2} \quad \text{Eq 13}$$

Example 2: Compute the principal acoustic modes in a combustion chamber having the following dimensions:

length (cylindrical portion), 5 in.

length (convergent portion), 6 in.

radius, 7 in.

assumed velocity of sound, 5500 ft/sec.

3.1, Determining Stability (cont.)

Table 3 -- Transverse Bessel Function Arguments

			$S_{\nu\eta}^*$
a.	Tangential Modes		
	First tangential:	S_{11} =	1.8413
	Second tangential:	S_{21} =	3.0543
	Third tangential:	S_{31} =	4.2012
	Fourth tangential:	S_{41} =	5.3175
	Fifth tangential:	S_{51} =	6.4154
b.	Radial Modes		
	First radial:	S_{02} =	3.8317
	Second radial:	S_{03} =	7.0156
	Third radial:	S_{04} =	10.1734
c.	Combined tangential-radial modes		
	1T-1R:	S_{12} =	5.3313
	1T-2R:	S_{13} =	8.5263
	1T-3R:	S_{14} =	11.7059
	2T-1R:	S_{22} =	6.7060
	2T-2R:	S_{23} =	9.9695
	2T-3R:	S_{24} =	13.1705
	3T-1R:	S_{32} =	8.0151
	3T-2R:	S_{33} =	11.3459
	3T-3R:	S_{34} =	14.5858

*The first subscript, ν , represents the order of the Bessel function and agrees with the order of the corresponding tangential mode. The radial modes ν is always zero. The second subscript, η , represents the order of occurrence of maxima and minima in the expansion of the Bessel function, and is always the first maximum for tangential modes. For the radial modes η equals the order of the mode increased by unity.

3.1, Determining Stability (cont.)

Thus the effective length

$$l_{\text{eff}} = 5 + 2/3 \times 6 = 9 \text{ in.}$$

Then for the longitudinal modes:

$$(f)_{\text{first longitudinal}} = \frac{5500 (1)}{2 (9/12)} = 3660 \text{ Hz}$$

$$(f)_{\text{second longitudinal}} = \frac{5500 (2)}{2 (9/12)} = 7320 \text{ Hz}$$

For the transverse modes:

$$(f)_{\text{first tangential}} = \frac{5500 (1.8413)}{2 \pi (7.0/12)} = 2770 \text{ Hz}$$

$$(f)_{\text{second tangential}} = \frac{5500 (3.0543)}{2 \pi (7.0/12)} = 5760 \text{ Hz}$$

For the combined 1T, 1L mode:

$$(f_{\text{req}})_{\text{combined transverse}} = (f)_{\text{transverse}}^2 + (f)_{\text{longitudinal}}^2$$

$$(f_{\text{req}})_{1\text{T}-1\text{L}} = (3660)^2 + (2770)^2 = 4700 \text{ Hz}$$

Step 4. Construction of Response Curves

Having determined the injector and chamber response and the acoustic modes of the combustion chamber from Steps 1, 2 and 3, the remaining tasks involve the mechanics of constructing the characteristic curves such as shown in Figure 4 and the interpretation of the results.

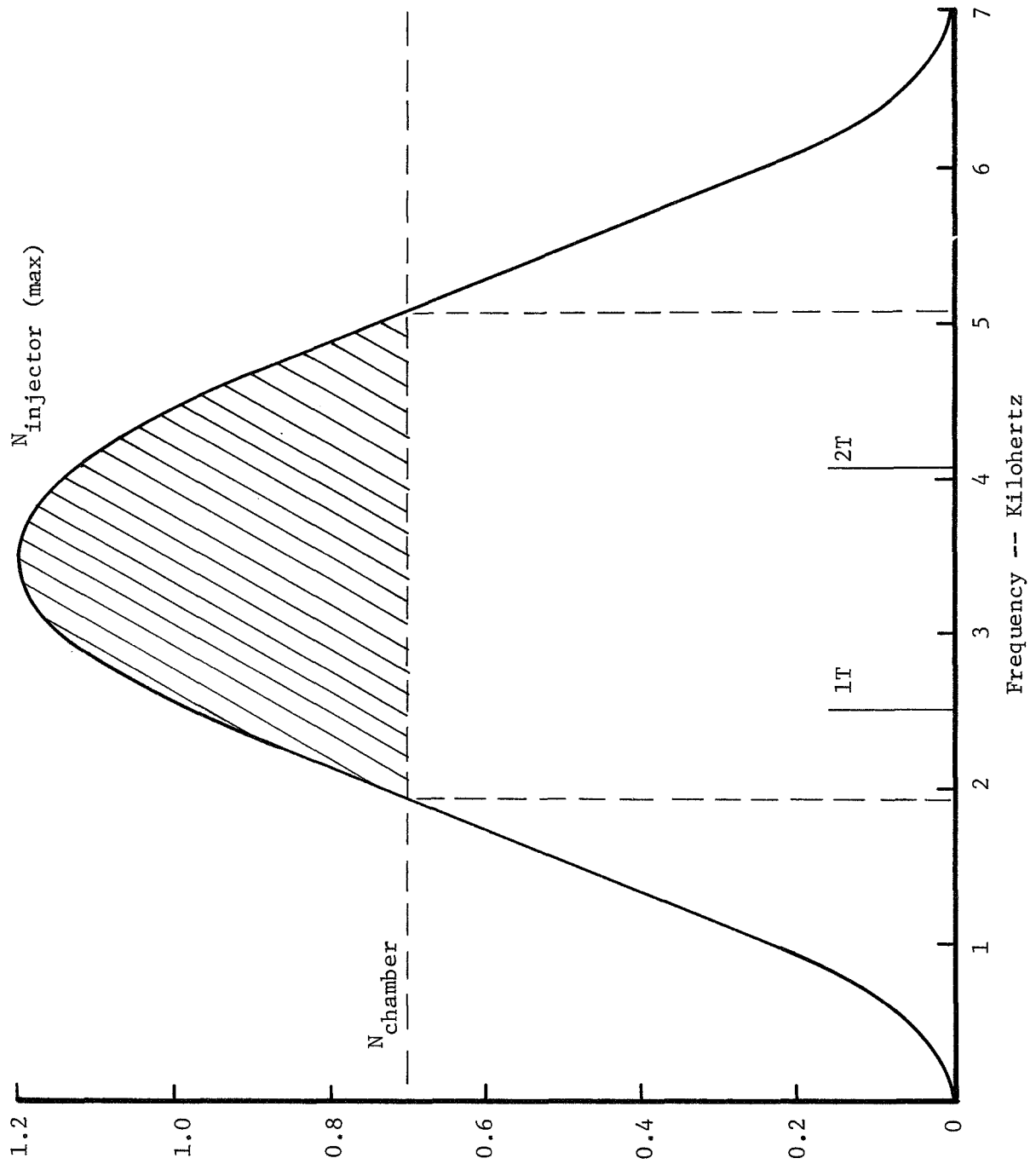


Figure 7 -- Comparing Injector and Chamber Response

3.1, Determining Stability (cont.)

Turning first to the mechanics of constructing a curve similar to Figure 4, the injector response curve is

$$N_{\text{injector}} = n_o \left(1 - \cos \pi \frac{f}{f_s}\right) \quad \text{Eq 10 (ref)}$$

which results in a peak in the response curve at $f = f_s$ and an intercept of the abscissa at $f = 0$ and $f = 2f_s$. As previously stated, n_o is assumed to be equal to 0.60.

Example 3: Construct the injector-chamber response diagram given the following injector and chamber operating conditions:

Injector type	Coaxial
Oxidizer orifice size	0.15 in.
Chamber pressure	300 psia
Chamber contraction ratio $\left(\frac{A_c}{A_t}\right)$	3.0
Propellants	H_2/O_2
Specific heat of combustion products $\left(\frac{C_p}{C_v} \text{ or } \gamma\right)$	1.2
Included angle ϕ	20°
Design velocity ratio	6.0
P_{crit} (oxygen)	730 psi
Chamber diameter	12.5 inches

From Equation 11 and Figure 5, the sensitive frequency is calculated to be 3500 Hz.* Letting the element response magnitude be 0.60, the curve for the injector response can be constructed by plotting Equation 10 as shown in Figure 7 for various values of f .

* Note that the difference in sensitive frequency compared to Example 1 is almost entirely due to d_o . P_r and F ($VR \sin \phi$) have small effect.

3.1, Determining Stability (cont.)

Proceeding to Step 2 and assuming the chamber to be used is cylindrical for the contraction ratio specified, the relationship

$$M_c = \frac{A_t}{A_c} \left(\frac{2}{\gamma+1} \right)^{\frac{\gamma+1}{2(\gamma-1)}} \quad \text{Eq 14}$$

$$= 0.20,$$

results. From Table 1 and the guidelines given in Step 2 this gives

$$N_{\text{chamber}} = 0.70.$$

This value for N_{chamber} is shown as a horizontal line on Figure 7. It is now apparent that the frequency range over which instabilities are likely to occur is 1900 to 5100 Hz. Calculations of the various acoustic modes for the 12.5 inch chamber using the relationships specified in Step 3 indicate that the likely modes of instability are the first tangential at 2500 Hz and the second tangential at 4000 Hz. Where selecting 5000 ft/sec for the speed of sound with these propellants at the given operating conditions.

$$f_{1T} = \frac{c S_{v\eta}}{2\pi r_c} = \frac{5000 (1.84) \times 12}{(6.28) 6.25} = 2800 \text{ Hz}$$

and

$$f_{2T} = \frac{5000 (3.05) \times (12)}{(6.28)(6.25)} = 4650 \text{ Hz}$$

where $S_{v\eta}$ was obtained from Table 3.

The longitudinal modes, which can also be calculated from a known chamber length, are not evaluated because experience shows these modes do not present a problem. This is believed to result from two factors--the higher

3.1, Determining Stability (cont.)

N_{chamber} values for these modes (of the order of 1/3 greater) and the distribution of combustion axially along the chamber which tends to give an effective increase in N_{chamber} . As estimated, the effective N_{chamber} for the longitudinal mode only is given by

$$N_{\text{chamber}}(\text{effective}) = N_{\text{chamber}} \left[\cos 2 \pi \frac{\ell}{\ell_{\text{eff}}} \right]^2 \quad \text{Eq 15}$$

where ℓ is the dimension from the injector face to the point of maximum combustion, which is generally 2 in. to 5 in. for most engines.

Knowing the modes of instability, certain design modifications can be made to improve stability (which is the topic for the next section) or it is possible now to design a stabilizing device such as discussed in Section 5.0.

As stated earlier, the proposed model only treats the problem of linear instability and not the case of those types of instability which are induced by perturbations. Thus, if a system is predicted to be stable by this method, it may be inferred that the system will not be spontaneously unstable.

Experience indicates that there are few, if any, systems which cannot be perturbed unstable by start transient spikes or other sources of perturbation. Based on experience to date, it would appear to be good design practice to consider as a minimum that some sort of stability device is required for man-rated systems and should be evaluated as a possible development requirement.

The approach just discussed in Step 2 can be used to identify whether such a device would be required and what its design characteristics should be. Experience has shown that transverse acoustic modes in the vicinity of the sensitive frequency (f_s) are the most likely modes to be pulsed unstable in a

3.1, Determining Stability (cont.)

system that is not spontaneously unstable. Thus, the injector response curve can be used to identify what modes are most likely to be pulsed unstable and Section 5.0 can be used to design the damping device or as a minimum to evaluate the impact of such a device if later developments should show it to be necessary.

Guidelines

Several basic "rules of thumb" have been developed from experience which will help the designer begin his stability evaluation task:

(1) The sensitive frequency should be less than the lowest fundamental mode frequency. Since the gain of the injection process is maximum at the sensitive frequency, it behooves the designer to remove any possible chamber modes from this vicinity. By setting the frequency lower than the fundamental, it can be assured that the harmonic modes also will be higher than the sensitive frequency and even further displaced.

(2) In the event Item (1) is impractical, the chamber should be designed so that a minimum number of modes will fall within the sensitive frequency curve above the minimum gain line. This would have the effect of limiting the protection requirements for the lower order modes.

(3) The value for velocity ratio used in the injection correlation equation should (if possible) exceed 10. Hydraulic considerations, propellant pump requirements, etc., may preclude adherence to this rule; however, data obtained thus far on two test programs (ref NASA TN D-3373 and Final Report 11741/SA6-F) demonstrate the worth of using large velocity ratios to suppress instability.

3.1, Determining Stability (cont.)

(4) For chambers with low contraction ratios (i.e., Mach numbers above 0.20) the mode frequencies and chamber interaction indices should be calculated solely by the computer program. The acoustic equations, however, will give good approximations for chamber frequencies at low Mach numbers, and corresponding N_{chamber} may be approximated from Table 1.

3.2 MANIPULATING INITIAL DESIGN

The calculations performed as indicated in Section 3.1 may show that the initial design is stable with respect to all conceivable modes. This is most likely to be true for very small chambers where the fundamental modes have frequencies much higher than that of the combustion response. In this case the only additional requirement is to demonstrate dynamic stability by pulse testing with prototype hardware.

In most instances, however, the designer will need to alter his original configuration in order to achieve stability and will also have a certain flexibility of choice in the manipulation of one or more of the design parameters. It is advantageous then to examine the effect upon stability of permitting these parameters to vary. This is relatively simple if there is only one free parameter. Quick calculations at the mean and both extremes of parameter variability may show whether there is a good prospect for a successful solution.

The approach may be made from two directions: (1) by shifting the sensitive frequency through operating on the injector pattern, or (2) by moving the resonant frequencies of the respective chamber modes by redesigning the chamber contours.

3.2, Manipulating Initial Design (cont.)

3.2.1 Calculating Limiting Injector Parameters

In each instance it is first necessary to determine how much the sensitive frequency must be displaced to provide neutral stability for the mode in question. This is equivalent to letting the combustion response equal the chamber response for the mode in question and solving for the sensitive frequency f_s .

Example 4: The frequency of the first tangential mode for a given chamber is 3720 Hz. Given the following data determine whether the system is stable and if not to what value must the sensitive frequency be shifted to assure stability.

$$\begin{aligned}
 f_s &= 3500 \text{ Hz} \\
 f_{1T} &= 3720 \text{ Hz} \\
 n_o &= 0.6 \\
 N_{\text{chamber}} &= 1.0 \\
 N_{\text{inj}} &= n_o \left(1 - \cos \pi \frac{f_{1T}}{f_s} \right) && \text{Eq 10 (Ref)} \\
 &= 0.6 \left(1 - \cos \pi \frac{3720}{3500} \right) \\
 &= 0.6 (1 - \cos 3.34 \text{ (rad)}) \\
 &= 0.6 (1 + 0.98) = 1.19
 \end{aligned}$$

Since $N_{\text{inj}} > N_{\text{chamber}}$ the system will be unstable in the 1T mode. To obtain a sensitive frequency that will have neutral stability in the 1T mode,

3.2, Manipulating Initial Design (cont.)

$$\begin{aligned}
 \text{Let } N_{\text{chamber}} &= n_o \left(1 - \cos \pi \frac{f_{1T}}{f_s}\right) \\
 \cos \pi \frac{f_{1T}}{f_s} &= 1 - \frac{N_{\text{chamber}}}{n_o} = -0.67 \\
 \pi \frac{f_{1T}}{f_s} &= \pi \pm 0.84 \text{ (rad)} \\
 f_s &= \frac{\pi f_{1T}}{\pi \pm 0.84} \\
 f_s &= \frac{3.14}{2.30} \times 3720 = 5070 \text{ Hz}
 \end{aligned}$$

or

$$f_s = \frac{3.14}{3.98} \times 3720 = 2940 \text{ Hz}$$

As can be seen from Figure 8, the first solution would move the sensitive frequency to a higher value where it would be within the range of modes of higher order than the 1T, which would be undesirable. The second solution would not only meet the requirement for the 1T mode but would lessen the response to the higher order modes as well.

3.2.2 Manipulating Sensitive Frequency

The sensitive frequency for coaxial elements may be calculated using Equation 11,

$$f_s = 4550 \left(\frac{M_c}{d_o} \right)^{0.15} \frac{(P_c/P_{\text{crit}})^{1/3}}{F (VR \sin \phi)} \quad \text{Eq 11 (Ref)}$$

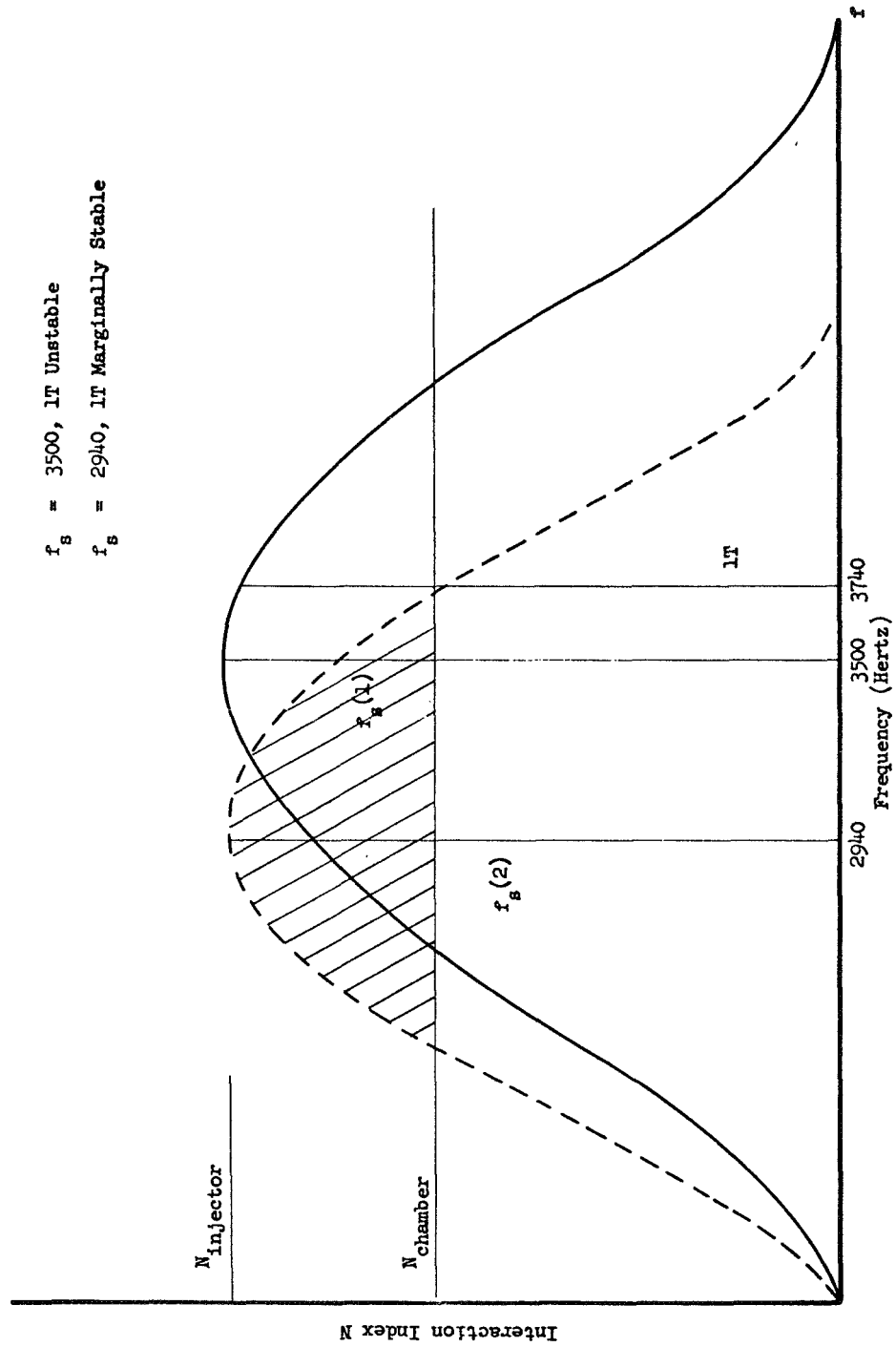


Figure 8 -- Effect of Displacing Sensitive Frequency

3.2, Manipulating Initial Design (cont.)

This equation contains six variable terms:

Mach number, M_c
 Orifice diameter, d_o (less volatile propellant)
 Chamber pressure, P_c
 Critical pressure, P_{crit} (less volatile propellant)
 Injection velocity ratio, $\frac{V_f}{V_o} = VR$, and
 Impingement angle, ϕ .

One of these, the critical pressure, is a physical property of the propellants selected and therefore not subject to variation. The other parameters may be manipulated to some extent depending upon the design operating requirements and the type of injector and chamber selected.

Mach Number

Mach number is a function of the contraction ratio and the ratio of specific heats

$$M_c = \frac{A_t}{A_c} \left(\frac{2}{\gamma + 1} \right)^{\frac{\gamma + 1}{2(\gamma - 1)}} \quad \text{Eq 14 (Ref)}$$

As the ratio of specific heats is a function of the propellants burning at a given mixture ratio, it may also be considered constant at 1.2, permitting variation only in the contraction ratio. For nearly all applications the contraction ratio falls between 1.5 and 6.0, giving a Mach number range of 0.10 to 0.40 for a total variation of ± 12 percent in sensitive frequency.

The sensitive frequency varies in the same direction as Mach number. Therefore, f_s may be reduced slightly either by constricting the throat, with attendant rise in chamber pressure, or by enlarging the chamber gas sectional area.

3.2, Manipulating Initial Design (cont.)

Pressure Ratio

The term $\left[\frac{P_c}{P_{crit}} \right]^{1/3}$ represents the effect of varying chamber pressure on sensitive frequency when the chamber pressure is below the critical pressure.

Using 50 psia as a lower limit for a O_2/H_2 system and 730 psia as the critical pressure of O_2 , the maximum variation in $\left[\frac{P_c}{P_{crit}} \right]^{1/3}$ is 0.41 to 1.00.

Because f_s varies in the same direction as P_c , the frequency of maximum sensitivity would be reduced to less than half by reducing the chamber pressure from 730 psia to 50 psia. For applications where $P_c > P_{crit}$ this parameter does not enter into consideration.

Velocity Ratio and Impingement Angle (co-axial element only)

Figure 5 shows $F (VR \sin \phi)$ as a combined function of the ratio of the propellant velocities and impingement angles. The curve, developed from experimental data, expresses both momentum effects, most noticeable at high velocity ratios and large angles of impingement, and shear effects, predominating where the velocities are nearly equal and where the stream directions are parallel (showerhead) or nearly so. From Figure 5 it can be seen that the range of variation of $F (VR \sin \phi)$ is from 1.0 to 1.4.

Oxidizer Orifice Diameter

The sensitive frequency can also be changed by varying the diameter of the oxidizer (less volatile propellant) orifice. In contemporary engines the orifice diameters range from approximately 0.020 in., for very small engines to somewhat in excess of 1/2 in. for engines on the order of a million pounds of thrust. The limits are set primarily by considerations of performance,

3.2, Manipulating Initial Design (cont.)

hydraulics, and fabrication. For any specific application, therefore, only a portion of the range is available for the designer to manipulate.

The effect of increasing the oxidizer orifice diameter is to lower the sensitive frequency. For the range of diameters 0.020 in. to 0.500 in. taken to the 0.15 power, $(d_o)^{0.15}$ ranges from 0.56 to 0.90, giving a variation in sensitive frequency by a factor of nearly 2.

Total Variation

The upper and lower limits of sensitive frequency may now be evaluated.

$$\begin{aligned}
 f_s &= 4550 \left(\frac{M_c}{d_o} \right)^{0.15} \frac{\left(P_c / P_{crit} \right)^{1/3}}{F (VR \sin \phi)} & \text{Eq 11 (Ref)} \\
 &= 4550 \frac{(0.708 \rightarrow 0.874)}{(0.901 \rightarrow 0.556)} \frac{(0.41 \rightarrow 1.00)}{(1.4 \rightarrow 1.0)} \\
 &= 1045 \text{ Hz} \rightarrow 7150 \text{ Hz}
 \end{aligned}$$

Naturally only a fraction of this range is available for any specific rocket application, the extent of the variation being limited by the operating conditions and design constraints.

3.2.3 Varying Frequency of Chamber Modes

In the same manner that the sensitive frequency can be moved to avoid one particular chamber mode it is also possible to displace a class of modes with respect to the sensitive frequency. The factors involved are the speed of sound and the chamber dimensions. For practical purposes the speed of sound must be assumed constant as it is based on the thermodynamic properties of the propellants and the operating conditions.

3.2, Manipulating Initial Design (cont.)

The frequencies of the longitudinal modes vary inversely with the length of the chamber, those of the transverse modes with the chamber diameter. As all modes of a class (i.e., transverse or longitudinal) are affected, it is generally preferable to raise rather than to lower their frequencies. Hopefully by raising their frequencies, the fundamental modes will have values higher than the sensitive frequency associated with the injector, and consequently harmonic modes will be even further removed. This is accomplished by minimizing the appropriate dimension. However, as minimum chamber size is most generally a design objective for other reasons, it is to be expected that all possible has been done that would increase the acoustic frequencies. The exception would be where, because of design constraints, it is impractical to move the fundamental mode to the right (ascending frequency) of the sensitive frequency peak. Then the fundamental and the first harmonic should span the sensitive frequency and added damping should be applied to suppress interaction with the combustion.

3.2.4 Injector Index (N_o)

As mentioned in Section 3.1, N_o for the injector is not adaptable to direct calculation but must be determined experimentally. In Section 6.1 a short test program is outlined by which the interaction index of a limited number of injector configurations may be approximated. If the designer does not have this option he had best assume the conservative value of 0.6.

3.2.5 Maximimizing Chamber Response (N_{chamber})

The response for the combustion chamber is conditioned by both geometric and combustion parameters. These effects are interdependent so that as yet there is no precise knowledge of their individual impact. In Table 1, Section 3.1, the range of the response is given for various types of chambers.

3.2, Manipulating Initial Design (cont.)

This represents a fairly comprehensive listing of analytical data which has been partially verified by experimental results. The designer is advised to assume the lower limit of these ranges if he is not prepared to conduct a detailed parameter study.

Based on parameter studies conducted to date, the following variations tend to increase the chamber response.

1. Decreasing the chamber contraction ratio or increasing Mach number.
2. For annular chambers, placing the nozzle throat nearer the chamber outer wall.

3.2.6 Propellant Distribution

One factor that is known to affect the chamber interaction index for transverse modes is the radial density distribution of the propellants. The relationship is expressed by the term A_{vn} equation

$$N_{\text{chamber (nu)}} = \frac{N_{\text{chamber (u)}}}{A_{vn}} \quad \text{Eq 16}$$

where:

- $N_{\text{chamber (u)}}$ = chamber response with uniform injection,
- $N_{\text{chamber (nu)}}$ = chamber response with non-uniform injection, and
- A_{vn} = pressure distribution coefficient.

3.2, Manipulating Initial Design (cont.)

The pressure distribution coefficient has the following characteristics:

- a. It measures the combustion sensitivity of the system with non-uniform injection of propellants.
- b. It applies only to the transverse modes (tangential and radial),
- c. The numerical value for the coefficient is different for each transverse mode (except for uniform distribution when the coefficient is unity for all modes.
- d. It assumes one-dimensional flow in the chamber with no mixing of streamlines, and
- e. It is assumed that the combustion process is pressure sensitive.

The influence of A_{vn} may be stabilizing or destabilizing depending upon the apportionment of the injected propellant in relation to the nodal points of the respective modes. In the nominal condition the propellant has a uniform radial distribution with reference to the chamber axis. That portion of the burning taking place near the pressure nodes of a particular oscillation will do little to sustain the oscillation. On the other hand, that portion of the combustion occurring near the pressure antinodes of a specific mode will have a driving effect. Theoretically, then, if all the propellant could be injected through an annulus of zero width at the location of a pressure node (e.g., the axis for the 1T), combustion would not reinforce acoustic oscillations and any disturbance would be attenuated for the particular mode in question. The problem is therefore to apportion some propellant flow to each radial zone (to prevent lateral migration) while restricting the flow at radii corresponding to the antinodes of modes with frequencies in the

3.2, Manipulating Initial Design (cont.)

vicinity of the sensitive frequency. The residual propellant would then be injected near the pressure nodes of the more prominent modes. The objective would be to make the coefficient A_{vn} as small as possible for each of the modes lying near the sensitive frequency.

Many injectors have distribution patterns such that the coefficient A_{vn} may be closely approximated using simple manual calculations. For example for the injection distribution depicted in Figure 9 and mode frequencies of 2000 and 3300 and 5800 Hz for the 1T, 2T and 1T-1R modes and a sensitive frequency of 2500 Hz, A_{vn} may be obtained by performing the following calculation.

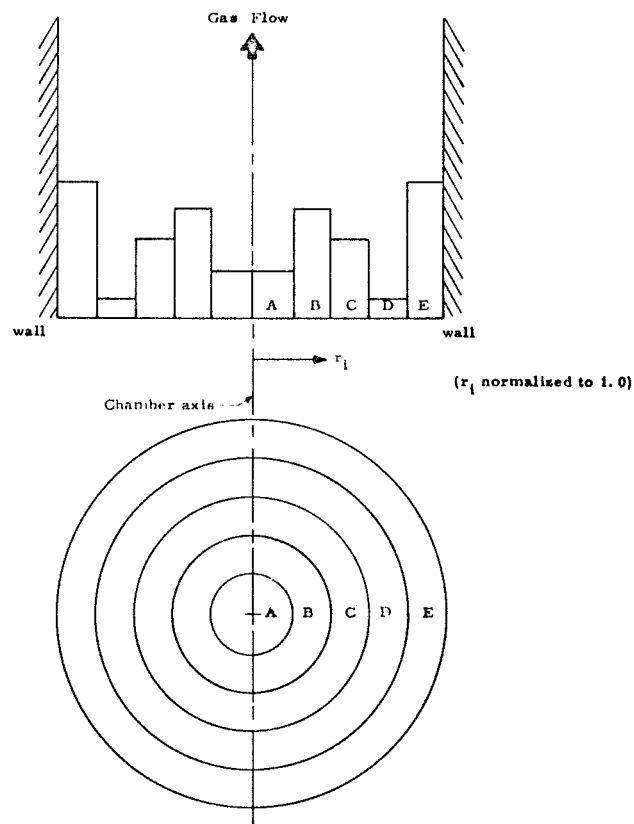


Figure 9 -- Varying Injector Distribution

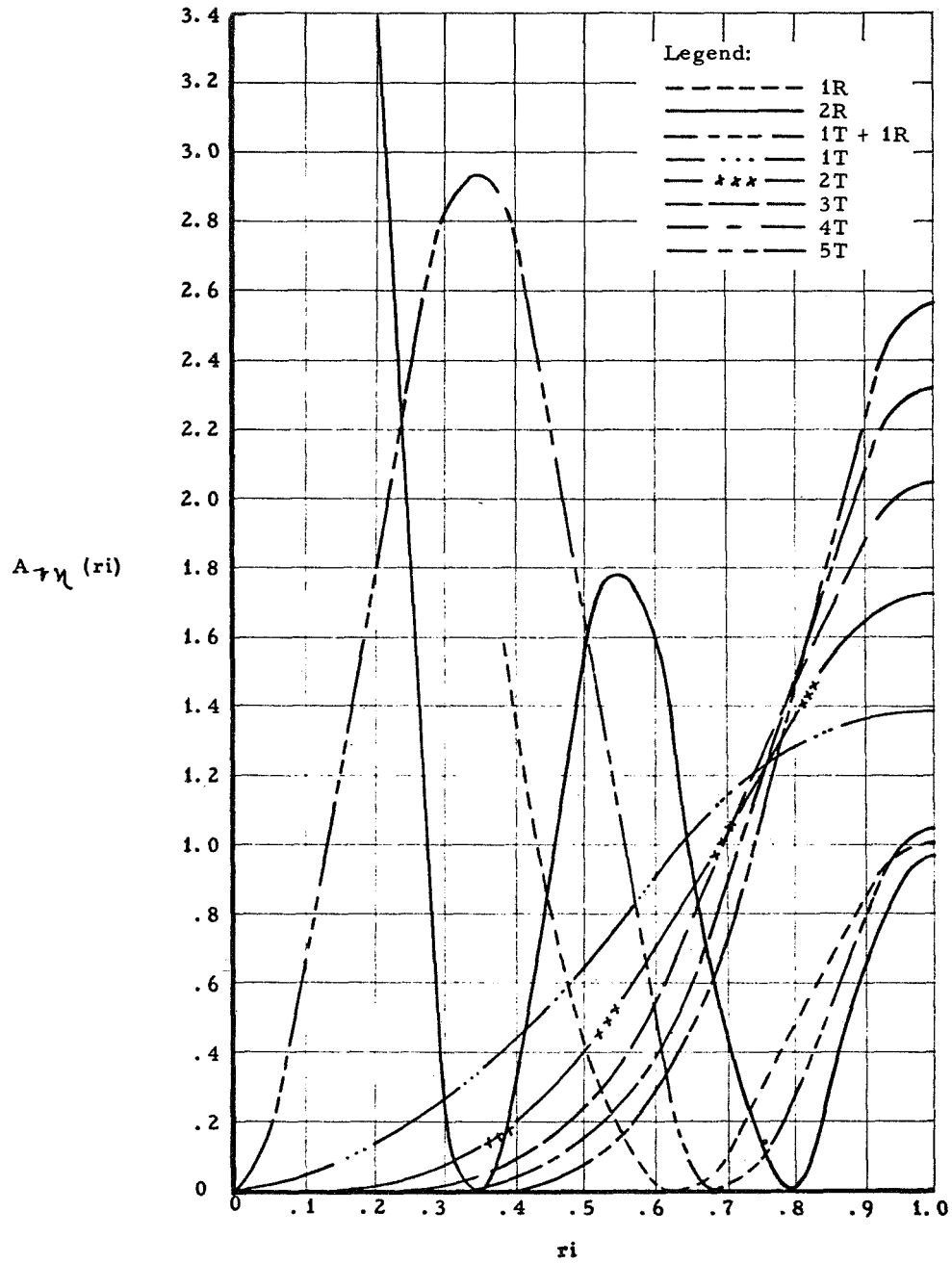


Figure 10 -- A_{vn} as Function of Chamber Radius

3.2, Manipulating Initial Design (cont.)

Example:

Given: $\dot{w}_t = w_A + w_B + w_C + w_D + w_E$

$$(A_{vn})_{mode} = \sum_i^j \left(\frac{\dot{w}_i}{\dot{w}_t} \right) A_{vn}(r_i) \quad \text{Eq 17}$$

where:

$$\begin{aligned} \dot{w}_t &= \text{Total weight flow} \\ \dot{w}_i &= \text{Weight flow through } i^{\text{th}} \text{ annulus} \\ A_{vn}(r_i) &= \text{Functional relationship found from Figure 10.} \\ r_i &= \text{Mean radial distance from the chamber axis to the} \\ &\quad \text{centroid of the } i^{\text{th}} \text{ annulus, normalized from zero} \\ &\quad \text{at the chamber axis to 1.0 at the wall.} \end{aligned}$$

Procedure:

- Step 1. Subdivided injection distribution into five annular zones (A through E), Figure 9.
- Step 2. Determine A_{vn} for the first tangential mode and first tangential-first radial combined mode.
- Step 3. Calculate new $N_{chamber}$ from equation 16.

Note in Table 4a how the majority of the A_{vn} integral comes from Zone E. This is partly because the area of Zone E is greater (high propellant flux) than for the other zones, but mostly because of the greater interaction exhibited by the tangential modes near the wall. In contrast, in Table 4c it is Zone B that contributes the largest percentage to the A_{vn} integral, the result from the antinode of the radial component of the 1R-1T mode occurring at $r_i = 0.35$.

Table 4 -- A_{vn} as Function of Injection Zonea. First Tangential Mode

<u>Zone</u>	\dot{w}_i/\dot{w}_t	r_i	$A_{vn}(r_i)$	$(\dot{w}_i/\dot{w}_t) A_{vn}(r_i)$
A	10%	0.1	0.05	0.005
B	30%	0.3	0.25	0.075
C	20%	0.5	0.57	0.114
D	5%	0.7	1.12	0.056
E	<u>35%</u>	0.9	1.35	<u>0.472</u>
	100%			0.722

Hence, $(A_{vn})_{1T} = 0.722$ b. Second Tangential Mode

<u>Zone</u>	\dot{w}_i/\dot{w}_t	r_i	$A_{vn}(r_i)$	$(\dot{w}_i/\dot{w}_t) A_{vn}(r_i)$
A	10%	0.1	0.0	~ 0
B	30%	0.3	0.08	0.024
C	20%	0.5	0.40	0.080
D	5%	0.7	1.05	0.052
E	<u>35%</u>	0.9	1.65	<u>0.577</u>
	100%			0.733

Hence, $(A_{vn})_{2T} = 0.733$ c. First Tangential/First Radial Mode

<u>Zone</u>	\dot{w}_i/\dot{w}_t	r_i	$A_{vn}(r_i)$	$(\dot{w}_i/\dot{w}_t) A_{vn}(r_i)$
A	10%	0.1	0.60	0.06
B	30%	0.3	2.80	0.84
C	20%	0.5	1.60	0.32
D	5%	0.7	0.0	0
E	<u>35%</u>	0.9	0.8	<u>0.28</u>
	100%			1.50

Hence, $(A_{vn})_{1T-1R} = 1.50$

3.2, Manipulating Initial Design (cont.)

It should be re-emphasized that the values of A_{vn} do not themselves express whether the system is stable. They merely compare the stability of a single nonuniform injector pattern with that from a uniform or "flat" distribution.

For a cylindrical chamber having a N_{chamber} of 0.70 (see Table 1) for uniform injection the new values of N_{chamber} for the 1T, 2T, and 1T-1R modes are:

$$\begin{aligned} N_{\text{chamber}} (1T) &= 0.97 \text{ (more stable)} \\ N_{\text{chamber}} (2T) &= 0.96 \text{ (more stable)} \\ N_{\text{chamber}} (1T-1R) &= 0.47 \text{ (less stable)} \end{aligned}$$

Since the sensitive frequency of the injection elements was much closer to the 1T and 2T frequencies versus the 1T-1R frequency it is more important to stabilize for those modes.

Often a non-uniform injection distribution pattern will exist that does not readily divided into a small number of zones similar to the example problem. In this case the designer should use subprogram (J) of the Sensitive Time Lag Computer Program to obtain his distribution coefficient. This subprogram uses the spatial element location, orifice diameters and hydraulic resistances, pressure drops, and film coolant orifices (considered to be non-reacting) and integrates the value of the coefficient over the injector face.

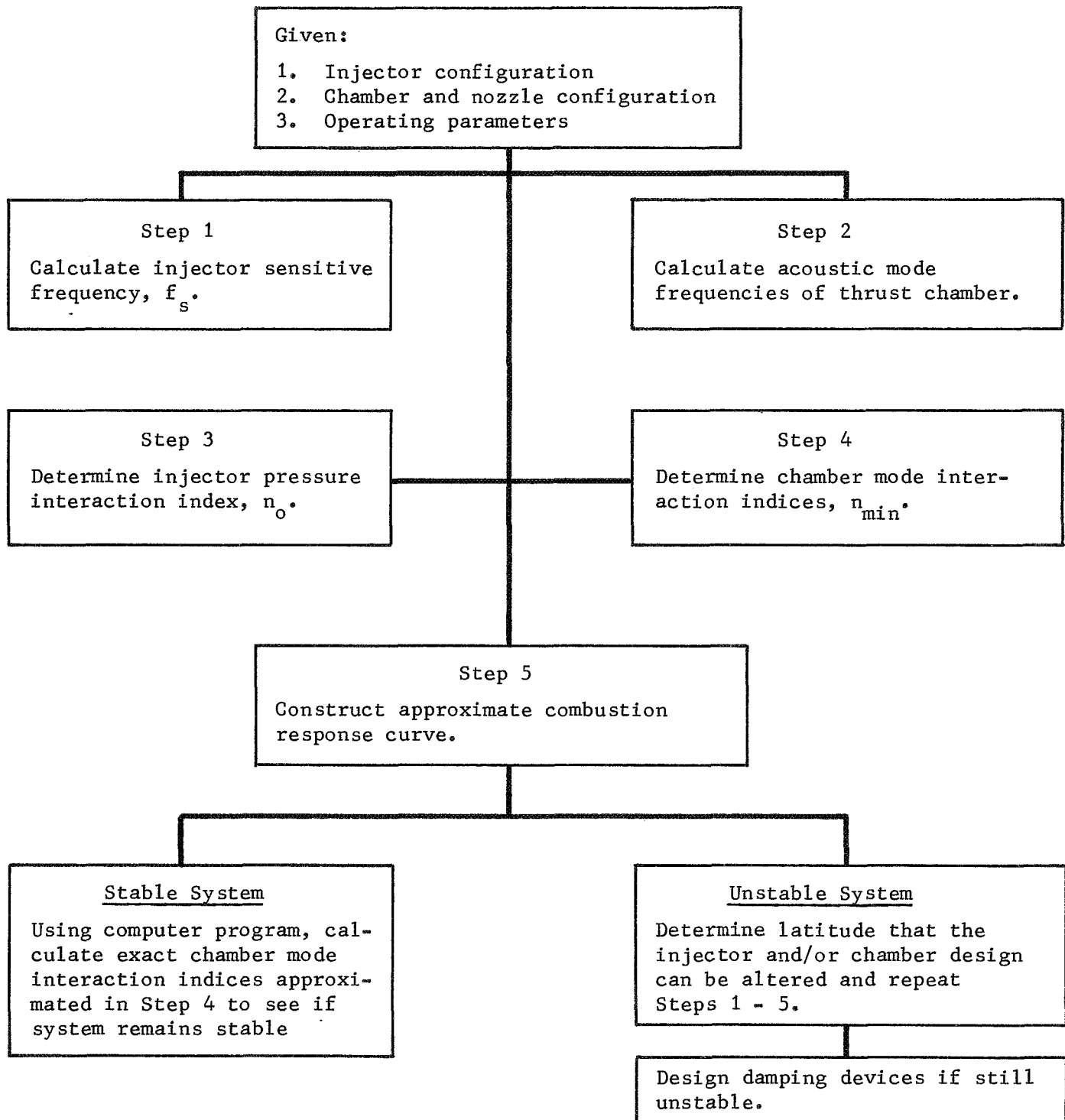


Figure 11 - Decision Diagram -- Evaluating Stability

3.3 ILLUSTRATIVE DESIGN PROBLEMS

Practical case studies are helpful to the designer by introducing problems which commonly occur during the development programs. In practice, the application of stability theory to design is best illustrated by three general cases:

- (1) Given the chamber and injector configurations and the flow parameters, determine the stability of the system.
- (2) Given the injector pattern and the operating conditions, assist in the selection of a chamber design.
- (3) Given the dimensions of the chamber and the design operating conditions, design a stable injector.

Decision diagrams describing the recommended approaches are shown in Figures 11, 12, and 15. An illustrative problem representing the various considerations facing the designer follows for each of the three cases.

3.3.1 Case I--Evaluating System Stability

The most frequent calculation required of the designer is the evaluation of the stability of the system with respect to the most prominent acoustic modes. This evaluation is necessary after designing a chamber or an injector with specific stability characteristics (Cases II and III) as well as when the design has been established previously and it is desired to know whether the system is inherently stable or whether additional damping is required.

The procedure divides into four steps:

Step 1. Calculate the injector sensitive frequency (f_g) for the given injector design utilizing the correct correlation equation and operating

3.3, Illustrative Design Problems (cont.)

conditions. Assume the injector pressure interaction index (n_o) = 0.60 (see Section 3.1) and plot the injector response curve.

Step 2. Calculate the various chamber modes which have frequencies in the region of the injector sensitive frequency. Depending upon whether the purpose is to give the designer a sense of the nature of his problem or whether he requires documentation for a design review, there are two approaches:

a. An approximate method disregarding combustion and using only the acoustic equations (hand calculations in Section 3.1).

b. A more rigorous method using the sensitive time lag computer program which considers combustion process along with the basic conservation equations (Section 4).

Step 3. Determine the combustion chamber response from Table 1 and draw the line N_{chamber} parallel to the abscissa or calculate the chamber response for each mode using the same computer program as in Step 2b.

Example 6: Evaluation of Stability

For purpose of illustration, let it be assumed that the system configuration and operating conditions are as follows:

Injector Design Parameters

- a. Coaxial element, centrally located oxidizer tube
- b. Oxidizer tube diameter = 0.15 in.
- c. Propellant velocity ratio = 6.0
- d. Propellant impingement angle = 20°
- e. Injector pressure interaction index (n_o) equals 0.6

3.3, Illustrative Design Problems (cont.)

Operating Parameters

- a. $\text{LO}_2/\text{hydrogen}$ propellants
- b. $\text{MR} = 5.0$
- c. $c = \text{acoustic velocity} = 5500 \text{ ft/sec}$
- d. Oxygen critical pressure (P_{crit}) = 730 psi
- e. Chamber pressure (P_c) = 300 psi
- f. Ratio of specific heats (γ) = 1.20

Chamber Design Parameters

- a. Chamber diameter = 14.0 in.
- b. Effective chamber length (ℓ_{eff}) = 9.0 in.
- c. Contraction ratio ($\frac{\text{area of chamber}}{\text{area of throat}}$) = 3.0
- d. No acoustic liners, baffles, or other damping techniques considered in the chamber

Step 1. Solve for Sensitive Frequency

$$(f_s) = 4550 \left(\frac{M_c}{d_{\text{ox}}} \right)^{0.15} \frac{(P_r)^{0.33}}{F(V.R. \sin\phi)} \quad \text{Eq 11 (Ref)}$$

where

M_c	=	Mach number	
d_{ox}	=	oxidizer diameter, in.	
P_r	=	critical pressure ratio	$\frac{P_c}{P_{\text{crit}}} = \frac{300}{730} \text{ or } 0.412$
$F(V.R. \sin\phi)$	=	functional relationship of the velocity ratio and the impingement angle (see Figure 5)	

3.3, Illustrative Design Problems (cont.)

$$M_c = \frac{A_{\text{throat}}}{A_{\text{chamber}}} \left(\frac{2}{\gamma+1} \right)^{\frac{\gamma+1}{2(\gamma-1)}} = 0.20$$

$$f_s = \frac{4550 \left(\frac{0.20}{0.15} \right)^{0.15} (0.412)^{0.33}}{1.03}$$

$$= 3440 \text{ Hz}$$

Step 2. Solve for the Acoustic Mode Frequency

From Section 3.1, the transverse and longitudinal chamber acoustic frequencies may be calculated from the following equations:

$$(\text{freq})_{\text{transverse modes}} = \frac{c S_{\nu\eta}}{2 \pi r_c}$$

where

a = acoustic velocity, ft/sec

r_c = chamber radius, ft

$S_{\nu\eta}$ = Bessel function argument (Table 3)

$$(f)_{\text{first tangential}} = \frac{5500(1.8413)}{2\pi (7.0/12)} = 2770 \text{ Hz}$$

$$(f)_{\text{second tangential}} = \frac{5500(3.0543)}{2\pi (7.0/12)} = 4600 \text{ Hz}$$

$$(f)_{\text{first radial}} = \frac{5500(3.8317)}{2\pi (7.0/12)} = 5760 \text{ Hz}$$

$$(\text{freq})_{\text{longitudinal modes}} = \frac{c S}{2 l_{\text{eff}}}$$

3.3, Illustrative Design Problems (cont.)

where S = order of longitudinal mode (1, 2, . . . n)
 eff = length of cylindrical portion of chamber plus 2/3 of the
 nozzle convergence length

$$(f)_{\text{first longitudinal}} = \frac{5500(1)}{2(9/12)} = 3660 \text{ Hz}$$

$$(f)_{\text{second longitudinal}} = \frac{5500(2)}{2(9/12)} = 7320 \text{ Hz}$$

$$(freq)_{\text{combined transverse longitudinal mode}} = (f)_{\text{transverse}}^2 + (f)_{\text{longitudinal}}^2$$

$$(freq)_{1T-1L} = \sqrt{(2770)^2 + (3660)^2}$$

$$(freq)_{1T-1L} = 4600 \text{ Hz}$$

The high order transverse, longitudinal or combined modes are disregarded since their frequencies would be considerably above the sensitive frequency and, consequently, would receive very little driving energy from the injection process.

Step 3. Plot Frequency Response Curve (Figure 4)

The plotting of the frequency response curve requires only supplying a sufficient number of arbitrary values for $\frac{f}{f_s}$ over the interval 0 to 2π to facilitate plotting the curve. It is most convenient to normalize all frequencies with respect to f_s , thereby eliminating the need to plot a new curve for each occasion. The following points shown in Table 5 are generally sufficient:

3.3, Illustrative Design Problems (cont.)

Table 5 -- Generalized Injector Response Tabulation

f/f_s	Radians	$\cos \pi \frac{f}{f_s}$	$1 - \cos \pi \frac{f}{f_s}$	N
0	0.0000	1.0000	0	0
0.25	0.7854	0.7071	0.2929	0.1757
0.5	1.5708	0.0000	1.0000	0.6000
0.75	2.3562	-0.7071	1.7071	1.0243
1.0	3.1416	-1.0000	2.0000	1.20-0
1.25	3.9270	-0.7071	1.7071	1.0243
1.5	4.7124	0.0000	1.0000	0.6000
1.75	5.4978	0.7071	0.2929	0.1757
2.0	6.2832	1.0000	0.0000	0.0000

Step 4. Plot Chamber Interaction Index

To use the approximate method, consult Table 1. The chamber response index for a cylindrical chamber with 3.0 contraction ratio utilizing LO_2/LH_2 is nominally 0.80. The horizontal line N_{chamber} crosses the frequency response curve at 0.61 and 1.39 frequency ratio, corresponding to chamber frequencies of 2100 Hz and 4780 Hz. The intervening zone is unstable. By inspection, therefore, it can be noted that the first (2770 Hz) and second (4700 Hz) tangential modes and the first longitudinal mode (3660 Hz) lie within the unstable zone. The first radial (5760 Hz) and second longitudinal (7320 Hz) are outside the unstable zone.

No corrective action is taken for the 1L mode because, as discussed previously in Section 3.1, this mode is highly damped by the nozzle losses and the distribution of combustion along the chamber axis.

3.3, Illustrative Design Problems (cont.)

For a design solution to the problem of the tangential modes using baffles, an illustrative case is presented in Section 5.1. Assuming the designer has followed this course, the chamber interior has been modified to incorporate radially oriented baffles extending into the chamber 3.5 inches beyond the interface between the injector and chamber.

3.3.2 Case II, Design of Combustion Chamber (Figure 12)

This situation arises when a high performing injector is available from previous development but the chamber design either is inadequate or must be adapted to a new application. In this case, the designer has some flexibility in selecting the chamber length and volume, contraction ratio, and nozzle contour. These selections will be strongly influenced by considerations of performance and compatibility; but for the present example, they will be assumed to be soluble within the framework required to assure stability.

The procedure involves the following steps:

Step 1. Calculate the injector response.

Step 2. Design the chamber/nozzle assembly using the following criteria:

- a. The acoustic modes of the chamber should have their frequencies displaced from the injector's sensitive frequency.
- b. The combustion chamber response should be maximized (i.e., N_{chamber} maximized).

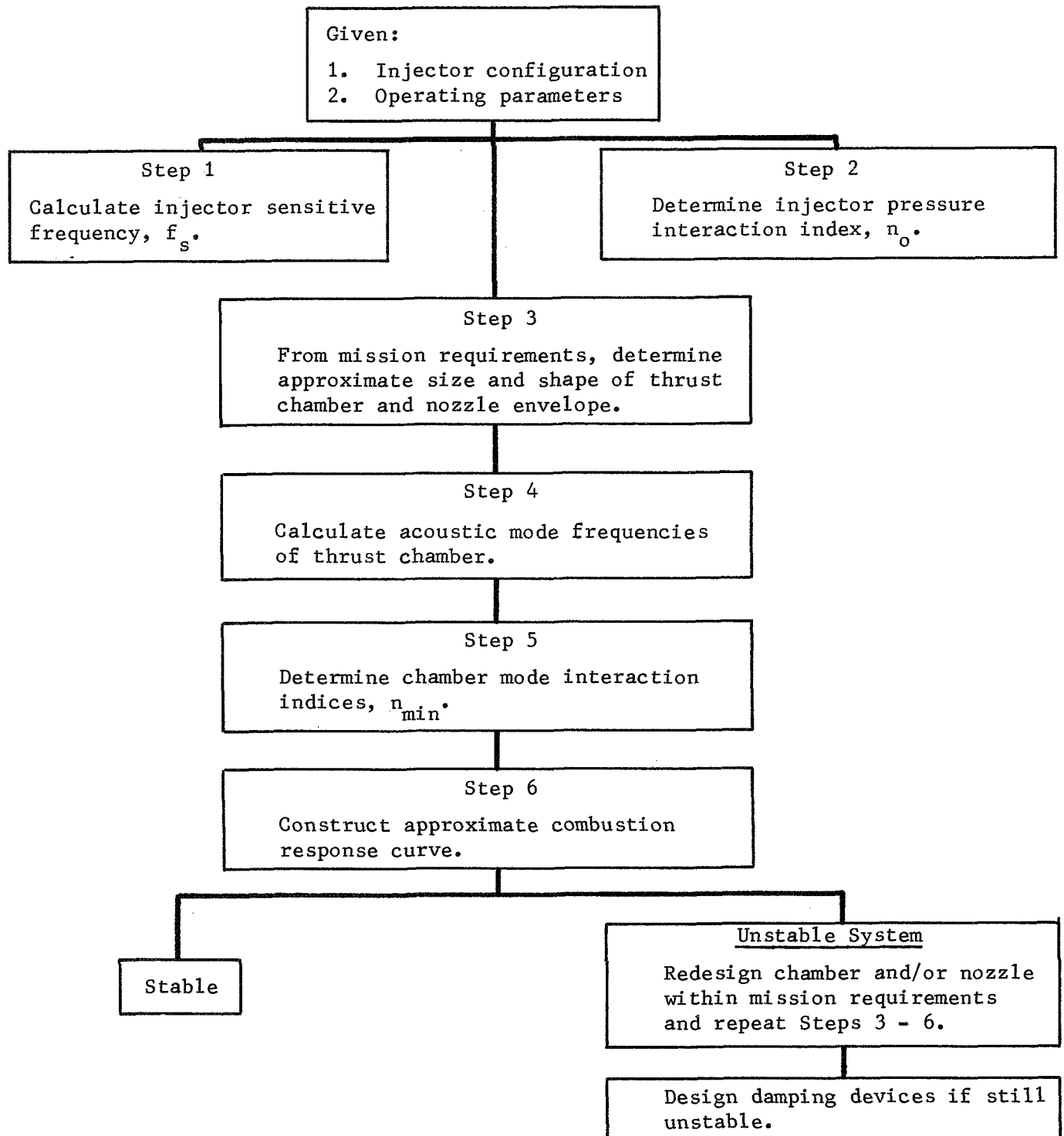


Figure 12 -- Decision Diagram -- Selecting Chamber Design

3.3, Illustrative Design Problems (cont.)

Example 7: Design of Combustion Chamber

For purposes of continuity as well as simplicity, it will be assumed that the same injector element will be employed as in Case I and, likewise, the operating conditions remain the same. For this example, the contraction ratio will be the major parameter investigated. Three values will be studied: 1.5, 3.0, and 4.5, which is a practical range of contraction ratios for the major engine systems. The engine for this design problem will be required to operate at a thrust of 15,000 pounds and a specific impulse of 375 seconds. The ratio of specific heats (γ) is assumed to be 1.20.

$$M_c = \frac{1}{\text{Contraction Ratio}} \left(\frac{2}{\gamma+1} \right)^{\frac{\gamma+1}{2(\gamma-1)}}$$

$$= \frac{1}{\text{C.R.}} (0.606) = 0.405 \text{ (C.R. = 1.5) and } 0.135 \text{ (C.R. = 4.5)}$$

The effect of these values on the sensitive frequency in the coaxial injector correlation equation (see Section 3.1) yields:

$$(M_c)^{0.15} = 0.87 \text{ (C.R. = 1.5) and } 0.74 \text{ (C.R. = 4.5)}$$

thus altering the sensitive frequency by approximately 15% over the range of contraction ratios of 1.5 to 4.5. Uncertainty about the contraction ratio therefore permits a variation of up to 15 percent in the sensitive frequency. This variation is small enough that a nominal value for contraction ratio of 3.0 can be assumed for a first trial, following the procedure described in Section 3.1.

$$f_s = 4550 \frac{M_c^{0.15} \times P_r}{d_o^{0.15} F (VR \sin \phi)} \quad \text{Eq 11 (Ref)}$$

$$= 3440 \text{ Hz, with a possible range from 3240 Hz to 3820 Hz.}$$

3.3, Illustrative Design Problems (cont.)

For the assumed injector response N_o of 0.6 (see Section 3.1), the frequency distribution curve calculated for Case I may also be used here.

Step 2. Design Chamber and Nozzle

From the design operating conditions

$$\dot{w}_t = \frac{F}{I_{sp}} = \frac{15000}{375} = 40 \text{ lb/sec}$$

$$A_t = \frac{c^* \dot{w}_t}{P_c g} = \frac{7600 \times 40}{300 \times 32.2} = 31.5 \text{ in.}^2$$

and (for cylindrical chambers)

$$d_t = \sqrt{\frac{4A}{\pi}} = 6.34$$

$$r_t = 3.17$$

Table 6 can now be constructed in which the frequencies of the primary chamber modes are calculated as single variable function of the contraction ratio. Chamber One ($A_c/A_t = 1.5$) has transverse modes which exceed the 3200 to 3650 Hz sensitive frequency range, but because of its length-to-diameter ratio low frequency longitudinal oscillations may be initiated. Chamber Two ($A_c/A_t = 3.0$) is potentially the least stable chamber with many frequencies close to the sensitive frequency range, with the higher order modes not shown on the table.

Longitudinal modes are seldom observed. This would lead to the selection of a contraction ratio of 1.5 as the most attractive design. Figure 13 shows the predicted stability characteristics of the selected injector

Table 6 -- Primary Response Frequency as Function of Chamber Design

Contraction Ratio	Throat Radius, in.	Chamber Radius, in.	L* (Minimum)	Effective Chamber Length	(1) f_{1T} , Hz	(2) f_{1L} , Hz	(3) f_{1R} , Hz	(4) f_{1T-1L} , Hz
1.5	3.17	4.75	35	23.30	4060	1430	8450	4325
3.0	3.17	9.50	35	11.65	2040	2830	4250	3490
4.5	3.17	14.25	35	7.75	1360	4250	2830	4460

$$(1) \quad f_{1T} = \frac{c}{2\pi} \frac{S}{r_c} \frac{\nu\eta}{c} \quad (c = 5500 \text{ ft/sec})$$

$$(2) \quad f_{1L} = \frac{c}{2} \frac{S}{\ell_{eff}} \frac{\nu\eta}{c}$$

$$(3) \quad f_{1R} = \frac{c}{2\pi} \frac{S}{r_c} \frac{\nu\eta}{c}$$

$$(4) \quad f_{1T-1L} = \sqrt{(f_{1T})^2 + (f_{1L})^2}$$

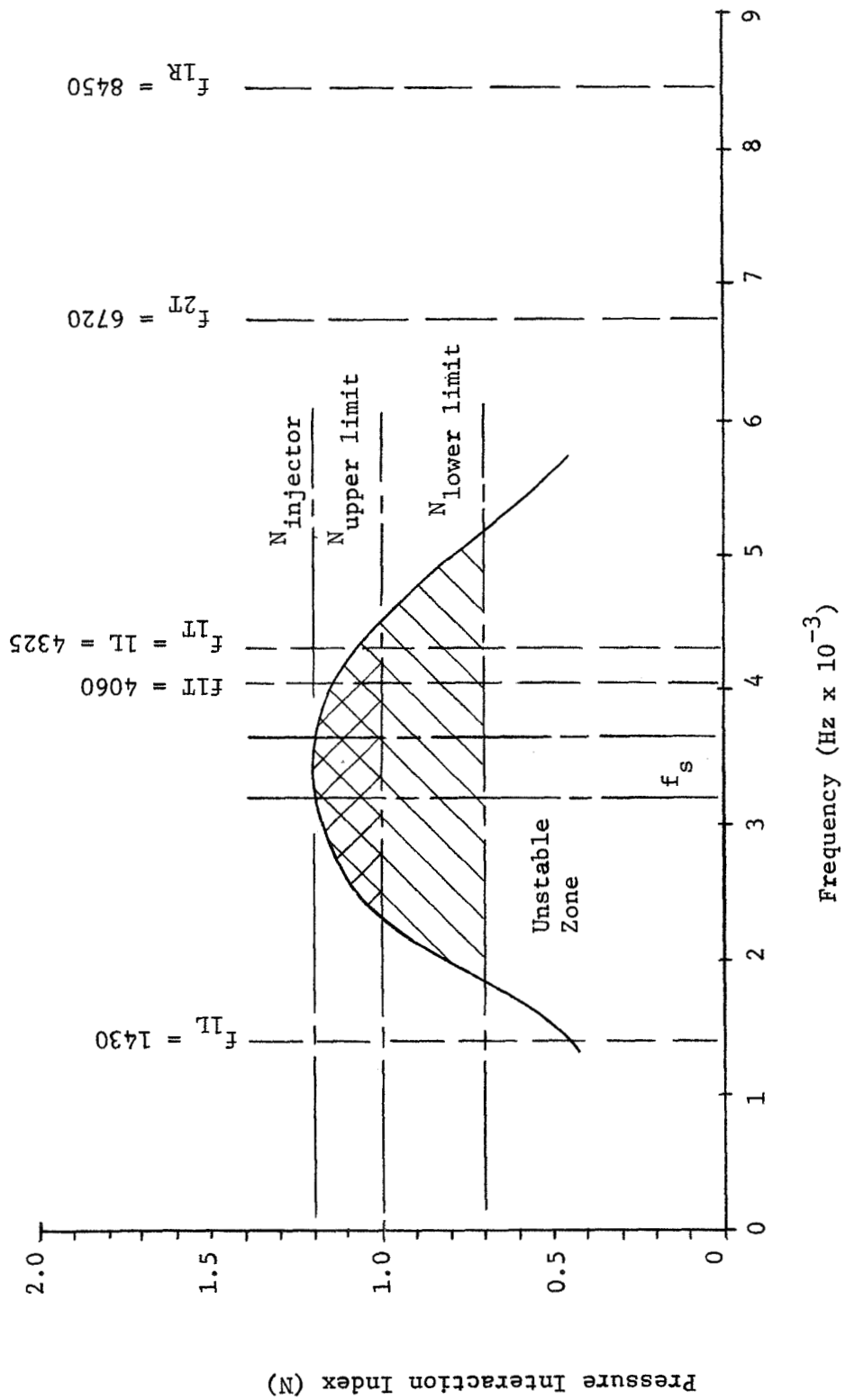


Figure 13 -- Predicted Stability Characteristics -- 1.5 Contraction Ratio

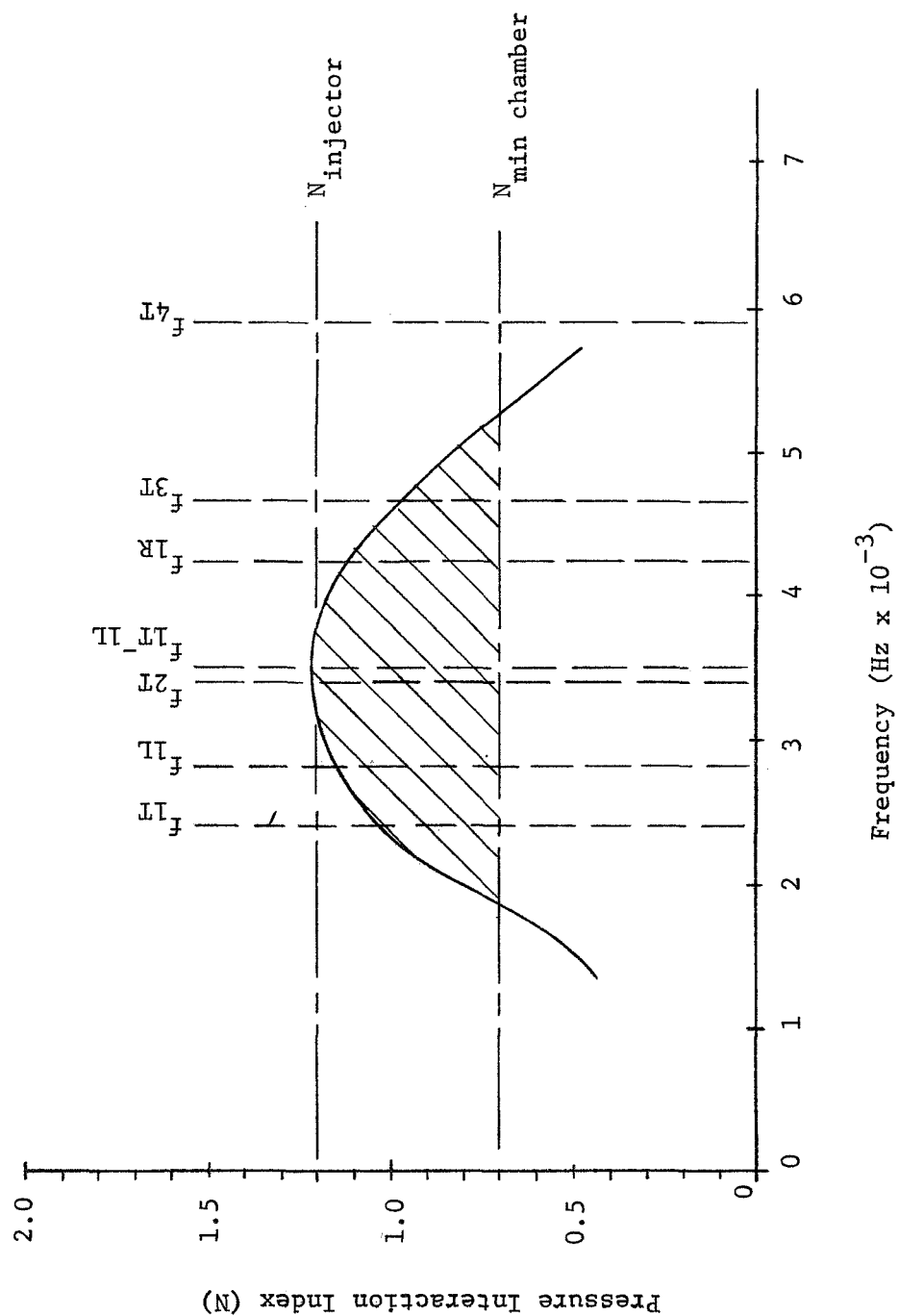


Figure 14 -- Predicted Stability Characteristics -- 3.0 Contraction Ratio

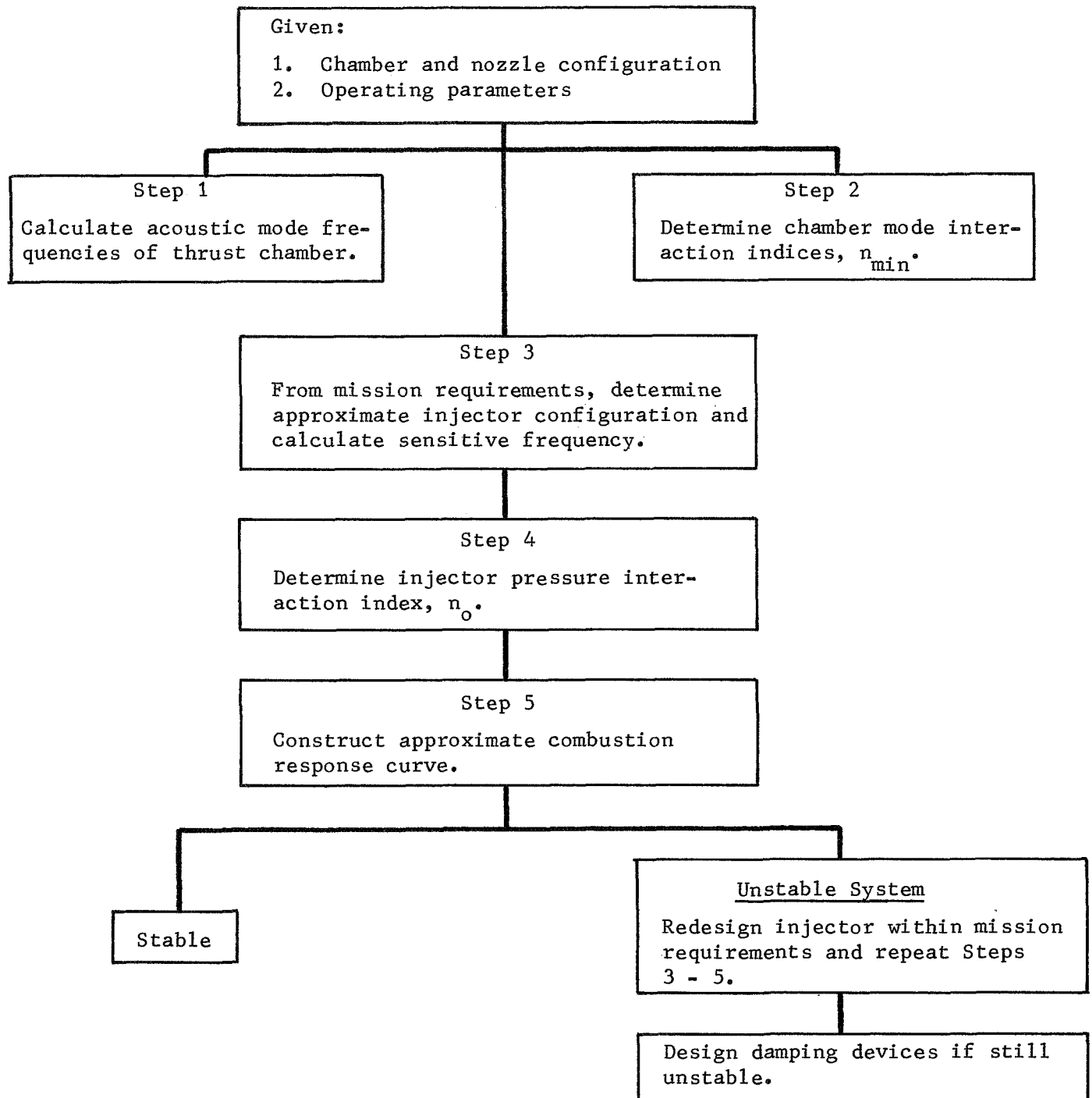


Figure 15 -- Decision Diagram -- Designing Stable Injector

3.3, Illustrative Design Problems (cont.)

in a chamber with a contraction ratio of 1.5. The value for N_{\min} of the chamber will, in most probability, be restricted to the nominal values shown in Table 1, Section 3.1; however, since values as low as 0.7 may be encountered with cylindrical chambers of large contraction ratios, the lower limit for the unstable zone is shown as that value. From Figure 13 two modes of instability other than the 1L mode may be identified as potential problems; these are the 1T and the 1T-1L modes. To illustrate the potential problems encountered by using a larger diameter - larger contraction ratio chamber, Figure 14 is included. Besides the six predicted problem modes of instability, additional combined modes may be included. The value of 0.7 as N_{\min} for the chamber is realistic in that the contraction ratio is becoming quite large.

Stabilization of the system presented in Figure 13 at a contraction ratio of 1.5 may be conveniently accomplished by using an acoustic liner which would have a minimum of interference with the injector pattern. Design principles for acoustic liners are elaborated in Section 5.2.

3.3.3 Case III, Design of Stable Injector (Figure 15)

This is the case that presents the most difficulties for the designer. Essentially, it is a matter of tradeoff between specified requirements for system performance and compatibility and the need for combustion stability in order to ensure safety and reliability. Usually this results in the introduction of damping devices.

The recommended procedure is as follows:

Step 1. Determine chamber acoustic mode frequencies.

Step 2. Write sensitive frequency equation for a selected type of injector and input all known parameters.

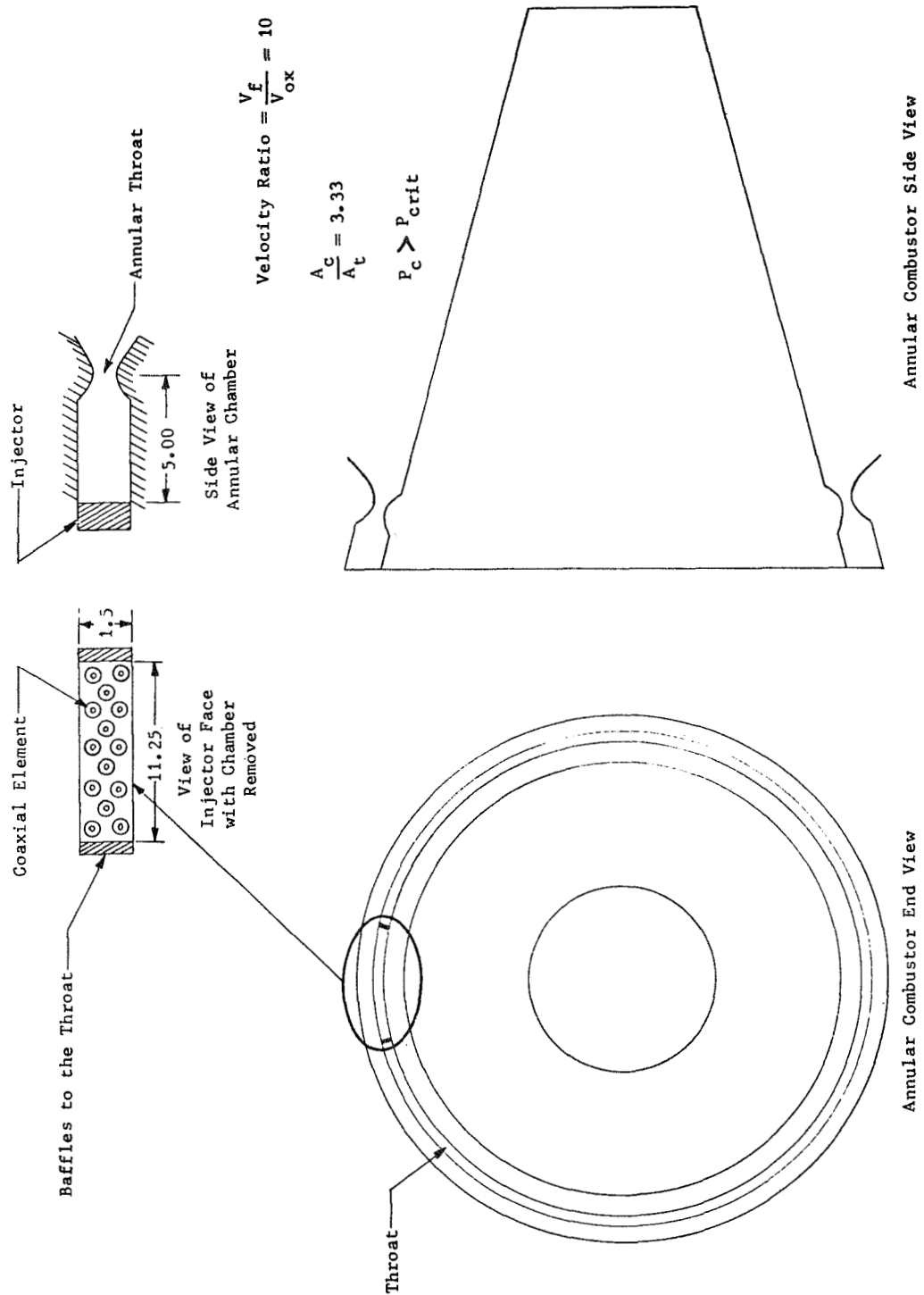


Figure 16 -- Annular Combustor

3.3, Illustrative Design Problems (cont.)

Step 3. Using an iterative technique, tabulate the sensitive frequency as a function of different orifice diameters and impingement angles. The orifices of the less volatile propellant are controlling. Other factors will limit the values associated with these two parameters, such as performance, L^* , design considerations, etc.

Step 4. Investigate injector pressure drops, propellant inlet velocities, and other injector hydraulic considerations to assure that these values meet reasonable design criteria limits.

Step 5. Compare the sensitive frequency value with the chamber acoustic mode frequencies to see if damping is required. Also at this step, it is possible to visualize the stabilizing or destabilizing effects of altering the various independent variables used in the sensitive frequency equation. When this frequency lies between the frequencies of two modes, it is possible to make design changes which will shift the sensitive frequency toward one mode and away from the other. Effective damping devices then need be designed for only one mode rather than two.

Step 6. Repeat Steps 2 through 5 with injectors of other types that appear feasible if design limitations permit.

The following illustrative example considers the case of an annular combustion chamber with a coaxial injector utilizing LO_2/LH_2 propellant. Given design conditions are shown on Figure 16.

3.3, Illustrative Design Problems (cont.)

Example 8: Design Stable Injector

Step 1. Calculate thrust chamber modes using acoustic theory.

$$f = \frac{c_o}{2\ell}$$

where: $c_o = 95\% (c_o)_{\text{theo}} = 0.95 (5300)$
 $= 5000 \text{ ft/sec}$

Injector Width (11.25 in. dimension)

$$f_{1T} = \frac{5000}{2 \left(\frac{11.25}{12} \right)} = 2670 \text{ Hz}$$

$$f_{2T} = 2 f_{1T} = 5340 \text{ Hz}$$

Injector Height (1.5 in.)

$$f_{1T} = \frac{5000}{2 \left(\frac{1.5}{12} \right)} = 20,000 \text{ Hz}$$

Chamber Axial Length (5.00 in.)

$$f_{1L} = \frac{5000}{2 \left(\frac{5.00}{12} \right)} = 6000 \text{ Hz}$$

Step 2. Write the sensitive frequency equation (f_s).

Input all known parameters and establish which parameters are variable and the limits of variation:

3.3, Illustrative Design Problems (cont.)

$$\text{Mach No.} = 0.182 \text{ from } A_c/A_t = 3.33 \text{ and } \gamma = 1.2$$

$$\text{Pr} = 1.0 \text{ since } P_c > P_{\text{crit}}$$

$$\text{VR} = 10.0$$

Therefore:

$$\begin{aligned} f_s &= \frac{4550 (0.182)^{0.15} (1.0)}{(d_{\text{ox}})^{0.15} F(10 \sin \phi)} \\ &= \frac{3520}{(d_{\text{ox}})^{0.15} F(10 \sin \phi)} \end{aligned}$$

Since values of $F(\text{VR} \sin \phi)$ attained from Figure 5 vary between 1.0 and 1.3, it may be noted that the sensitive frequency can be rewritten as:

$$f_s = \frac{3520}{(d_{\text{ox}})^{0.15} (1.0 \rightarrow 1.3)} = \frac{3520}{(d_{\text{ox}})^{0.15}} \rightarrow \frac{2700}{(d_{\text{ox}})^{0.15}}$$

In order for the sensitive frequency to be depressed below the frequency of the fundamental mode (2670 Hz) regardless of the $F(\text{VR} \sin \phi)$ value, the oxidizer diameter would have to be larger 1.0 in. This is not practical from a design viewpoint and a serious degradation of performance would be anticipated.

Since f_s must therefore lie above the fundamental frequency, a value will be chosen midway between the fundamental and first harmonic frequency (i.e., approximately 4000 Hz) and this value will be used as a starting point for the iteration process involving the oxidizer diameter and impingement angle.

3.3, Illustrative Design Problems (cont.)

Step 3. Tabulate the sensitive frequency for the acceptable range of oxidizer diameters (Table 7).

Table 7 -- Sensitive Frequency as Function of Oxidizer Orifice Diameter

d_{ox} , in.	$(d_{ox})^{0.15}$	Sensitive Frequency, f_s	
		$F(VR \sin \phi) = 1.0$	$F(VR \sin \phi) = 1.3$
0.040	0.617	5700	4400
0.050	0.648	5430	4182
0.060	0.656	5350	4130
0.070	0.671	5240	4040
0.080	0.685	5140	3953
0.090	0.697	5050	3888
0.100	0.708	4960	3830
0.110	0.718	4900	3770
0.120	0.728	4830	3723
0.140	0.745	4730	3638
0.175	0.770	4570	3520
0.200	0.785	4500	3450
0.250	0.812	4340	3340
0.500	0.903	3900	3000

Performance will require a minimum oxidizer diameter for completion of combustion in the 5.00-in. chamber length. It is assumed for this problem that an upper limit is set at 0.110 in. diameter based on performance considerations.

Since the sensitive frequency desired was around 4000 Hz (maximum distance from two modes), it may be noted from the table that the choice of $F(VR \sin \phi)$ should be closer to 1.3 than 1.0.

3.3, Illustrative Design Problems (cont.)

Step 4. Review other injector parameters.

Having established a value for $F(VR \sin \phi)$ and knowing the velocity ratio, the angle ϕ may be found from Figure 5.

$$VR \sin \phi = 5.5 \text{ or } 0.4$$

$$10 \sin \phi = 5.5 \text{ or } 0.4$$

$$\sin \phi = \frac{5.5}{10} \text{ or } \frac{0.4}{10}$$

$$\phi \approx 33^\circ \text{ or } 2^\circ$$

The 2° angle of impingement is essentially a "showerhead pattern" and would require a longer chamber for proper mixing and combustion to take place; therefore, only the 33° angle need be considered.

The final design consideration is the injector hydraulics--injection pressure drops, propellant injection absolute velocities, number of elements, etc. From the velocity ratio equation, the ratio of oxidizer to fuel area can be calculated:

$$VR = \frac{V_{\text{fuel}}}{V_{\text{ox}}} = \frac{\rho_{\text{ox}}}{\rho_{\text{fuel}}} \times \frac{A_{\text{ox}}}{A_{\text{fuel}}} \times \frac{\dot{w}_{\text{fuel}}}{\dot{w}_{\text{ox}}}$$

where $\rho_{\text{ox}} = 70 \text{ lb/ft}^3$
 $\rho_{\text{fuel}} = 1.3 \text{ lb/ft}^3$ (200°R and 1500 psi, assuming a 300 psi pressure drop across chamber)
 $\frac{\dot{w}_{\text{ox}}}{\dot{w}_{\text{fuel}}} = MR = 6.0$

$$VR = 10 = \frac{70}{1.3} \times \frac{A_{\text{ox}}}{A_{\text{fuel}}} \times \frac{1}{6}, \therefore \frac{A_{\text{ox}}}{A_{\text{fuel}}} = \frac{78}{70} = 1.11$$

3.3, Illustrative Design Problems (cont.)

Calculating the fuel area assuming an injector pressure drop of 300 psi and $C_D = 0.70$ yields:

$$A_{\text{fuel}} = \frac{\dot{w}_f = 4.6}{C_D (2g\rho\Delta P)^{1/2}} = 0.496 \text{ in.}^2$$

Consequently:

$$A_{\text{ox}} = 1.11 A_f = 0.55 \text{ in.}^2$$

The number of elements (n_e) required to attain this area with a 0.110-in. oxidizer orifice diameter is:

$$\begin{aligned} A_{\text{ox}} &= \frac{\pi}{4} (d_{\text{ox}})^2 (n_e) = 0.55 \\ n_e &= \frac{0.55}{0.785} \left[\frac{1}{d_{\text{ox}}} \right]^2 \\ &= 0.70 \left(\frac{1}{0.11} \right)^2 \\ &= 57 \text{ elements} \end{aligned}$$

The oxidizer velocity may be found from the continuity equation:

$$V_{\text{ox}} = \frac{w}{\rho A} = \frac{27.4}{70 \left(\frac{0.55}{144} \right)} = 103 \text{ ft/sec}$$

and the fuel injection velocity equals:

$$V_f = 10 V_{\text{ox}} = 1030 \text{ ft/sec}$$

3.3, Illustrative Design Problems (cont.)

The oxidizer pressure drop equals:

$$\Delta P_{ox} = \frac{(\dot{w}_{ox})^2}{(A_{ox} C_D)^2 (2g\rho)} = \frac{(27.4)^2}{(0.55 \times 0.7)^2 \frac{772}{1728} \times 70}$$

$$= 125 \text{ psi}$$

Step 5. An analysis can now be made using the sensitive frequency value (e.g., 3770 Hz for the case where $d_{ox} = 0.110$ in. and $F(VR \sin \phi) = 1.3$) and the first and second tangential mode frequencies (2670 and 5340 Hz, respectively).

The computer program should be run to obtain (1) the combustion response (pressure interaction index, n ,) and (2) the sensitive time lag, τ , or analogously its reciprocal frequency ($\tau = \frac{1}{2f}$) for each of the two transverse modes. The frequencies at N_{min} obtained from the computer program will be approximately equal to the acoustic mode frequencies calculated in Step 1. They will be more exact in that they are derived from a more complex set of equations which consider the combustion process which the acoustic equations do not. The interaction index will give the relative sensitivity of the two modes. It is possible for one mode to have a significantly smaller value for N_{min} which could cause the combustion to go unstable at that mode even though the injector sensitive frequency was chosen equal numerically to the frequency of the other mode. For this sample problem, both modes are assumed to have the same response ($N_{min} = 1.10$); consequently, an injector having its sensitive frequency midway between both mode frequencies could respond to either mode.

Prior experience with coaxial elements and information provided in previous sections of this report have shown values of n_o to be between 0.4 and 0.6. Choosing the higher value for the most conservative design will give a value of N as 1.2 ($N = 2 n_o$). This value, being larger than the N_{min} values

3.3, Illustrative Design Problems (cont.)

for the various modes ($N_{\min} = 1.08$), indicates that the system could be unstable or driven unstable. A graphical representation of the predicted injector response is given in Figure 17. The two curves shown are the two velocity ratios investigated. It is concluded from the response curve that the best design provides an oxidizer diameter of 0.110 in. and a velocity ratio of 10 [$F(VR \sin \phi) = 1.3$]. It may also be observed that the nearest potential instability modes are the first and second tangential modes. Since the propellants are hydrogen and oxygen, significant variation in velocity ratio might be experienced due to density variations in the hydrogen during transient portions of operation of the engine which would tend to increase the sensitive frequency and place it nearer the second tangential mode. Within the guidelines of this problem the optimum design has been selected and two potential problem stability modes identified (1T and 2T). Design changes for stability improvements may be evaluated by considering the effect of varying injection distribution as discussed in Section 3.2 and/or inclusion of stabilizing devices in the system as described in Section 5.

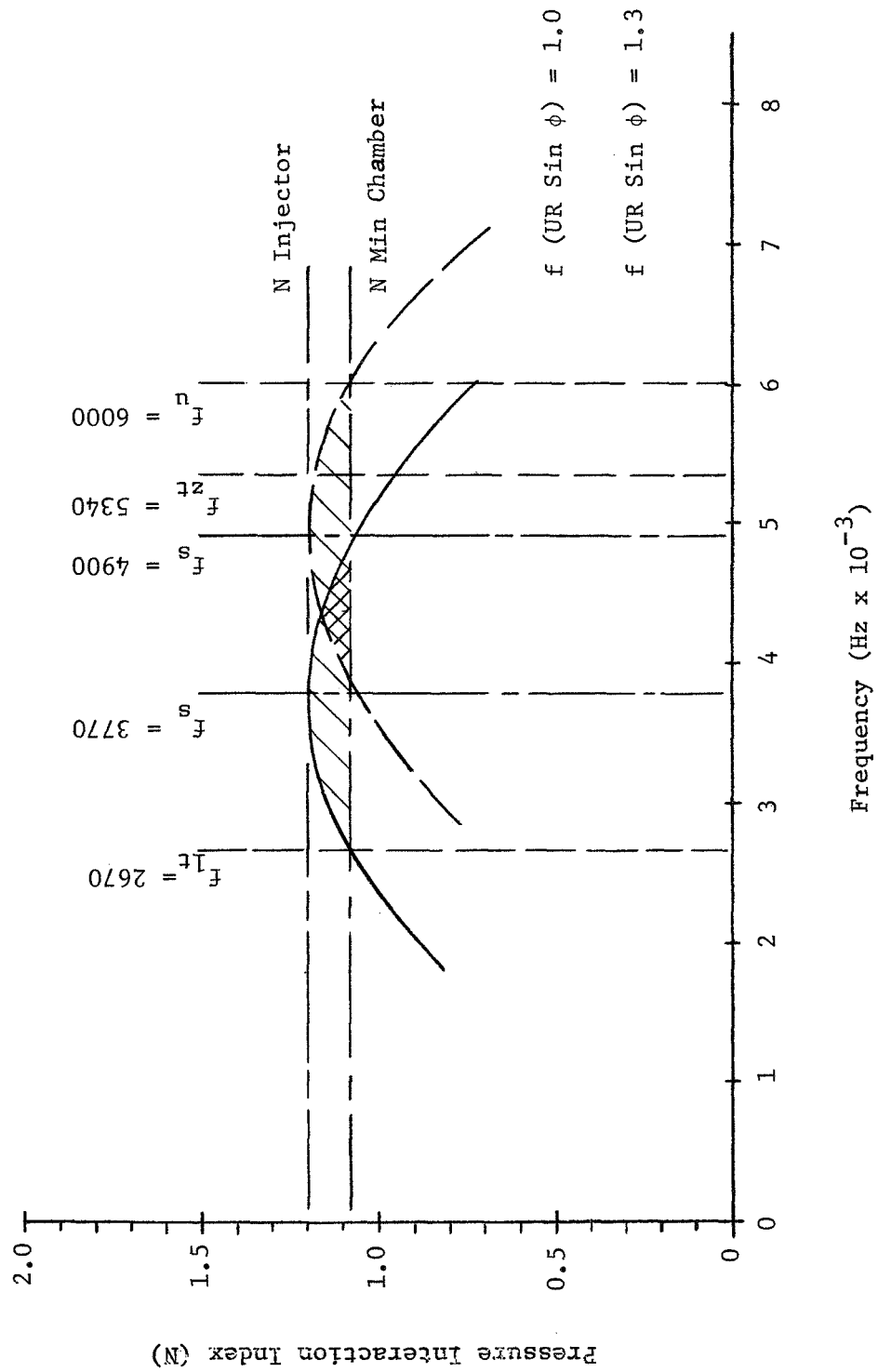


Figure 17 -- Effect of $F VR \sin \phi$ on Combustion Response

4. USE OF COMPUTER PROGRAMS

It is recommended that the designer resort to the use of one or more of the computer programs discussed in this section whenever the following situations arise:

- a) After the initial design calculations to confirm the results obtained by manual calculation and for increased accuracy.
- b) Multiple variable parametric studies are desired to evaluate the effect of trade-offs.
- c) Additional test data have been obtained
- d) Data are required for the design of stabilizers.

Best results will be obtained from a judicious mixture of manual calculation with the use of computer printouts. To illustrate how the designer may use the programs to best advantage several illustrative design problems are furnished in Section 4.3.

4.1 DESCRIPTION OF COMPUTER PROGRAM

The stability solution for any given liquid rocket engine must consider the three main components: (1) the injector, (2) the combustion chamber, and (3) the exhaust nozzle. Furthermore, oscillatory conditions can exist in both the longitudinal and the transverse (i.e., tangential and radial) directions. These considerations serve as the basis for building the computer program.

4.1, Description of Computer Program (cont.)

The complete program consists of nine separate subprograms which may be used independently or in various combinations depending upon the data available and the information required by the designer. Figure 18 shows the interrelationships of the programs and the optional routes for proceeding with the calculation. The individual programs are:

- A. Longitudinal Mode Chamber Analysis, used to obtain η , τ stability mapping for longitudinal modes.
- B. Transverse Mode Chamber Analysis. For simplicity only the analysis is performed; the η , τ mapping is done later in Program F.
- C. Nozzle Admittance. Here the resistive effects of the nozzle are calculated for both longitudinal and transverse modes.
- D. Expansion of results from Program B by interpolation.
- E. Injector Nonuniformity Coefficients. This subprogram calculates the modulating coefficients for the effects resulting from uneven injection distribution and nonlinear combustion response.
- F. Stability Mapping (η , τ) for Transverse Modes.
- G. (Not in use.)
- H. High Combustion Chamber Mach Number Analysis. (Not operational.)
- I. Nonlinear Combustion Response. Input to Program E.
- J. Injected Mass Distribution Effects

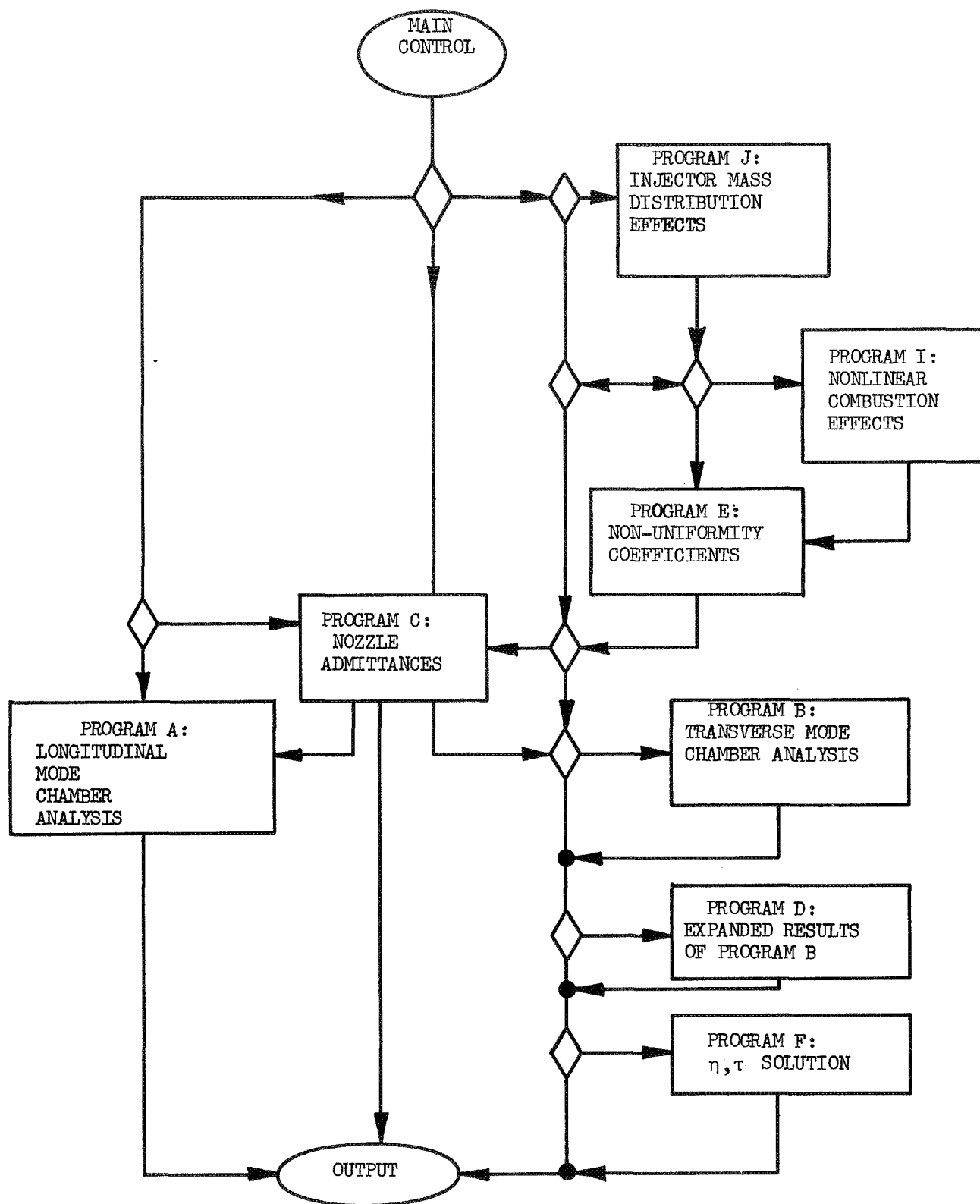


Figure 18 -- General Flow Diagram of the Computer Program

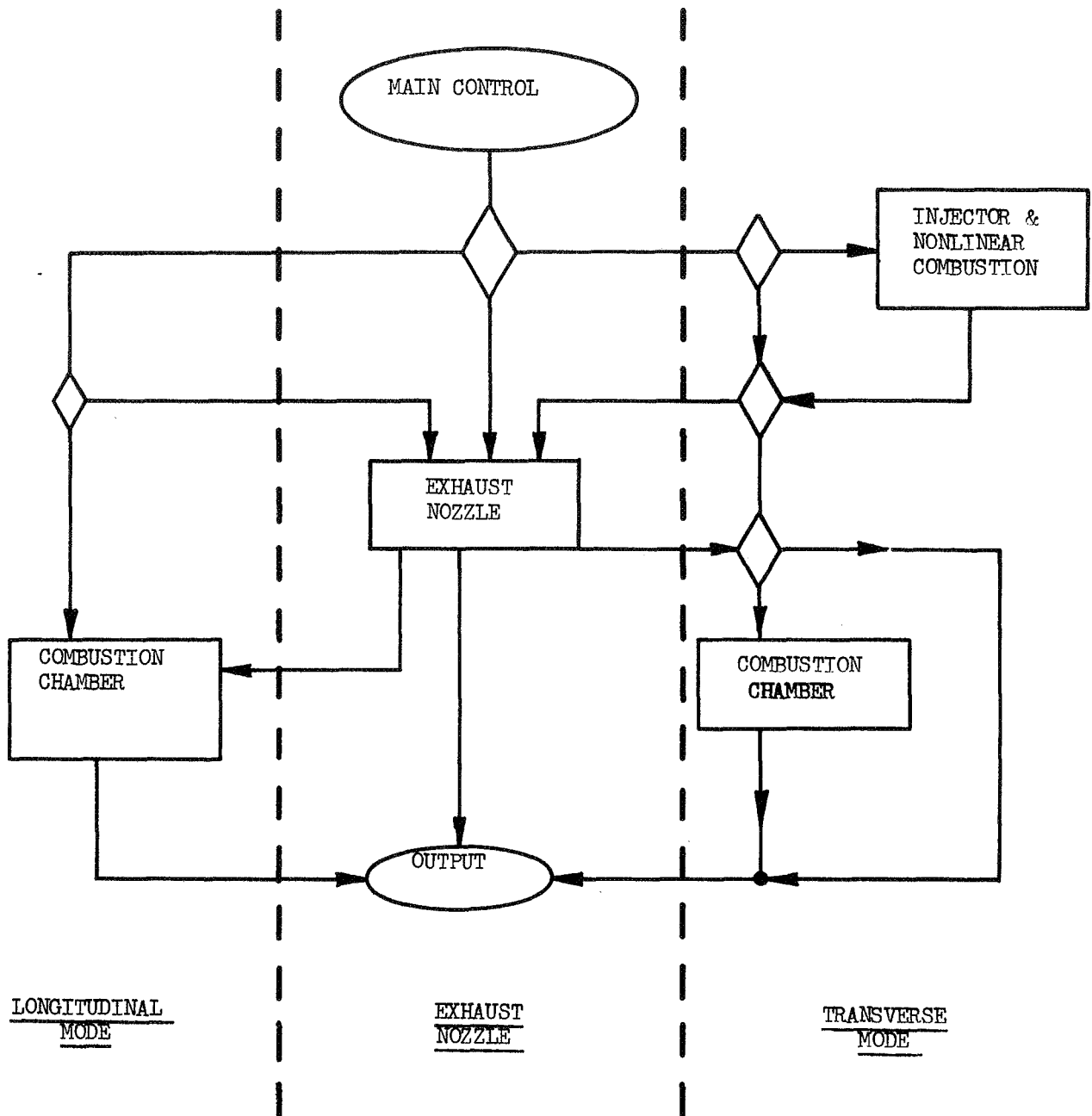


Figure 19 -- Overall Schematic of Computer Program

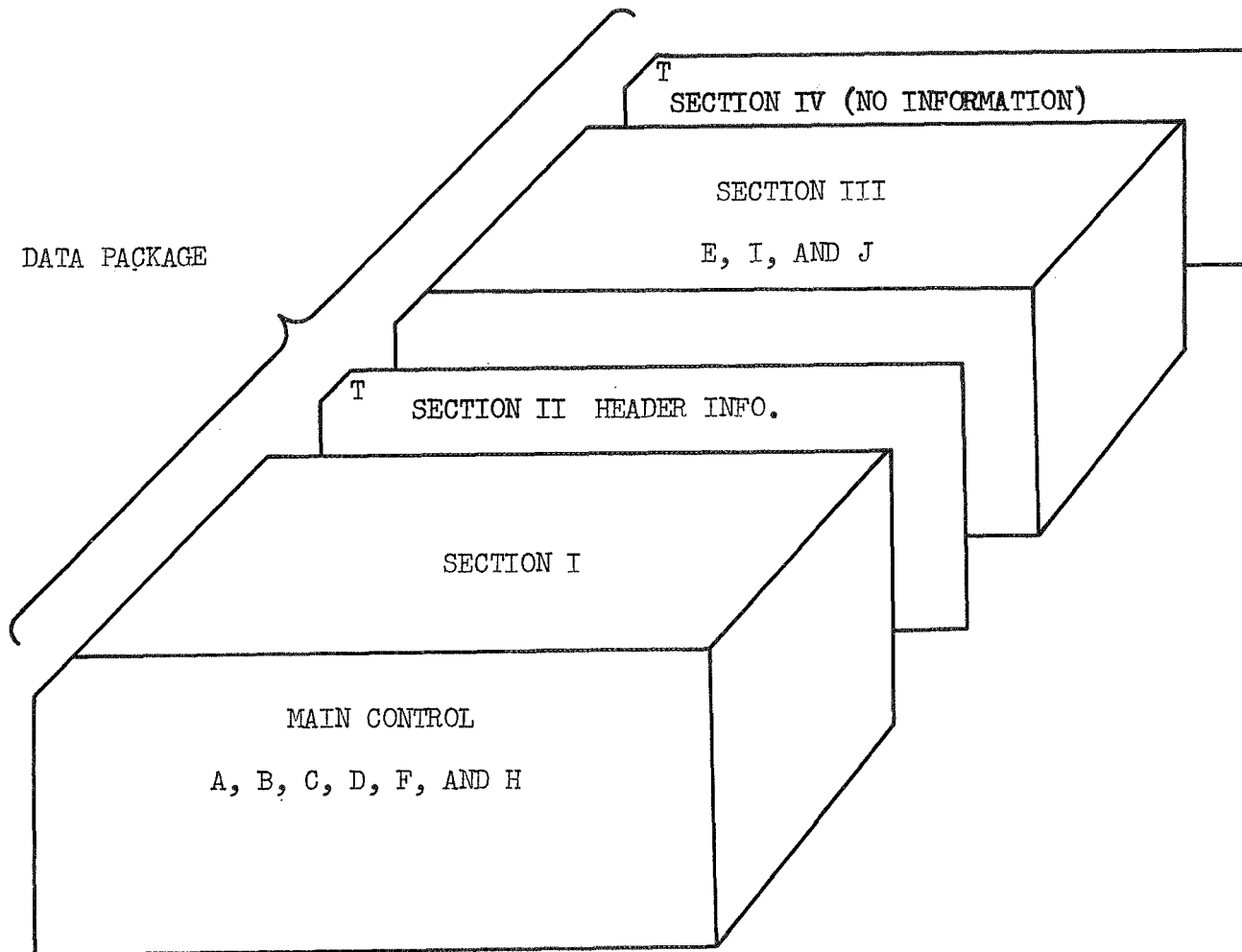
4.1, Description of Computer Program (cont.)

To assure that the proper subprograms are requested it is necessary to introduce a regulatory device that monitors the course of the entire program as it proceeds from one portion of the engine to another. This regulatory device is called MAIN CONTROL and serves to direct the flow of the solution in a consistent manner. Figure 18 illustrates the basic framework of the computer program. The diamond-shaped symbols can be considered as switches that are turned on if the particular item is to be analyzed by the program or turned off if the item is not needed. It is the function of MAIN CONTROL to turn these switches on or off according to the dictates of the problem.

It can be seen in Figure 19 that the program is divided into 3 parts: (1) longitudinal modes, (2) transverse modes, and (3) exhaust nozzle. The exhaust nozzle portion has been carried over from the program's early development when nozzle parametric studies were conducted.

The versatility of the program is illustrated in Figure 18 by the various flow-paths that can be constructed. For example, if the required injector and nozzle data were known before hand, one could determine the transverse stability of the engine by merely running the combustion chamber program. If, on the other hand, all the data were unknown, proper use of MAIN CONTROL would initiate the injector, nozzle, and chamber programs. Therefore, the program is as suitable for parametric studies as it is for analysis of specific designs.

It can be seen that the transverse portion of the program is more detailed than the longitudinal portion. Programs, J, I, and E are required to evaluate the injector parameters that affect stability. The chamber analysis requires Programs B, D, and F. It should be noted that Program D is more of a convenience than a necessity while Program F determines the solution of η and τ .



IF SECTION III IS NOT USED, SECTION IV MUST NOT BE USED.

Figure 20 -- Input Load Sequence Required by the Computer Program

4, Use of Computer Programs (cont.)

4.2 OPERATING THE PROGRAM

It is necessary to discuss the general organization of the data as well as how the data actually get into the computer before proceeding to further discussion of the computer program. The input data deck will always be referred to as a set of data packages.

Assembling the Data Package

The manner in which the data deck is assembled is shown in Figure 20. It can be seen that the data package (one package required per case), is divided into four sections. The first section contains the data for MAIN CONTROL and Programs A, B, C, D, F, and H. The second section is one card that has the letter T punched in card column one. This card serves the purpose of an end-data signal and of a header card such that all information that follows the T will be printed on the top of each output page. The third section contains the data for Programs E, I, and J. The fourth section is a T-card that is used only to signal the end of data.

It should be noted that if neither Programs E, I nor J are run, Sections III and IV are not needed. However, Sections I and II must always be in the data package.

Running Multiple Cases

The flexibility of the program is such that stacking cases (i.e., running multiple cases) is an easy task. All that is required is to add the required number of data packages to the data deck. There is no restriction as to the flow paths of individual data packages; therefore, data packages

4.2, Operating the Program (cont.)

of parametric studies involving the use of one program can be intermingled with data packages that use any of the other program combinations for an analysis.

Getting the Data onto the Card

Inputting of the data is accomplished in a flexible fashion called "scatter load." This method has a minimum number of restrictions as to how and in what manner the data are punched on the card. Examples are given below that will illustrate the flexibility of scatter load.

Load and Terminal Flags

The letter T or the letter L must be punched on each card. The L signals the computer that there are data on the card whereas the T signifies that the computer has received all of the data for that section of the data package.

Data Input

Immediately after the L will appear one to four numbers; therefore, the card thus far has been punched with L followed by 4 digits, e.g., L4175. This tells the computer to start loading the data that will follow into computer core starting at Location 4175. Following this number will be a plus or minus sign and data, another plus or minus sign and additional data, etc. Since the signs serve to separate the data, the second data point will automatically be loaded into core location 4176. This process continues across the first 72 locations of the data card.

4.2, Operating the Program (cont.)

Consider the following example of input data:

L0 + 10.0
L1 + 19.4
L2 + 0.0
L3 - 0.92
L8 + 6.4

This may be punched on a single card as

(Example 1) L0 + 10.0 + 19.4 + 0.0 - 0.92 L8 + 6.4
(Example 2) L0 + 1000 + 19.4 + -0.92 + + + + + 6.4
(Example 3) L8 + 6.4 L0 + 10.0 + 19.4 + -0.92
(Example 4) L39 + 0.21 + 3.14 + 5.0 + 1.5 -35.5 L39 + 1545.

Example 1 illustrates a normal load sequence for the given input. No data are transferred into core locations L4 through L7; therefore, any previous data stored there remains there. Example 2 illustrates how algebraic signs can be used alternatively to index the data to the proper core location. Note also the L2, which is zero, has no number punched on the card. This illustrates that the computer, when it sees no number following the sign, loads the value of zero into that core location. If data have been previously stored in Locations L4 and L8 and are to be used again, the use of indexing presented in Example 2 will load zeros into those core locations; consequently, the data will be lost.

Example 3 illustrates that the L-numbers do not have to be punched in sequential order. Example 4 illustrates the method of correcting data. Specifically, L39 was initially loaded with 0.21 and later loaded with 1545.0; therefore, the former number is erased on core and the latter included in its

4.2, Operating the Program (cont.)

place. The most convenient method for correcting data cards is to punch all the corrections on one or more cards and place these cards immediately before the T-card of that data section.

Presented below are some basic rules to employ when punching data cards:

1. DO start each input card with L. The L does not have to be punched in card column 1 but it must appear before any data.
2. DO pay close attention to the sequence of the remaining data included on the card so that data are not loaded into the wrong core location.
3. DO NOT use more than 8 significant digits (including decimal point) for the input data. Exponential notation is permitted. That is, the number 0.0625 can be loaded as 6.25 E-02 (where E is the base 10 and -02 denotes the exponent).
4. DO NOT start the data on one card and complete it on another.
5. DO NOT use more than 72 card columns for data input. The computer looks at 73 to 80 but does not transfer that information to core. Therefore, columns 73 and 80 can be used for the card sequence number in the data deck or identification of some significant aspect of the data so that it can be identified at some later date.
6. DO include a T-card at the end of a data section in the data package. The T must be punched in card column 1. If the T appears anywhere else on the card, the computer will dump the entire run.

4.2, Operating the Program (cont.)

7. DO include a description of the case on the T-card of Section 2. This information serves as a header for each output page. This is a convenience more than a necessity.

8. DO NOT use two or more T-cards for a header. This can confuse the computer's input logic.

Thus far the storage locations for the individual data bits have not been noted. It is sufficient here to note that the input data have reserved locations in core and that these data remain in those locations unless over-written by the next set of input data. Therefore, it is not necessary to input all the data on the next run if only one parameter (e.g., the ratio of the specific heats) is to be changed. Only those data which change from one case to the next need be input in successive data packages.

Operation of MAIN CONTROL

Since the computer obeys every command explicitly, it is necessary to indicate correctly to the computer the programs that are desired for a particular case. Furthermore, this must be done for every case because the computer will turn off the switch that activated the subprogram after it is through with that program. This is done purposely to avoid using a program that is not needed for the second case.

The first 10 core locations are reserved for MAIN CONTROL in the following order:

4.2, Operating the Program (cont.)

- L0: Program A, Longitudinal Mode Chamber Analysis and Stability Zones
- L1: Program B, Transverse Mode Chamber Analysis
- L2: Program C, Exhaust Nozzle Admittance Coefficients for Longitudinal and Transverse Modes
- L3: Program D, Expansion of Results from Program B
- L4: Program E, Injector Nonuniformity Coefficients
- L5: Program F, Final Solution of Instability Zones
- L6: Program G, (not used in this package)
- L7: Program H, High Combustion Chamber Mach Number Analysis
- L8: Program I, Nonlinear Combustion Response Analysis
- L9: Program J, Injected Mass Distribution Effects

A zero value (except Program H which requires a negative value) in any of the locations indicates that this program will not be used. Any number greater than zero instructs the computer to execute this subprogram at the time it is required. The program instructions determine when to execute the subprogram and the number in the proper place tells the computer whether or not to execute the program.

Program Options

Most subprograms have various options concerning the desired output to be printed. These options are exercised by the same control number that executes the program and are keyed by the magnitude of the number. These print options are presented in the discussion of the individual programs. However, a few examples are presented here to illustrate this point:

4.2, Operating the Program (cont.)

EXAMPLE 1: EXECUTE PROGRAM C - PRINT NO OUTPUT

LO + + + 9.0 + + + + + + + (0 < L2 ≤ 9.0)

EXAMPLE 2: EXECUTE PROGRAM C - PRINT OUTPUT

LO + + + 99.0 + + + + + + + (10 < L2 ≤ 99.0)

EXAMPLE 3: EXECUTE PROGRAM C - PRINT INPUT AND OUTPUT

LO + + + 99.0 + + + + + + + (100 < L2 ≤ 199.0)

Determination of Design Criteria

Table 8 shows the program combinations that are required to obtain stability maps for the longitudinal and transverse modes and to make certain parameter studies.

Table 8 -- Program Combinations for Design Criteria

Desired Output	Critical Data Requirements		Required Programs
η , τ Map for Longitudinal Modes	Nozzle Admittance Coefficient, A	Known Not known	A A,C
	Nozzle Admittance Coefficients, A,B,C	A,B,C known One not known	B,F B,C,F
	Non uniformity Coefficients, $A_{\nu\eta}$, $B_{\nu\eta}$, $C_{\nu\eta}$	All known One not known	B,F B,E,F
	Chamber Mach number	> 0.1 ≤ 0.1	B,F,H B,F
Parameter Studies	Number of Data Points	10 Sufficient More than 10 required	B,F B,D,F
	Nozzle Effects		C
	Variation of Nonuniformity Effects with Respect to Mass Distribution		J,E
	Variation of Nonuniformity Effects with Respect to Nonlinear Combustion Response		I,E
	Variation of Stability Zones with Respect to Nozzle Effects		A, C or B,C,D,F
	Variation of Stability Zones with Respect to Nonuniformity Coefficients		B,D,E,F

Report 20672-P2D

PROGRAM INDEX

<u>Program</u>		<u>Page</u>
A	Longitudinal Mode Chamber Analysis and Instability Zones	91
B	Transverse Mode Chamber Analysis	94
C	Exhaust Nozzle Admittance Coefficients for Longitudinal and Transverse Modes	97
D	Expansion of Results from Program B	104
E	Injector Nonuniformity Coefficients	106
F	Final Solution of Instability Zones	109
G	(Obsolete and deleted from the listing)	111
H	High Combustion Chamber Mach Number Analysis	111
I	Nonlinear Combustion Response	111
J	Injected Mass Distribution Effects	113

4.2, Operating the Program (cont.)

Program A: Longitudinal Mode Chamber Analysis and Instability Zones

a. Input Requirements

<u>Core Location</u>	<u>Mnemonic</u>	<u>Description</u>
L0	-	Execute Program A. Magnitude of number depends upon print options given below.
L10	γ	Ratio of the specific heats.
L11	\bar{u}_e	Steady state Mach number at the entrance to the exhaust nozzle. This can be determined by the contraction ratio or by Program C. In the latter case, leave L11 blank.
L13	r_c	Chamber radius, in. also loaded in L3804, Program G.
L14	L_c	Length of cylindrical portion of chamber, in.
L15	c_o	Speed of sound in the chamber, ft/sec
L16	\bar{u}_{L0}	Weighted liquid injection velocity, ft/sec See Equation (18) at the end of this section.
L17	k	Gas/liquid momentum interchange coefficient. ($k = 0$ for no droplet momentum effects)
L20	$S_{v\eta}$	Set equal to zero.
L21	$N_{\omega c}$	Number of chamber frequencies to be used. Leaving this column blank will turn on Program GENMEC which will select 10 frequencies according to the relationship given by Equation (19).
L22 : : : : L49	ω_c	Table of nondimensional, chamber frequencies arranged in ascending order. A zero must be included at the end of the table. The maximum number of frequencies is 28 (including the zero point). This is left blank if L21 is blank.

4.2, Operating the Program (cont.)

<u>Core Location</u>	<u>Mnemonic</u>	<u>Description</u>
L50 : : L69	L_z	Table of ascending axial positions at which the combustion distribution (i.e., the variation of the local Mach number with respect to Z) is known. Dimensioned in inches. A zero value must appear at the last point. Minimum of four real data points is required.
L70 : : L89	\bar{U}_x	The local steady state Mach number that corresponds to the given L_z . A zero <u>must</u> appear as the last value.
L600 : : L629	$\omega_{c,\alpha}$	The ascending table of chamber frequencies for which the longitudinal, real and imaginary parts of the nozzle admittance coefficients (to be input next) are known. If Program C is run to determine the admittances, these frequencies will be automatically transferred. The last point in the table <u>must</u> be zero.
630 : : 659	A_r	The real part of the admittances corresponding the above frequencies. The last point in the table <u>must</u> be zero. These can be determined by running Program C.
L660 : : L689	A_i	The imaginary part of the admittances corresponding to the above frequencies. The last point in the table <u>must</u> be zero. These can be determined by running Program C.

b. Print Options

There are no print options available with this program. Any LO number greater than zero will cause a program execution as well as an output of the input data and the results of the program.

4.2, Operating the Program (cont.)

c. Placement of the Data into the Data Package

These data maybe inserted anywhere in Section I of the data package.

d. Output

The following output results from the efforts of this program:

- f, the longitudinal chamber frequency for the given value of ω , cps
- ω , the nondimensional value of the chamber frequency
- τ , the sensitive time lag, millisec
- η , the pressure interaction index

e. Auxiliary Equations

(1) Axial Liquid Velocity (Weighted)

$$\bar{U}_{LO} = \frac{(MR)v_x \cos \theta_x + v_F \cos \theta_F}{MR+1}, \text{ ft/sec} \quad \text{Eq. 18}$$

$$MR = \text{mixture ratio} = \dot{w}_x / \dot{w}_F$$

$$v_x = \text{oxidizer injection velocity, ft/sec}$$

$$v_F = \text{fuel injection velocity, ft/sec}$$

$$\theta_{x,F} = \text{oxidizer and fuel impingement angle}$$

4.2, Operating the Program (cont.)

(2) Selection of Frequencies by GENMEG

$$(\text{First Longitudinal}) = (1 \pm 0.10) \pi \quad \text{Eq. 19}$$

$$(\text{Transverse}) = (1 \pm 0.10) S_{v\eta}$$

where

π = 3.14159 + = resonant frequency (non-dimensional) for longitudinal modes

$S_{v\eta}$ = transverse acoustic mode number given in the Program B writeup. (Table 3, Section 3.1)

f. Other Information

In order to run higher order longitudinal modes the frequencies must be input using core locations L21, L22 ... L49.

This program is specifically concerned with concentrated combustion located at position xx in the chamber. Therefore, this program converts the general combustion distribution profile to a concentrated profile.

Program B: Transverse Mode Chamber Analysis

a. Input Requirements

<u>Core Location</u>	<u>Mnemonic</u>	<u>Description</u>
L1	-	Execute Program B. Magnitude of number depends on print options given in Paragraph b.
L20	$S_{v\eta}$	Transverse acoustic mode number is given in Table 3 for various modes.

4.2, Operating the Program (cont.)

<u>Core Location</u>	<u>Mnemonic</u>	<u>Description</u>
L10 : L89		These are identical to Program A except L19 is not needed. Refer to the writeup of Program A for these requirements.
L3017	N_{ω}	The number of input frequencies at which the transverse nozzle admittance coefficients are known. This number must be greater than 2 and less than 30. If the admittance for a nozzle is unknown and Program C is run, C will provide this number.
L3019 : L3048	$\omega_{c,e}$	The values of the chamber frequencies, arranged in ascending order, for which the transverse admittances are known. Program C will provide them if it is run. The last value must be zero.
L3049 : L3078	E_R	The values of the real part of the transverse nozzle admittance coefficient. The last value must be zero. Program C will supply these values.
L3079 : L3108	E_i	The values of the imaginary part of the transverse nozzle admittance coefficient. The last value <u>must</u> be zero. Program C will supply these values.
L3109 : L3138	C_R	The values of the real part of the third transverse nozzle admittance coefficient. This is needed only for high Mach number chambers. The last value must be zero. Program C will supply these values.
L3139 : L3168	C_i	The values of the imaginary part of the third transverse nozzle admittance coefficient. This is needed only for high Mach number chambers. The last value must be zero. Program C will supply these values.

b. Print Options

$0 < L1 \leq 9$: Execute B, do not print input or output

$10 \leq L1 \leq 99$: Execute B, print output

4.2, Operating the Program (cont.)

100 \leq L1 \leq 199: Execute B, print input and output
(recommended)

200 \leq L1 \leq 299: Execute B, print input and output,
print steady state tables and values
of integrals associated with high
Mach number cases.

c. Placement of the Data into the Data Package

These data may be inserted anywhere in Section I of the data
package.

d. Output

The following output results from this program:

ω : nondimensional chamber frequencies

$h_R(\omega)$: the real part (damping effects) of the
chamber admittance in the chamber

$h_i(\omega)$: the imaginary part of the chamber
admittance

e. Tabulation of Transverse Acoustic Mode Number ($S_{v\eta}$)

(1) Tangential Modes

First tangential: $S_{11} = 1.8413$

Second tangential: $S_{21} = 3.0543$

Third tangential: $S_{31} = 4.2012$

Fourth tangential: $S_{41} = 5.3175$

Fifth tangential: $S_{51} = 6.4154$

4.2, Operating the Program (cont.)

(2) Radial Modes

First radial: $S_{02} = 3.8317$
 Second radial: $S_{03} = 7.0156$
 Third radial: $S_{04} = 10.1734$

(3) Combined Tangential-Radial Modes

IT-1R: $S_{12} = 5.3313$
 IT-2R: $S_{13} = 8.5263$
 IT-3R: $S_{14} = 11.7059$
 2T-1R: $S_{22} = 6.7060$
 2T-2R: $S_{23} = 9.9695$
 2T-3R: $S_{24} = 13.1705$
 3T-1R: $S_{32} = 8.0151$
 3T-2R: $S_{33} = 11.3459$
 3T-3R: $S_{34} = 14.5858$

(4) Combined transverse-longitudinal Modes can not be Programmed

Program C: Exhaust Nozzle Admittance Coefficients for Longitudinal and Transverse Modes

a. Input Requirements

<u>Core Location</u>	<u>Mnemonic</u>	<u>Description</u>
L3801	MDESIR	= 1.: the table of velocity potential values within the nozzle is input and the Mach number to the entrance of the nozzle is input.

4.2, Operating the Program (cont.)

<u>Core Location</u>	<u>Mnemonic</u>	<u>Description</u>
		= 2.: The Mach number at the entrance to the nozzle is input but the velocity potential table must be calculated.
		= 3.: the Mach number and the velocity potential table must be calculated.
L3803	RAT	Radius of the throat, in.
L3804	RAC	Radius of the chamber, in., also loaded in L13, Program A.
L3805	RCC	Radius of chamber curvature at the nozzle entrance, in.
L3806	RCT	Radius of curvature at the throat, in.
L3807	ALPHA	Nozzle convergent half-angle, deg.
L90	RATI	Radius of centerbody throat, in.
L91	RCTI*	Radius of curvature of the centerbody throat, in.
L92	RACI	Radius of chamber of centerbody, in.
L93	RCCI*	Radius of curvature of centerbody at the nozzle entrance.
L94	HANGI*	Centerbody nozzle convergent half-angle, deg.
L20	S	Transverse acoustic mode number given in Table 3 for cylindrical chambers.
L3808	KN	If $L3801 \geq 2$, then KN is either <ul style="list-style-type: none"> a. An odd integer less than 200 telling the desired size of the program generated velocity potential table, or b. Blank and program will assume $K_N = 101$ (recommended)

*Note 1: These values may be plus or minus, see Figures 21 and 22.

Note 2: For cylindrical chambers, leave L90 through L94 blank.

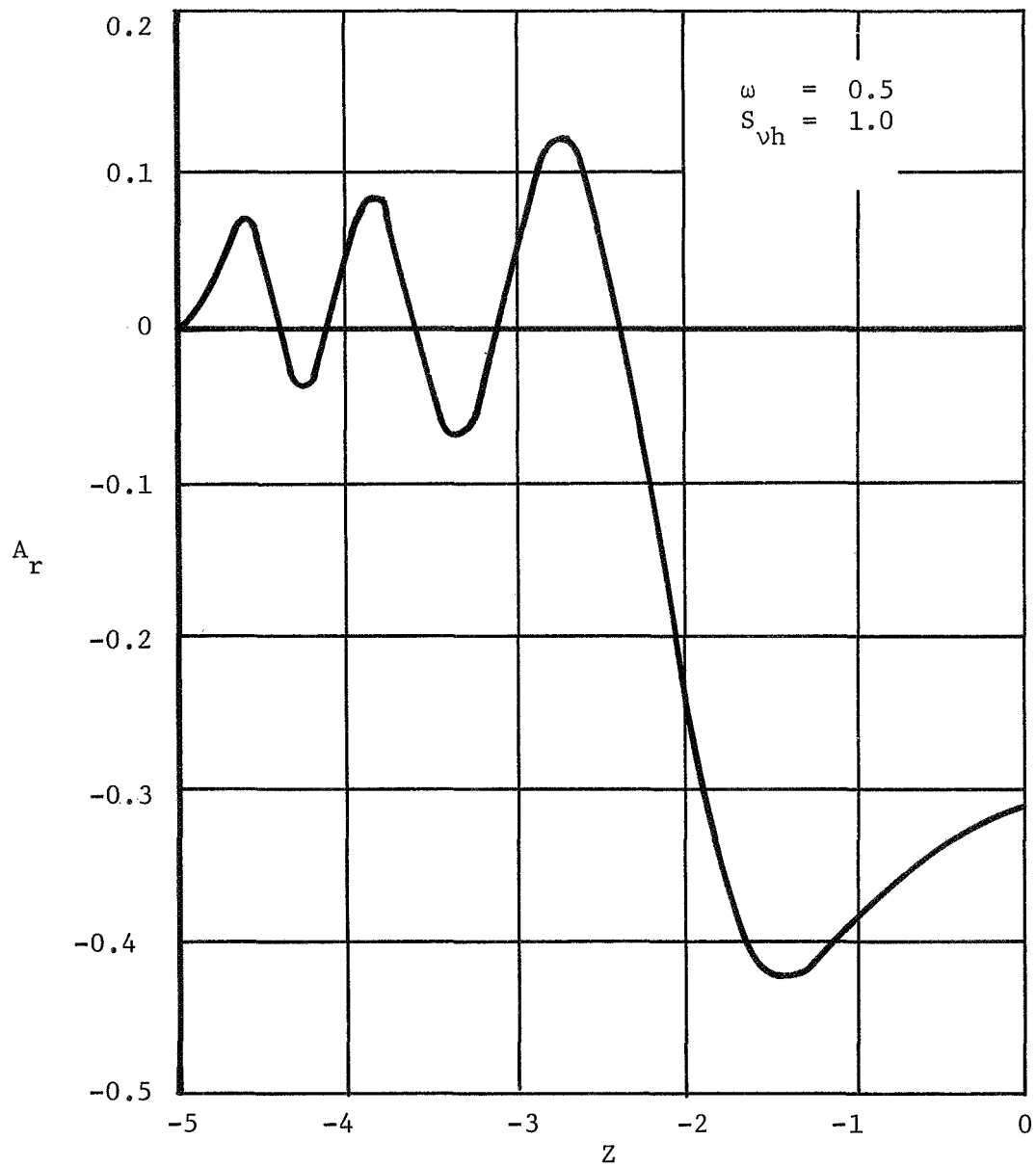


Figure 21 -- Real Part of Pressure Admittance Coefficient
Versus Axial Distance

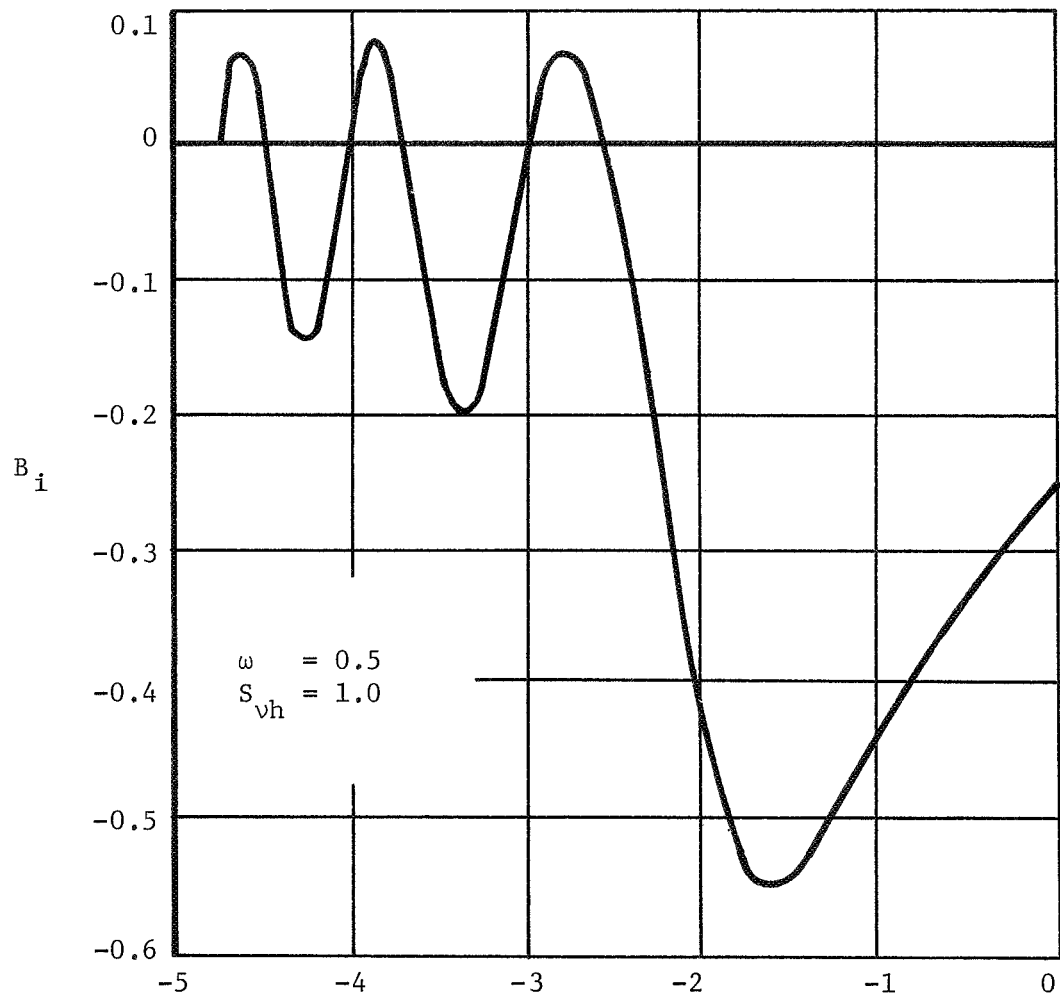


Figure 22. Imaginary Part of Radial Velocity Admittance Coefficient Versus Axial Distance

4.2, Operating the Program (cont.)

<u>Core Location</u>	<u>Mnemonic</u>	<u>Description</u>
L3809 L3811 L3813 L4205	X(Z)	Dimensionless velocity potential table (199 values maximum) in the odd numbered locations only. If $L3801 \geq 2$, this is not necessary.
L3810 L3812 L3814 L4206	$V^2(Z)$	Squares of the reduced velocity table (199 values maximum) in the even numbered locations only. If $L3801 \geq 2$, this is not necessary.

b. Print Options

$0 < L2 \leq 9$:	Execute Program C, print no output
$10 \leq L2 \leq 99$:	Execute Program C, print output
$100 \leq L2 \leq 199$:	Execute Program C, print input and output (recommended)
$200 \leq L2 \leq 299$:	Execute Program C, print input and output, and print the nondimensional velocity potential table.

c. Placement of the Data in the Data Package

These data may be inserted anywhere in Section I of the data package.

d. Output

The transverse acoustic mode number, $S_{v\eta}$, in the chamber and nozzle. The variation of $S_{v\eta}$ in the nozzle is given by Eq. 22 at the end of this section.

4.2, Operating the Program (cont.)

The nondimensionalized frequency, ω in the chamber and nozzle.
The variation of the ω in the nozzle is given by Equations 21 and 22 at the end of this section.

The Mach number, \bar{u}_e ; at the entrance of the nozzle.

The ratio of the specific heats, G .

The real and imaginary portions of the first, second, and third (i.e., A, B, C) admittance parameters.

The real and imaginary portions of the transverse nozzle admittances (i.e., T1, T2).

The frequency, F , in chamber, Hz.

e. Auxiliary Equations

- (1) The Selection of the Chamber Frequencies to be Used

Because of the long execution time of this program for a given value of ω , the program starts with the first chamber frequency and uses every other frequency thereafter; that is if n is the total number of chamber frequencies, Program C will use m number of frequencies according to the relationship

$$m = \frac{n}{2} + 1$$

4.2, Operating the Program (cont.)

In computer language, m and n are whole numbers. Therefore,
if n = 11

$$m = \frac{11}{2} + 1$$

$$m = 5 + 1 \text{ (where 0.5 has been truncated out)}$$

$$m = 6$$

(2) Nondimensional chamber frequency

$$c = \frac{(2\pi f_c^*) (\nu_{AC}^*)}{c_c^*} \quad \text{Eq. 20}$$

where

* = denotes dimensional variables
subscript c denotes chamber
conditions

f_c = chamber frequency, cps

c_c = chamber speed of sound, ft/sec

ν_{AC} = chamber length L_c^* or radius R_c^*
(depending if longitudinal or
transverse modes respectively
are desired).

(3) Nondimensional Nozzle Frequency

$$\omega_N + \frac{\omega_c}{K} \frac{(\gamma+1)^{1/2}}{2} \frac{r_{AT}^*}{r_{AC}^*} \quad \text{Eq. 21}$$

4.2, Operating the Program (cont.)

where

$$K = \left(\frac{2}{\gamma+1} \frac{r^*_{AT}}{r^*_{CT}} \right)^{1/2}$$

(4) Nozzle Transverse Acoustic Nozzle Number

$$(S_{v\eta})_N = \frac{(S_{v\eta})_c}{K} \quad \text{Eq. 22}$$

The listing of this program is presented in Volume 2.

Program D: Expansion of Results from Program B

a. Input Requirements

<u>Core Location</u>	<u>Mnemonic</u>	<u>Description</u>
L3405	ℓ_r/n	The ratio of the radial velocity coefficient to the pressure interaction index. Generally set equal to zero.
L3406	ℓ_θ/n	The ratio of the tangential velocity coefficient to the pressure interaction index. Generally set equal to zero.
L3407	N_ω, I	= 1 for linear combustion response, > 1 for nonlinear combustion response. This parameter indicates the number of frequencies for which the injector nonuniformity coefficients, $A_{v\eta}$, $B_{v\eta}$, and $C_{v\eta}$, are known. The running of Program I will determine this number. (Not required if Program B is run.)
L3408	$\eta_{\omega,c}$	The number of chamber frequencies (≥ 29) (Not required if Program B is run.)

4.2, Operating the Program (cont.)

<u>Core Location</u>	<u>Mnemonic</u>	<u>Description</u>
L3409 : : L3437	ω_c	The table of frequencies arranged in ascending order. The last value must be zero. (Not required if Program B is run.)
L3439 : : L3467	$h_R(\omega)$	Real part of the damping effects computed in Program B. The last value must be zero. (Not required if Program B is run.)
L3469 : : L3497	$h_i(\omega)$	Imaginary part of the damping effects computed in Program B. The last value must be zero. (Not required if Program B is run.)
L4522 : : L4538	$\omega_{c,I}$	The values of chamber frequencies for which the non-uniformity coefficients are known. Use only if data are available.
L4539 : : L4555	$(A_{v\eta})_R$	The real part of the pressure nonuniformity coefficient corresponding to the above frequencies ($\omega_{c,I}$). $A = 1.0$ for uniform injection distribution.
L4556 : : L4572	$(B_{v\eta})_R$	The real part of the radial velocity nonuniformity coefficient corresponding to the above frequencies ($\omega_{c,I}$). Generally set equal to zero.
L4573 : : L4589	$(C_{v\eta})_R$	The real part of the tangential velocity nonuniformity coefficient corresponding to the above frequencies ($\omega_{c,I}$). Generally set equal to zero.
L4590 : : L4606	$(C_{v\eta})_i$	The imaginary part of the tangential velocity non-uniformity coefficient corresponding to the above frequencies ($\omega_{c,I}$). Generally set equal to zero.

- NOTES:
- All these data, with the exception of ℓ_r/n and ℓ_θ/n , can be calculated using Programs B, E, and I.
 - This program was used specifically to include the effects of the nonuniformity coefficients for the low Mach number cases. With the new high Mach analysis, these effects are taken into account by the chamber program.

4.2, Operating the Program (cont.)

b. Print Options

$0 < L3 < 9$: Execute D, print no output or input

$10 \leq L3 \leq 99$: Execute D, print output only

$100 \leq L3 \leq 199$: Execute D, print input and output

c. Placement of the Data into the Data Package

These data can be inserted anywhere in Section I of the data package.

d. Output

An expanded table (50 values) of ω , $h_R(\omega)$, and $h_i(\omega)$.

A listing of this program is presented in Volume 2.

Program E: Injector Nonuniformity Coefficients: $A_{v\eta}$, $B_{v\eta}$, $C_{v\eta}$

a. Input Requirements (not programed for annular chambers)

MAIN CONTROL requires L4

<u>Core Location</u>	<u>Mnemonic</u>	<u>Description</u>
L1	IZZIT	Indicates whether the mode is standing or spinning: Standing: $IZZIT < 0$ Spinning: $IZZIT > 0$

4.2, Operating the Program (cont.)

<u>Core Location</u>	<u>Mnemonic</u>	<u>Description</u>
L2	XM	The number of radial divisions desired on the injector face ($10 \leq XM \leq 21$). This does not need to be input if Program J is run because Program J sets this equal to 20.
L3	XN	The number of angular divisions desired around the injector face ($20 \leq XN \leq 181$). This does not need to be input if Program J is run because Program J sets this equal to 180.
L4	SECTOR	The number of symmetrical sectors that the injector can be divided into, ($1 \leq SECTOR \leq 180$).
L5	v	Longitudinal mode number 1, 2, 3, etc. For radial modes $v = 0$.
L7	$S_{v\eta}$	Transverse acoustic mode number given by tabulation presented in Program B write-up.
L9573	R_{inj}	Injector radius, in.
L9570	NE	Number of elements per symmetrical sector. The maximum number of elements is 1000. Ignore if Program J is run.
L1920 : : L2919	r_E	The radial position of each element within the symmetrical sector, in. Program J supplies these data when it is run.
L2920 : : L3919	θ_E	
L3920 : : L4919	μ_E	The element injection distribution given by Equation 23 at the end of this section. Usually Program J provides this information to Program E.

4.2. Operating the Program (cont.)

b. Print Options

$0 \leq L4 \leq 9$: Execute E, do not print input or output

$10 \leq L4 \leq 99$: Execute E, print output only

$100 \leq L4 \leq 199$: Execute E, print input and output

c. Placement of the Data into the Data Package

Main control data: Section I of data package.

All other data: Section III of data package. Section IV must be included in the data package.

d. Output

The following output is obtained from this program:

$A_{v\eta}$, $B_{v\eta}$, and $C_{v\eta}$.

e. Auxiliary Equations

Distribution coefficient, μ_E

$$\mu_E = \frac{(\dot{w}_T)_E / (A_s)_E}{\dot{w}_T / A_{inj}} = \frac{1}{x_m \cdot x_N} \frac{(w_T)_E}{\dot{w}_T} \quad \text{Eq. 23}$$

where

$(w_T)_E$ = total weight flow rate of element, lb/sec

w_T = total weight flow rate of injector, lb/sec

$(A_s)_E$ = surface area serviced by the element, in.²

A_{inj} = total surface area of injector, in.²

4.2, Operating the Program (cont.)

f. Other Information

The listing of this program is presented in Volume 2.

Program F: Final Solution of Instability Zones

a. Input Requirements

The input for this program comes directly from Program D and consists of the following parameters:

The frequency in the chamber, ω

The radius of the chamber r_{AC} , in.

Speed of sound in the chamber, c_o , ft/sec

Real and imaginary parts of the damping parameters corresponding to the above frequencies

This program can be run by itself if the data are inserted into those locations specified by Program D.

b. Print Options

$0 < L5 \leq 9$: Execute Program F, print no input and output

$10 \leq L5 \leq 99$: Execute Program F, print output only

$100 \leq L5 \leq 199$: Execute Program F, print input and output

4.2, Operating the Program (cont.)

c. Placement of the Data into the Data Package

These data are included into Section I of the data package.

d. Output

The following output results from this program:

f = frequency of oscillation, Hz

ω = nondimensional frequency

τ = sensitive time lag corresponding to the
above frequency, millisec

n = pressure interaction index

At the bottom of the page, an effort is made to locate the minimum interaction index. In most cases, this information is valid. However, effects from an adjacent mode will intervene occasionally thereby invalidating this information.

e. Other Information

This program obtains its result by the solution of the following equations:

Frequency, cps

$$f = \frac{\omega}{2\pi} \frac{c_o}{r_{AC}} \quad \text{Eq. 24}$$

4.2, Operating the Program (cont.)

Pressure interaction index, n

$$n = \frac{h_R^2 + h_i^2}{2h_R} \quad \text{Eq. 25}$$

Sensitive time lag, τ , millisecc

$$\tau = (83.33) \frac{r_c}{c_o} \frac{1}{f} \tan^{-1} \frac{h_i}{n-h_R} \quad \text{Eq. 26}$$

Program G: Not in Use

Program H: High Combustion Chamber Mach Number Analysis

Program H is not operational. Recommended procedure is to place a negative number in load location L7 of MAIN CONTROL.

Program I: Nonlinear Combustion Response (Option for Program E)

a. Input Requirements

<u>Core Location</u>	<u>Mnemonic</u>	<u>Description</u>
--------------------------	-----------------	--------------------

ALL THE DATA REQUIRED TO RUN PROGRAM E AS WELL AS:

L0	E1	The permissible error. If blank, the program will assume E1 = 0.001.
L12	P _{oo}	The ratio of the maximum pressure amplitude at the injector face to the steady-state pressure value.
L19 L68	IPP	The values of the pressure perturbation associated with the pressure-dependent nonlinear element.

4.2, Operating the Program (cont.)

<u>Core Location</u>	<u>Mnemonic</u>	<u>Description</u>
L69 L118	OPP	The values of the combustion perturbation corresponding to the above IPP values.
L119 L168	IPR	The values of the radial velocity perturbation associated with the velocity-dependent nonlinear element.
LI69 L218	OPR	The values of the combustion perturbation corresponding to the above IPR values.
L219 L268	IPT	The values of the tangential velocity perturbation associated with the velocity dependent nonlinear element.
L269 L318	OPT	The values of the combustion perturbation corresponding to the above IPT values.
L9595	TFLP	The linear transfer function for equivalent linear operation associated with the pressure-dependent nonlinear element.
L9596	TFLR	The same as TFLP except for radial velocity-dependent nonlinear element.
L9597	TFLT	The same as TFLP except for tangential velocity-dependent nonlinear elements.
L9598	NUMBR	The number of steps to be used in the integration scheme associated with this problem. If left blank, the computer will assume 20, which is sufficient for most cases.

b. Print Options

$0 < L8 \leq 9$: Execute I, print no input or output data
 $10 \leq L8 \leq 99$: Execute I, print output only
 $100 \leq L8 \leq 199$: Execute I, print input and output

4.2, Operating the Program (cont.)

c. Placement of the Data into the Data Package

These data are included in Section III of the data package. Along with these data, Section IV must be included.

d. Output

The output of this program is as follows:

The frequency, ω

The element number, location, and fractional flow rate f_p , f_R , and f_T necessary for Program E

This will automatically change the output Program E as follows:

The frequency, ω

The frequency dependent expansion coefficients $A_{v\eta}$, $B_{v\eta}$, and $C_{v\eta}$.

Program J: Injected Mass Distribution Effects (Not Programed for Annular Chambers)

a. Input Requirements

<u>Core Location</u>	<u>Mnemonic</u>	<u>Description</u>
L319 L323	n	Element number (maximum = 1000) within symmetrical sector.
L327 L319 + 4n L320		

4.2, Operating the Program (cont.)

<u>Core Location</u>	<u>Mnemonic</u>	<u>Description</u>
L324 L328 L320 + 4n L321	X_n or v_n	Element location, in.
L325 L329 L321 + 4n L322	X_n or θ_n	Element location
L326 L330	T_n	Type of injection element. The details concerning this type number are given next.
L4	DX	Number of symmetrical sectors, DX = 1 for no symmetry.
L4944 : L9568	-	The data input in this section serve to define the element types and consist of a maximum of 100 variable length data sets. Each set contains: <ol style="list-style-type: none"> The element type number (≤ 100) Number of oxidizer orifices for that type Diameters of all the oxidizer orifices Number of fuel orifices for that type Diameters of all the fuel orifices

EXAMPLE

```

let       $T_i$    = ith element type
          $NX_i$   = number of oxidizer orifices for the ith type element
          $DX_{ij}$  = diameter of the jth oxidizer orifice in the ith type
                   element
          $NF_i$   = number of fuel orifices for the ith type element
          $DF_{ij}$  = diameter of the jth fuel orifice in the jth type
                   element

```

4.2, Operating the Program (cont.)

Then a typical input would read

L4944 + T₁ + NX₁ + DX_{1,1} + DX_{1,2} + DX_{1,3} + NF₁ + DF_{1,1} + DF_{1,2} + T₂ + NX₂
 + DX_{2,1} +

If NF_L or NX_L is zero, then do not set DF_{i,1} = 0 or DX_{i,1} = 0.

Assume NX₁ ≡ 0.0, then

L4944 + T₁ + NX₁ + NF₁ + DF_{1,1} + DF_{1,2} + DF_{1,3} + T₂ + NX₂ + DX_{2,1} + . . .

<u>Core Location</u>	<u>Mnemonic</u>	<u>Description</u>
L9569	NT	Total number of injection types
L9570	NE	Number of elements per symmetrical sector
L9571	COORD	COORD = 0: elements are located using polar coordinates COORD > 0: elements are located using cartesian coordinates
L9572	WT	Total injector weight flow, lb/sec
L9573	R _{inj}	Injector radius, in.
L9574	MR	Injector mixture ratio
L9575	NFFC	Total number of fuel film cooling holes
L9576	DFFC	Diameter of fuel film cooling holes

In the event of fuel or oxidizer film cooling, either the percent film cooling or the actual orifice dimensions can be used to describe the cooling. Place a zero(s) in the one(s) not used.

4.2, Operating the Program (cont.)

<u>Core Location</u>	<u>Mnemonic</u>	<u>Description</u>
L9588	PFFC	Percent fuel film cooling
L9578	ROX	Oxidizer density, lb/ft ³
L9579	ROF	Fuel density, lb/ft ³
L9584	CDX	Oxidizer orifice loss coefficient
L9585	CDF	Fuel orifice loss coefficient
L9589	PFFX	Percent oxidizer film cooling
L9590	NFFX	Total number of oxidizer film cooling orifices
L9591	DFFX	Diameter of oxidizer film cooling orifices

L2, L3, and L4 from Program E.

b. Print Options

$0 < L9 \leq 9$:	Execute J, do not print output or input data
$10 \leq L9 \leq 99$:	Execute J, print output only
$100 \leq L9 \leq 199$:	Execute J, print input and output
$L9 \leq 500$:	Execute J, print input and output, and, if error occurs in J, dump error message with input data.

c. Placement of the Data into the Data Package

Main control data: Section I of the data package.

All other data: Section III of the data package. Section IV must be included in the data package.

4.2, Operating the Program (cont.)

d. Output

The following output results as a consequence of this program:

Miscellaneous information concerning the total orifice area, circuit pressure drops, overall mixture ratio, etc.

Element number, injection type, and location.

Description of various parameters associated with the different types of injection elements.

Element number, location, and distribution coefficient.

The distribution coefficient as a function of the radius across the face of the injector.

Table 9 -- Input Data for Mode Example Problem

```

L0+100++100
L10+1.218+0
L13+6.4+14.8+3800+20.42+0.0
L20+0.0
L21+15+2.0+2.5+3.0+3.25+3.5+3.75+4.0+4.25+4.5+4.75+5.0
+5.5+6.0+6.5+7.0
L50+0.0+2.5+5.0+6.3+6.35+6.38+6.39+6.40+6.41+6.42+6.43+6.5
+7.5+12.5+25.+50.+0.00000
L70+0.0+2.5+5.0+6.3+6.35+6.38+6.39+6.395+6.4+6.4+6.4+6.4
+6.4+6.4+6.4+6.4+0.00000
L3801+3.0+0.+3.58+0.+3.0+7.16+15.0+0.
TEXAMPLE PROBLEM... LONGITUDINAL MODE FOR HYPOTHETICAL ENGINE
L1+100+10+10+100+10L9+100
L3407+1
L20+1.8411838+0.0
L7-100
T EXAMPLE PROBLEM... FIRST TANGENTIAL MODE, HYPOTHETICAL ENGINE
L0+0+1+20+180+180+1++1.8411838
L4944+1+1+.0785+1+.0785
+2+2+.0785+.0785+1+.0785
+3+1+.0785+4+.0785+.0785+.0785+.0785+.0785
L319+1+2.0+1.0+1
L323+2+4.0+1+2
L327+3+6.0+1.0+3
L9569+3+3+0+150+6.4+2.0++
L9578+89.52+56.1
L9584+0.75+0.75
T
L1+100+10+10+100+10
L20+3.0542369+0.0
L7-100
T EXAMPLE PROBLEM... SECOND TANGENTIAL MODE, HYPOTHETICAL ENGINE
L0+0+1+20+180+180+2++3.0542369
T
L4+200
L8+50
L20+1.8411838+0.0
L3405+1.0
T 1T MODE, SHOWING EFFECTS OF DEADBAND NONLINEARITY
L0+0+1+20+180+180+1++1.8411838
L12+1.0L9596+1.0
L119-5.1-2.1-1.1-0.60-0.20-0.15-0.11-0.10-0.09-0.05
L169-5.0-2.0-1.0-0.50-0.10-0.05-0.01+0.00+0.00+0.00
L129-0.01+0.01+0.05+0.09+0.10+0.11+0.15+0.20+0.60
L179+0.00+0.00+0.00+0.00+0.00+0.01+0.05+0.10+0.50
L138+1.10+2.1+5.1+0.000000
L188+1.00+2.0+5.0+0.000000

```

4, Use of Computer Programs (cont.)

4.3 ILLUSTRATIVE DESIGN PROBLEMS

Example 9: Longitudinal Mode Analysis

The following data concerning a hypothetical engine will be used for this example. The location of these data in the input is described in Program A and Program C in Section 4.2.

Main control (L0 and L2)

Engine geometry: see Figure 21 (L13, 14, 18, 3803-3807)

$\gamma = 1.218$ (L10)

Mach number: will be calculated from contraction ratio and (L11)

$C_o = 3800$ ft/sec (L15)

Weighted liquid injection velocity (L16)

Momentum interchange coefficient = 0.0 (L17)

Combustion distribution: a linear combustion distribution with complete combustion occurring at 6.4 in. (L50..., L70...)

The problem is to find the n, τ zone for the first longitudinal mode. The input data package is shown in Table 9 and the output is shown in Table 10.

The output of this program is a neutral stability curve which describes the system pressure interaction index, n , as a function of the sensitive time lag, τ . Engine systems whose injector characteristics coincided with this line could neither amplify nor dampen small linear disturbances in the combustion process. The injector characteristics are not obtainable from this nor any existing computer program. They are divided into two parts: (1) sensitive frequency (relatable to τ by the equation $f_s = \frac{1}{2\tau}$) and (2) an experimentally determined injector pressure interaction index, n .

Table 10 -- Output of Longitudinal Mode Example Problem

```

DATE      03 NOV 69

  A    B    C    D    E    F    G    H    I    J
100.   0. 100.  0.  0.  0.  0.  0.  0.  0.

***** THE FOLLOWING MAIN CONTROL DATA WILL BE USED IN THIS CASE *****
RATIO OF SPECIFIC HEAT (GAMMA) = 1.2180
DESIRED MACH NUMBER = .00000 (=0 IF BEING CALCULATED)
CHAMBER RADIUS = 6.400 (INCHES)
CHAMBER LENGTH = 14.800 (INCHES)
SPEED OF SOUND = 3800.000 (FT/SEC)
CHAMBER MODE DESCRIPTION = .00000 (=0 FOR LONGITUDINAL MODES)

***** CHAMBER FREQUENCIES (WC) *****

  2.00000      2.50000      3.00000      3.25000      3.50000
  3.75000      4.00000      4.25000      4.50000      4.75000
  5.00000      5.50000      6.00000      6.50000      7.00000

***** MACH DISTRIBUTION IN CHAMBER AS A FUNCTION OF LENGTH *****

CHAMBER LENGTH      MACH DISTRIBUTION      CHAMBER LENGTH      MACH DISTRIBUTION
.00000      .00000      6.40000      6.39500      25.00000      6.40000
2.50000      2.50000      6.41000      6.40000      50.00000      6.40000
5.00000      5.00000      6.42000      6.40000      .00000      .00000
6.30000      6.30000      6.43000      6.40000      .00000      .00000
6.35000      6.35000      6.50000      6.40000      .00000      .00000
6.38000      6.38000      7.50000      6.40000      .00000      .00000
6.39000      6.39000      12.50000      6.40000

```

Table 10 -- Output of Longitudinal Mode Example Problem (cont.)

DATE 03 NOV 69
 PROGRAM C INPUT - CALCULATES NOZZLE ADMITTANCE COEFFICIENTS USING 8052
 G = 1.218 , MDESIR = 3
 RAT = 3.580, RAC = 6.400, RCC = 3.000, RCT = 7.160, ALFA = 15.000, KN = 101

WN	(SNH)N	DES
.758748+00	.000000	.000000
.113812+01	.000000	.000000
.132781+01	.000000	.000000
.151750+01	.000000	.000000
.170718+01	.000000	.000000
.189687+01	.000000	.000000
.227625+01	.000000	.000000
.614112+01	.000000	.000000

Table 10 --- Output of Longitudinal Mode Example Problem (cont.)

DATE 03 NOV 69									
PROGRAM C OUTPUT									
(SNH)C (SNH)N	WC WN	MACH NO G	-AR/(MACH NO)	AI -AI/(MACH NO)	BR T1	BI T2	CR -CR/(MACH NO)	CI -CI/(MACH NO)	
.0000	2.0000	.1885	-.83951+00	-.12120+01	.00000+00	.00000+00	-.10709+00	.66309-03	
.0000	.7587	1.2180	.44530+01	.64285+01	.00000	.00000	.56803+00	-.35172-02	
FC(CPS)= 980.7386									
.0000	3.0000	.1885	-.14485+01	-.35432-01	.00000+00	.00000+00	.41367-01	-.60754-01	
.0000	1.1381	1.2180	.76831+01	.18794+00	.00000	.00000	-.21942+00	.32226+00	
FC(CPS)= 1471.1079									
.0000	3.5000	.1885	-.10632+01	.45579-01	.00000+00	.00000+00	-.45013-01	-.12225-01	
.0000	1.3278	1.2180	.56396+01	-.24176+00	.00000	.00000	.23876+00	.64846-01	
FC(CPS)= 1716.2925									
.0000	4.0000	.1885	-.89968+00	-.77292-01	.00000+00	.00000+00	-.38491-02	.35508-01	
.0000	1.5175	1.2180	.47721+01	.40998+00	.00000	.00000	.20417-01	-.18835+00	
FC(CPS)= 1961.4772									
.0000	4.5000	.1885	-.88698+00	-.21135+00	.00000	.00000	.27857-01	.21121-02	
.0000	1.7072	1.2180	.47047+01	.11211+01	.00000	.00000	-.14776+00	-.11203-01	
FC(CPS)= 2206.6618									
.0000	5.0000	.1885	-.96782+00	-.29622+00	.00000	.00000	-.90676-03	-.20969-01	
.0000	1.8969	1.2180	.51336+01	.15712+01	.00000	.00000	.48097-02	.11123+00	
FC(CPS)= 2451.8464									
.0000	6.0000	.1885	-.111663+01	-.20603+00	.00000	.00000	.72719-02	.14955-01	
.0000	2.2762	1.2180	.61862+01	.10928+01	.00000	.00000	-.38572-01	-.79327-01	
FC(CPS)= 2942.2157									
.0000	7.0000	.1885	-.10462+01	-.35016-01	.00000	.00000	-.16828-01	-.42143-02	
.0000	6.1411	1.2180	.55494+01	.18573+00	.00000	.00000	.89261-01	.22354-01	
FC(CPS)= 3432.5850									

Table 10 -- Output of Longitudinal Mode Example Problem (cont.)

DATE	03 NOV 69				
U1BAR =	.18852762+00	GAMMA =	.12180000+01	K =	.00000000+00
		X =	.21651235+00	ULM =	.20420000+02
RESULTS FOR LONGITUDINAL MODE					
FC(CPS)	OMEGA	TAU(MS)	N		
980.7	2.00000	.43362	1.25433		
1029.8	2.10000	.35794	1.45551		
1078.8	2.20000	.30058	1.73711		
1127.8	2.30000	.25804	2.07726		
1176.9	2.40000	.22678	2.45271		
1225.9	2.50000	.20395	2.83985		
1275.0	2.60000	.18742	3.21606		
1324.0	2.70000	.17565	3.56120		
1373.0	2.80000	.16750	3.85876		
1422.1	2.90000	.16211	4.09681		
1471.1	3.00000	.15876	4.26857		
1495.6	3.05000	.15772	4.32019		
1520.1	3.10000	.15699	4.34120		
1544.7	3.15000	.15632	4.33802		
1569.2	3.20000	.15548	4.31784		
1593.7	3.25000	.15425	4.28862		
1618.2	3.30000	.15245	4.25877		
1642.7	3.35000	.14999	4.23684		
1667.3	3.40000	.14685	4.23075		
1691.8	3.45000	.14312	4.24688		
1716.3	3.50000	.13903	4.28885		
1740.8	3.55000	.13462	4.35705		
1765.3	3.60000	.12986	4.45234		
1789.8	3.65000	.12489	4.57541		
1814.4	3.70000	.11987	4.72577		
1838.9	3.75000	.11493	4.90170		
1863.4	3.80000	.11017	5.10032		
1887.9	3.85000	.10569	5.31781		
1912.4	3.90000	.10154	5.54971		
1937.0	3.95000	.09773	5.79130		
1961.5	4.00000	.09428	6.03807		
1986.0	4.05000	.09117	6.28815		
2010.5	4.10000	.08841	6.53915		
2035.0	4.15000	.08599	6.78644		
2059.6	4.20000	.08389	7.02600		
2084.1	4.25000	.08208	7.25456		
2108.6	4.30000	.08053	7.46986		
2133.1	4.35000	.07919	7.67075		
2157.6	4.40000	.07802	7.85724		
2182.1	4.45000	.07697	8.03053		
2206.7	4.50000	.07601	8.19293		
2231.2	4.55000	.07511	8.34374		
2255.7	4.60000	.07429	8.48226		
2280.2	4.65000	.07347	8.61268		
2304.7	4.70000	.07262	8.74054		
2329.3	4.75000	.07167	8.87247		
2353.8	4.80000	.07058	9.01610		
2378.3	4.85000	.06933	9.17983		
2402.8	4.90000	.06787	9.37265		
2427.3	4.95000	.06620	9.60393		

Table 10 -- Output of Longitudinal Mode Example Problem (cont.)

DATE	03 NOV 69	2451.8	5.00000	.06431	9.88329
		2500.9	5.10000	.06001	10.61243
		2549.9	5.20000	.05517	11.62190
		2599.0	5.30000	.05007	12.98562
		2648.0	5.40000	.04499	14.77940
		2697.0	5.50000	.04015	17.08252
		2746.1	5.60000	.03569	19.98102
		2795.1	5.70000	.03169	23.57412
		2844.1	5.80000	.02814	27.98557
		2893.2	5.90000	.02503	33.38315
		2942.2	6.00000	.02228	40.01144
		2991.3	6.10000	.01983	48.28128
		3040.3	6.20000	.01762	58.80177
		3089.3	6.30000	.01561	72.45483
		3138.4	6.40000	.01377	90.65824
		3187.4	6.50000	.01204	115.81549
		3236.4	6.60000	.01041	152.27425
		3285.5	6.70000	.00884	208.58000
		3334.5	6.80000	.00730	303.49994
		3383.5	6.90000	.00576	485.27914
		3432.6	7.00000	.00419	912.11401

4.3, Illustrative Design Problems (cont.)

Example 10: Transverse Mode Analysis

For the transverse case, the problem will be to find the n, τ zones for the first tangential and the second tangential modes. The data given in the longitudinal case will be supplemented by the following information:

Main control (L1, L3, L4, L5 and L9) which triggers Programs B, D, E and J

$S_{11} = 1.8413$ and $S_{21} = 3.0543$ (L20)

Injector pressure nonuniformity coefficient (L4539)

Number of radial baffle compartments = 180

(L4 Section III of data package not to be confused with L4 of main control)

Total weight flow = 150 lb/sec

Mixture ratio = 2.0

Injection occurs at three radii:

Unlike doublets at $r = 2.0$ in.

Triplets (X-F-X) at $r = 4.0$ in.

Pentads (4F-X) at $r = 6.0$ in.

(L9569-76, 79, 84, 85, 88-91)

Injector radius = chamber radius

No film cooling

Fuel and oxidizer loss coefficients = 0.75

Spinning modes (L1 Section III of data package)

Tangential mode numbers = 1 and 2 (L5 Section III of data package)

No radial or tangential velocity effects (L4556..., L4573..., and L4590... not needed)

The data package input is shown in Table 9 and the output is shown in Table 11. Pay close attention to arrangement of input cards (Figure 20) to make sure that the data for Programs E and J go into Section III of package. Do not forget Sections II and IV (T) cards. Once again, the problem is to find the n, τ neutral stability curve for both the first and second tangential modes.

Table 11 --- Output of Transverse Mode Example Problem

DATE 03 NOV 69

A B C D E F G H I J

0. 100. 10. 10. 100. 10. 0. -100. 0. 100.

***** THE FOLLOWING MAIN CONTROL DATA WILL BE USED IN THIS CASE *****

RATIO OF SPECIFIC HEAT (GAMMA) = 1.2180

DESIRED MACH NUMBER = .00000 (=0 IF BEING CALCULATED)

CHAMBER RADIUS = 6.400 (INCHES)

CHAMBER LENGTH = 14.800 (INCHES)

SPEED OF SOUND = 3800.000 (FT/SEC)

CHAMBER MODE DESCRIPTION = 1.84118 (=0 FOR LONGITUDINAL MODES)

***** CHAMBER FREQUENCIES (WC) *****

1.69389 1.73071 1.76754 1.80436 1.84118

1.87801 1.91483 1.95165 1.98848 2.02530

***** MACH DISTRIBUTION IN CHAMBER AS A FUNCTION OF LENGTH *****

CHAMBER LENGTH	MACH DISTRIBUTION	CHAMBER LENGTH	MACH DISTRIBUTION	CHAMBER LENGTH	MACH DISTRIBUTION
.00000	.00000	6.40000	6.39500	25.00000	6.40000
2.50000	2.50000	6.41000	6.40000	50.00000	6.40000
5.00000	5.00000	6.42000	6.40000	.00000	.00000
6.30000	6.30000	6.43000	6.40000	.00000	.00000
6.35000	6.35000	6.50000	6.40000	.00000	.00000
6.38000	6.38000	7.50000	6.40000	.00000	.00000
6.39000	6.39000	12.50000	6.40000		

Table 11 -- Output of Transverse Mode Example Problem (cont.)

DATE 03 NOV 69

SECTION 1....MISCELLANEOUS INFORMATION FOR INJECTOR DESIGNED BY PROJECTS

A.....PROPELLENT ORFICE AREAS

ELEMENT TOTAL OXIDIZER AREA	= 3.48462972 SQ. IN.	ELEMENT TOTAL FUEL AREA	= 5.22700441 SQ. IN.
TOTAL OXIDIZER FILM COOLING AREA	= .00000000 SQ. IN.	TOTAL FUEL FILM COOLING AREA	= .00000000 SQ. IN.
INJECTOR TOTAL OXIDIZER AREA	= 3.48462972 SQ. IN.	INJECTOR TOTAL FUEL AREA	= 5.22700441 SQ. IN.

B.....INJECTOR PRESSURE DROPS FOR ABOVE INJECTOR DESIGN

OXIDIZER PRESSURE DROP	= 36.6PSI	FUEL PRESSURE DROP	= 6.5 PSI
------------------------	-----------	--------------------	-----------

C.....PROPELLANT FLOWS AND INJECTOR VELOCITIES FOR ABOVE INJECTOR DESIGN

TOTAL WEIGHT FLOW = 150.0 LB/SEC	
AVERAGE MIXTURE RATIO OF THE ELEMENTS	= 2.000
OVERALL MIXTURE RATIO FOR THE INJECTOR	= 2.000

ELEMENT TOTAL OXIDIZER FLOW	= 100.0 LB/SEC	ELEMENT TOTAL FUEL FLOW	= 50.0 LB/SEC
TOTAL OXIDIZER FILM COOLING FLOW	= .0 LB/SEC	TOTAL FUEL FILM COOLING	= .0 LB/SEC
INJECTOR TOTAL OXIDIZER FLOW	= 100.0 LB/SEC	INJECTOR TOTAL FUEL FLOW	= 50.0 LB/SEC
OXIDIZER OVERALL INJECTION VELOCITY	= 61.5 FT/SEC	FUEL OVERALL INJECTION VELOCITY	= 32.7 FT/SEC

D.....INPUT INFORMATION USED IN COMPUTATIONS

TOTAL PROPELLANT FLOW	= 150.0 LB/SEC
TOTAL NUMBER OF ELEMENT TYPES (SYMMETRICAL SECTION ONLY)	= 3
TOTAL NUMBER OF ELEMENTS (SYMMETRICAL SECTION ONLY)	= 3
OXIDIZER LOSS COEFFICIENT	= .750
FUEL LOSS COEFFICIENT	= .750
PERCENT FUEL FILM COOLING	= .0
PERCENT OXIDIZER FILM COOLING	= .0
DIAMETER OF FUEL FILM COOLING ORFICE	= .00000 IN. (NOTE..THIS MIGHT BE AN EQUIVALENT DIAMETER FOR MULTIPLE-ROW COOLING
DIAMETER OF OXIDIZER FILM COOLING ORFICE	= .00000 IN. (SEE ABOVE NOTE)
NUMBER OF FUEL FILM COOLING ORFICES PER INJECTOR	= 0.
NUMBER OF OXIDIZER FILM COOLING ORFICES PER INJECTOR	= 0.
OXIDIZER DENSITY	= 89.52 PCF
FUEL DENSITY	= 56.1 PCF

Table 11 -- Output of Transverse Mode Example Problem (cont.)

DATE		03 NOV 69		SECTION 2.... ELEMENT LOCATION AND INJECTION TYPE			
ELEMENT NO.	TYPE NO.	R (INCHES)	THETA (DEGREE)	X (INCHES)	Y (INCHES)		
1	1	2.00000	1.00000	1.99970	.03490		
2	2	4.00000	1.00000	3.99939	.06981		
3	3	6.00000	1.00000	5.99909	.10471		

Table 11 --- Output of Transverse Mode Example Problem (cont.)

DATE		03 NOV 69											
SECTION 3...TYPE DESCRIPTION,ORIFICE AREA, PROPELLANT FLOW, AND MIXTURE RATIO													
TYPE		***** FUEL ORIFICE DATA -----*											
		NUMBER OF ORIFICE	DIAMETER IN.	AREA SQ. IN.	FLOW LB/SEC	NUMBER OF ORIFICES	DIAMETER IN.	AREA SQ. IN.	FLOW LB/SEC	TOTAL OXIDIZER AREA SQ. IN.	TOTAL FUEL AREA SQ. IN.	TOTAL PROPELLANT FLOW RATE LB/SEC	MIXTUR RATIO
1	1		.0785	.004840	.138889	1							
2	2		.0785	.004840	.138889		.0785	.004840	.046296	.00484	.00484	.1852	3.000
			.0785	.004840	.138889	1							
3	1		.0785	.004840	.138889		.0785	.004840	.046296	.00968	.00484	.3241	6.000
						4							
			.0785	.004840	.046296		.0785	.004840	.046296				
			.0785	.004840	.046296		.0785	.004840	.046296				
			.0785	.004840	.046296		.0785	.004840	.046296				
										.00484	.01936	.3241	.750

Table 11 -- Output of Transverse Mode Example Problem (cont.)

DATE	03 NOV 69	ELEMENT RESULTS			
		ELEMENT NO.	RADIUS	ANGLE RADIANS	DISTRIBUTION COEFFICIENT MU
		1	2.000	.0175	4.4444
		2	4.000	.0175	7.7778
		3	6.000	.0175	7.7778

Table 11 -- Output of Transverse Mode Example Problem (cont.)

DATE 03 NOV 69

SECTION 4..RESULTANT FLOW DISTRIBUTION (MU) AS A FUNCTION OF ONLY THE RADIUS, I.E.. AVERAGE OF MU IN A RADIAL BAND

RADIUS IN.	MU(R)	MU(R)/MU(MAX)
1.431	.000	.0000
2.024	4.444	.5714
2.479	.000	.0000
2.862	.000	.0000
3.200	.000	.0000
3.505	.000	.0000
3.786	.000	.0000
4.048	7.778	1.0000
4.293	.000	.0000
4.525	.000	.0000
4.746	.000	.0000
4.957	.000	.0000
5.160	.000	.0000
5.355	.000	.0000
5.543	.000	.0000
5.724	.000	.0000
5.901	.000	.0000
6.072	7.778	1.0000
6.238	.000	.0000
6.400	.000	.0000

Table 11 -- Output of Transverse Mode Example Problem (cont.)

```

DATE      03 NOV 69

INPUT TO INJECTION DISTRIBUTION PROGRAM

CONSTANTS

NUMBER OF OMEGAS = 1
NUMBER OF ELEMENTS = 3 FOR EACH OF 180 SYMMETRIC SECTIONS.
RADIAL DIVISIONS(XM) = 20.
ANGULAR DIVISIONS (XN) = 180.
ACOUSTIC MODE NUMBER(SVN) = 1.8412
ORDER OF BESSEL FUNCTIONS(V) = 1.
INJECTOR RADIUS = 6.400, IN.
RATIO OF SPECIFIC HEATS(GAMMA) = 1.2180
MAXIMUM PRESSURE AMPLITUDE RATIO(P00) = .000

TRANSFER FUNCTIONS FOR LINEAR OPERATION

PRESSURE(TFLP) = .000
RADIAL VELOCITY(TFLR) = .000
TANGENTIAL VELOCITY(TFLT) = .000

```

Table 11 -- Output of Transverse Mode Example Problem (cont.)

DATE 03 NOV 69

ELEMENT INFORMATION

ELEMENT NO.	RADIUS IN.	ANGLE RADIANS	DISTRIBUTION COEFFICIENT MU
1	2.000	.0175	4.4444
2	4.000	.0175	7.7778
3	6.000	.0175	7.7778

Table 11 -- Output of Transverse Mode Example Problem (cont.)

DATE	03 NOV 69	RESULTS OF INJECTION DISTRIBUTION EFFECTS			
	OMEGA	AVN REAL	BVN REAL	CVN REAL	CVN IMAG
	ALL	1.2745	.8766	.0000	-1.8125
***** THESE VALUES PERTAIN TO A SPINNING MODE *****					

Table 11 -- Output of Transverse Mode Example Problem (cont.)

DATE	03 NOV 69	PROGRAM C OUTPUT							
(SNH)C (SNH)N	WC WN	MACH NO G	AR -AR/(MACH NO)	AI -AI/(MACH NO)	BR T1	BI T2	CR -CR/(MACH NO)	CI -CI/(MACH NO)	
1.8412	1.6939	.1885	-.60983-03	.48540+00	-.22887-01	-.21780+00	.43915-02	-.38873-03	
2.7421	1.4861	1.2180	.32347-02	-.25747+01	.21724+00	.42368+00	-.23294-01	.20619-02	
FC(CPS)= 1920.8346									
1.8412	1.7675	.1885	.12592-01	.40557+00	-.27694-01	-.20090+00	.35139-02	-.28287-02	
2.7421	1.5507	1.2180	-.66792-01	-.21513+01	.21299+00	.36166+00	-.18639-01	.15004-01	
FC(CPS)= 2004.3491									
1.8412	1.8412	.1885	.26283-01	.32326+00	-.30799-01	-.18321+00	.12002-02	-.34923-02	
2.7421	1.6153	1.2180	-.13941+00	-.17147+01	.20950+00	.29246+00	-.63661-02	.18524-01	
FC(CPS)= 2087.8636									
1.8412	1.9148	.1885	.41969-01	.23916+00	-.34388-01	-.16317+00	-.63995-03	-.79534-03	
2.7421	1.6799	1.2180	-.22261+00	-.12686+01	.20681+00	.21434+00	.33945-02	.42187-02	
FC(CPS)= 2171.3781									
1.8412	1.9885	.1885	.65749-01	.13721+00	-.23057-01	-.13333+00	.23384-02	-.74945-03	
2.7421	1.7445	1.2180	-.34875+00	-.72779+00	.20433+00	.12513+00	-.12404-01	.39753-02	
FC(CPS)= 2254.8926									
1.8412	2.0253	.1885	.70360-01	.76014-01	-.79474-02	-.12608+00	.16016-02	-.32095-02	
2.7421	1.7768	1.2180	-.37321+00	-.40320+00	.20348+00	.75668-01	-.84956-02	.17024-01	
FC(CPS)= 2296.6498									

Table 11 -- Output of Transverse Mode Example Problem (cont.)

DATE 03 NOV 69											
TRANSVERSE STABILITY PROGRAM... CALCULATES HR, HI OR HTR, HTI											
INPUT DATA											
SNH	ZE	GAMMA	UE	SOUND (FT/SEC)	ULM (FT/SEC)	XK (DRAG)	XCOMPL (IN)				
1.84118374	2.31250000	1.21800	.18852762	3800.00	20.420000	.000000	.000000				
INCREMENTS	LR/N	LT/N									
.0	.0000000	.0000000									
NOZZLE ADMITTANCES INPUT											
OMEGA(CH)	ERT	EIT	CRT	CIT							
1.6938890	.21723997+00	.42368060+00	.43915419-02	-.38872861-03							
1.7675363	.21299294+00	.36165724+00	.35139393-02	-.28287281-02							
1.8411837	.20949743+00	.29246183+00	.12001764-02	-.34922587-02							
1.9148310	.20681402+00	.21434183+00	-.63995426-03	-.79533766-03							
1.9884783	.20433431+00	.12512822+00	.23384384-02	-.74945183-03							
2.0253019	.20347937+00	.75667907-01	.16016490-02	-.32095248-02							
CALCULATED RESULTS...											
OMEGA	H REAL	H IMAG	HT REAL	HT IMAG							
1.6938890	.17957059+01	-.27574364+01									
1.7307127	.17782917+01	-.22796713+01									
1.7675364	.17530309+01	-.17919479+01									
1.8043600	.17150791+01	-.12867290+01									
1.8411837	.16552088+01	-.75276300+00									
1.8780073	.15548406+01	-.17326547+00									
1.9148310	.13731123+01	.47663003+00									
1.9516547	.10097995+01	.12250634+01									
1.9884783	.21071993+00	.20269546+01									
2.0253020	-.14794744+01	.22718191+01									
PROGRAM D OUTPUT											
OMEGA(C)	HTR	HTI									
1.693889	1.408977	-2.163586									
1.730713	1.395313	-1.788714									
1.767536	1.375492	-1.406028									
1.804360	1.345714	-1.009615									
1.841184	1.298738	-.590645									
1.878007	1.219985	-.135950									
1.914831	1.077394	.373981									
1.951655	.792326	.961230									

Table 11 --- Output of Transverse Mode Example Problem (cont.)

EXAMPLE PROBLEM - FIRST TANGENTIAL MODE FOR HYPOTHETICAL ENGINE			
1.988478		.165339	1.590423
2.025302		-1.160850	1.782553

Table 11 -- Output of Transverse Mode Example Problem (cont.)

DATE 03 NOV 69

OMEGA	HTRINT	HTIINT
1.693889	1.408977	-2.163586
1.702387	1.406370	-2.077770
1.710885	1.403435	-1.991539
1.719382	1.400173	-1.904891
1.727880	1.396583	-1.817828
1.736378	1.392702	-1.730407
1.744876	1.388591	-1.642721
1.753373	1.384121	-1.554571
1.761871	1.379152	-1.465738
1.770369	1.373575	-1.376047
1.778867	1.367628	-1.285807
1.787364	1.361180	-1.194872
1.795862	1.353964	-1.102917
1.804360	1.345714	-1.009616
1.812858	1.336698	-.915203
1.821355	1.327006	-.819804
1.829853	1.316099	-.722934
1.838351	1.303440	-.624108
1.846849	1.289011	-.523215
1.855346	1.273668	-.420881
1.863844	1.256370	-.316484
1.872342	1.235935	-.209306
1.880840	1.211498	-.098749
1.889338	1.185488	.014342
1.897835	1.156400	.130284
1.906333	1.121336	.249892
1.914831	1.077395	.373978
1.923329	1.028341	.503359
1.931826	.974968	.637437
1.940324	.909922	.774907
1.948822	.825851	.914467
1.957320	.721702	1.060091
1.965817	.607907	1.220061
1.974315	.472976	1.378341
1.982813	.303737	1.517271
1.991311	.088156	1.620716
1.999808	-.168239	1.696089
2.008306	-.461870	1.748186
2.016804	-.792735	1.777007
2.025302	-1.160835	1.782553

Table 11 --- Output of Transverse Mode Example Problem (cont.)

DATE	03 NOV 69	PROGRAM	F	OUTPUT	FC(CPS)	(OMGA)D,	TAU(MS)	N
					1920.8	.42495		2.36566
					1930.5	1.70239		2.23803
					1940.1	1.71088		2.11476
					1949.7	1.71938		1.99586
					1959.4	1.72788		1.88136
					1969.0	1.73638		1.77135
					1978.7	1.74488		1.66598
					1988.3	1.75337		1.56507
					1997.9	1.76187		1.46846
					2007.6	1.77037		1.37605
					2017.2	1.77887		1.28825
					2026.8	1.78736		1.20503
					2036.5	1.79586		1.12619
					2046.1	1.80436		1.05159
					2055.7	1.81286		.98166
					2065.4	1.82136		.91673
					2075.0	1.82985		.85660
					2084.7	1.83835		.80114
					2094.3	1.84685		.75069
					2103.9	1.85535		.70637
					2113.6	1.86384		.66805
					2123.2	1.87234		.63569
					2132.8	1.88084		.60977
					2142.5	1.88934		.59283
					2152.1	1.89784		.58554
					2161.7	1.90633		.58851
					2171.4	1.91483		.60360
					2181.0	1.92333		.63736
					2190.7	1.93183		.69586
					2200.3	1.94032		.78492
					2209.9	1.94882		.91922
					2219.6	1.95732		1.13942
					2229.2	1.96582		1.52828
					2238.8	1.97432		2.24486
					2248.5	1.98281		3.94152
					2258.1	1.99131		14.94228
					2267.7	1.99981		-8.63362
					2277.4	2.00831		-3.53939
					2287.0	2.01680		-2.38805
					2296.6	2.02530		-1.94904

THE FOLLOWING ARE VALUES INTERPOLATED AT SLOPE OF N=0.0

```

NMIN=      .58525
TAU(MS)=   .21238
(OMEGA)D=  1.89958
FC(CPS)=   2154.1

```

Table 11 -- Output of Transverse Mode Example Problem (cont.)

DATE 03 NOV 69

A	B	C	D	E	F	G	H	I	J
0.	100.	10.	10.	100.	10.	0.	-100.	0.	0.

***** THE FOLLOWING MAIN CONTROL DATA WILL BE USED IN THIS CASE *****

RATIO OF SPECIFIC HEAT (GAMMA) = 1.2180

DESIRED MACH NUMBER = .00000 (=0 IF BEING CALCULATED)

CHAMBER RADIUS = 6.400 (INCHES)

CHAMBER LENGTH = 14.800 (INCHES)

SPEED OF SOUND = 3800.000 (FT/SEC)

CHAMBER MODE DESCRIPTION = 3.05424 (=0 FOR LONGITUDINAL MODES)

***** CHAMBER FREQUENCIES (WC) *****

2.80990	2.87098	2.93207	2.99315	3.05424
3.11532	3.17641	3.23749	3.29858	3.35966

***** MACH DISTRIBUTION IN CHAMBER AS A FUNCTION OF LENGTH *****

CHAMBER LENGTH	MACH DISTRIBUTION	CHAMBER LENGTH	MACH DISTRIBUTION	CHAMBER LENGTH	MACH DISTRIBUTION
.00000	.00000	6.40000	6.39500	25.00000	6.40000
2.50000	2.50000	6.41000	6.40000	50.00000	6.40000
5.00000	5.00000	6.42000	6.40000	.00000	.00000
6.30000	6.30000	6.43000	6.40000	.00000	.00000
6.35000	6.35000	6.50000	6.40000	.00000	.00000
6.38000	6.38000	7.50000	6.40000	.00000	.00000
6.39000	6.39000	12.50000	6.40000		

Table 11 -- Output of Transverse Mode Example Problem (cont.)

```

DATE      03 NOV 69

INPUT TO INJECTION DISTRIBUTION PROGRAM

CONSTANTS

NUMBER OF OMEGAS = 1
NUMBER OF ELEMENTS = 3 FOR EACH OF 180 SYMMETRIC SECTIONS.
RADIAL DIVISIONS(XM) = 20.
ANGULAR DIVISIONS (XN) = 180.
ACOUSTIC MODE NUMBER(SVN) = 3.0542
ORDER OF BESSEL FUNCTIONS(V) = 2.
INJECTOR RADIUS = 6.400, IN.
RATIO OF SPECIFIC HEATS(GAMMA) = 1.2180
MAXIMUM PRESSURE AMPLITUDE RATIO(P00) = .000

TRANSFER FUNCTIONS FOR LINEAR OPERATION

PRESSURE(TFLP) = .000
RADIAL VELOCITY(TFLR) = .000
TANGENTIAL VELOCITY(TFLT) = .000

```

Table 11 -- Output of Transverse Mode Example Problem (cont.)

DATE 03 NOV 69

ELEMENT INFORMATION

ELEMENT NO.	RADIUS IN.	ANGLE RADIANS	DISTRIBUTION COEFFICIENT MU
1	2.000	.0175	4.4444
2	4.000	.0175	7.7778
3	6.000	.0175	7.7778

RESULTS OF INJECTION DISTRIBUTION EFFECTS

OMEGA	AVN REAL	CVN REAL	CVN IMAG
ALL	1.2761	1.2828	.0000 -3.2524

***** THESE VALUES PERTAIN TO A SPINNING MODE *****

Table 11 -- Output of Transverse Mode Example Problem (cont.)

DATE	03 NOV 69										
PROGRAM	C	OUTPUT									
(SNH)C	WC	MACH NO	AR	AI	BR	BI	CR	CI			
(SNH)N	WN	G	-AR/(MACH NO)	-AI/(MACH NO)	T1	T2	-CR/(MACH NO)	-CI/(MACH NO)			
3.0542	2.8099	.1885	.14637-01	.45547+00	-.50957-02	-.20204+00	.68186-03	-.20889-03			
4.5487	2.4651	1.2180	-.77641-01	-.24159+01	.21550+00	.41394+00	-.36168-02	.11080-02			
FC(CPS)= 3186.3651											
3.0542	2.9321	.1885	.19685-01	.36188+00	-.46909-02	-.19214+00	.67167-03	-.64559-03			
4.5487	2.5723	1.2180	-.10441+00	-.19195+01	.21103+00	.34271+00	-.35627-02	.34244-02			
FC(CPS)= 3324.9026											
3.0542	3.0542	.1885	.24287-01	.26445+00	-.39316-02	-.18399+00	-.19082-03	-.66101-03			
4.5487	2.6795	1.2180	-.12882+00	-.14027+01	.20827+00	.26052+00	.10122-02	.35062-02			
FC(CPS)= 3463.4402											
3.0542	3.1764	.1885	.31553-01	.16051+00	-.35605-02	-.17486+00	-.22172-03	.27431-03			
4.5487	2.7867	1.2180	-.16737+00	-.85140+00	.20768+00	.16337+00	.11761-02	-.14550-02			
FC(CPS)= 3601.9778											
3.0542	3.2986	.1885	.39549-01	.40666-01	.11319-02	-.16749+00	.83306-04	.41939-04			
4.5487	2.8939	1.2180	-.20978+00	-.21571+00	.21020+00	.45052-01	-.44188-03	-.22245-03			
FC(CPS)= 3740.5154											
3.0542	3.3597	.1885	.42122-01	-.24369-01	.13055-02	-.16696+00	-.44631-03	.77124-03			
4.5487	2.9474	1.2180	-.22343+00	.12926+00	.21329+00	-.25501-01	.23674-02	-.40909-02			
FC(CPS)= 3809.7841											

Table 11 -- Output of Transverse Mode Example Problem (cont.)

DATE 03 NOV 69											
TRANSVERSE STABILITY PROGRAM... CALCULATES HR, HI OR HTR, HTI											
INPUT DATA											
SNH	ZE	GAMMA	UE	SOUND (FT/SEC)	ULM (FT/SEC)	XK (DRAG)	XCOMPL (IN)				
3.05423680	2.31250000	1.21800	.18852762	3800.00	20.420000	.000000	.000000				
INCREMENTS	LR/N	LT/N									
.0	.0000000	.0000000									
NOZZLE ADMITTANCES INPUT											
OMEGA(CH)	ERT	EIT	CRT	CIT							
2.8098978	.21550144+00	.41393717+00	.68185882-03	-.20889010-03							
2.9320672	.21103374+00	.34271131+00	.67167071-03	-.64559413-03							
3.0542367	.20827204+00	.26051853+00	-.19082022-03	-.66101016-03							
3.1764061	.20767955+00	.16337189+00	-.22172432-03	.27430632-03							
3.2985756	.21019855+00	.45051624-01	.83306136-04	.41938501-04							
3.3596603	.21329456+00	-.25500607-01	-.44631177-03	.77123835-03							
CALCULATED RESULTS...											
OMEGA	FIRST-ORDER SOLN (UNIF INJ)			SECOND-ORDER SOLUTION							
	H REAL	H IMAG	HT REAL	HT IMAG							
2.8098978	.18477270+01	-.33330533+01									
2.8709826	.18420358+01	-.26730276+01									
2.9320673	.18303127+01	-.20026718+01									
2.9931520	.18046849+01	-.13051752+01									
3.0542367	.17417167+01	-.54798279+00									
3.1153214	.15558282+01	.33303596+00									
3.1764061	.85958605+00	.13542701+01									
3.2374909	-.74346371+00	.94920009+00									
3.2985756	.19871684+00	-.42130306-02									
3.3596603	.94748507+00	.65183567+00									
PROGRAM D OUTPUT											
OMEGA(C)	HTR	HTI									
2.8098988	1.447911	-2.611838									
2.870983	1.443451	-2.094630									
2.932067	1.434264	-1.569328									
2.993152	1.414182	-1.022758									
3.054237	1.364839	-.429409									
3.115321	1.219174	.260973									
3.176406	.673586	1.061229									
3.237491	-.582591	.743809									

Table 11 --- Output of Transverse Mode Example Problem (cont.)

DATE	OMEGA	HTIRINT	HTIINT
	2.809898	1.447911	-2.611838
	2.820862	1.447458	-2.519602
	2.831826	1.446853	-2.427105
	2.842790	1.446097	-2.334347
	2.853754	1.445187	-2.241329
	2.864717	1.444126	-2.148050
	2.875681	1.442929	-2.054546
	2.886645	1.441697	-1.961031
	2.897609	1.440358	-1.867354
	2.908573	1.438806	-1.773285
	2.919537	1.436934	-1.678596
	2.930501	1.434634	-1.583059
	2.941465	1.432068	-1.486881
	2.952429	1.429461	-1.390447
	2.963393	1.426503	-1.293327
	2.974357	1.422876	-1.195080
	2.985321	1.418260	-1.095263
	2.996284	1.412447	-.993531
	3.007248	1.406766	-.891013
	3.018212	1.400807	-.787487
	3.029176	1.393407	-.682079
	3.040140	1.383402	-.573920
	3.051104	1.369629	-.462136
	3.062068	1.353722	-.346415
	3.073032	1.340228	-.227741
	3.083996	1.324383	-.105974
	3.094960	1.300921	.019111
	3.105924	1.264575	.147735
	3.116888	1.210281	.280510
	3.127851	1.145059	.436696
	3.138815	1.070803	.611631
	3.149779	.982123	.784023
	3.160743	.873631	.932577
	3.171707	.739937	1.035998
	3.182671	.564687	1.076864
	3.193635	.313983	1.065218
	3.204599	.026978	1.014156
	3.215563	-.249402	.935611
	3.226527	-.468232	.841518
	3.237491	-.582590	.743812

FOLLOWING WILL BE INTERPOLATION WITHIN HTR HTI TABLE GIVEN ABOVE

Table 11 --- Output of Transverse Mode Example Problem (cont.)

DATE 03 NOV 69
PROGRAM F OUTPUT

FC(CPS)	(OMGA)D,	TAU(MS)	N
3186.4	2.80990	.26327	3.07966
3198.8	2.82086	.26073	2.91667
3211.2	2.83183	.25812	2.75917
3223.7	2.84279	.25544	2.60715
3236.1	2.85375	.25268	2.46062
3248.5	2.86472	.24983	2.31961
3261.0	2.87568	.24689	2.18417
3273.4	2.88665	.24385	2.05457
3285.8	2.89761	.24069	1.93065
3298.3	2.90857	.23741	1.81216
3310.7	2.91954	.23398	1.69892
3323.1	2.93050	.23040	1.59074
3335.6	2.94146	.22664	1.48793
3348.0	2.95243	.22270	1.39098
3360.4	2.96339	.21855	1.29954
3372.9	2.97436	.21417	1.21331
3385.3	2.98532	.20953	1.13204
3397.7	2.99628	.20459	1.05565
3410.2	3.00725	.19932	.98556
3422.6	3.01821	.19372	.92175
3435.0	3.02918	.18774	.86364
3447.5	3.04014	.18134	.81075
3459.9	3.05110	.17445	.76278
3472.3	3.06207	.16696	.72118
3484.8	3.07303	.15886	.68946
3497.2	3.08400	.15024	.66643
3509.6	3.09496	.14113	.65060
3522.1	3.10592	.13145	.64092
3534.5	3.11689	.12095	.63765
3546.9	3.12785	.10827	.65580
3559.4	3.13882	.09406	.71008
3571.8	3.14978	.07995	.80400
3584.2	3.16074	.06685	.93457
3596.6	3.17171	.05489	1.09523
3609.1	3.18267	.04260	1.30914
3621.5	3.19363	.02519	1.96392
3633.9	3.20460	.00233	19.07532
3646.4	3.21556	.11438	-1.87964
3658.8	3.22653	.09248	-.99031
3671.2	3.23749	.07858	-.76612

THE FOLLOWING ARE VALUES INTERPOLATED AT SLOPE OF N=0.0

NMIN= .63752
TAU(MS)= .12561
(OMGA)D= 3.11224
FC(CPS)= 3529.12

4.3, Illustrative Design Problems (cont.)

Example 11: Nonlinear Combustion Response Analysis

For this case, the first tangential mode will be examined using a deadband nonlinear element. In addition to the above injector data, the following additional information will be used:

$$P_{\infty} = 1.0$$

$$TFLP = 1.0$$

The data package is shown in Table 9 and the output is shown in Table 12.

Table 12 --- Output of Nonlinear Mode Example Problem

```

DATE      03 NOV 69      T LODE2 RHOWING EFFECTS OF DEADBAND-NONLINEARITY
A   B   C   D   E   F   G   H   I   J
0.   0.   0.   0.  200.  0.   0.   0.   50.   0.

***** THE FOLLOWING MAIN CONTROL DATA WILL BE USED IN THIS CASE *****
RATIO OF SPECIFIC HEAT (GAMMA) = 1.2180
DESIRED MACH NUMBER = .00000 (=0 IF BEING CALCULATED)
CHAMBER RADIUS = 6.400 (INCHES)
CHAMBER LENGTH = 14.800 (INCHES)
SPEED OF SOUND = 3800.000 (FT/SEC)
CHAMBER MODE DESCRIPTION = 1.84118 (=0 FOR LONGITUDINAL MODES)

***** CHAMBER FREQUENCIES (WC) *****
1.69389      1.73071      1.76754      1.80436      1.84118
1.87801      1.91483      1.95165      1.98848      2.02530

***** MACH DISTRIBUTION IN CHAMBER AS A FUNCTION OF LENGTH *****
CHAMBER      MACH      CHAMBER      MACH      MACH
LENGTH        DISTRIBUTION      LENGTH      DISTRIBUTION      DISTRIBUTION
.00000        .00000        6.40000        6.39500        25.00000        6.40000
2.50000        2.50000        6.41000        6.40000        50.00000        6.40000
5.00000        5.00000        6.42000        6.40000        .00000        .00000
6.30000        6.30000        6.43000        6.40000        .00000        .00000
6.35000        6.35000        6.50000        6.40000        .00000        .00000
6.38000        6.38000        7.50000        6.40000        .00000        .00000
6.39000        6.39000        12.50000        6.40000

```

Table 12 --- Output of Nonlinear Mode Example Problem (cont.)

DATE 03 NOV 69 T LODE2 SHOWING EFFECTS OF DEADBAND NONLINEARITY

INPUT TO INJECTION DISTRIBUTION PROGRAM

CONSTANTS

NUMBER OF OMEGAS = 6

NUMBER OF ELEMENTS = 3 FOR EACH OF 180 SYMMETRIC SECTIONS.

RADIAL DIVISIONS(XM) = 20.

ANGULAR DIVISIONS (XN) = 180.

ACOUSTIC MODE NUMBER(SVN) = 1.8412

ORDER OF BESSEL FUNCTIONS(V) = 1.

INJECTOR RADIUS = 6.400, IN.

RATIO OF SPECIFIC HEATS(GAMMA) = 1.2180

MAXIMUM PRESSURE AMPLITUDE RATIO(P00) = 1.000

TRANSFER FUNCTIONS FOR LINEAR OPERATION

PRESSURE(TFLP) = .000

RADIAL VELOCITY(TFLR) = 1.000

TANGENTIAL VELOCITY(TFLT) = .000

INPUT FREQUENCIES

1.6939	1.7675	1.8412	1.9148	1.9885
2.0253				

Table 12 -- Output of Nonlinear Mode Example Problem (cont.)

DATE 03 NOV 69 T LODE2 SHOWING EFFECTS OF DEADBAND NONLINEARITY

ELEMENT INFORMATION

ELEMENT NO.	RADIUS IN.	ANGLE RADIAN	DISTRIBUTION COEFFICIENT MU
1	2.000	.0175	4.4444
2	4.000	.0175	7.7778
3	6.000	.0175	7.7778

Page 151

Table 12 -- Output of Nonlinear Mode Example Problem (cont.)

DATE	03 NOV 69	T LODE2 SHOWING EFFECTS OF DEADBAND NONLINEARITY					
RESULTS OF DESCRIBING FUNCTION							
OMEGA	ELEMENT NO.	RADIUS	ANGLE RAD	FRACTIONAL FLOW-RATE	FP	FR	FT
1.6939	1	.313	.0175	.00123	1.000000	.678814	1.000000
1.6939	2	.625	.0175	.00216	1.000000	.493693	1.000000
1.6939	3	.938	.0175	.00216	1.000000	.000000	1.000000

Table 12 --- Output of Nonlinear Mode Example Problem (cont.)

DATE	03 NOV 69	T LODE2 SHOWING EFFECTS OF DEADBAND NONLINEARITY						
RESULTS OF DESCRIBING FUNCTION								
OMEGA	ELEMENT NO.	RADIUS	ANGLE RAD	FRACTIONAL FLOW-RATE	FP	FR	FT	
1.7675	1	.313	.0175	.00123	1.000000	.665192	1.000000	
1.7675	2	.625	.0175	.00216	1.000000	.472795	1.000000	
1.7675	3	.938	.0175	.00216	1.000000	.000000	1.000000	

Table 12 --- Output of Nonlinear Mode Example Problem (cont.)

DATE	03 NOV 69	T LODE2 SHOWING EFFECTS OF DEADBAND NONLINEARITY						
RESULTS OF DESCRIBING FUNCTION								
OMEGA	ELEMENT NO.	RADIUS	ANGLE RAD	FRACTIONAL FLOW-RATE	FP	FR	FT	
1.8412	1	.313	.0175	.00123	1.000000	.651640	1.000000	
1.8412	2	.625	.0175	.00216	1.000000	.452589	1.000000	
1.8412	3	.938	.0175	.00216	1.000000	.000000	1.000000	

Table 12 --- Output of Nonlinear Mode Example Problem (cont.)

DATE	03 NOV 69	T LODE2 SHOWING EFFECTS OF DEADBAND NONLINEARITY						
RESULTS OF DESCRIBING FUNCTION								
	OMEGA	ELEMENT NO.	RADIUS	ANGLE RAD	FRACTIONAL FLOW-RATE	FP	FR	FT
	1.9148	1	.313	.0175	.00123	1.000000	.637977	1.000000
	1.9148	2	.625	.0175	.00216	1.000000	.432330	1.000000
	1.9148	3	.938	.0175	.00216	1.000000	.000000	1.000000

Table 12 --- Output of Nonlinear Mode Example Problem (cont.)

DATE	03 NOV 69	T LODE2 SHOWING EFFECTS OF DEADBAND NONLINEARITY						
RESULTS OF DESCRIBING FUNCTION								
OMEGA	ELEMENT NO.	RADIUS	ANGLE RAD	FRACTIONAL FLOW-RATE	FP	FR	FT	
1.9885	1	.313	.0175	.00123	1.000000	.624504	1.000000	
1.9885	2	.625	.0175	.00216	1.000000	.412330	1.000000	
1.9885	3	.938	.0175	.00216	1.000000	.000000	1.000000	

Table 12 --- Output of Nonlinear Mode Example Problem (cont.)

DATE	03 NOV 69	T LODE2 SHOWING EFFECTS OF DEADBAND NONLINEARITY						
RESULTS OF DESCRIBING FUNCTION								
OMEGA	ELEMENT NO.	RADIUS	ANGLE RAD	FRACTIONAL FLOW-RATE	FP	FR	FT	
2.0253	1	.313	.0175	.00123	1.000000	.617796		1.000000
2.0253	2	.625	.0175	.00216	1.000000	.402424		1.000000
2.0253	3	.938	.0175	.00216	1.000000	.000000		1.000000

Table 12 -- Output of Nonlinear Mode Example Problem (cont.)

DATE	03 NOV 69	T LODE2 RHOWING EFFECTS OF DEADBAND NONLINEARITY					
RESULTS OF INJECTION DISTRIBUTION EFFECTS							
	OMEGA	AVN REAL	BVN REAL	CVN REAL	CVN IMAG		
	1.6939	1.2745	.4300.	.0000	-1.8125		
	1.7675	1.2745	.4158	.0000	-1.8125		
	1.8412	1.2745	.4020	.0000	-1.8125		
	1.9148	1.2745	.3881	.0000	-1.8125		
	1.9885	1.2745	.3744	.0000	-1.8125		
	2.0253	1.2745	.3676	.0000	-1.8125		
		***** THESE VALUES PERTAIN TO A SPINNING MODE *****					

5. STABILIZATION DEVICES

In a sense, any combustion system for a rocket engine is potentially unstable. It may even be true that all high-performing systems require some measure of supplemental damping besides that afforded by the nozzle. This view is emphasized by the illustrative problems presented in Section 3, where only the exotic designs were manageable solely by controlling the injector pattern and the nozzle admittance, and these only at the expense of a potential degradation in performance.

Stabilization devices have been employed in all major systems since the second generation ballistic missiles. They should be viewed by the designer, therefore, not as a crutch to a workable system that has exhibited a latent defect, but as an essential component which supplies stability in the same way that the injector supplies propellants and the nozzle supplies thrust.

Baffles are the stabilizer most frequently employed because they are relatively simple to design and can be installed in a system already operating without major redesign. The only significant alternative to baffles is the acoustic liner. Compared to baffles, this device is relatively new, and while theoretically quite feasible, has not been utilized as extensively. Moreover, it has the disadvantage with respect to existing systems of requiring inclusion in the original design before the chamber geometry, fabrication technique, and cooling system have become fixed.

The balance of Section 5 is a detailed review of the state-of-the-art as it relates to baffles and liners.

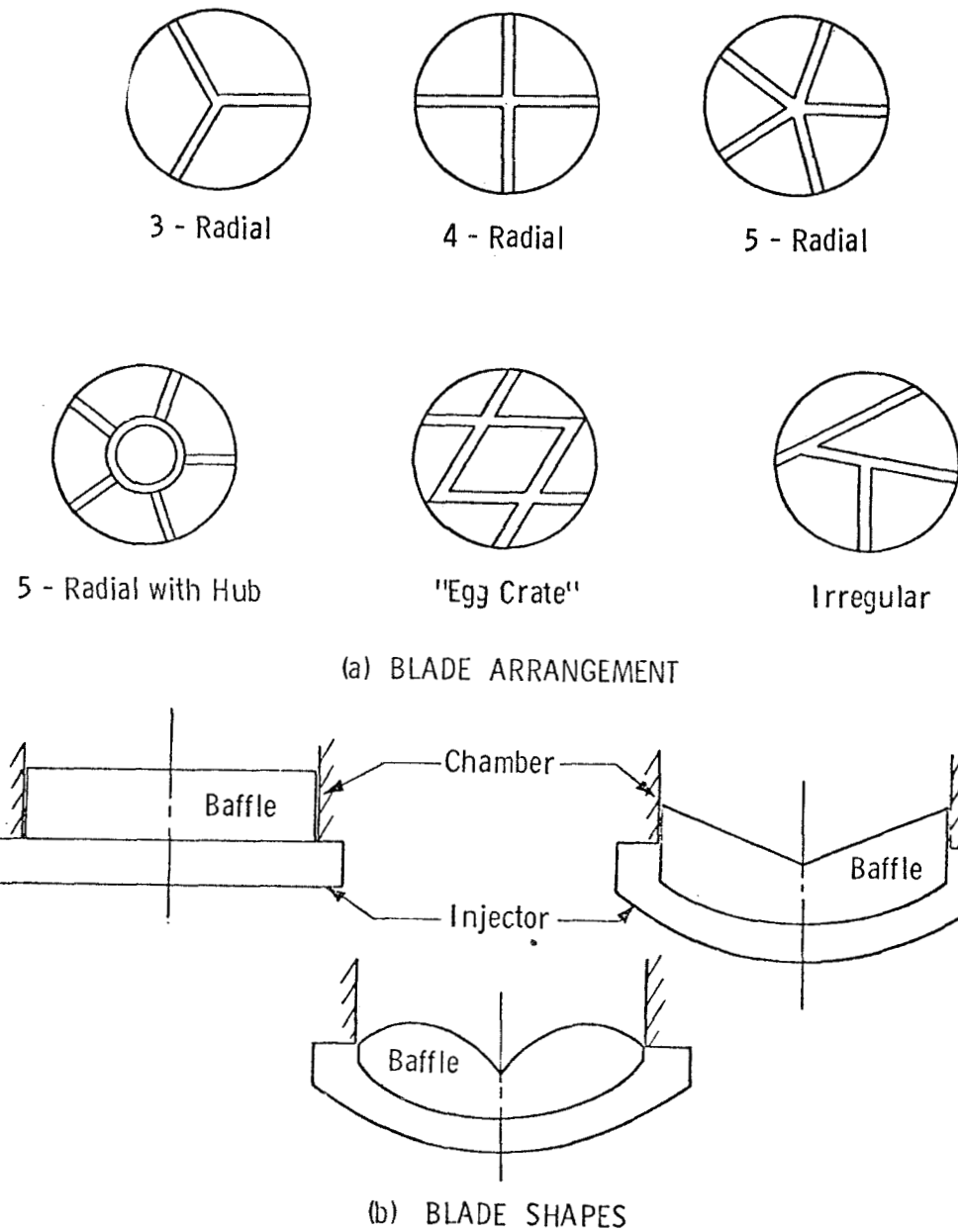


Figure 23 -- Baffle Shapes and Blade Arrangements

5, Stabilization Devices (cont.)

5.1 BAFFLES

There are innumerable baffle configurations possible, not all of which can be covered in this text. Therefore, emphasis is placed on understanding the underlying principles of baffle design in order that the designer be able to extend the basic concepts of baffle design to new and original designs.

5.1.1 Principles Governing Baffle Design

Injector-face baffles are intended as a damping device for the high frequency modes of instability referred to in Section 3 as the transverse modes and are characterized by acoustic oscillation parallel to the injector face. In a cylindrical chamber, the acoustic pressure and velocity vary in both the radial and circumferential directions for the tangential modes and only in the radial direction for the radial modes.

The tangential modes of instability can be further divided into spinning modes, which are the result of a single pressure wave traveling tangentially in either a clockwise or counterclockwise direction and a corresponding velocity perturbation in phase with the pressure, or standing modes, which consist of two counter-rotating waves with the velocity perturbation $\frac{90^\circ}{n}$ out of phase with the pressure in space dimensions.

The addition of baffles to a rocket engine prevents continuous motion of the gas particles in a tangential direction because the baffle, extending radially outward as shown in Figure 23, introduces a boundary condition incompatible with the spinning tangential mode. Therefore, it is the latter class of tangential instability, along with the radial modes, that are of major concern in the design of baffles.

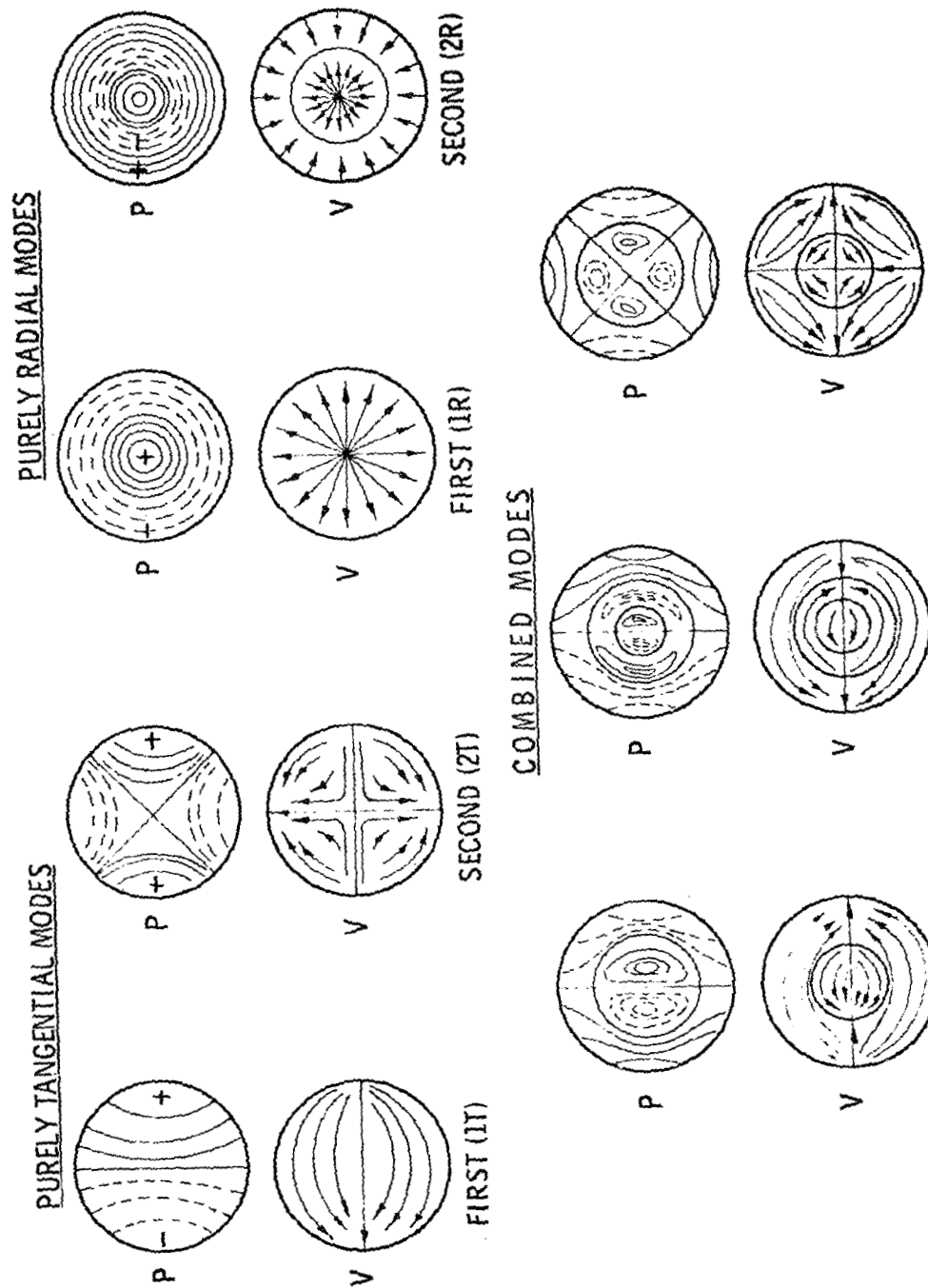


Figure 24 --- Transverse Mode Characteristics

5.1, Baffles (cont.)

The standing tangential and the radial modes of instability are depicted in Figure 24, which shows the particle paths and the pressure anti-nodes for the tangential and radial modes of the first and second order. Also shown are the three most common combined transverse modes: the first tangential-first radial; first tangential - second radial; and second tangential - first radial modes.

A number of references* discuss the pure transverse modes, as well as the combined tangential and radial modes. In general, the principles of design for baffles to damp the pure transverse modes apply equally well for the combined modes.

Of major concern in the design of an effective baffle is the location of the baffles relative to the particle paths, since the baffles constitute an obstruction to particle motion. There are a few general comments concerning the tangential modes that can be helpful in understanding baffle design. For example, with the exception of the first tangential mode the transverse velocity at the center of the injector is zero. In general, as the tangential modes become of higher order, the major motions and pressure variations of the gas particles are limited to the outer circumference of the chamber. This characteristic becomes important in considering placement of baffles to suppress the higher order modes. A second consideration is that each mode has its characteristic pattern of pressure and velocity gradients. The pattern of the specific mode for which correction is required should be analyzed in deciding on the placement of the baffles because what may suppress a tangential mode of one order may not be effective against modes of higher (or lower) order. (Cf Figure 10, Page 46 and discussion pp 43 ff.)

*See General References, Page 233

5.1, Baffles (cont.)

In the case of the pure radial modes, the velocity perturbations are limited to the radial direction, with the axis of symmetry being the chamber axis at the center of the injector and again, as in the case of the tangential modes of higher than the first order, no velocity perturbations occur at the center of the injector. The order of a radial mode is determined by the number of velocity antinodes, as shown in Figure 24.

The several stabilizing effects attributed to baffles can each be related to the physical characteristics of the baffle, such as baffle compartment size, baffle placement, and baffle length. However, it cannot be shown conclusively in which way the baffle produces its major stabilizing effect, because each effect is improved by altering the same physical dimensions of the baffle.

The mechanisms suggested by which baffles effect damping fall into three categories: (1) protection of the sensitive flame region (2) phase stabilization, (3) and gain stabilization, or increased damping. By protecting the sensitive flame region it is postulated that baffles make the precombustion processes (e.g., mixing and vaporization) less sensitive to perturbations. Phase stabilization results from significant changes in resonant acoustic modes of the combustion chamber so that the sensitive frequencies associated with the combustion process are not in resonance with the chamber modes. Two mechanisms have been adduced as the cause of gain stabilization, or increased damping: additional viscous losses resulting from the increased surface area introduced by the baffles; and the scattering of energy into other modes that are easily damped. The former is considered a second order effect.

5.1.2 Baffle Geometry

In the design of an effective blade arrangement it is necessary to provide a logical basis for the selection of the minimum or the maximum number

5.1, Baffles (cont.)

of baffle blades or hubs, and whether a symmetric or asymmetric blade arrangement should be used. Each of these is discussed in the following.

The optimum number of blades for any baffle configuration depends primarily on the mode of instability to which the system is most susceptible. For example, consider the first tangential mode illustrated in Figure 24. Of the three mechanisms by which baffles are postulated to produce stability, phase stabilization and gain stabilization are affected by the number of blades.

The phase and gain stabilizing characteristics depend upon the baffle system altering the acoustics properties of the combustion chamber by interfering with or altering the particle paths. Referring to Figure 25a, the selection for a symmetrical baffle configuration to damp a first tangential mode would be a three-bladed baffle. It is also apparent from Figure 25a that a one- or two-bladed baffle could, at the most, only cause the mode to stand in the baffle cavity with the velocity antinodes located 90° from the baffle. The same reasoning applied to a second tangential mode as depicted in Figure 25b indicates that a symmetrical three-bladed baffle would be effective and that the two- and one-bladed baffle would not be. Not as obvious but equally true, a symmetrical four-bladed baffle would have little or not effect because the mode can be contained within the baffle cavity with the velocity antinodes located 45° from the baffle radial legs.

Extension of these considerations to the higher order tangential modes leads to the generalization that a radial baffle system having an odd number of blades (with the exception of a single blade) would offer protection from modes which are of the order less than the number of blades and, to some degree, protection from modes of an order higher than the number of blades provided the order of the mode divided by the number of blades is not equal to an integer. This then gives the designer a criterion for the minimum number of blades required in the case of a symmetrical baffle system.

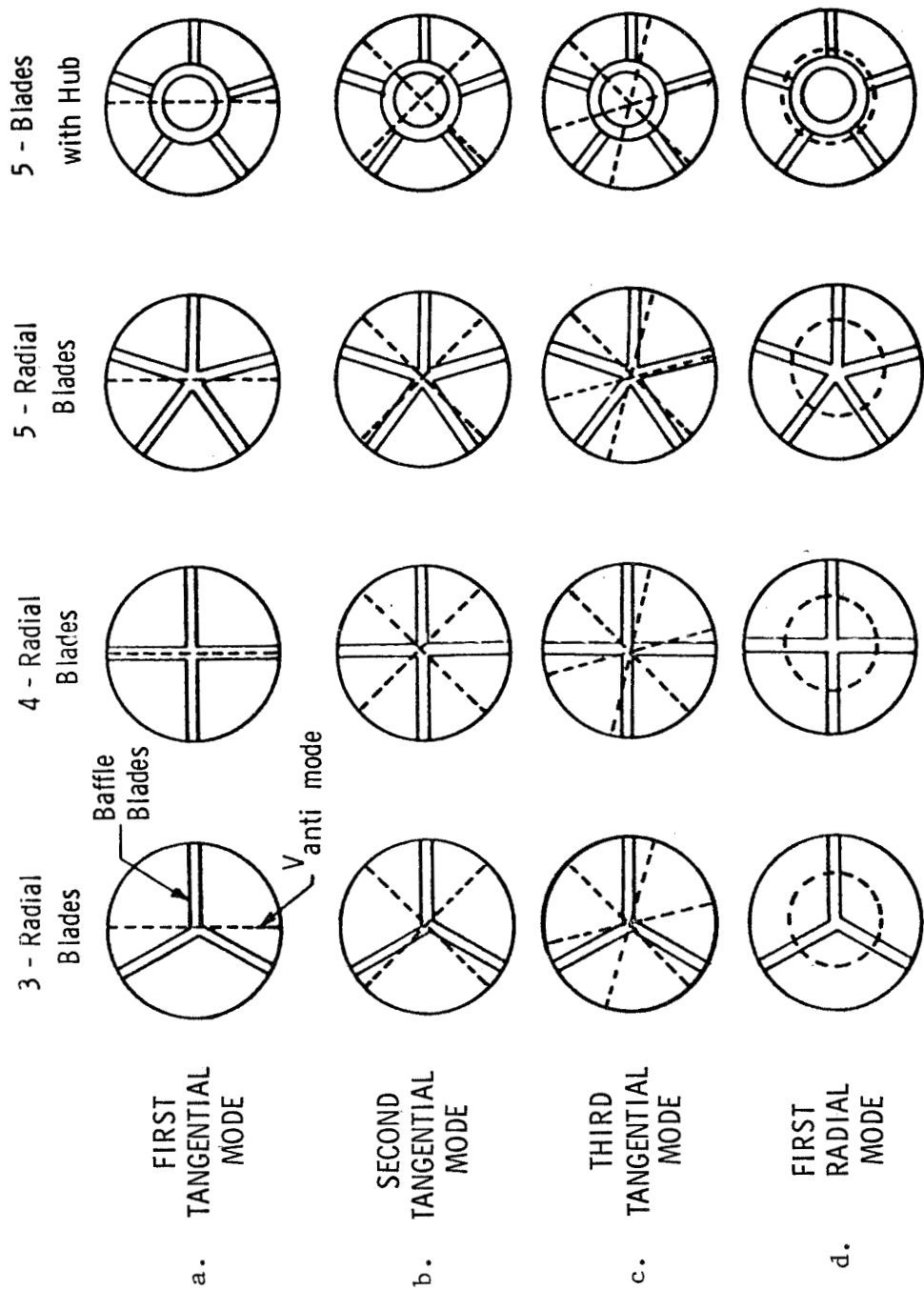


Figure 25 -- Possible Mode Orientations for Various Baffles

5.1 Baffles (cont.)

The generalization previously made only indicates the minimum number of blades required, but indicates nothing concerning the optimum number of blades to maximize damping and changing of chamber resonant frequencies. For example, in the case of Titan III, Stage I, satisfactory stabilization with respect to the 1T mode was reached only with a 7-blade baffle. Some resistance to the 1T and 2T modes was exhibited by a 5-blade baffle, but not enough to meet program requirements. For this information as to the most effective configuration we must turn to experimental data on the effects of baffle pocket size.

5.1.3 Design Optimization

Of interest to the injector designer is the trade-off between baffle length and compartment size because of system considerations such as heat transfer, performance, system pressure drop and compatibility. There are little quantitative data available; however, what are available indicate that, as might be expected, as the order of the mode approaches the number of baffles, the trade-off becomes quite significant in terms of gain stabilization, as can be seen from Figure 26.

These data, which are summarized in Figure 27, relate to the first tangential mode and are consistent with what would be expected. The boundary between the stable and unstable regions appears to be approaching asymptotically a horizontal line at a value of 0.92, which represents a baffle configuration having two blades which is compatible with the first tangential mode.

From the results shown in Figure 28, decreasing the baffle cavity characteristic dimension any further may, in fact, prove detrimental. Where the wave length (λ) is determined by the frequency of the first tangential mode (i.e., $\lambda = c/f$) the characteristic cavity dimension (w) is the

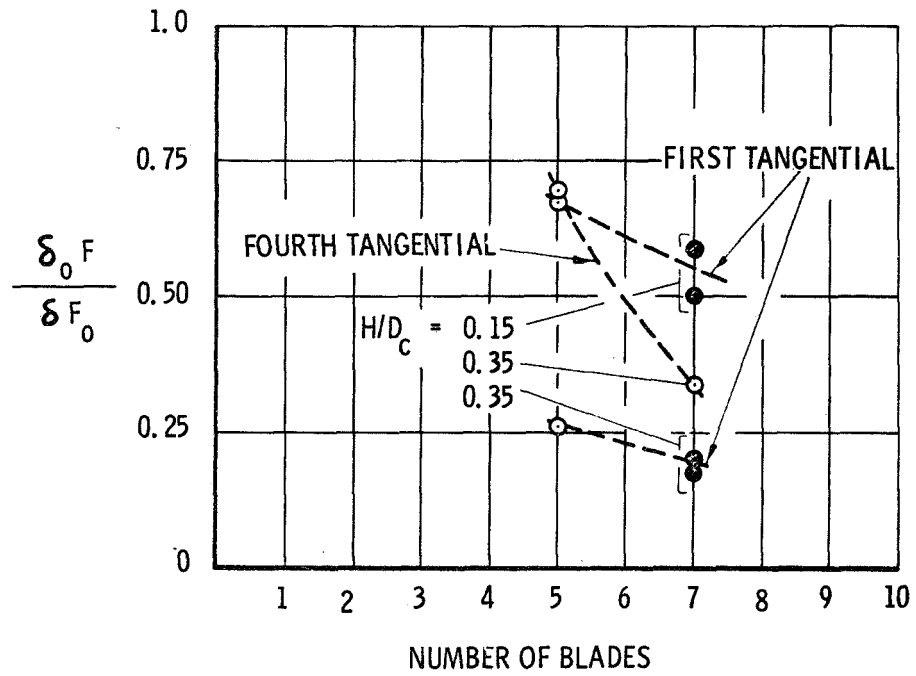


Figure 26 -- Effect of Number of Baffle Blades

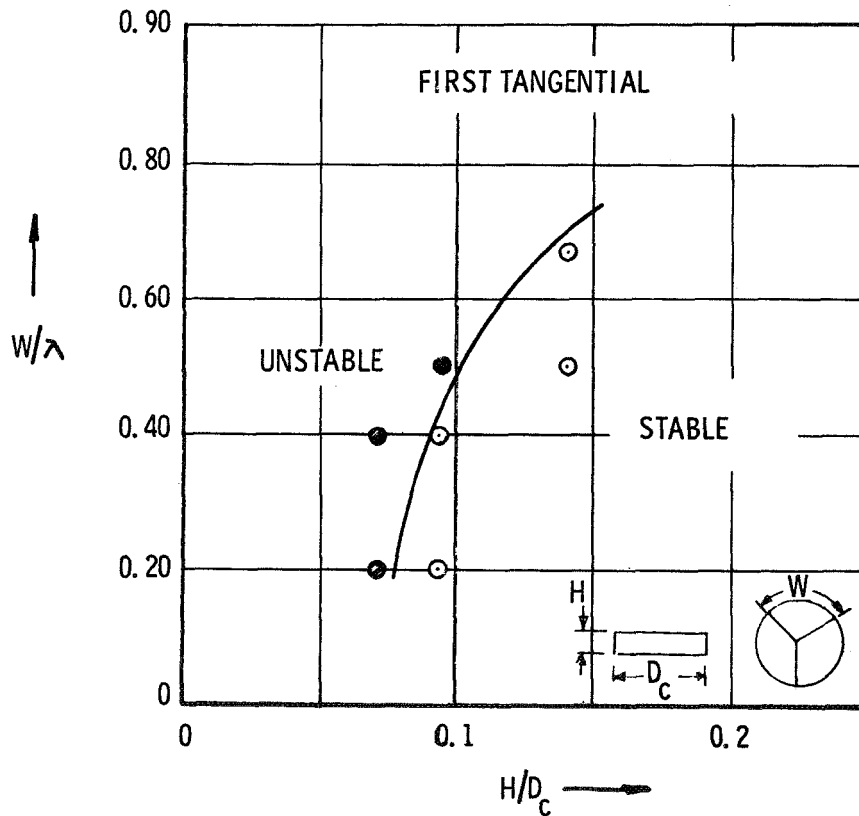


Figure 27 -- Effect of Baffle Spacing vs Baffle Length

5.1, Baffles (cont.)

circumferential distance between baffle legs at the chamber wall. Additional support for this conclusion can be found in Figures 29 and 30 where the degree of both gain and phase stabilization -- as indicated from acoustic tests -- was not significantly altered for the first tangential mode by going from a five-bladed symmetrical baffle ($w/\lambda = 0.37$) to a seven bladed baffle ($w/\lambda = 0.26$).

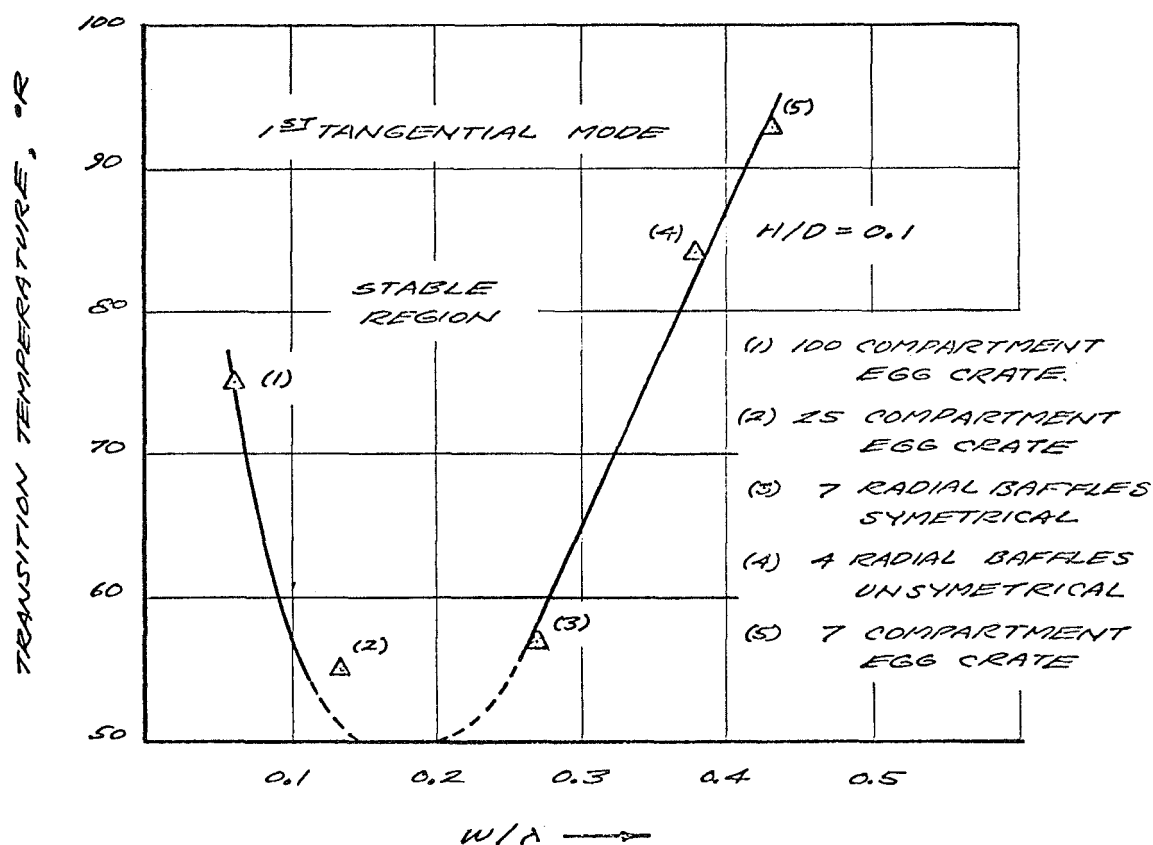


Figure 28 -- Effect of Baffle Spacing on First Tangential Mode

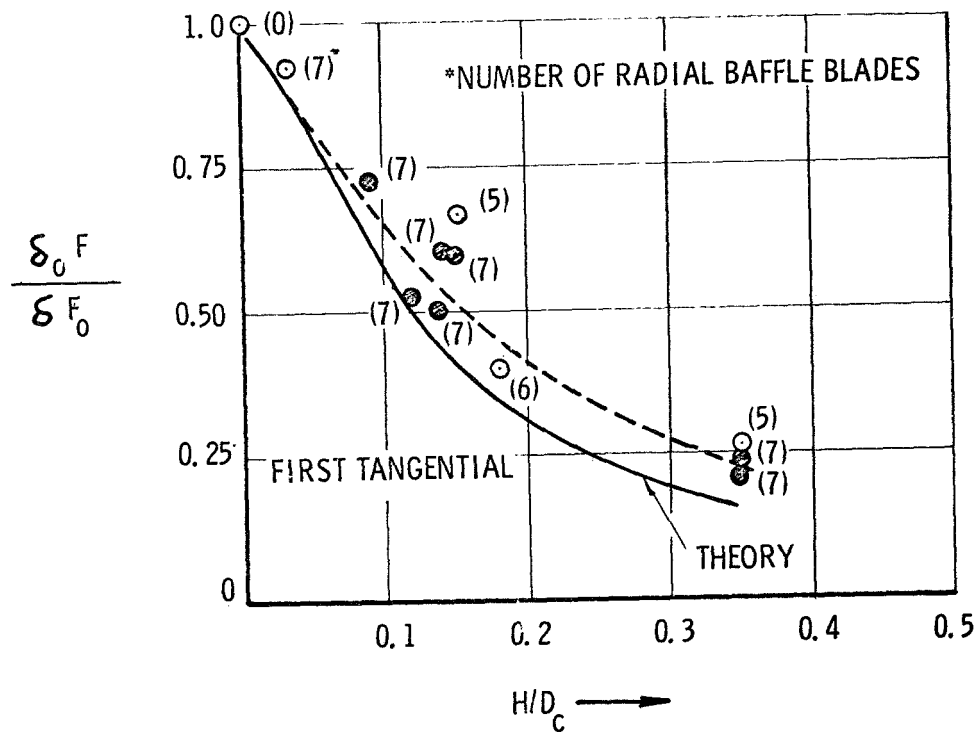


Figure 29 -- Damping versus Baffle Length and Number of Blades

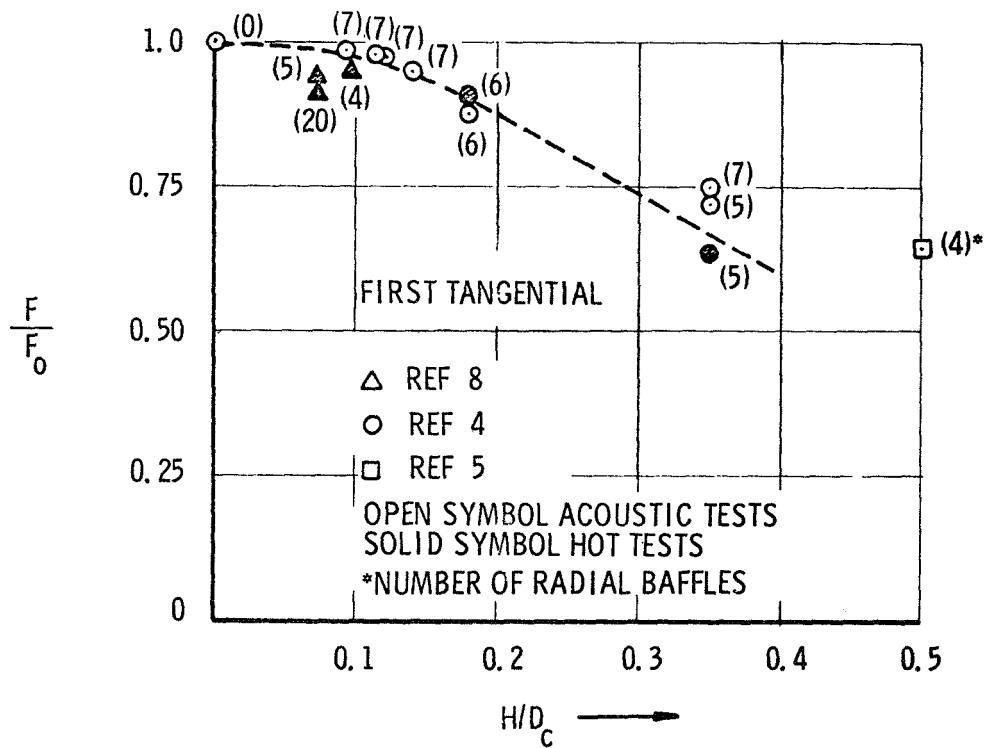


Figure 30 -- Frequency Depression versus Baffle Length

5.1, Baffles (cont.)

The discussion thus far has been limited to the tangential modes, principally the first tangential mode. However, there are data available which indicate that similar trends are present for the higher order tangential modes and the radial modes. For the radial modes, w is the maximum dimension along the chamber radius.

A possible explanation of the trend which indicates that excessively small baffle compartments can be detrimental is found in considering the limiting case where the baffle compartments are a series of close-open tubes which have cross-sectional dimensions in the order of $1/16$ wave length. For this case the baffles would exhibit the characteristics of a quarter-wave tube such as shown in Figure 31 which exhibits only narrow band effectiveness (high Q) and makes the baffle length a critical parameter. Acoustic data which support this observation can be found in the work by Wieber which has been included in Figure 32 along with data from Hannum.* The latter data are normalized by the hydrogen temperature at which the unbaffled injector went unstable (T_0). The Wieber data are normalized by the inverse of the decay rate (F_0/δ_0) for the unbaffled injector. Wieber evaluated a four-bladed baffle and a baffle configuration which consisted of an array of 65 solid posts, 3 inches in length and of varying diameter. The characteristic dimensions for the injector having the posts was determined by subtracting the total area of the cross-section of the posts from the area of the injector and dividing by 65, the characteristic dimension being the diameter of a circle having this area. Applying this method, values for the term w/λ range from 0.05 to 0.07, which is in the range of w/λ for the 100-compartment egg crate baffle, evaluated by Hannum. The two sets of results indicate the same trend, that too small a baffle compartment can be detrimental.

-
- *1. Wieber, P. R., "Acoustic Decay Coefficients of Simulated Rocket Combustors", Lewis Research Center, NASA TN D-3425, May 1966.
2. Hannum, N. P. Bloomer, H. E., and Goelz, R. R., "Stabilizing Effects of Several Injector Face Baffle Configurations on Screech in a 20,000 lb-Thrust Hydrogen-Oxygen Rocket", Lewis Research Center NASA TN D-4515, April 1968.

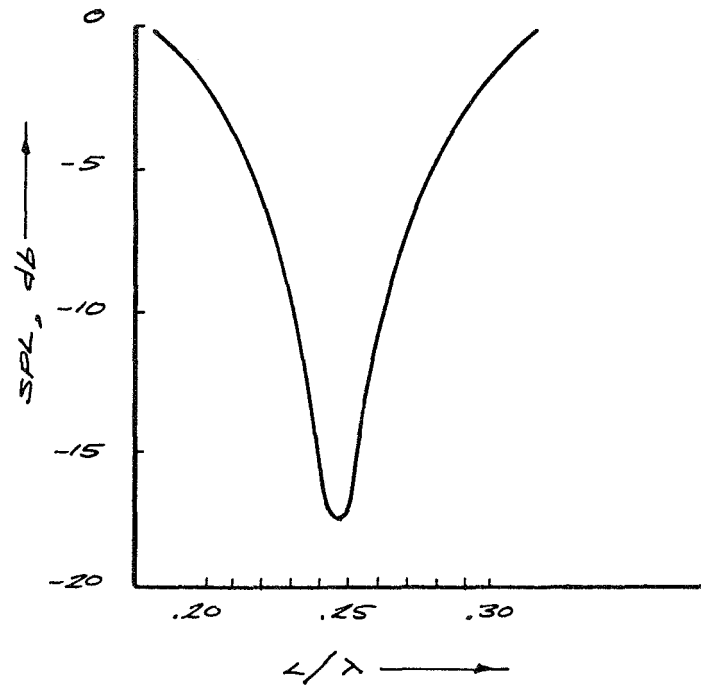


Figure 31 -- Attenuation in Closed-Open Tube

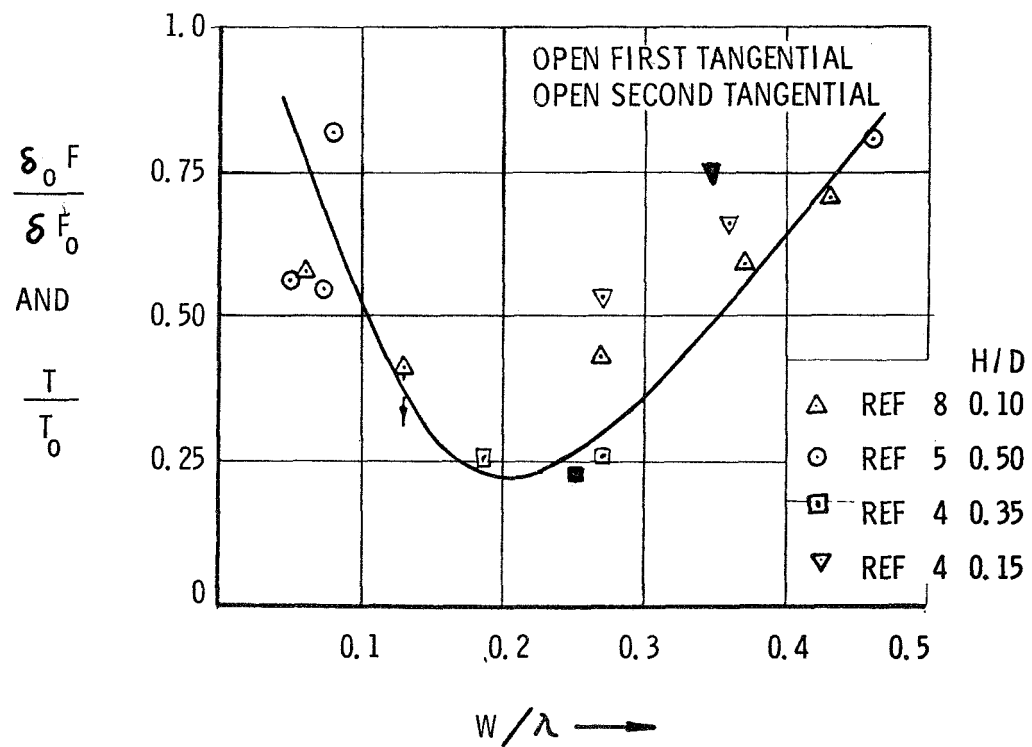


Figure 32 -- Rocket Spacing versus Damping

5.1, Baffles (cont.)

There is at present a tendency to use symmetrical baffles in rocket engines. This is primarily because of the difficulties associated with feeding coolants to an asymmetric baffle system from a feed system that is generally symmetric. However, some experimental work has been done with asymmetric baffles of the type shown in Figure 23. Several reasons have been stated as to why an asymmetric baffle system would be superior to a symmetric system, all of which basically revolve about the idea that asymmetrically placed baffles will "scatter" the energy generated in a random manner. No data have been accumulated on what could be considered a truly asymmetric baffle. However, some data are available on configurations in which the radial blades of the baffle have unequal sector angles or in which the baffle legs are directed in other than a radial direction. The results from tests with units of this type indicate no apparent superiority for this type of baffle over a symmetrical baffle having the same number of baffle blades.

5.1.4 Blade Design

One aspect of baffle design, the size of the baffle pocket, is discussed in Section 5.1.3. The data accumulated indicate that ratios of characteristic cavity dimension to wave length in the order of 0.20 is desirable, where the wave length is based on the frequency of the unstable mode and the characteristic dimension is defined as the average of the maximum circumferential dimension of each of the baffle cavities for the tangential modes of instability or the average of the maximum radial dimensions of the baffle cavities for the radial modes.

It is next necessary to determine the optimum baffle length and shape viewed from the side of the baffle, such as shown in Figure 23b and, finally, design considerations related to cooling of the baffles. The mean baffle height is defined by

5.1, Baffles (cont.)

$$H = \frac{1}{r_c} \int_0^{r_c} H(r) dr \quad \text{Eq. 27}$$

for the tangential modes. This definition is used throughout in defining baffle length and is reasonable for the configurations discussed. However, significant deviation from a baffle system in which the blades do not extend to the center of the chamber will require some judgement in specifying the baffle height since, in the case of the tangential modes, baffle height at the wall of the chamber is more effective in increasing phase and gain stabilization. This is because the major portion of the gas motion in tangential modes occurs near the chamber walls. This gas motion becomes more concentrated at the chamber wall as the order of the mode increases, which would indicate that the effective height may change, depending on the mode being considered.

On the evidence of acoustics as represented in Figure 29, it is indicated that the baffle length has the maximum effect on gain as the ratio of the baffle height to the chamber diameter approaches 0.10. Increasing this ratio to 0.30 adds only 25% to the damping, or the rate of increase in damping is reduced by a half, and from this point very little increase in damping is realized. Similar trends have been noted in test firing data, which are also presented in Figure 29.

However, a word of caution is warranted. Consider the feedback mechanisms such as those proposed by Dykema and Priem, discussed in Appendix A. Response curves from these mechanisms are typically of the shape depicted in Figure 33. It can be deduced that, if the unbaffled resonance of the chamber is to the left of the peak response, increasing the baffle length will indeed increase the stability of the system in both a phase and gain stabilizing manner. However, if the unbaffled resonance is to the right of the peak

5.1, Baffles (cont.)

response of the controlling feedback mechanism and if the rate of increase in gain for this mechanism as a function of frequency is greater than the damping increase due to increasing the baffle length, the system will become less stable.

The relationship of injector element design to the effectiveness of a given baffle can be found in the data obtained from GEMSIP where both a seven and a five-bladed baffle configuration, having the acoustic characteristics

indicated in Figures 29 and 30, exhibited dynamically stable combustion characteristics when tested with a coarse injector pattern. This same configuration, when tested with a fine injector pattern, failed to stabilize combustion. This shows the necessity for considering the injector pattern characteristics in the design of the baffles. The designer must in his selection of an injector-baffle system use an analytical technique such as discussed in Section 3.1 to determine, as a minimum, the sensitive frequency range of his candidate patterns, and evaluate how the baffles will alter the chamber resonances relative to the estimated sensitive frequency. Although this technique will not necessarily insure the design of a stable system, it will minimize the amount of development work required.

Consider now the stabilizing aspect of a baffle attributed to protection of the sensitive flame zone. This mechanism was postulated from observation of the combustion process in a transparent thrust chamber. In these experiments it was noted that a certain length of baffle was required to

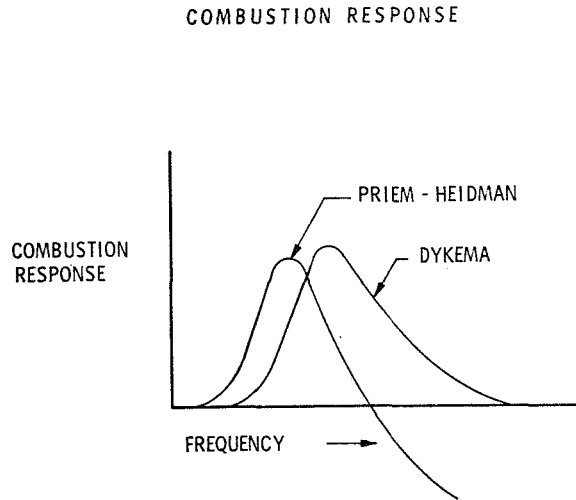


Figure 33 -- Combustion Response

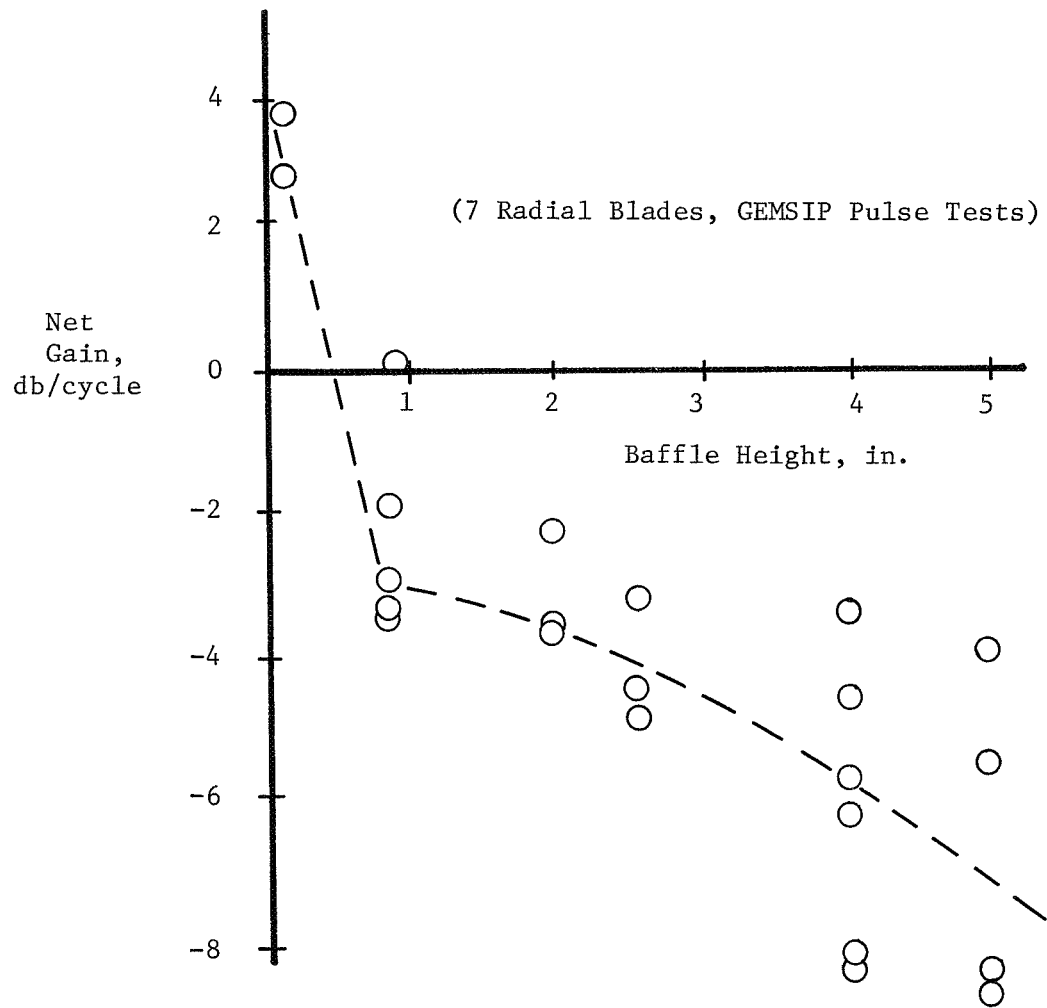


Figure 34 -- Decay Rate vs Baffle Height (Effect on Flame Zone)

5.1, Baffles (cont.)

minimize the interaction between adjacent streams of propellants when perturbed by a bomb. From the observations it was concluded that baffle lengths which covered 70 to 80% of the combustion zone were most effective in reducing stream interaction. Additional support can be found for this mechanism in the data presented by Hefner* where he postulated that the initial high decay rate with baffle length measured from test firing data (Figure 34) was significantly greater than that measured in acoustic tests at room temperature and therefore could be attributed to the concept of flame zone protection. From the data available it is apparent that selection of a baffle length that produces the optimum phase and gain stabilizing effects should likewise be sufficient to satisfy the baffle length criterion for the flame zone protection concept, since the major portion of the combustion occurs within two to three inches of the face. This criterion of flame zone protection may not be satisfied for small diameter chambers. However, where baffles have been selected for small engines on the basis of the phase and gain stabilization criteria, success has been possible. In these cases the baffle lengths were in the order of 1/4 inch and the injector patterns were very fine.

Data on the acoustic effects of baffle shape are limited to that reported by Wieber** and others. In the case of the Wieber data, the change in baffle shape was the result of a change in the contour of the injector face. The test results are not conclusive because the variation in the contour of the injector face itself has a significant effect on the decay rates measured, making the effect of baffle shape difficult to interpret. However, the results do indicate that based on the average height, as determined using the relationship given by Equation 27, the baffle is more effective.

*Hefner, R. J., "A Review of the Combustion Dynamics Aspects of the Gemini Stability Improvement Program", Second Combustion Conference, CPIA Publication 105, Volume 1, pp 13-22, May 1966.

**Wieber, op cit.

5.1, Baffles (cont.)

The same trend is indicated in the case of the data from GEMSIP. However, the variations in the baffle shape are not significant, making correlations between the baffle shape and the damping characteristics impractical. Additional work in this area is required. The trends indicated are consistent with the observation made earlier that the major gas motion for the tangential modes occur at the chamber wall. This effect becomes more noticeable for the higher order modes.

The effectiveness of radial baffles extending approximately 1/3 the chamber radius from the chamber wall has been demonstrated by Moberg with a 1750-lb-thrust engine. In this demonstration, dynamic stability was not evaluated.

From the discussion and data presented the following general rules can be used in designing a baffle.

1. An odd number of baffle blades is best for the tangential modes. The order of the mode divided by the number of blades should not be an interger.
2. For the radial modes, hubs located at the velocity antinodes, indicated in Figure 25, are best. The minimum number of hubs required is equal to the order-of-the-mode (i.e., 1st radial requires one hub).
3. Making the baffle compartments too small may be detrimental. A baffle characteristic cavity dimension (w) in the range $0.4 > \frac{w}{\lambda} \leq 0.2$ where $\lambda = \frac{c}{f}$ appears to be most desirable.

5.1, Baffles (cont.)

4. Ratios of baffle length to chamber diameter in the range of 0.2 to 0.3 appear to be optimum.

An example is given to show how a designer applies these rules.

Example 12: Design Baffle to Suppress Transverse Mode

Assume that the injector pattern and propellant combination has been found to have its greatest frequency sensitivity (i.e., peak response) at 3400 Hz. This value for f_s may have been determined analytically from Section 3 or experimentally from test data such as obtained from the transverse excitation chamber discussed in Section 6.

Inserting this frequency (f_s) into the wave equation together with the speed of sound (a) for the combustion gases (approximately 5000 ft/sec for H_2/O_2) one can calculate the wave length (λ).

$$\lambda = \frac{a}{f_s} = 1.5 \text{ ft}$$

Assuming that the chamber diameter is 10.4 in., the frequency of 3400 Hz corresponds to the first tangential mode.

From Recommendation 3 the baffle spacing, w , should be in the range of 3.6 in. to 7.2 in. Since w for the first tangential mode is the circumferential distance between the radial baffle legs, this yields a minimum of 5 and a maximum of 9 for the number of baffles. In accordance with Recommendation 1 an odd number of baffles is advisable. A nominal value of seven appears to be a reasonable choice. From Recommendation 4 the baffle height should be between 2 in. and 3 in.

5.1, Baffles (cont.)

5.1.5 Other Design Considerations

In addition to the stabilizing effects of baffles, consideration must be given to such factors as methods for baffle cooling, the effect that the baffle will have on performance, and the magnitude of the system pressure losses that can be attributed to the addition of baffles. Detail consideration of each of these factors is beyond the scope of this guide and is, in general, influenced by the injector systems in which the baffles are to be installed. However, some discussion is warranted.

The effect of baffles on the performance of rocket engines has never been documented in the open literature; however, limited data are available for a few engine systems and they are summarized in Table 13 below.

Table 13 -- Effect of Baffles on Engine Performance

<u>System</u>	<u>Change in Specific Impulse (sec)</u>
Atlas	-0.3
Thor	+1.1
F-1	+5.3
H-1	-0.5
Titan	-0.9 (Stage I)
Titan	+5.0 (Stage II)

Though these data would seem to indicate that there is no significant performance loss attendant to the addition of baffles to the injector, this conclusion must be tempered by the probability that the injector pattern was altered during the process. Since, with the addition of baffles, the system would be considerably less susceptible to instability, the injector

5.1, Baffles (cont.)

pattern could have been modified to produce more efficient combustion. The net result would be very little loss--or perhaps, even a small gain--in performance for the baffled system.

A survey of several engine systems indicates that a properly designed, regeneratively cooled baffle system will require an increase in the propellant feed pressure on the order of 7% of the chamber pressure in order to operate reliably. However, this is strongly dependent on the cooling technique used. For example, with tip-injecting baffles, the pressure drop in some cases has to be maintained at the same pressure drop as the matrix.

At least one set of experimental measurements of the thermal environment in which the baffle must operate is available, as well as several related articles on similar design problems with cooled chambers. The most complete set of baffle design cooling data is a result of work performed for GEMSIP. This experimental study of blade cooling utilized a highly instrumented water-cooled baffle. The significant results of this work are presented in Figures 35 and 36.

The first figure gives what is referred to as the calorimetric heat fluxes from three separate tests. The calorimetric heat flux, defined by

$$q/A = \frac{w_t C_p \Delta T_s}{A_s}, \quad \text{Eq. 28}$$

represents an average heat flux for a series of coolant channels located at various distances from the injector face. The values of heat flux are determined from the bulk temperature rise of the coolant in the individual channels. The variation in the heat flux as a function of the baffle length is apparently the result of combustion intensity, as a function of the distance from the

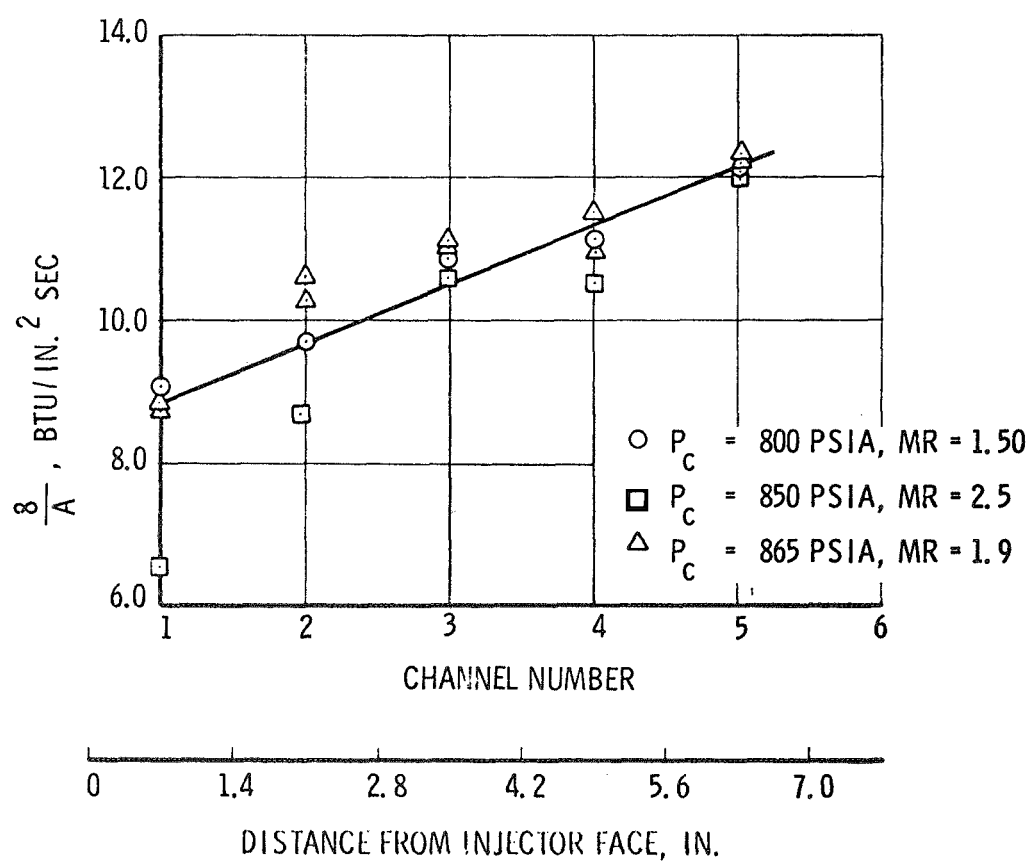


Figure 35 -- Calorimetric Heat Flux

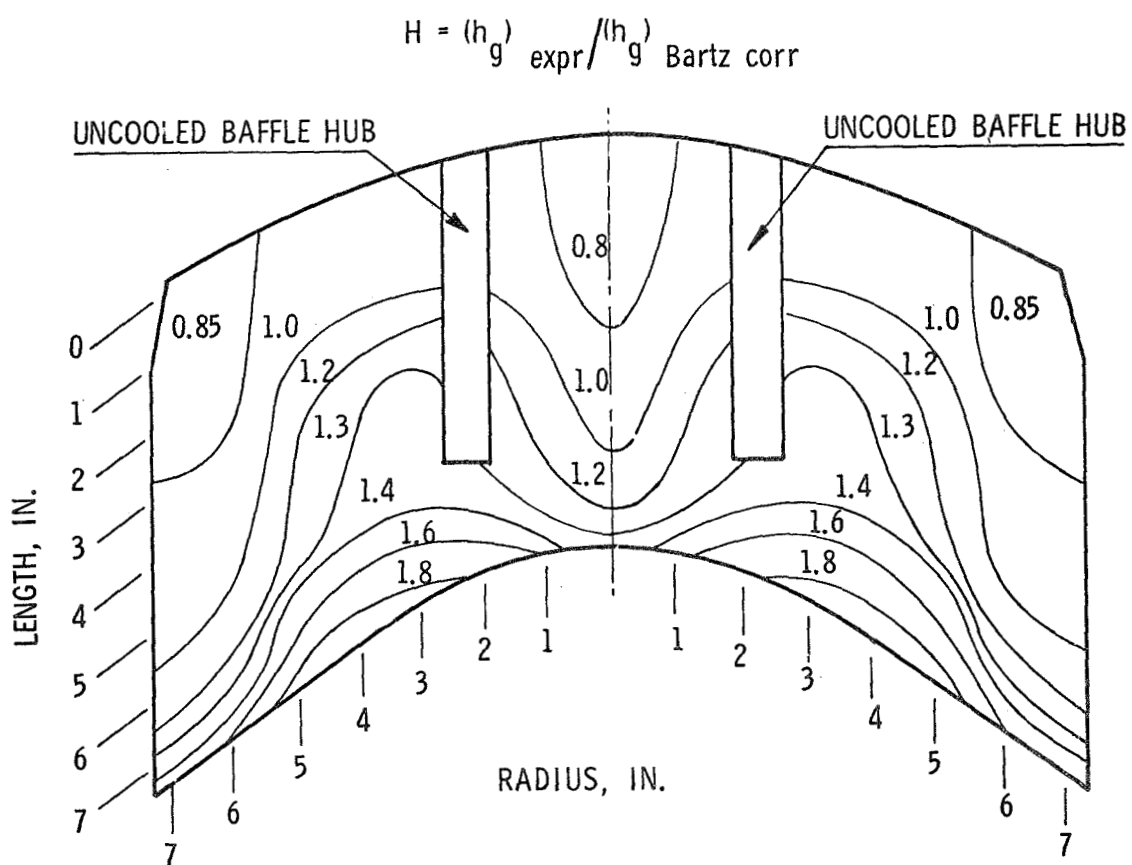


Figure 36 -- Gas Side Film Coefficient Profile

5.1, Baffles (cont.)

injector face. Perhaps the most significant observation from the data from the standpoint of the designer arises from the comparison of the predicted gas side film coefficients based on the simplified Bartz correlation defined by

$$h_{g(\text{Bartz})} = \frac{0.026}{D_e^{0.2}} \left(\frac{0.2 C_p}{P_r^{0.6}} \right) f \left(\frac{W}{A} \right)^{0.8} \left(\frac{T_s}{T_f} \right)^{0.8} \quad \text{Eq. 29}$$

where:

$$T_f = \frac{T_g + T_s}{2}$$

T_s is the static temperature defined by

$$T_s = \eta^3 T_o \quad ,$$

with the calculated film coefficient $h_{(\text{data})}$ defined by

$$\eta_{\text{data}} = \frac{q/A}{T_s - T_{g(\text{data})}}$$

Plotted in Figure 36 is the ratio of film coefficients (H) defined by

$$H = h_{g(\text{data})}/h_{g(\text{Bartz})} \quad \text{Eq. 30}$$

The results indicate that the gas-side film as estimated by the Bartz equation can be in error by as much as 50% on the low side. It should be noted that no film cooling was used on the experimental baffle.

In general, two methods have been used for cooling baffles, the first being a single-pass cooling system in which the coolant is discharged into the chamber at the tips of the baffle, and the second being a double-pass

5.1, Baffles (cont.)

system in which the coolant is returned through the baffle to the injector manifold and enters the combustion zone through the injector orifices.

The method of discharging the coolant from the tip of the baffle has been the subject of much discussion because it could introduce a secondary flame front downstream of the baffle and be detrimental to stability. Injector development data have in fact, indicated such a possibility; however, to date no conclusive evidence has been obtained.

5, Stabilization Devices (cont.)

5.2 ACOUSTIC LINERS

One manner of depressing or damping combustion oscillation in liquid rocket engines is through the use of an acoustic device based on the classical Helmholtz resonator, a sketch of which is shown in Figure 37. There have

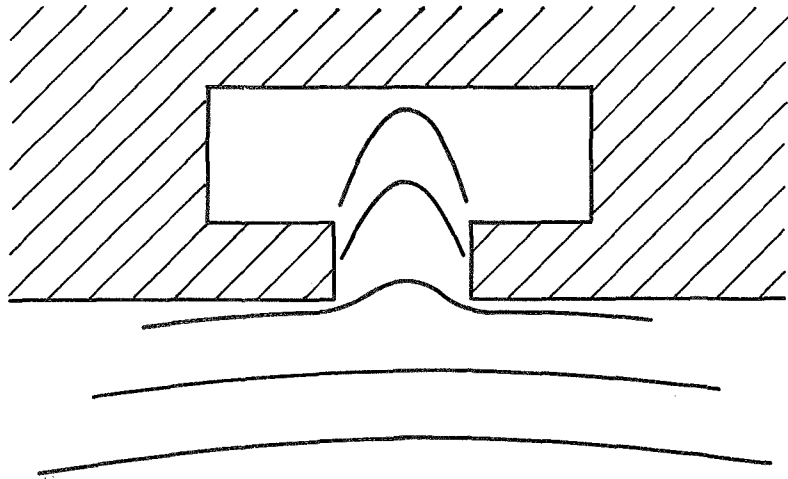


Figure 37 -- Helmholtz Resonator

been many applications of this method of stabilization and much discussion in the literature of the theory involved and the experience gained from a variety of programs. A bibliography of important theoretical and experimental work in this field follows this section. This bibliography will aid the designer by providing the basic information necessary to design and to evaluate a state-of-the-art acoustic liner for a liquid rocket engine. The essential concepts involved are introduced and discussed and an example design calculation is presented.

5.2, Acoustic Liners (cont.)

An acoustic liner is basically an array of Helmholtz resonators designed to damp an observed combustion oscillation. The liner departs from the resonator concept in that it is not mandatory that each resonator volume be physically separate from all other cavities. The usual practice is to have several resonator orifices opening on a common cavity whose volume is equivalent to the total volume of the several individual resonators. The liner generally includes only enough cavity separators to preclude any flow of combustion gases through the liner (i.e., in one orifice and out another). If flow through the resonator orifices were to occur, hot gas erosion could result in damage to the liner. In the case of tangential modes of instability the mode could also occur inside the resonator cavity and possibly add to the instability.

Another departure from the theoretical resonator concept is the use of openings as continuous slots instead of discrete orifices. Although a departure from the classic Helmholtz resonator, the analytical procedures remain the same.

Positioning of a liner or individual resonators must be dictated by the particular mode of instability observed. To have the maximum effectiveness, the liner should be positioned so as to present orifices at the point of maximum pressure oscillation. In the case of most transverse instabilities, the pressure maximum occurs at or near the chamber wall within a few inches of the injector face. It has been observed that liners which have been positioned in a chamber with the forward most row of elements several inches downstream of the injector have little or no effect on the instabilities. Although most work has been done with liners placed in the combustion chamber wall, some work has begun on placing resonators in the face of the injector in the region of the anticipated pressure maximum. The placement of the acoustic resonator in the injector face could detract from the area available for active injection elements; however, the installation is simpler.

5.2, Acoustic Liners (cont.)

One question which arises in the design of an acoustic liner is the number of elements required to damp an observed instability. There is no rule, postulate (experimental or theoretical), or mathematical formulation which will give a general answer to this question. The common procedure is to incorporate as much acoustic liner as physically possible. In order to reduce the size of the liner, a trial-and-error procedure must be followed.

A resonator must be "tuned" for resonance at the frequency of the combustion chamber pressure oscillation. The resonant frequency of a Helmholtz resonator is given by:

$$f = \frac{12 \times c_r}{2\pi} \sqrt{\frac{A_o}{\ell_{eff} V}} \quad \text{Eq 31}$$

where $\ell_{eff} = t + 0.85 d_o (1 - 0.7 \sqrt{\sigma})$

and

- f = resonator resonant frequency, Hertz
- c_r = γgRT = acoustic velocity of gases in resonator, ft/sec
- A_o = $\pi d_o^2/4$ = area of orifice, in.²
- d_o = resonator orifice diameter, in.
- V = resonator cavity volume, in.³
- ℓ_{eff} = effective length of resonator orifice, in.
- t = thickness of resonator wall, in.
- σ = open area ratio at the face of the resonator, A/A_f
- A_f = face area of resonator, in.²
- γ = ratio of specific heats of gases in resonator
- g = gravitational constant, ft/sec
- R = gas constant, ft-lb/lb °R
- T = absolute temperature of gases in resonator cavity, °R

5.2, Acoustic Liners (cont.)

The simple Helmholtz resonator can be discussed in terms of an analogous simple mechanical oscillator. The gas in the opening is considered to move as a unit and provides the mass element of the system. The stiffness element of the system is provided by the gas pressure in the cavity as it is alternately compressed and expanded by the influx and efflux of gas through the orifice. The resistance element is provided by a combination of viscous losses associated with the oscillating gases in the orifice and the dissipation of acoustic energy by the radiation of sound into the surrounding medium.

The mass term described above is a function of the orifice area, the average gas density and the effective length of the orifice. The use of an effective length rather than simply the physical orifice length is because some of the gases beyond the ends of the actual constriction move as a unit with the gas in the constriction or orifice. The formulation given in Equation 31 assumes that the flow along the face of the resonator has no effect on the oscillating gases. This is a valid assumption when designing resonators for applications near the injector where the axial velocity of the combustion gases has not become established.

An example of the application of the aforementioned equations follows:

Example 13: Design of Acoustic Resonator

It is first necessary to obtain the acoustic and thermodynamic conditions from design data or assumption and then fit the acoustic liner to these. For this particular example, it will be assumed that a combustor has been tested and found to operate with oscillatory combustion at a frequency of 1200 Hertz.

5.2, Acoustic Liners (cont.)

Next, in order to design the resonator itself, some physical design constraints and assumptions must be fixed. A cavity gas temperature and composition must be assumed (unless there are pertinent data available) to calculate the acoustic velocity in the cavity. For this purpose it will be assumed that the cavity acoustic velocity is 2400 ft/sec.

Thirdly, the geometry of the resonator must often be designed to conform to an existing chamber configuration; i.e., the resonator is often fitted to a chamber subsequent to the final design and manufacture. This may limit volumetrically the amount of liner which can be considered in the original design. Another example of a physical design constraint is the thickness of the face (or length of the orifice). From a resonator standpoint, it is often desired to have a short orifice length and, hence, a thin wall on the liner face. A thin-walled resonator will generally have higher effectiveness than a thick-walled resonator tuned for the same conditions. For other reasons, however, the walls may need to be thicker than desired and the design compromised from an acoustic standpoint. For example, due to the elevated thermal environment to which a liner is necessarily exposed, the wall of a resonator must be designed more from a stress and heat transfer point of view than from combustion stability considerations. Keeping the above restrictions in mind, assume that the example design requires a wall 0.40 in. thick for the face of the resonator and that there is a maximum available volume of 19.35 in.³ for the installation of this liner.

Now assuming an open area ratio of 2 percent and an orifice diameter of 0.13 in., the size of the resonator element of the liner can be calculated from the following equation:

$$\begin{aligned} \ell_{\text{eff}} &= t + 0.85 (d_o) (1 - 0.7 \sqrt{\sigma}) \\ &= 0.40 + 0.85 (0.13) (1 - 0.7 \sqrt{0.02}) \\ &= 0.50 \text{ in.} \end{aligned}$$

5.2, Acoustic Liners (cont.)

Then from Equation 31

$$f = \frac{12 \times c_r}{2\pi} \sqrt{\frac{A_o}{\ell_{eff} V}}$$

or

$$\begin{aligned} V &= \left(\frac{12 \times C_r}{2\pi f} \right)^2 \frac{A_o}{\ell_{eff}} \\ &= \left(\frac{12 \times 2400}{2\pi \times 1200} \right)^2 \frac{\pi/4 (0.13)^2}{0.50} \\ &= 0.387 \text{ in.}^3 \end{aligned}$$

Therefore, since there was a maximum of 19.35 in.³ available in the system for the liner cavity and each resonator element requires 0.387 in.³, there will be room for only 50 elements in an array so arranged to maintain the specified open area ratio of 2 percent.

The foregoing example has been designed to illustrate the basic principles using an extremely simplified set of restrictions and assumptions. Nothing has been said, for example, about the bandwidth effectiveness of a resonator design, i.e., the frequency spectrum over which any resonator or liner will be effective in damping a pressure oscillation. This would be extremely important in the case where, instead of one mode of unstable operation, there are two or more modes predicted. Accordingly, it is necessary to know if it can be expected that all modes can be controlled by a liner designed for a single resonant frequency or if, in fact, a liner tuned to several frequencies must be designed. These problems are very specific in nature and are most often unique. The designer is therefore directed to the bibliography for further and more detailed information.

BIBLIOGRAPHY FOR DESIGN OF ACOUSTIC LINERS

1. Anonymous, Absorbing Liners for Rocket Combustion Chambers - Theory and Design Techniques, Pratt and Whitney Aircraft, PWA FR 2007, Florida Research and Development Center, AFRPL-TR-66-234.
2. Anonymous, A Study of the Suppression of Combustion Oscillations with Mechanical Damping Devices Pratt and Whitney Aircraft, Report FR-1007, September 1964.
3. Bailey, Curtis R.; An Investigation of the Use of Acoustic Energy Absorbers to Damp LOX/RP-1 Combustion Oscillations. NASA TN D-4210, November 1967.
4. Beranek, L. L., Acoustics, McGraw-Hill, Inc., New York, 1952.
5. Blackman, A. W.; "Effect of Nonlinear Losses on the Design of Absorbers for Combustion Instabilities." ARSJ., Vol. 30, No. 11, November 1960, 11 1022-1028.
6. Bucher, R. E., "A Mathematical Analysis of the Suppression of High Frequency Combustion Instabilities by a Sound Absorbing Liner". AIAA 2nd Aerospace Sciences Meeting, Paper No. 65-107, New York, N. Y., January 1965.
7. Conrad, E. William; Bloomer, Harry E.; Wanhainer, John P., and Vincent, David D.; Interim Summary of Liquid Rocket Acoustic-Mode-Instability Studies at a Nominal Thrust of 20,000 Pounds. NASA TN-D-4968, December 1968.
8. Culick, Fred E., Stability of High Frequency Oscillations in Gas and Liquid Rocket Combustion Chamber, TR 480, Massachusetts Institute of Technology Aerophysic Laboratory, June 1961.
9. Gordon, Colin; and Smith, P. W. Jr.; "Acoustic Losses of a Resonator with Steady Gas Flow", J. Acoust. Soc. Am., Vol. 37, No. 2, February 1965, pp 257-267.
10. Ingard, Uno, "On the Theory and Design of Acoustic Resonators", J. Acoust. Soc. Amer., Vol. 25, No. 6, November 1953, pp 1037-1061.
11. Ingard, Uno; and Hartmut Ising; "Acoustic Nonlinearity of an Orifice." J. Acoust. Soc. Am.; Vol 42, No. 1, July 1967, pp 6-17.
12. McAuliffe, C. E., The Influence of High Speed Air Flow on the Behavior of Acoustical Elements, M. Sc. Thesis, Massachusetts Institute of Technology, 1950.

Bibliography (cont.)

13. Marino, Jr., P. A.; Bohn, N; and Garrison, G.D.; "Measurement of Acoustical Resistance at Sound-Pressure Levels to 171dB." J. Acoust. Soc. Am., Vol. 41, No. 5, May 1967, pp 1325-1327.
14. Mechel, F., et al, Research on Sound Propagation in Sound Absorbent Ducts with Superimposed Air Streams, Report No. AMRL-TDR-62-140, USAF Aerospace Medical Division, Wright Patterson Air Force Base, Ohio, December 1962.
15. Meyer, Erwin; Mechel, Fridolin; and Kurtze, Gunther; "Experiments on the Influence of Flow on Sound Attenuation in Absorbing Ducts," J. Acoust. Soc. Am., Vol. 30, No. 3, March 1958, pp 165-174.
16. Morse, P. M., Vibration and Sound, 2nd Edition, McGraw-Hill Book Co., Inc., N. Y., 1948, p 235f.
17. Morse, Philip M. and Ingard, Uno K.; Theoretical Acoustics, McGraw-Hill Inc., New York, 1968, p 467.
18. Obert, C. L. and Kulva, N. M., Acoustic Liners for Large Engines - Final Report, NAS 8-21345 (Rocketdyne), George C. Marshall Space Flight Center, Alabama, March 1969.
19. Phillips, Bert; and Morgan, Joe C.; Mechanical Absorption of Acoustic Oscillations in Simulated Rocket Combustion Chambers, NASA TN D-3792.
20. Phillips, Bert; Experimental Investigation of an Acoustic Liner with Variable Cavity Depth, NASA TN D-4492.
21. Phillips, Bert; Hannum, Ned P.; Russell, Louis M.; On the Design of Acoustic Liners for Rocket Engines: Helmholtz Resonators Evaluated with a Rocket Combustor, NASA TN D-5171, April 1967
22. Phillips, Bert; Effects of High-Wave Amplitude and Mean Flow on a Helmholtz Resonator, NASA TM X-1582.
23. Phillips, Bert; On the Design of Acoustic Liners for Rocket Engines; Maximum Damping as a Design Objective, NASA TM X-1720, January 1969.
24. Priem, Richard J. and Rice, Edward J.; Combustion Instability with Finite Mach Number Flow and Acoustic Liners, NASA TM X-52412, May 1968.
25. Rayleigh, Lord, J. W. S., The Theory of Sound, Vol. II, Dover Publications, p 172f and p 192f.

Bibliography (cont.)

26. Smith, P. W. and Feldman, B., Influence of Vent Design on Flow Dependent Acoustic Losses of a Resonator with Steady Gas Flow, Bolt Beranek and Newman, Inc., Final Technical Report for Ballistics Research Laboratories, Contract No. DA-19-020-AMC-00527(X), April 1966.
27. Tabata, William K.; Antl, Robert J.; and Vincent, David W.; Storable Propellant Combustion Instability Program at Lewis Research Center, Paper No. 66-602, AIAA, June 1966.
28. Vincent, David W.; Phillips, Bert; and Wanhainer, John P.; Experimental Investigation of Acoustic Liners to Suppress Screech in Storable Propellant Rocket Motors, NASA TN-D-4442, March 1968.
29. Wanhainer, John P.; Bloomer, Harry E.; Vincent, David W.; and Curley, Jerome K.; Experimental Investigation of Acoustic Liners to Suppress Screech in Hydrogen-Oxygen Rockets, NASA TN D-3822, February 1967.
30. Wieber, Paul R.; Acoustic Decay Coefficients of Simulated Rocket Combustors, NASA TN D-3425, May 1966.
31. Wood, Alexander, Acoustics, Dover Publications, p 103.

6. TEST PROGRAMS

The preceding sections of the report cover in detail the approach used in the design of a injector chamber combination using one of two element types, the coaxial intersecting cones or the conventional impinging injector stream elements. This section is devoted to discussing methods for obtaining sufficient experimental data to characterize other element types, methods for instrumenting the test piece and finally the technique to be used for demonstrating the stability characteristics of the injector.

6.1 SUBSCALE AND MODEL TESTING

6.1.1 Evaluation of the Transverse Mode

Transverse modes of instability are defined as pressure perturbations perpendicular to the flow direction. Instability modes categorized as transverse modes include: tangential, radial, and pocket modes for baffled compartments. To evaluate these, a test device was designed and demonstrated for Contract NAS 8-20672. This device is termed a "transverse excitation chamber" or TEC. The TEC has high acoustic losses for the longitudinal modes of instability, and is generally spontaneously unstable in the transverse modes when operating near an injector's sensitive frequency range. The term "sensitive frequency range" is used in conjunction with excitation chamber test results and simply means that there exists a range of frequencies which represents the most unstable operating condition.

The TEC shown in Figure 38, utilizes removable injector inserts and wedges for the combustion chamber. The wedges are used to change the chamber cavity size, thereby changing the transverse mode frequency. Chamber pressure may be varied by changing the area of the throat for tests at constant injection density or by using the same throat and varying the flow rate for constant Mach number. The removable injector inserts allow a variety of injection patterns to be evaluated using the same chamber hardware.

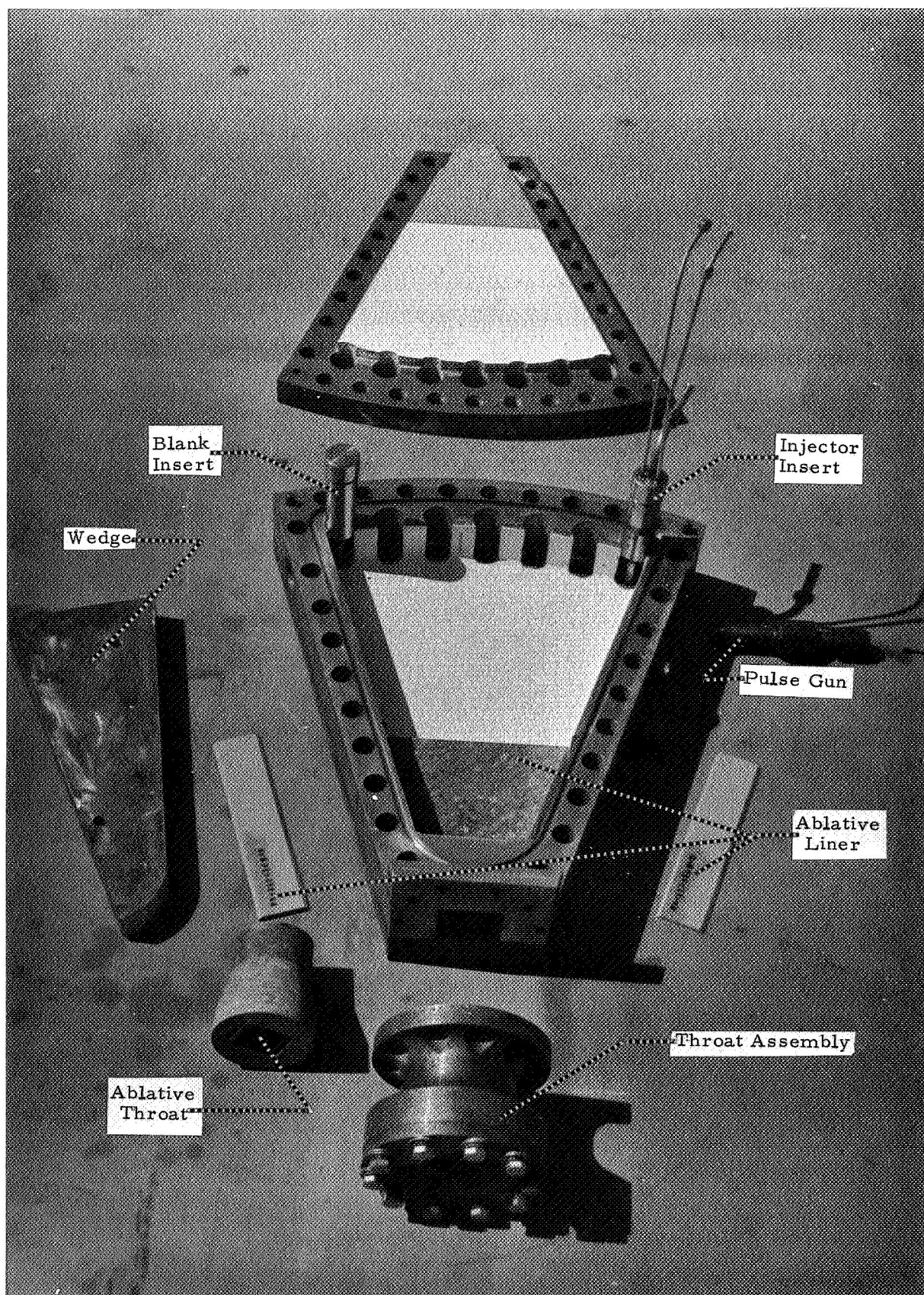


Figure 38 -- Transverse Excitation Chamber (exploded view)

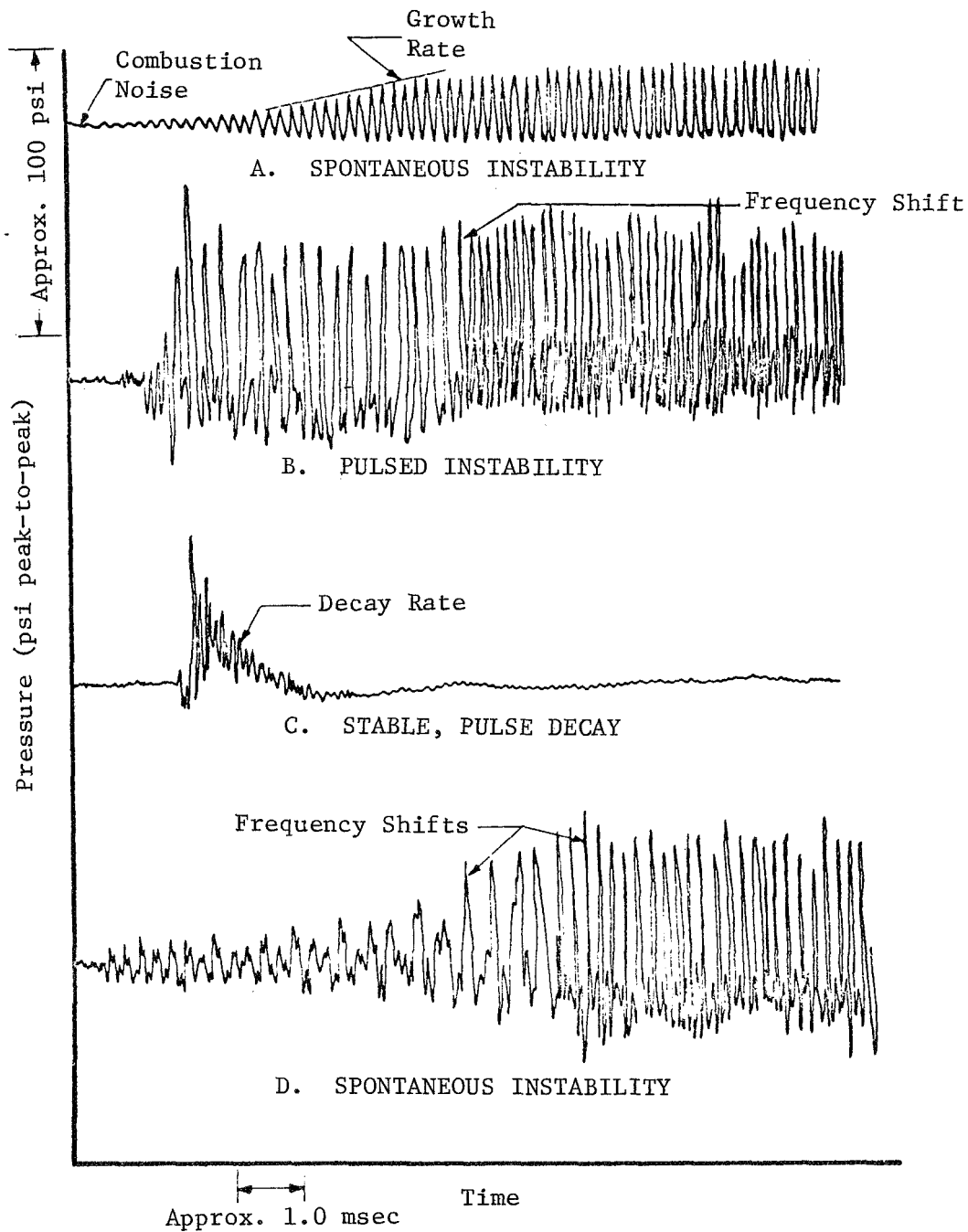


Figure 39 -- Instability and Damping

6.1, Subscale and Model Testing (cont.)

The required test data include a continuous high frequency analog record of the growth rates of the spontaneous instabilities. A pulse, fired in the transverse direction when the system has attained steady-state operation, is used to excite an instability when required.

Typical instabilities are shown in Figure 39; these instabilities were obtained directly from test records. The topmost trace shows the growth of a spontaneous instability which then grows through a linear wave form into a steep-fronted nonlinear wave. The second trace is the result of a pulse; the system is changed from stable to unstable almost instantaneously by reaching the limit cycle amplitude of the instability. The system is initially unstable in the fundamental mode and shifts to the second mode soon after instability is established. The third record shows the decay of a pulse during a stable test. The fourth record shows the spontaneous growth of an instability in the fundamental mode and a shift to the second mode once the limiting amplitude has been attained.

Figure 40 shows an established instability in the second mode during a pulse: the pulse results in a pressure spike which decays in the fundamental mode and the start of a regrowth of the second mode is seen.

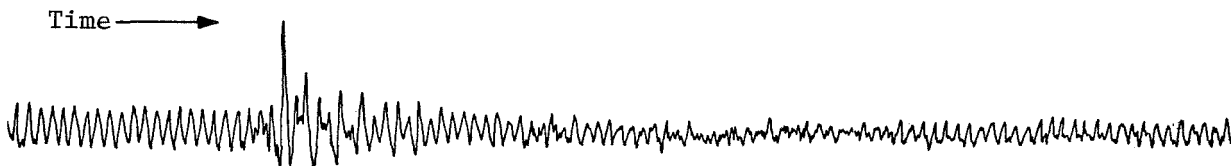


Figure 40 -- Decay of Fundamental Mode and Regrowth of Second Mode

6.1, Subscale and Model Testing (cont.)

Test records such as those shown in Figures 39 and 40 are analyzed by determining the rate of change of pressure during the period of growth or decay of an instability. (This growth rate or decay rate is interpreted as the response of combustion to the frequency of instability). These results are commonly expressed in terms of sound pressure level. An analog record of a high-frequency instability is seen in Figure 41. This record shows the growth

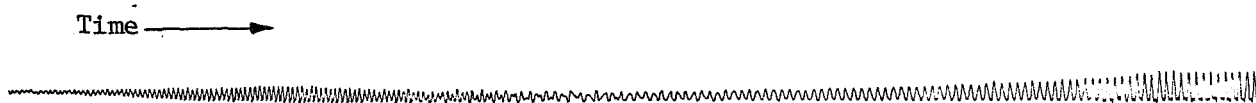


Figure 41 -- Growth of Second Mode and Decay into Fundamental

of a second order mode and its decay into the fundamental mode. Figure 42 is a series of log decrement plots of sound pressure level vs time obtained from the same record by using a Brüel and Kjaer analyzer to separate the sound levels of the various modes of instabilities. At the top of the figure is a plot of the unfiltered record showing the growth of both modes of instability. The second record was filtered at 2500 Hz, thereby recording the growth of the fundamental mode. The third record was filtered at 4000 Hz and shows only the growth of the second mode.

6.1.2 Evaluation of Longitudinal Modes

Longitudinal modes are evaluated in subscale testing in the same manner as transverse modes, and the analysis of the data is the same as that described in the prior section.

Testing for an injector's sensitivity to longitudinal modes is done by using a research device which has high system gains in the longitudinal direction and whose tangential mode frequencies are high enough that they are above the system's sensitive frequency. The mode excited by this device is in the direction of flow.

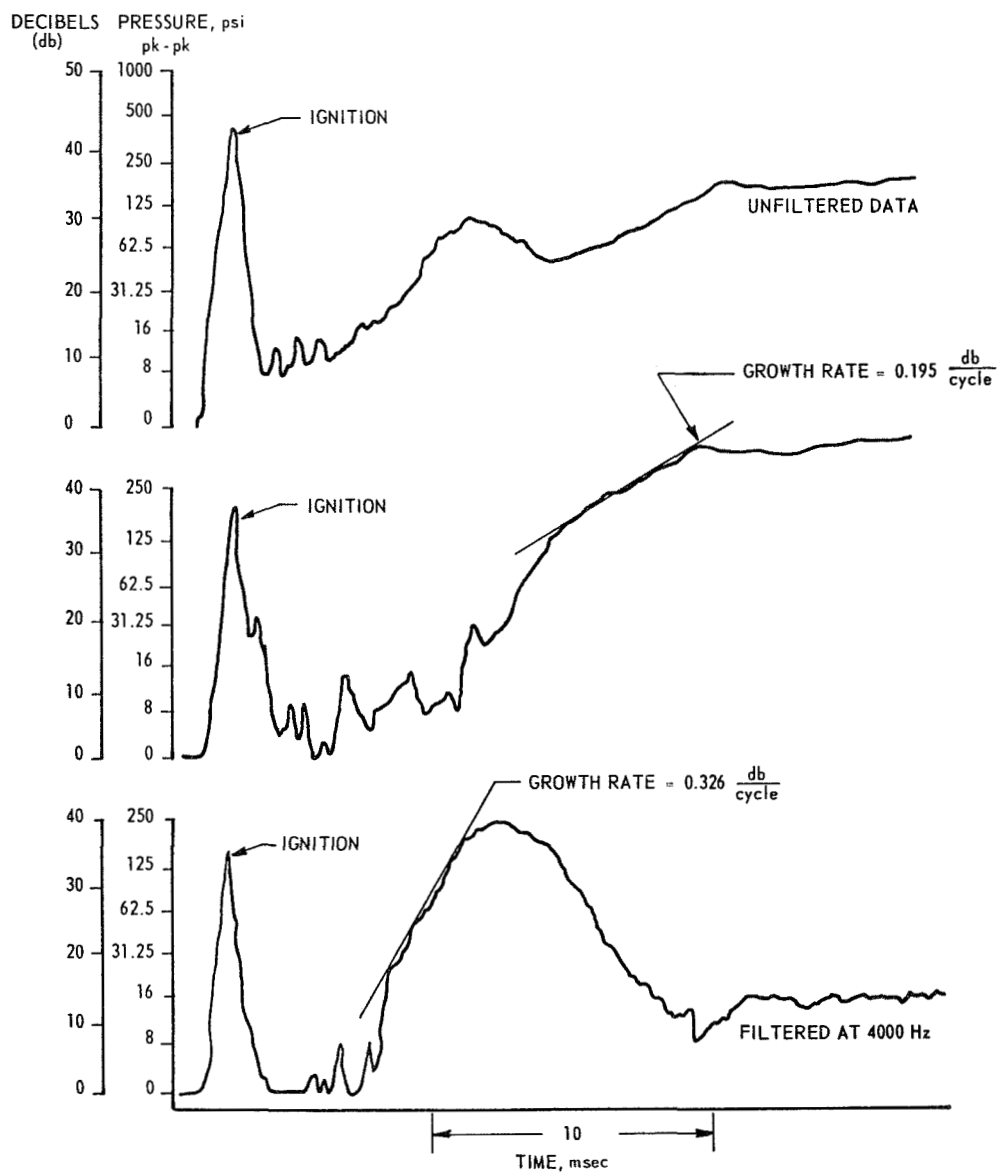


Figure 42 -- Amplitude Plots Showing Growth and Decay Rates

6.1, Subscale and Model Testing (cont.)

The sensitivity of the longitudinal mode in connection with multi-orifice injectors using earth storable propellants was evaluated at Aerojet by a company-sponsored independent research and development program. An artist's concept of the device used for these investigations is shown in Figure 43. The injectors are located at each end of the combustion chamber and the throat is located in the center of the chamber in the form of an annular slit. A baffle inserted through the throat and across the full diameter of the chamber is removed once steady-state operation is attained. This reduces system losses allowing an instability to grow at a frequency corresponding to the fundamental longitudinal mode for the un baffled chamber length. Data are recorded in a manner similar to that for transverse modes. Growth rates or decay rates are used to characterize the injector's sensitivity.

These data are interpreted in a manner similar to the transverse mode in that the growth rate is a measure of the system's responsiveness to the frequency of a particular longitudinal mode. A decay rate represents the amount of the damping present when operating at a given set of testing conditions and at the frequency of the fundamental longitudinal mode.

6.1.3 Planning Subscale Test Program

A test program to evaluate an injector concept for sensitivity in the transverse or longitudinal mode should include where possible evaluations of single parameters. The parameters to be evaluated during these tests may be correlated by using experience from other stability evaluation programs*. For example, velocity ratio, combustion chamber mode number, chamber pressure, and diameter of the oxidizer orifice were found to be important under this contract. In addition, the work of Wanhainen, Feiler, and Morgan at NASA's Lewis Research Center showed that the pressure drop through the fuel circuit, the density of the hydrogen and of the oxygen, and the propellant mixture ratio can be used as a guide in designing a test plan.†

*5th ICRPG, "Correlations of Sensitive-Time-Lag Theory Combustion Parameters with Thrust Chamber Design and Operating Variables," F. H. Reardon, 1968.

†"Effects of Chamber Pressure, Flow per Element, and Contraction Ratio on Acoustic-Mode Instability in Hydrogen-Oxygen Rockets," J. P. Wanhainen, C. E. Feiler, C. J. Morgan, LeRD THD 4733, August 1968.

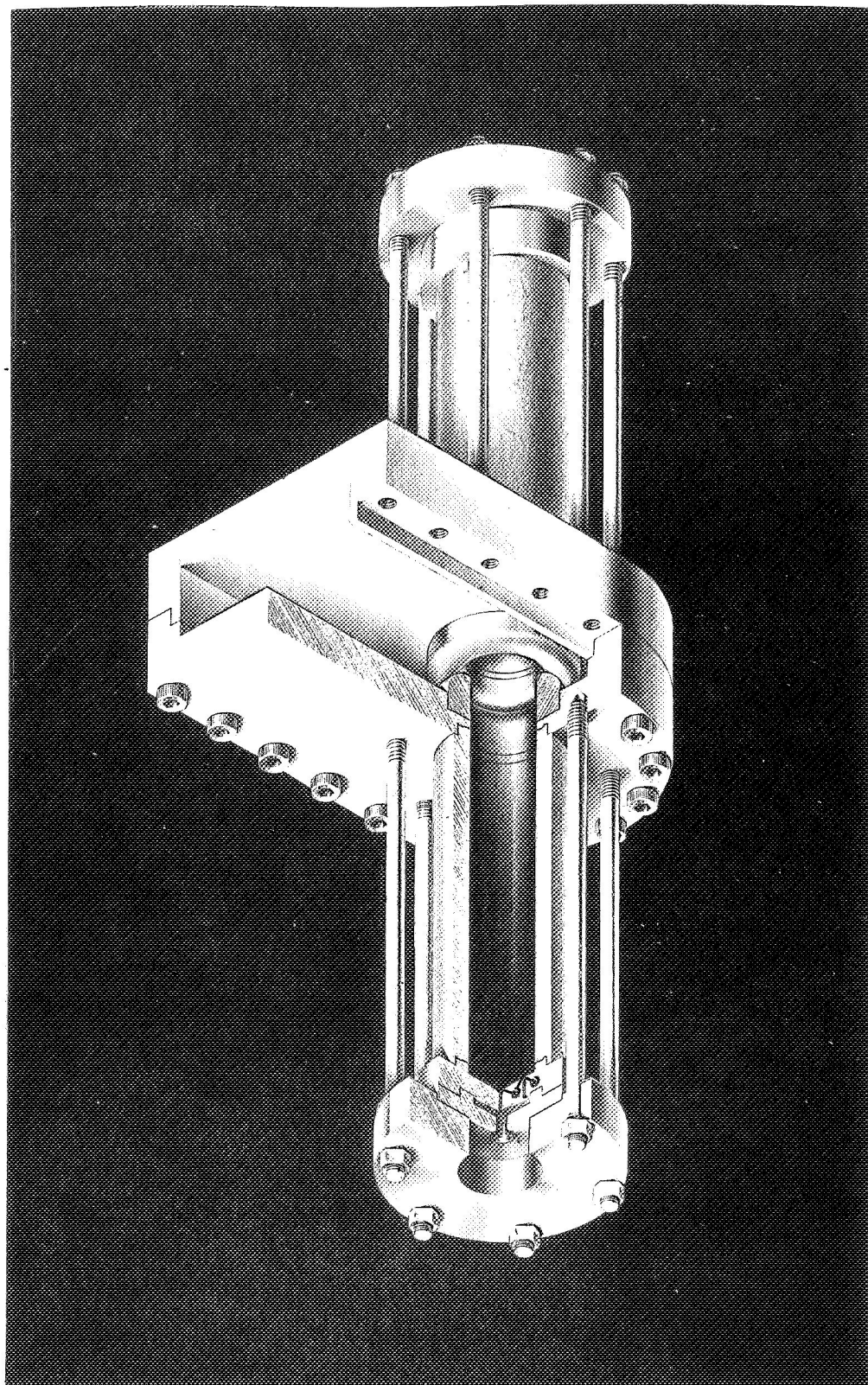


Figure 43 -- Longitudinal Excitation Chamber (sectional view)

6.1, Subscale and Model Testing (cont.)

In devising a test matrix to evaluate the effect of the parameters in question on stability, consideration should be given to the expected overall effect of these parameters. This may be done by using available correlation equations. If, from this study, it is found that the effect of a parameter is only slight [e.g., $(M_c)^{0.15}$], then evaluation of the parameter should be conducted over a sufficient range to separate its effect from the normal scatter of test data.

A test program may be used which will concentrate testing around nominal engine operating conditions. The test parameters should then be varied on either side of these nominal values. Initial testing should concentrate on nominal test conditions to determine the frequency response characteristics of the injector element. Having first determined the sensitive frequency, one may then evaluate the effect of variations in the operating conditions on the gain. The test matrix should consider a minimum of two possibilities: shifts in gain and/or shifts in the sensitive frequency range due to changes in the operating conditions.

6.2 DEVELOPMENT TESTING

6.2.1 General

The use of high-frequency instrumentation in the test program is an absolute necessity to enable the designer to identify the effects of modifications to the injector or chamber designed by applying the principles in Section 3 of this design manual. The data obtained from this source will enable him to evaluate the stability of a given design, to determine the range of sensitive frequencies by mode identification, or to design a baffle configuration or acoustic liner for stabilizing a potentially unstable design. Stability rating of the system should be obtained by using either directional pulses or nondirectional bombs or both.

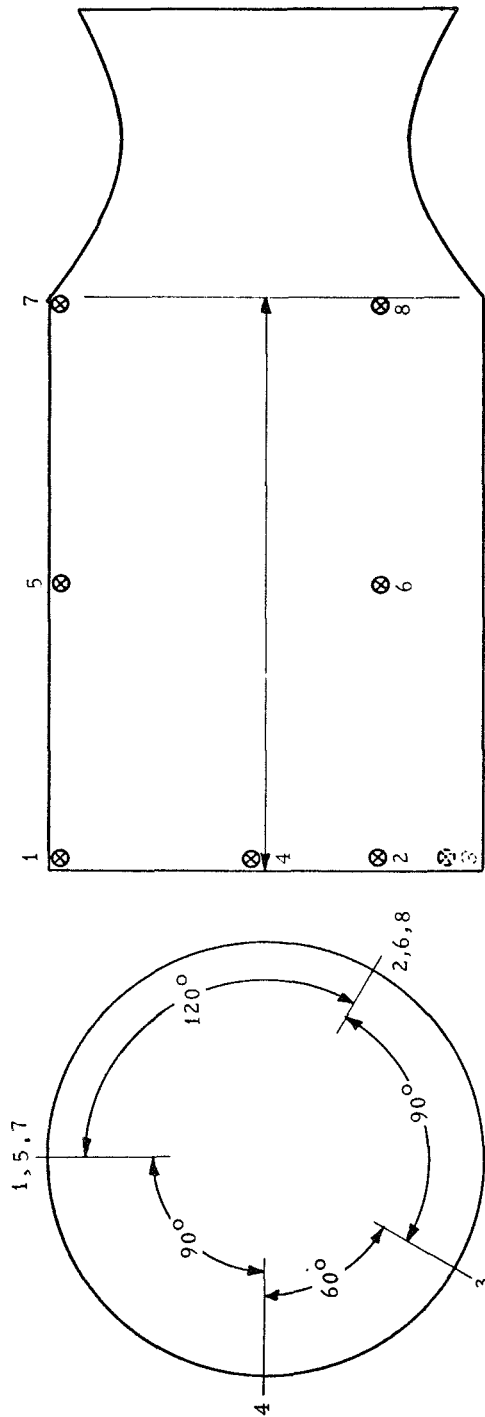


Figure 44 -- Recommended Transducer Locations in Order to Identify Modes of Instability

6.2, Development Testing (cont.)

The location of the high frequency pressure transducers can assist in determining the important modes (e.g., 1T, 2T, 1T-1L, 2T-1L, etc.), thereby supplying requirements for selecting a particular baffle configuration. The type of high frequency pressure transducer used is important in that there is a variety of pressure transducers on the market with different ranges of frequency response. The mounting of these transducers is also important in order to avoid resonance, which will yield misleading results. The use of power spectral density plots and fixed-bandwave analyzer (B&K plots) data may be used effectively to determine the sensitivity at specific frequencies.

Testing requirements that will determine adequately the stability characteristics of a system should include sufficient variation of operating parameters to characterize the system over its entire range. Particular attention should be given to the parameters which most affect the stability of the system. As an example, the injection velocity ratio, the mixture ratio, and the chamber pressure have significant effect on the stability of systems employing coaxial and impinging multi-orifice injectors.

6.2.2 Instrumentation

6.2.2.1 Instrumentation Locations

The intent of this section is to prescribe the best locations for high frequency pressure transducers such that a maximum number of instability acoustic modes may be identified and to describe the mechanics for analyzing stability data. Figure 44 has been used at Aerojet to identify modes as high as 2T-3L. Theoretically, this arrangement of transducers can be used to identify transverse modes of as high an order as 5T and longitudinal modes as high as 4L. Additional information on instrumentation can be found in the References.*

*Selection of Instrumentation for Analyzing Combustion Instability in Liquid Propellant Rocket Engines prepared by the Committee on Instrumentation and Test Data, ICRPG, Chemical Propulsion Information Agency CPIA Publ. 148, July 1967.

6.2, Development Testing (cont.)

Example 14: Determination of Transverse Modes

The modes to be considered should be selected on the bases of the frequencies observed and those calculated using the method described in Section 3.1, Examples 1 and 2. For this case, a standing 3T mode (shown in Figure 24, Section 5) is assumed.

- Step 1. Place the plot of nodal planes over the sketch of transducer locations with one nodal line passing through the location of the transducer.
- Step 2. If a standing 3T mode were to appear in this position, transducers No. 1 and No. 2 would record no pressure oscillation since a nodal plane coincides with each transducer. Pressure transducers No. 3 and No. 4 would record the maximum amplitude of the instability 180° out of phase since the two transducers are located at a pressure maximum and a pressure minimum (antinodes).
- Step 3. Rotate the nodal planes 7.5° . At this location, all transducers will record pressure oscillations. Transducer No. 2 is now near a pressure antinode and will record a maximum amplitude. Transducers No. 1 and No. 3 are in phase and transducer No. 4 is 180° out of phase with transducer 3.
- Step 4. Rotate the nodal planes 7.5° beyond the position of Step 3 or 15° from the original position (Step 1). At this location, transducers No. 1 and No. 2 are located at pressure antinodes and will record maximum amplitudes in phase. Transducers No. 3 and No. 4 are at pressure nodes and will record no pressure oscillations.

6.2, Development Testing (cont.)

Determination of Longitudinal Modes

The identification of longitudinal modes is accomplished by using transducers in locations along the chamber axis. Mode pressure profiles up to 4L are shown on Figure 45. The identification of modes is accomplished in much the same manner as for transverse modes. As an example, transducers No. 1 and No. 7 read maximum pressure oscillations 180° out of phase; transducer No. 5 is at a pressure node and no pressure oscillation will be recorded. For a 2L mode, transducers No. 1 and No. 7 record maximum pressure oscillation in phase and transducer No. 5 records maximum pressure oscillations 180° out of phase. For a 3L mode, the transducers record the same phase relationships as the 1L mode; however, the frequency is increased to approximately three times the frequency of the 1L. In a similar manner, this type of mode identification may be applied to modes of higher order.

If the pressure transducers are not equally spaced or do not coincide with pressure antinodes, the amplitude of the pressure oscillation may be determined by the location of the transducer with respect to the pressure profile. By assuming the pressure oscillations are acoustic in nature, the actual amplitude may be adjusted by assuming a sinusoidal pressure profile (shown in Figure 45). The proportion of maximum amplitude to measured amplitude may be determined by the point at which the transducer location intercepts the curve for the given mode.

6.2.2.2 Types of Instrumentation

The severe environment encountered in a combustion chamber imposes stringent requirements on the instrumentation. Considerable research and development has been conducted in development of high-frequency response instrumentation for measurement of pressure oscillations in rocket combustion chambers. It is often necessary to isolate this instrumentation from the

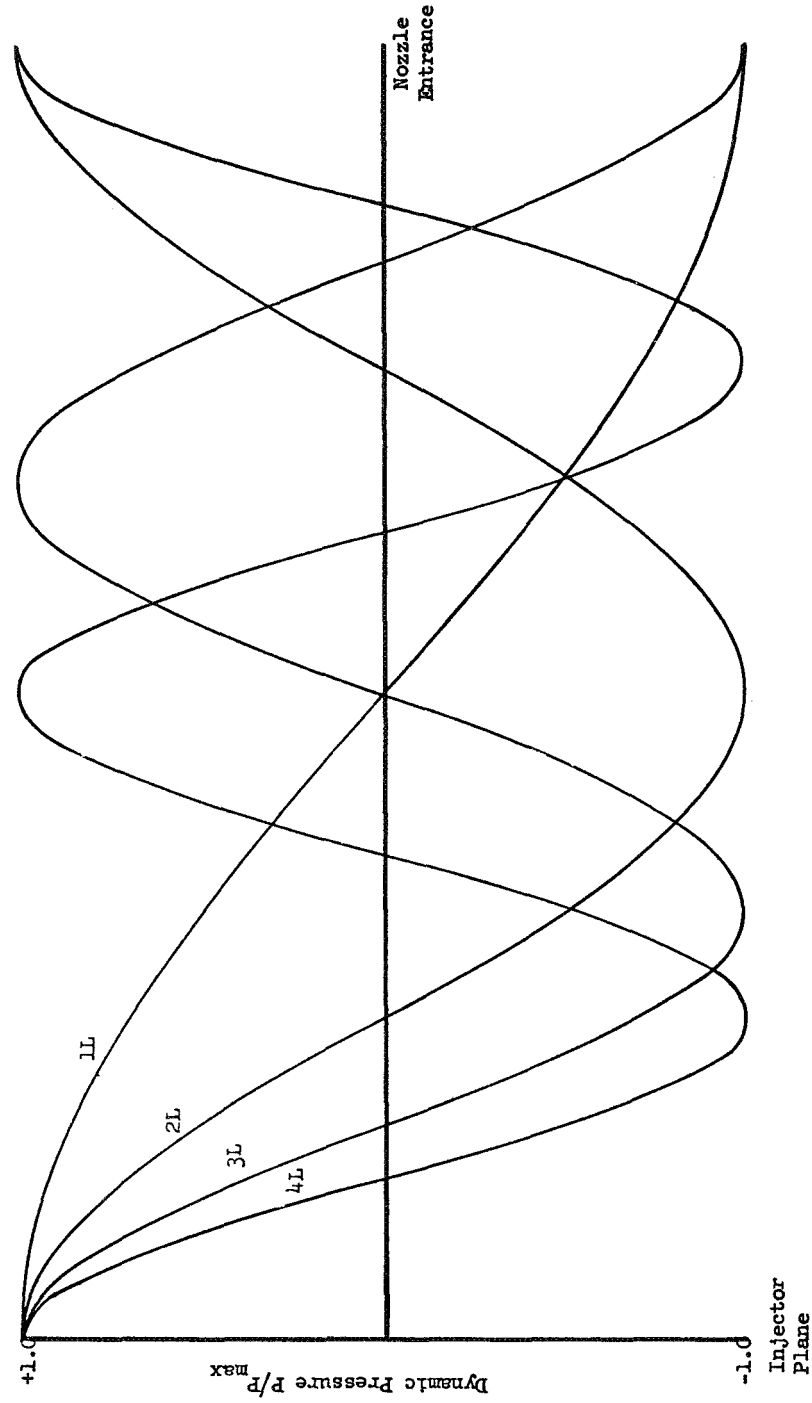


Figure 45 -- Axial Pressure Profiles of Longitudinal Modes
in an Enclosed Cylinder

6.2, Development Testing (cont.)

thermal environment and from the vibration of the transducer mount on the combustion chamber in order to obtain data which reflect actual pressure oscillations in the combustion chamber. A detailed description of recent developments in instrumentation for measuring combustion instability is given in the References.* A detailed description of several pressure transducers is also given#, including the Photocon 352A and helium bleed Kistler transducers which have both been used extensively on Contract NAS 8-20672.##

The Photocon 352A transducer is especially suited for hardware intended for field use in that the transducer is ruggedly constructed and has a water-cooled heat shield which improves its thermal characteristics and reduces susceptibility to shrapnel damage from pulse charge fragments. This transducer is commonly used behind a flame shield in an attempt to protect it from the erosion resulting in chamber streaking because of injector incompatibilities. Care must be exerted in interpretation of data when using a flame shield in that the resonance of the transducer's mounting may distort amplitude or decay data. The resonance characteristics of transducers have been investigated analytically and are discussed in Section 6.2.2.3.

The helium bleed pressure transducer is well suited for use in a combustion chamber and has the advantage over Photocon transducers in that no part is exposed to combustion, and it is therefore protected from the thermal environment and damage from shrapnel. Another advantage of this type of transducer is that it provides a gas of known density between the transducer's sensor and the combustion gases, thereby permitting accurate calculation of the resonant frequency of the transducer assembly. By bleeding helium through

*Special Considerations for Combustion Instability Instrumentation and Data Representation, prepared by the Committee on Instrumentation and Test Data, ICRPG, Chemical Propulsion Information Agency, CPIA Publ. 170, June 1968.

#Gemini Stability Improvement Program, Contract AF 04(695)-517, Final Report, Vol. 6, Instrumentation Report GEMSIP FR-1 SSD-TR-66-2, 31 August 1965.

6.2, Development Testing (cont.)

the transducer during combustion, the sensor is thermally protected by the helium environment and provides a continual bleed of gases, purging the aperture of foreign particles generated during testing. Two models of helium bleed transducers were tested during this program. One model designed by Aerojet and designated HB3X uses a Kistler 601 transducer in the helium bleed housing. This transducer is particularly suited for insertion between regenerative cooling tubes or in ablative chambers. The other is the Model 615 transducer made by Kistler; it fits conveniently in a 1/4-in. AN fitting and is especially suited for use with workhorse hardware. The major problem with the Kistler transducers is that the electrical pickup is sensitive to the intrusion of moisture and the transducer may take a dc shift due to saturation of the charge amplifier during the engine's ignition.

6.2.2.3 Effect of Transducer Mounting Resonance on Decay Measurements

To get the most accurate measurements of pressure oscillations in a chamber, a pressure transducer should be mounted flush with the wall of the chamber. However, because of the high temperature of the chamber gases, it is sometimes necessary to recess the transducer from the wall. Depending on the configuration of this recess, some distortion may be introduced.

What follows is a discussion of the effect of transducer resonant frequency and damping. The comparison is between what is actually happening in the chamber versus what the output of the transducer is as the transducer resonant frequency approaches that of the chamber. The results presented were obtained from an analog computer using the following relationship for the transducer transfer function. (See Nomenclature for definitions.)

$$\frac{P_T}{P_c} = \frac{1}{-\frac{\omega^2}{\omega_{oT}^2} + \frac{j\omega 2\zeta_T}{\omega_{oT}} + 1} \quad \text{Eq 32}$$

6.2, Development Testing (cont.)

The response of the pressure transducer to an exponential sinusoid ($e^{\zeta_c t} \sin \omega_{oc} t$) can easily be obtained on an analog computer. To obtain the exponential sinusoid, it was decided to use the output of another second order system to a Dirac delta function.

$$P_c = \frac{1}{-\frac{\omega^2}{\omega_{oc}^2} + \frac{j\omega 2\zeta_c}{\omega_{oc}^2} + 1} \quad \text{Eq 32a}$$

To run cases on an analog computer, values must be established for ζ_T , ω_{oT} , ζ_c , ω_{oc} . The quantities α_c and ω_{oc} can be obtained from existing test data. The quantities α_T and ω_{oT} are determined by the configuration of the recess. For this study, ω_{oT} should be chosen at various fractions of the frequency ω_{oc} . The quantity α_T is determined by the damping characteristics of the recess. This must be estimated analytically. The resistance per unit length*, R, is given by:

$$R = \frac{2 \sqrt{2\rho\mu\omega}}{D} \quad \text{Eq 33}$$

The acoustic equation, including the frictional force described above, is given by:

$$\frac{\partial^2 P}{\partial x^2} - \frac{j\omega(j\omega\bar{\rho} + R)}{\bar{c}^2 \bar{\rho}} P' = 0 \quad \text{Eq 34}$$

The solution for the ratio of pressures in a dead-end tube can be given as:

$$\frac{P'}{P} = \frac{1}{\cosh Kx} \quad \text{where } K = \frac{j\omega(j\omega\bar{\rho} + R)}{(\bar{c})^2 \bar{\rho}}^{1/2} \quad \text{Eq 35}$$

*A Study of the Suppression of Combustion Oscillations with Mechanical Damping Devices, Pratt & Whitney Aircraft Final Report PWA FR-1922, Contract NAS 8-11038, July 1966.

6.2, Development Testing (cont.)

After algebraic manipulation, $\cosh Kx$ can be written as a complex number, $\theta + j\chi$. At resonance, $\chi = 0$. The value of θ at this point can then be compared to $\frac{2\alpha_T}{\omega_{OT}}$ to get an estimate for α_T .

Table 15 shows the result of evaluating the effect of transducer resonance on input frequencies. The ratio of the critical frequency for the system to the transducer resonance at selected damping ratios was studied at a variety of damping ratios for the chamber and transducer cavity.

The results from these studies illustrate significant decay rate characteristics that will aid in the analyses of test firing data. For example, analog Run No. 1 shown on Figure 46, with the transducer and chamber natural frequencies equal, shows that the decay rate within the chamber is different from that recorded by the transducer. It should also be noted that the transducer decay plot yields first a growth (positive slope), then a decay (negative slope).

Run No. 2, shown in Figure 47, is representative of a "beat" phenomenon with slopes being measured along both the high and low portions of the curve. Differences in the decay rates recorded by the pressure transducer and those actually occurring in the combustion chamber show different slopes. Run No. 23, shown on Figure 48, taken at the same natural frequency ratio as Run No. 2, shows the effect of the increased value of the transducer damping factor (three times that of the chamber). Two distinct slopes occur: the first, lasting for approximately 25 cycles, measures the rapid decay of the transducer system, while the second slope records the chamber decay. In such cases it is important to use the second slope, allowing an appropriate time to pass from the initiation of the impulse function. The reverse of this phenomenon (i.e., a greater chamber decay) is represented by Run No. 18 shown in Figure 49, which shows a transducer "ringing" after the chamber decay period. (Text continued on Page 222.)

Report 20672-P2D

Table 14 -- Results of Analog of Transducer Resonance to Input Frequencies

Run No.	ω_{oc}/ω_{oT}	$2\zeta_c$	$2\zeta_t$	Decay Rate of Chamber Pressure db/cycle	Decay Rate of Transducer db/cycle
1	1.0	0.01	0.01	0.22	0.12 ⁽¹⁾
2	0.9	0.01	0.01	0.20	0.28
3	0.8	0.01	0.01	0.28	0.32
4	0.7	0.01	0.01	0.22	0.32
5	0.7	0.01	0.05	0.24	0.26
6	0.8	0.01	0.05	0.26	0.26
7	0.9	0.01	0.05	0.28	0.28
8	1.0	0.01	0.05	0.24	0.24
9	1.0	0.02	0.05	0.46	0.40
10	0.9	0.02	0.05	0.54	0.50
11	0.9	0.02	0.05	0.46	0.60
12	0.7	0.02	0.05	0.48	0.48
13	0.7	0.02	0.03	0.50	0.48
14	0.8	0.02	0.03	0.56	0.44
15	0.9	0.02	0.03	0.44	0.50
16	1.0	0.02	0.03	0.46	1.60 & 0.45 ⁽²⁾
17	1.0	0.02	0.01	0.54	1.74 & 0.22 ⁽²⁾
18	0.9	0.02	0.01	0.46	0.32
19	0.8	0.02	0.01	0.54	0.34
20	0.7	0.02	0.01	0.46	0.36 & 0.26 ⁽³⁾
21	0.7	0.01	0.03	0.26	0.42 & 0.26 ⁽³⁾
22	0.8	0.01	0.03	0.24	0.40 & 0.30 ⁽³⁾
23	0.9	0.01	0.03	0.22	0.43 & 0.28 ⁽³⁾
24	1.0	0.01	0.03	0.28	1.80 & 0.28 ⁽²⁾
25	0.3333	0.01	0.03	0.24	0.26
26	0.4	0.01	0.03	0.22	0.30 & 0.24 ⁽³⁾
27	0.5	0.01	0.03	0.26	0.32 & 0.18 ⁽³⁾
28	0.6	0.01	0.03	0.24	0.26
29	1.1	0.01	0.03	0.22	0.52 ⁽¹⁾ & 0.12 ⁽³⁾

NOTE: (1) This decay rate appeared 40 cycles after the initiation of the impulse signal. Prior to this time a growth rate was recorded by the transducer.

(2) This decay rate appeared approximately 15 cycles after the initiation of the impulse signal. Prior to this time a growth rate was recorded by the transducer.

(3) Second decay rate recorded approximately 25 cycles after the impulse.

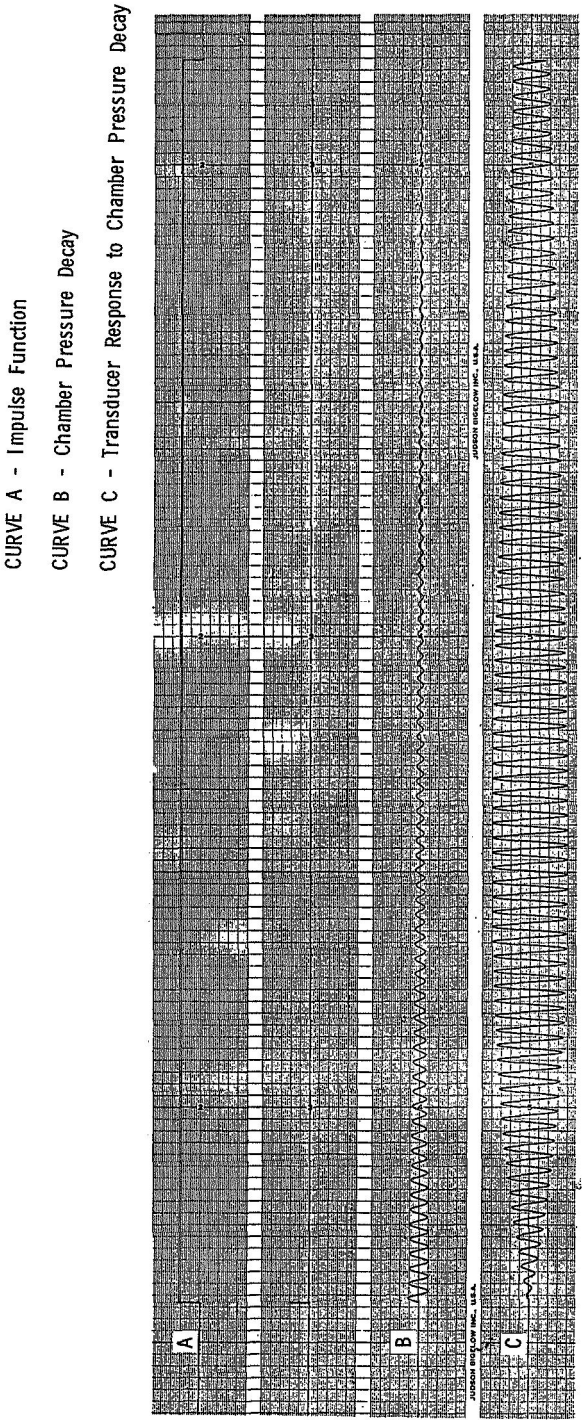


Figure 46 --- Analog Run No. 1

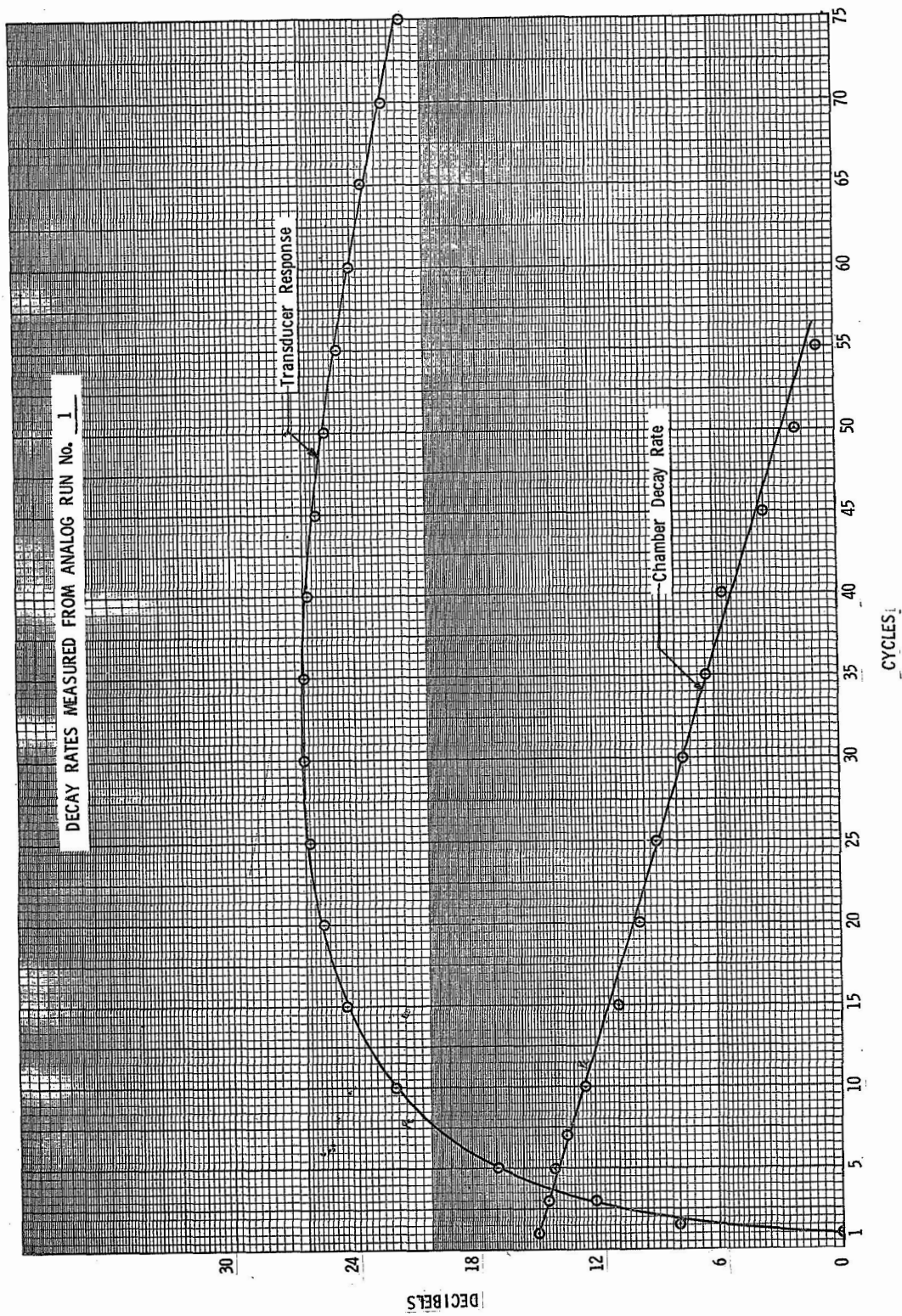
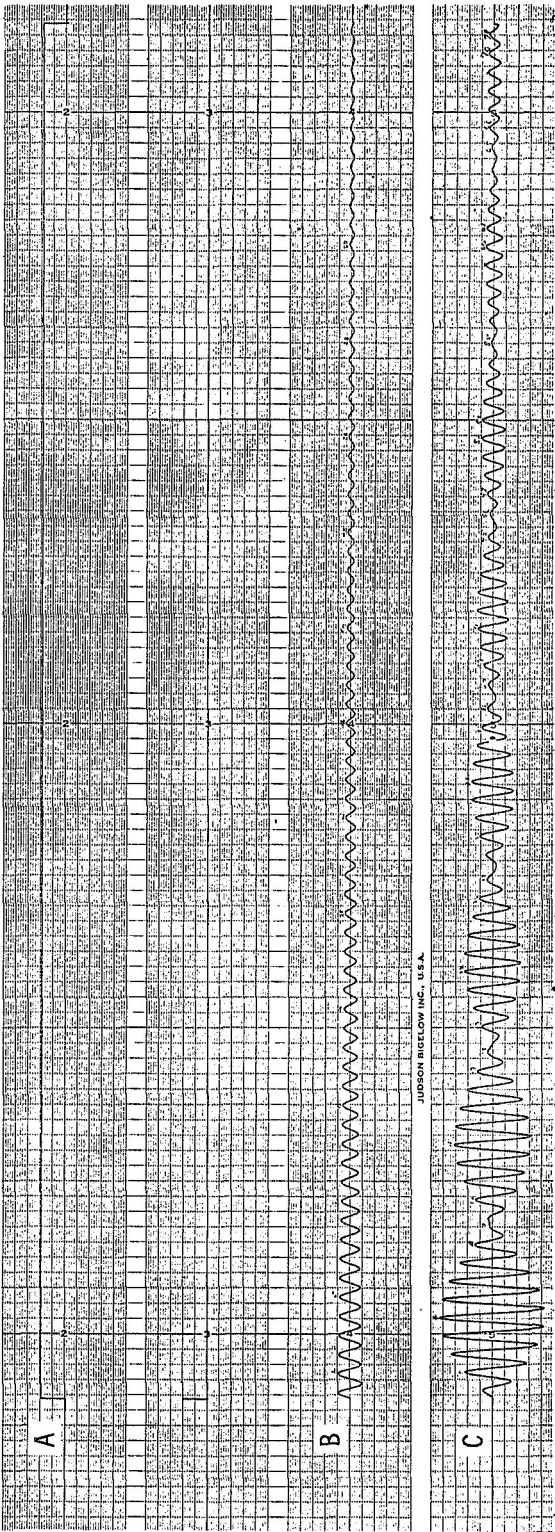


Figure 46 -- Analog Run No. 1



CURVE A - Impulse Function

CURVE B - Chamber Pressure Decay

CURVE C - Transducer Response To Chamber Pressure Decay

Figure 47 -- Analog Run No. 2

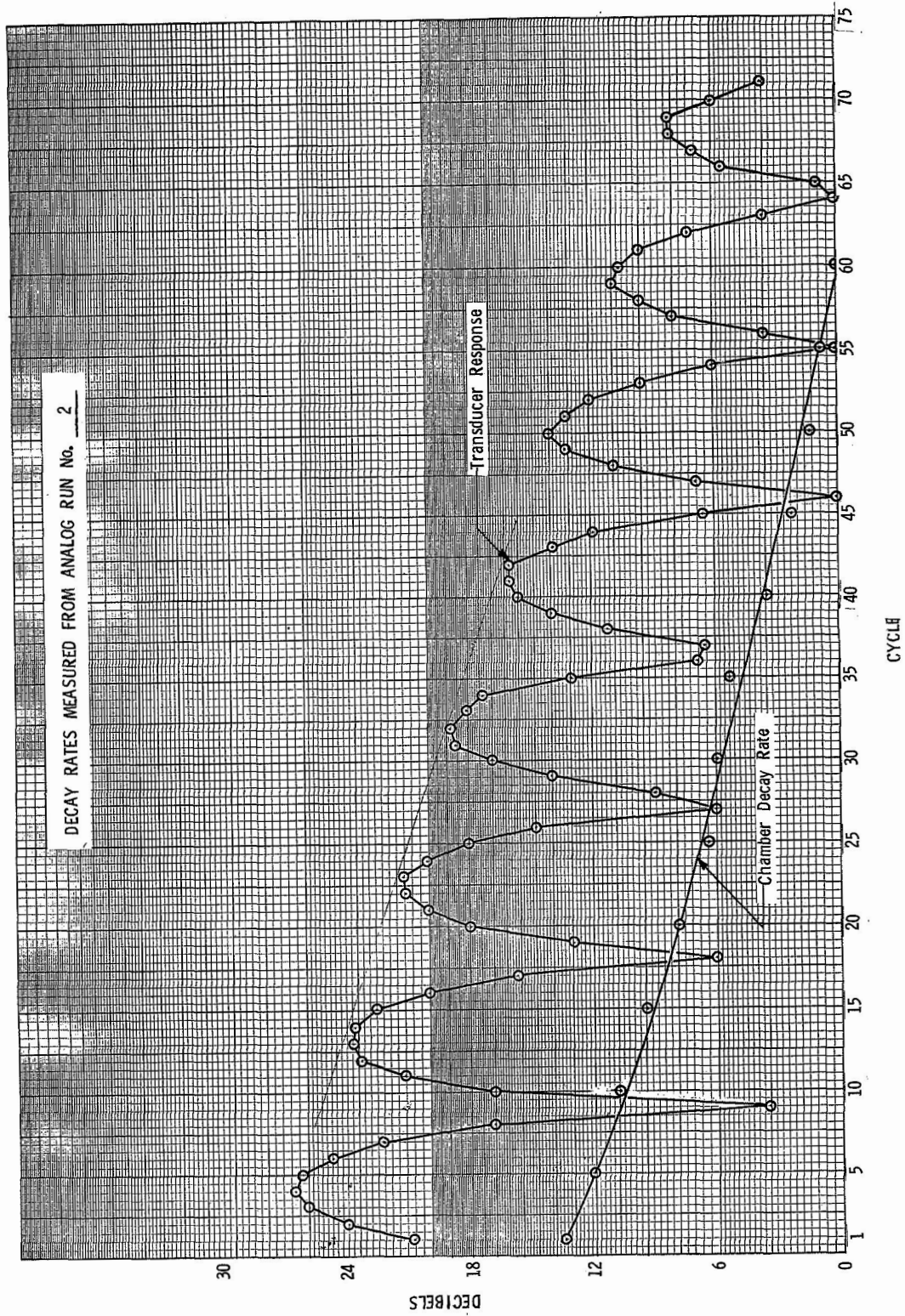
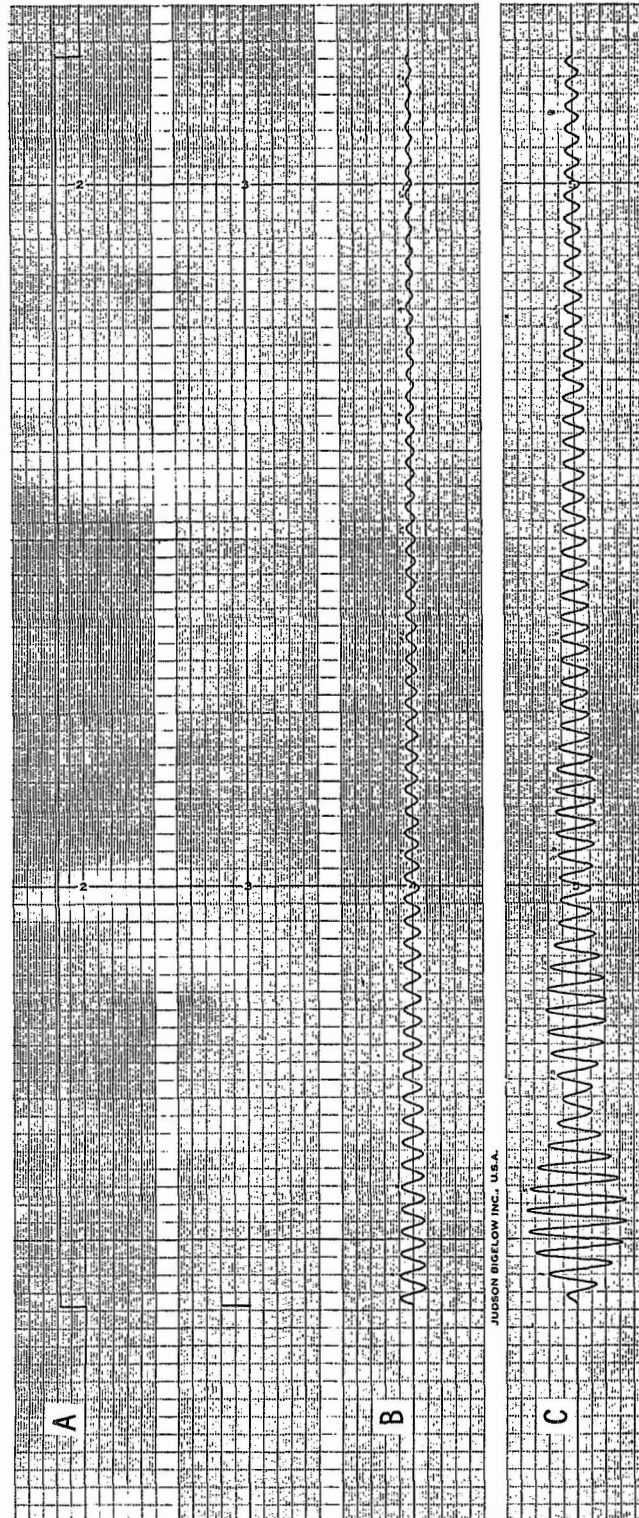


Figure 47 -- Analog Run No. 2



CURVE A - Impulse Function

CURVE B - Chamber Pressure Decay

CURVE C - Transducer Response To Chamber Pressure Decay

Figure 48 -- Analog Run No. 23

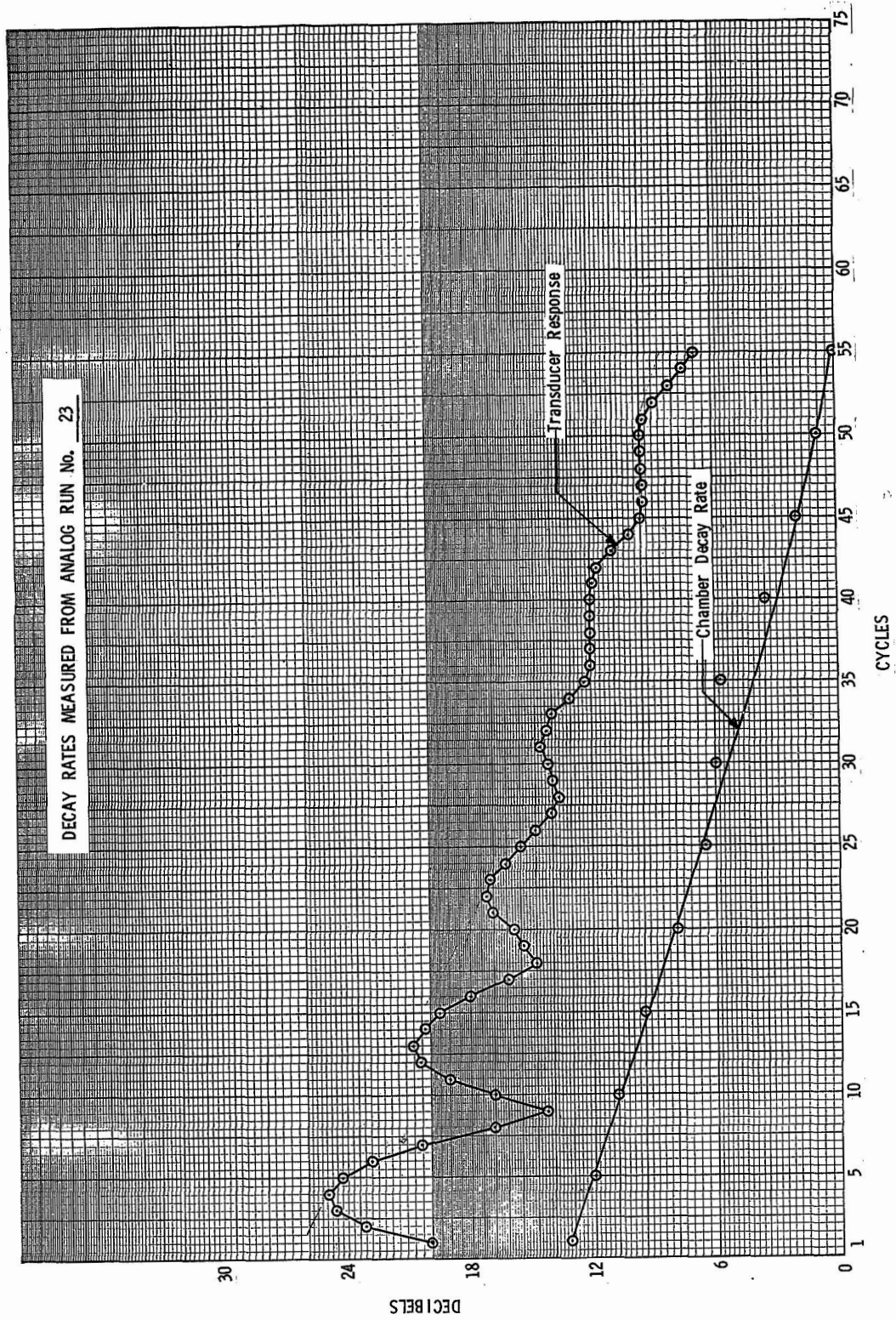


Figure 48 -- Analog Run No. 23

CURVE A - Impulse Function
CURVE B - Chamber Pressure Decay
CURVE C - Transducer Response to Chamber Pressure Decay

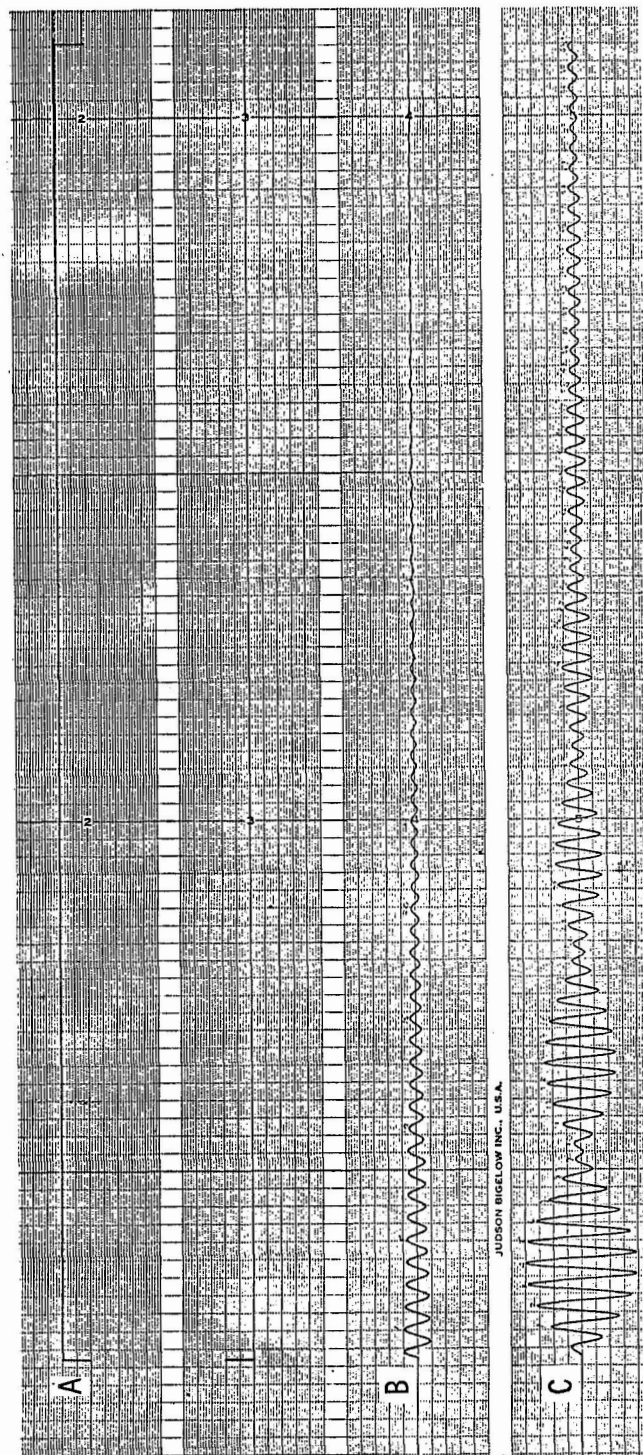


Figure 49 -- Analog Run No. 18

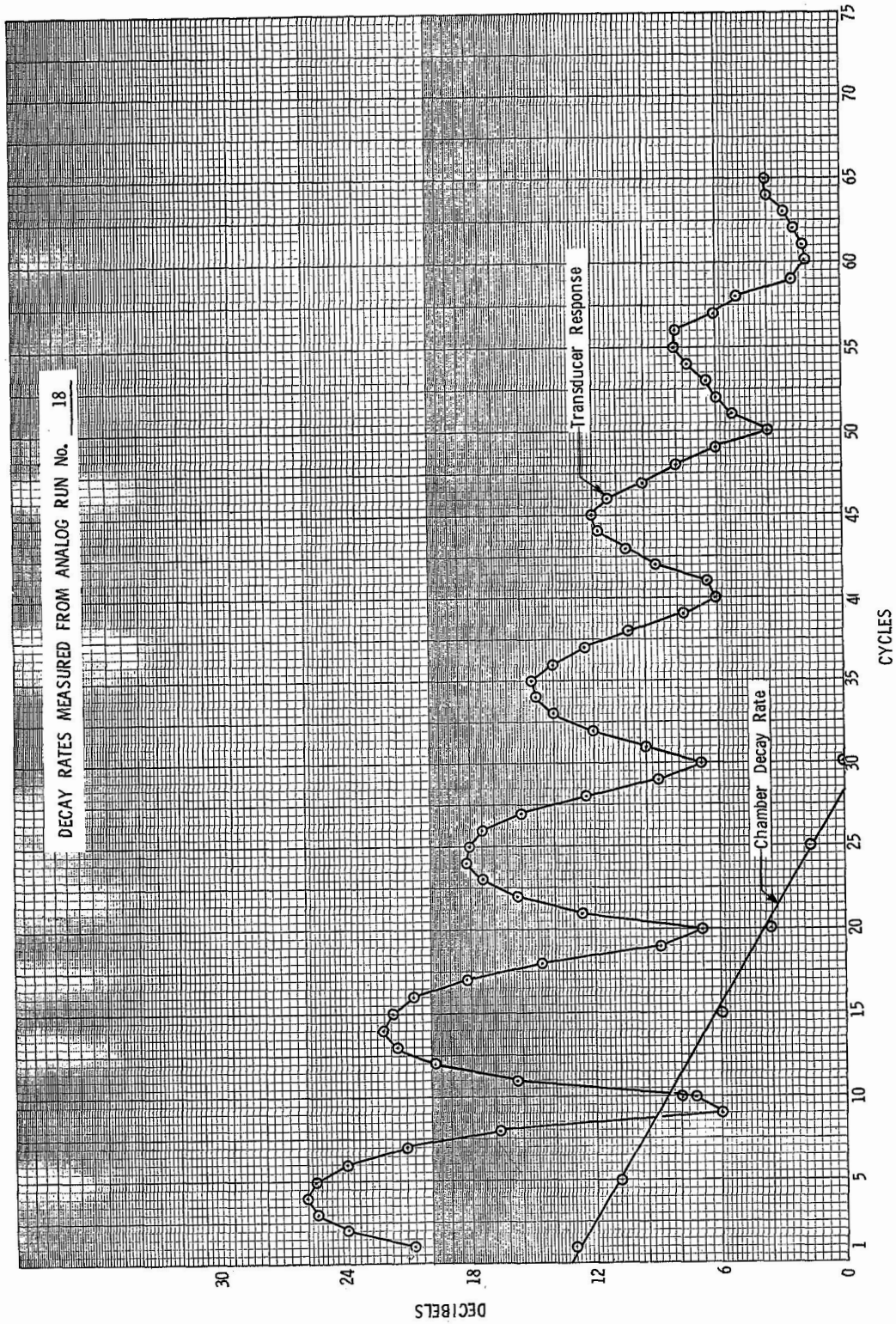


Figure 49 -- Analog Run No. 18

6.2, Development Testing (cont.)

In summary, these studies have shown that (1) the decay rate measured by the transducer may differ from the true chamber decay, (2) the decay may first appear as a growth followed by a delayed decay, (3) the significance of beating, and (4) the effect of varying the damping factor values of both the transducer and chamber.

These results are required to interpret correctly the logarithmic decrement data (B&K plots) for actual test firings. The limitations on the use of these curves are that knowledge of the resonant frequencies of the chamber and transducer are required and values for the damping factors must be obtained.

Though the results of the entire analog study of decay rates are most important for data analysis, it is highly important that the designer recognize that the dynamic pressure instrumentation he selects must have a natural frequency range at least 30% greater than the observed system frequency to reduce distortion to a minimum.

6.2.3 Testing Requirements

The rating of a thrust chamber assembly in terms of stability requires the use of high frequency instrumentation located as discussed in Section 6.2.2. Stability rating is accomplished by employing a pulsing device and recording the combustion chamber overpressure required to initiate a sustained instability. Of the variety of pulsing devices used, the tangential pulse gun and the nondirectional pulse change (NDPC) are most common. The pulse gun (shown in Figure 50) has been used exclusively during the stability rating on Contract NAS 8-20672. The NDPC is shown in Figure 51.

Several criteria have been used to evaluate engine stability such as the ratio of pulse amplitude to nominal chamber pressure required to induce

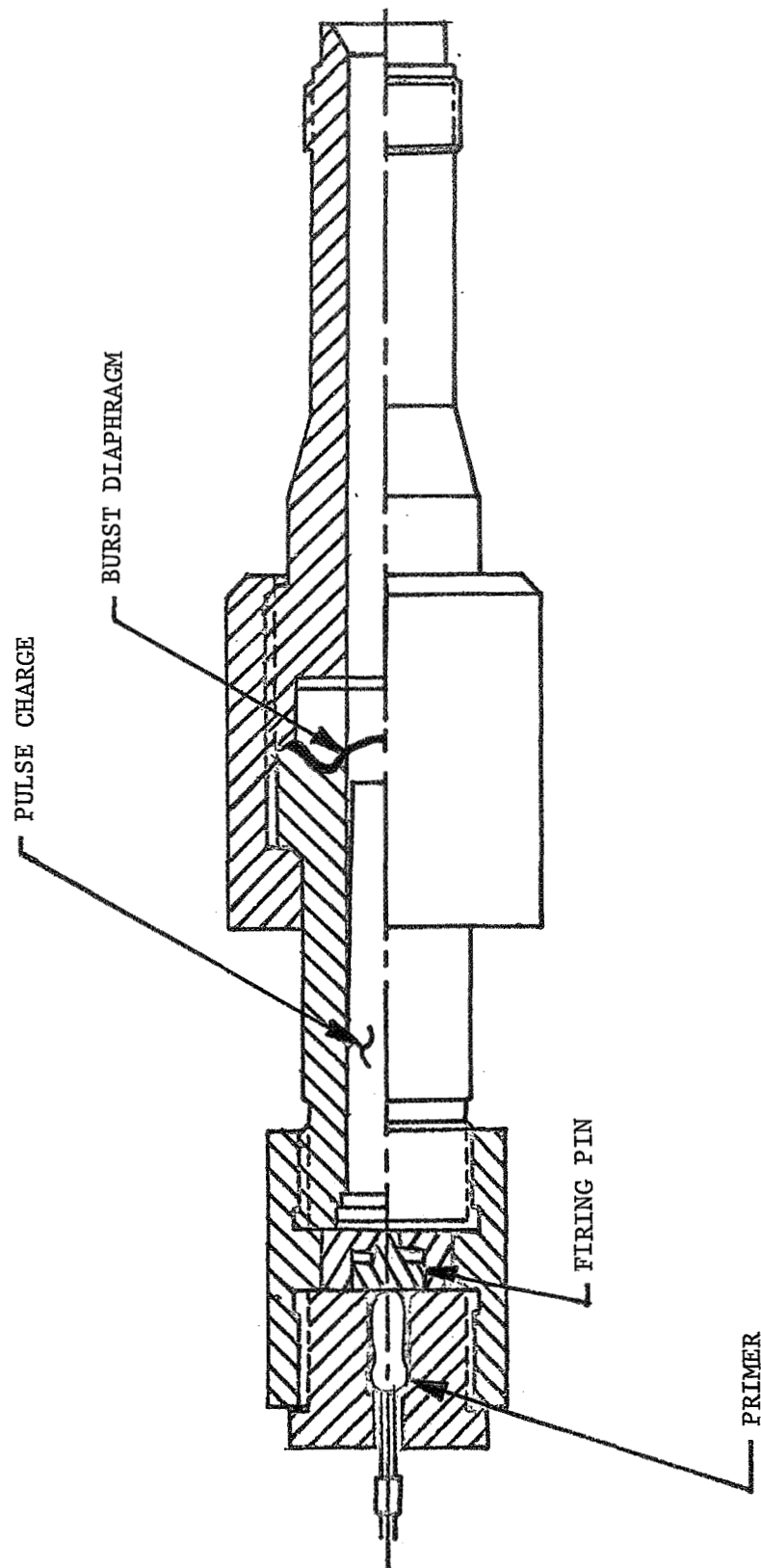


Figure 50 -- Tangential Pulse Gun

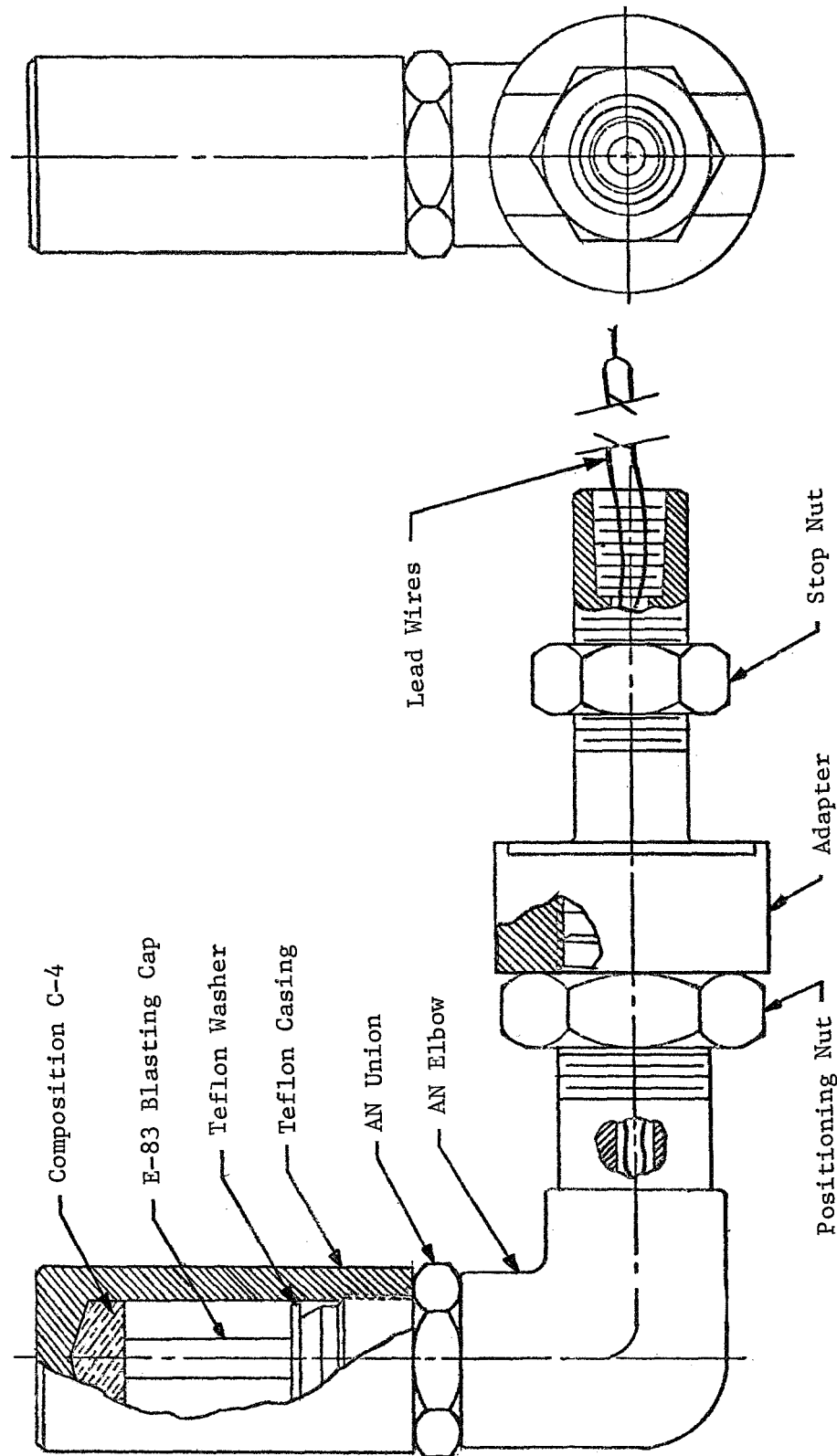


Figure 51 --- Nondirected Pulse Charge

6.2, Development Testing (cont.)

instability in a given system, a "go" or "no go" criteria where the various injectors are rated by their ability to damp a particular type of induced disturbance or the stability of the system to a certain minimum over pressure. This latter measure is the one generally used, although the degree of over-pressure specified varies from system to system. When more than one injector type successfully meets requirements the selection is then based on the rate of decay or the time to decay to a predetermined level (e.g., $\pm 5\% P_c$).

6.3 DATA ANALYSIS

6.3.1 High Frequency Analog Record

Of the methods available for analyzing the dynamic pressure characteristics of a system, the majority of data may be obtained directly from the high frequency analog record. The predominant frequencies in the instability may be determined by filtering the analog record with several band pass filters, or power spectral density plots may be used to identify frequencies present in the chamber and the magnitude of each. The phase relationship of these frequencies at the known transducer locations may be determined to identify each mode.

The filtered analog record is best used for determining a mode of instability in that high frequency oscillations due to transducer "ring" or simple combustion noise will be removed. Care must be taken to insure the filter is not also affecting the data. This is best accomplished by altering the filter characteristics or characterizing the filter response to a known input. Identification of the location of nodes must be done first to determine the amplitude relationship of the various pressure traces (see Section 6.2 for details of amplitude determinations). Secondly, the amplitude relationship for both transverse and longitudinal modes must be determined in terms of

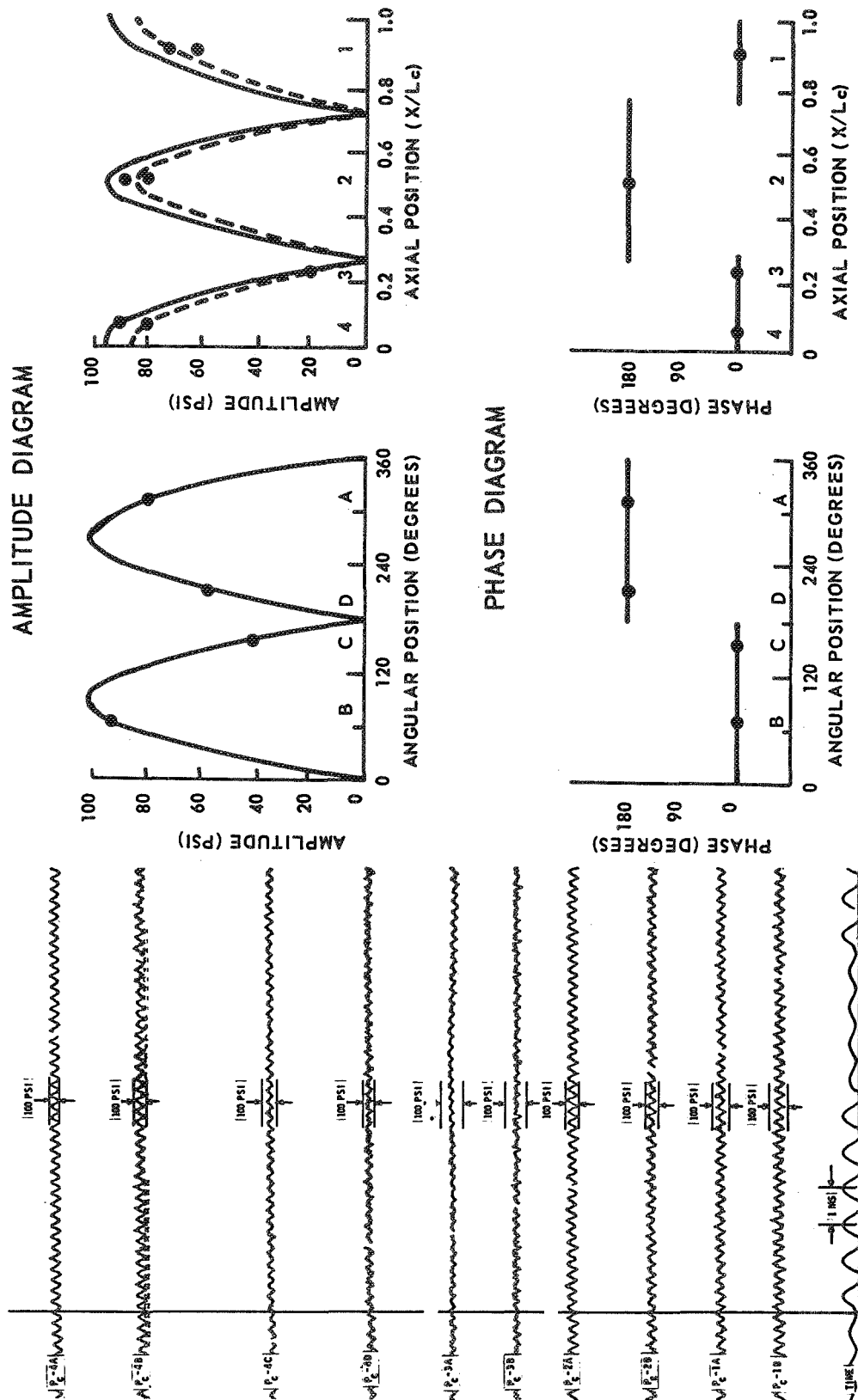


Figure 52 -- Identification of IT-2L Instability Mode

6.3, Data Analysis (cont.)

axial position down the chamber. Next, a time line on the analog record should be established together with the phase relationship of the instability as recorded at each transducer and these phase and amplitude data correlated with the theoretical mode relationships. A detailed description of this method of mode identification is given in Section 6.2. An example of the use of analog data in conjunction with amplitude and phase diagrams is shown in Figure 52. This figure demonstrates the technique for a more complex wave form in identification of a 1T-2L mode of instability.

6.3.2 Power Spectral Density Plots

Power spectral density plots are important in determining relative magnitudes of the various modal frequencies present in an instability. An example of a power spectral density plot of a complex mode form in which two modes predominate is shown in Figure 53. It is common for a test record to contain multiple modes which change during the test. (These changes may be caused by any number of effects such as changes in fuel temperature, mixture ratio variations, changing chamber pressures, and others.)

Often useful is a variation of the power spectral density data in which the test is analyzed using a fixed frequency band filter and observing the changes in amplitude of a particular mode throughout the test. Frequently a given test parameter affects the stability of a system. One may observe one mode at the beginning of a test and as the test progresses the mode will change to a mode of a higher or lower order. This may be caused by a change in one of the operation parameters which affect stability (e.g., chamber pressure, propellant density, or propellant phase and others). To evaluate an entire test, the predominant modes and the period during which each is sustained during a test should be determined. A fixed frequency band filter may be applied to the analog record and power spectral density plots run at a variety of frequency bands for the entire test duration.

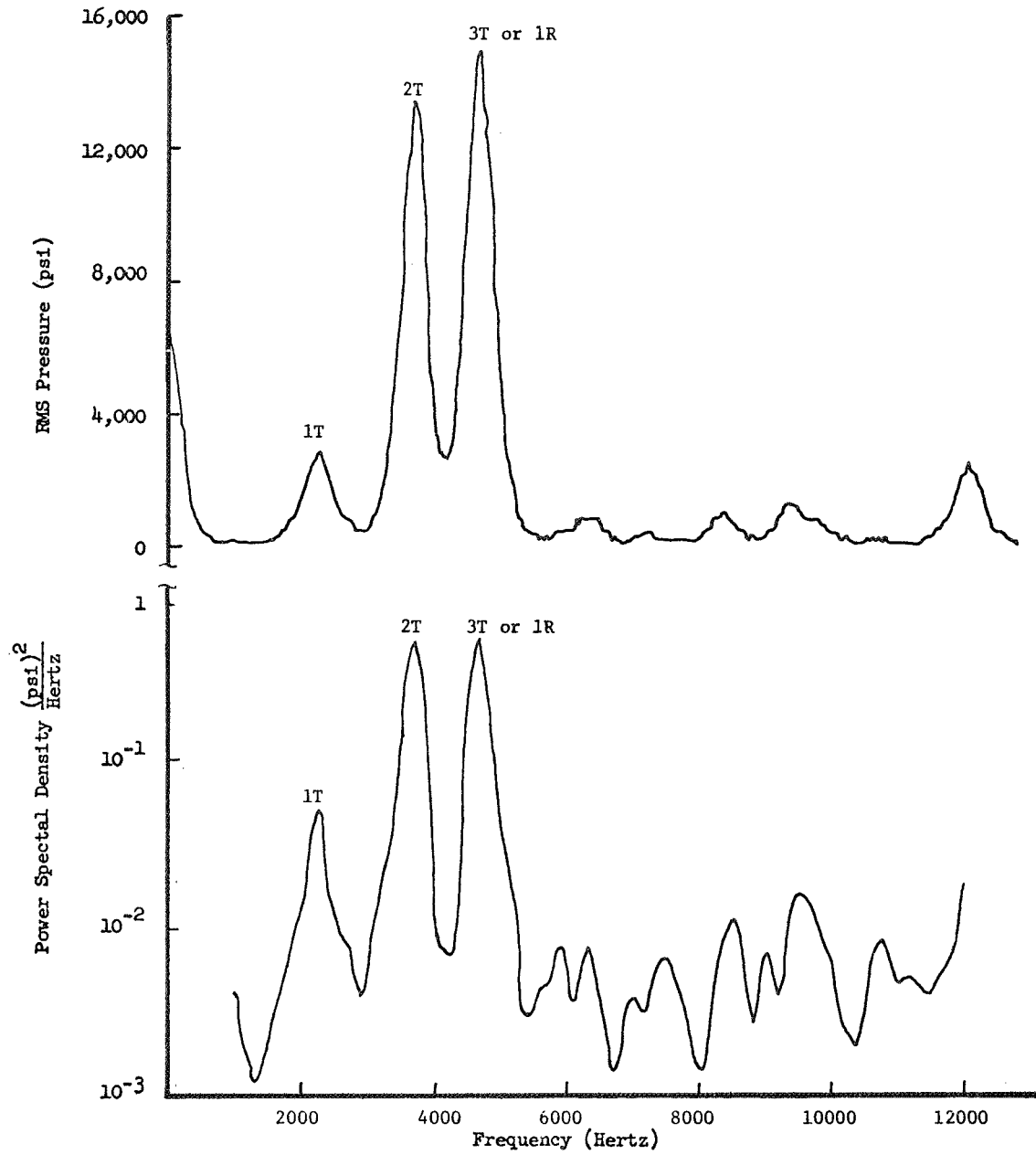


Figure 53 -- Power Spectral Density Plot

6.3, Data Analysis (cont.)

6.3.3 Fixed Frequency Bandwidth - Pressure Amplitude Data

This type of data is obtained by passing the unfiltered analog data through a fixed-frequency bandwidth filter and obtaining the sound pressure level (decibels) of the instability.

An instrument for obtaining this type of data is the Brüel and Kjaer spectrometer (B&K Analyzer). In this analyzer, the data are plotted in decibels on the ordinate against time on the abscissa. A measure of a system's susceptibility to instability is often given in terms of the time required for a given pressure perturbation (pulse) to decay. In the case of stability research with subscale hardware, as done with transverse or longitudinal excitation chambers, the decay rate and growth rate data may be obtained directly from the B&K record as db/sec, or when divided by the observed frequency from the analog record as db/cycle.

An example of B&K data used in conjunction with the analog record is shown in Figure 42. These data are characteristic of those obtained with the transverse excitation chamber. On this record, the second transverse mode occurred first, decayed, and the first transverse mode grew.

NOMENCLATURE

	<u>Latin</u>	<u>Dimensions</u>
A	Area, general	in. ²
A _c	Area, cross section of chamber plenum	in. ²
A _o	Area, orifice, injector or resonator	
A _t	Area, chamber throat	in. ²
A _{vn}	Injection distribution Coefficient	--
c	Acoustic velocity	ft/sec
c _p , c _v	Specific heat at constant pressure, constant volume	--
d	Diameter, general	in.
d _o	Diameter, oxidizer injector orifice, resonator orifice	in.
E	Energy	ft-lb
e	Base of natural logarithms	--
F	Function as in F (VR sin Ø)	--
f	Frequency	sec ⁻¹
f _s	Sensitive frequency	sec ⁻¹
G	Combustion response	
g	Acceleration due to gravity (32.2 ft/sec ²)	
H	Enthalpy	Btu/lb
h	Height, baffle	in.
i, j	Term in a sequence; also $\sqrt{-1}$	--
J	Bessel function of first kind	--
K	As defined in Equation 35, pg 211	--
L	Longitudinal mode	--
l	Length	in.
M _c	Mach number	--
n	Interaction index; also as n = 1,2,3 ...	--
N _{min}	Combustion response, chamber	--
N _o	Combustion response, injector at sensitive frequency	--
P	Pressure, general	psi
P _c	Chamber pressure	psi

NOMENCLATURE (cont.)

	<u>Latin</u>	<u>Dimensions</u>
P_{crit}	Critical pressure (usually of the less volatile propellant)	psi
P_r	Ratio to critical pressure (P_c/P_{crit})	--
P_t	Pressure at chamber throat	
Q	Burning rate	Btu/sec
q	Heat flux	Btu/in. ² sec
R	Radial mode	--
R	(Equations 33 ff) resistance per unit length	psi/ft
R	Universal gas constant (1545 Btu/lb°F)	
r	Radius	in.
S	Transfer function	--
$S_{v\eta}$	Argument to Bessel function for transverse modes	--
T	Tangential mode	--
T	Temperature	°R
t	Time	sec
t_w	Wall thickness (acoustic resonators)	in.
x	Linear displacement	ft
V	Volume	in. ³
VR	Velocity ratio (fuel to oxidizer)	--
<u>Greek</u>		
γ	Ratio of specific heats	--
ζ	(Table 15) damping ratio (damping ÷ critical damping)	--
ζ_{oc}	Chamber damping ratio	--
ζ_{oT}	Transducer damping ratio	
η	Order of radial mode (= number of derivatives of Bessel function)	--
θ	(1) Angular displacement	deg
	(2) Real part of argument of K_x	--
μ	Dynamic viscosity	$\frac{lb \text{ sec}}{ft^2}$

NOMENCLATURE (cont.)

	<u>Greek</u>	<u>Dimensions</u>
ν	Order of tangential mode (= order of Bessel function)	--
ρ	Density	lb/ft ³
σ	Area ratio of face of resonator (Acoustic Liners)	--
τ	Sensitive time lag	sec
ϕ	Angle of impingement between propellant streams	deg
χ	Imaginary part of argument K_x	--
ω	Angular velocity	rad/sec
ω_{oc}	Natural frequency of chamber	rad/sec
ω_{oT}	Natural frequency of transducer	rad/sec
	<u>Subscripts</u>	
eff	Effective	
f	Face	
r	Resonator	
c	Chamber	
t	Throat	
oc	Resonant frequency, chamber	
oT	Resonant frequency, transducer	
T	Transducer	

GENERAL REFERENCES

1. Beltran, M. R., Breen, B. P., et al, Liquid Rocket Engine Combustion Instability Studies, Dynamic Science Report No. AFRPL-TR-66-125, 1966.
2. Campbell, D. T., Combustion Instability Analysis at High Chamber Pressure, Rocketdyne, Report AFRPL-TR-67-222, 1967.
3. Crocco, L., "Theoretical Studies on Liquid Propellant Rocket Instability," Tenth Symposium (International) on Combustion, The Combustion Institute," 1965.
4. Crocco, L., Research on Combustion Instability in Liquid Propellant Rockets Twelfth Symposium (International) on Combustion, The Combustion Institute 1969.
5. Crocco, L. and Cheng, S. I., "Theory of Combustion Instability in Liquid Propellant Rocket Motors," AGARDograph No. 8, Butterworths Scientific Pub., Ltd., London, 1956.
6. Crocco, L., Grey, J., and Harrje, D. T., "Theory of Liquid Propellant Rocket Combustion Instability and Its Experimental Verification, ARS Journal, Vol. 30, No. 2, February 1960.
7. Dykema, O. W., An Engineering Approach to Combustion Instability, 2nd Combustion Conference, ICRPG, CPIA Publication No. 105, May 1966.
8. Feiler, C. E., and Heidmann, M. F., Dynamic Response of Gaseous-Hydrogen Flow System and Its Application to High Frequency Combustion Instability, NASA TN D-4040, 1967.
9. Hefner, R. J., "A Review of the Combustion Dynamics Aspects of the Gemini Stability Improvement Program", Second Combustion Conference, CPIA Publication 105, Volume 1, pp 13-22, May 1966.
10. Heidmann, M. F., and Wieber, P. R., An Analysis of the Frequency Response Characteristics of Propellant Vaporization, NASA TN D-3749, 1966.
11. Heidmann, M. F., and Wieber, P. R., Analysis of n-Heptane Vaporization in Unstable Combustor with Travelling Transverse Oscillations, NASA TN D-4324, 1966.
12. Heidman, M. F., and Groeneweg, J. F., Dynamic Behavior of Liquid Jet Atomization, Fifth ICRPG Combustion Conference, CPIA Publication No. 183, 1968.
13. Ingebo, R. D., Drop Size Distribution for Impinging Jet Breakup in Airstreams Simulating the Velocity Conditions in Rocket Combustors, NASA TN 4222, 1958.

GENERAL REFERENCES (cont.)

14. Priem, R. J., and Guentert, D. C., Combustion Instability Limits Determined by a Nonlinear Theory and a One-Dimensional Model, NASA TN D-1409, 1962.
15. Reardon, F. H., "Correlation of Sensitive-Time-Lag-Theory Combustion Parameters with Thrust Chamber Design and Operating Variables, Fifth ICRPG Combustion Conference, CPIA Publication No. 183, 1968.
16. Summerfield, Martin, "A Theory of Unstable Combustion in Liquid Propellant Rocket Systems," ARS Journal, Vol. 21, No. 5, September 1951, pp 108-114.
17. Hannum, N. P., Bloomer, H. E., and Goelz, R. R., Stabilizing Effects of Several Injector Face Baffle Configurations on Screech in a 20,000 lb-Thrust Hydrogen-Oxygen Rocket, Lewis Research Center NASA TN D-4515, April 1968.
18. Wieber, P. R., Acoustic Decay Coefficients of Simulated Rocket Combustors, Lewis Research Center, NASA TN D-3425, May 1966.
19. C. R. Wylie, Advanced Engineering Mathematics, Second Edition, McGraw-Hill Book Co., 1960.
20. "Effects of Chamber Pressure, Flow per Element, and Contraction Ratio on Acoustic-Mode Instability in Hydrogen-Oxygen Rockets," J. P. Wanhainen, C. E. Feiler, C. J. Morgan, LeRC THD 4733, August 1968.
21. 5th ICRPG, "Correlations of Sensitive-Time-Lag Theory Combustion Parameters with Thrust Chamber Design and Operating Variables," F. H. Reardon, 1968.
22. Gemini Stability Improvement Program (GEMSIP), Final Report, Aerojet-General Corp., Report GEMSIP FR-1, 1965.
23. Report 20672-PIF, Stability Characterization of Advanced Injectors, Final Report on Phase I, Contract NAS 8-20672, Aerojet-General Corporation, 25 October 1968.
24. Handbook of Astronautical Engineering, Heing Hermann Koelle, Editor, "Combustion Parameters and Interior Flow" by R. S. Levine, pp 20-57 through 70-68, McGraw-Hill Book Co., 1961.
25. Selection of Instrumentation for Analyzing Combustion Instability in Liquid Propellant Rocket Engines, prepared by the Committee on Instrumentation and Test Data, ICRPG, Chemical Propulsion Information Agency CPIA Publ. 148, July 1967.

GENERAL REFERENCES (cont.)

26. Special Considerations for Combustion Instability Instrumentation and Data Representation, prepared by the Committee on Instrumentation and Test Data, ICRPG, Chemical Propulsion Information Agency, CPIA Publ. 170, June 1968. Gemini Stability Improvement Program, Contract AF 04(695)-517, Final Report, Vol. 6, Instrumentation Report GEMSIP FR-1 SSD-TR-66-2, 31 August 1965.
27. A Study of the Suppression of Combustion Oscillations with Mechanical Damping Devices, Pratt & Whitney Aircraft Final Report PWA FR-1922, Contract NAS 8-11038, July 1966.

APPENDIX A

ANALYTICAL APPROACHES TO
COMBUSTION STABILITY

Although combustion stability problems encountered in engine development have usually been solved by trial-and-error methods, a number of analytical approaches have been originated. For purposes of discussion, it is convenient to group these analytical approaches into three categories:

- a. Response factor approach
- b. Mechanistic-numerical analysis
- c. Sensitive time lag theory

In the following paragraphs brief descriptions of each method are given and the general philosophy, advantages and limitations, and use in design and development are discussed. Since the Sensitive Time Lag approach is the subject of the manual to which this Appendix is attached, its discussion here will be appropriately short.

A. RESPONSE FACTOR APPROACH

Analytically, the simplest and perhaps most easily appreciated method is the response factor approach. The unsteady operation of the rocket engine is viewed as resulting from the cumulative effect of many separate combustion and flow processes. For example, if the chamber pressure oscillates, the combustion rate and the exhaust flow rate both oscillate. The combustion adds energy to the oscillation, whereas the exhaust flow takes energy away. Clearly, the growth or decay of the pressure oscillation depends on the balance between these two processes. The response factor approach thus consists of (a) the evaluation of the response of each significant process to a chamber pressure oscillation, and (b) the summation of the individual effects to determine whether there is a net positive energy addition to the oscillation. By Rayleigh's criterion, the energy must be added in phase with the oscillating pressure. The "response factor" is the in-phase component of the energy addition, divided by the pressure oscillation amplitude. Hence, it may be thought of as the real part of the process "transfer function." The response factor is usually nondimensionalized by use of suitable steady-state reference quantities.

A, Response Factor Approach (cont.)

Heidmann and Feiler*, who introduced the term "response factor," base their analysis on the mass flow rate. Attention is focused on the stability limit, at which the mass addition due to combustion (in phase with the pressure) is just equal to the in-phase component of the mass efflux through the exhaust nozzle. If several processes are considered in the mass addition term, the net effect is taken to be the sum of the individual process response functions, each weighted by the fraction of the total mass flow entering into the process. However, the analyses published to date have concentrated on a single combustion process and have been restricted to purely transverse modes. In addition, the nozzle loss has been taken as a constant.

Response factors have been derived for several possible rate-controlling processes. Both linear and nonlinear analyses of droplet vaporization have been performed by Heidmann and Wieber**. To explain the behavior of gaseous hydrogen/liquid oxygen combustors, Heidmann and Feiler determined theoretically the response of the gaseous hydrogen flow to high frequency chamber pressure oscillations. This analysis includes a combustion time delay, which must be empirically determined. The large response factor values found for hydrogen injection (compared to other processes considered) indicate that this process can be expected to have a significant effect on the stability of an O_2/H_2 engine. A relatively simple analysis of atomization has also been performed. #

* Feiler, C. E., and Heidmann, M. F., Dynamic Response of Gaseous-Hydrogen Flow System and Its Application to High Frequency Combustion Instability, NASA TN D-4040, 1967.

** Heidmann, M. F., and Wieber, P. R., An Analysis of the Frequency Response Characteristics of Propellant Vaporization, NASA TN D-3749, 1966.
Heidman, M. F., and Wieber, P. R., Analysis of n-Heptane Vaporization in Unstable Combustor with Travelling Transverse Oscillations, NASA TN D-4324, 1966.

Heidman, M. F., and Groeneweg, J. F., Dynamic Behavior of Liquid Jet Atomization, Fifth ICRPG Combustion Conference, CPIA Publication No. 183, 1968.

A, Response Factor Approach. (cont.)

Dykema* has taken the controlling process for unsteady combustion to be mass transfer by molecular diffusion from the surface of a liquid drop to the surrounding flame. The drop is assumed to be spherical and the relative velocity between the drop and the surrounding gas is essentially zero; hence, this model will be valid only at the location (near the injector face) where liquid and gas velocities are equal. In Dykema's analysis damping effects are not treated quantitatively. Further, because of the difficulty in evaluating many of the physical and chemical quantities in the response factor equation, it is used mainly as a correlating equation. That is, the frequency is normalized by a function of chamber pressure, injection orifice size, and mass flow rate, and includes an adjustable constant. The response function is positive only over a certain range of normalized frequency values. By comparing stability test data for a given engine with the theoretical response curve, a value of the adjustable constant can be inferred. It is then possible to predict the unstable frequency ranges for other engines using the same propellants.

B. MECHANISTIC-NUMERICAL ANALYSIS

Whereas the response function approach involves essentially an "open-loop" analysis, the mechanistic-numerical method originated by Priem and Guentert** incorporates the effects of the burning rate oscillation on the chamber pressure oscillation (feedback). The equations governing the unsteady flow in a rocket combustion chamber are written very generally to allow for non-sinusoidal waves and an arbitrary choice of the rate-controlling combustion process. Because of the nonlinearities associated with the conservation equations and the combustion rate equations the only practical method of solution is by numerical integration.

* Dykema, O. W., op. cit.

** Priem, R. J., and Guentert, D. C., Combustion Instability Limits Determined by a Nonlinear Theory and a One-Dimensional Model, NASA TN D-1409, 1962.

B, Mechanistic-Numerical Analysis (cont.)

The numerical solution begins with specified initial conditions, which correspond to steady-state operation with a disturbance superimposed. The governing equations, in difference form, are integrated at a number of locations in the combustor to determine time histories. If the initial disturbance decays, the combustor is stable. Usually, the disturbance amplitude is varied until the threshold at which the disturbance begins to grow is obtained. The accuracy of the solution, as well as the length of time required to obtain it, depends on the number of chamber locations at which calculations are performed and on the size of the time-step. At present, accurate solutions for two or three space dimensions are prohibitively expensive. Therefore, nearly all work has been based on an annular control volume that is very small in length and radial thickness.

Priem's initial calculations made use of a quasi-steady vaporization-controlled combustion model. The steady-state theory from which it was derived had been successful in correlating performance data from a large number of engines. Two parameters were shown to control both the threshold perturbation amplitude and the amplitude of the fully-developed oscillations. These parameters are a dimensionless burning rate

$$\ell = \frac{M_x R}{\epsilon_c}$$

(where M_x is the fractional burning rate per unit length, R is the mean radius of the annular control volume, and ϵ_c is the chamber contraction ratio) and the relative velocity between gas and liquid in the control volume. The most unstable condition corresponds to $\ell = 1$, approximately; that is, at this value of ℓ the disturbance threshold amplitude is a minimum. Decreasing the relative velocity always is destabilizing, probably because of the dependence of the burning rate on $Re^{1/2}$ (Re = Reynolds number based on relative velocity),

B, Mechanistic-Numerical Analysis (cont.)

as assumed in the theory. Usually a minimum value of the relative velocity is selected, corresponding roughly to the intensity of turbulence in the chamber.

A chemical-reaction-controlled combustion model has also been studied*. It was found that this process is normally so fast that it would not be controlling, except possibly for gaseous-propellant rocket engines. Atomization# and gas-phase mixing** have received a small amount of attention, but in most analyses the burning rates have been treated as vaporization-limited. Such additional features as monopropellant decomposition## and drop-let shattering** have been incorporated into some mechanistic-numerical models.

In practice, the stability analysis must be used in conjunction with a steady-state analysis, which generates liquid and gas velocities, temperatures, pressures, etc., at various locations within the chamber. Then the stability analysis is used to determine, for the given steady-state flow and controlling combustion mechanism, the threshold perturbation for continuous oscillations. When any of the design features or operating conditions are changed, the steady and unsteady analyses are repeated to determine a new threshold value. Clearly, a change that results in an increased threshold is a stabilizing effect.

* Priem and Guentert, op cit.

** Campbell, D. T., Combustion Instability Analysis at High Chamber Pressure, Rocketdyne, Report AFRPL-TR-67-222, 1967.

Ingebo, R. D., "Drop Size Distribution for Impinging Jet Breakup in Airstreams Simulating the Velocity Conditions in Rocket Combustors," NASA TN 4222, 1958.

Beltran, M. R., Breen, B. P., et al, Liquid Rocket Engine Combustion, Instability Studies, Dynamic Science, Report No. AFRPL-TR-66-125, 1966.

C. SENSITIVE TIME LAG THEORY

The sensitive time lag theory differs from both of the preceding types of analyses in that the combustion mechanism is not specified. Rather, a fairly simple, but general, combustion response function that involves two adjustable parameters (n and τ) is incorporated into a rigorous gas dynamic analysis of the combustion chamber flow. Although the most complete development of this approach has been that associated with very small perturbations (linear theory), several studies of finite-amplitude oscillations (nonlinear theories) have recently been published.*

There are both advantages and disadvantages in approaching the combustion process as a "black box." No initial assumptions or estimates of combustion response coefficients or exponents need to be made. As a result, very general theoretical results can be obtained, and some stability trends can be predicted. However, a complete stability analysis requires that values of the combustion response parameters be known. These parameters can only be determined by comparing extensive stability test data with the corresponding size, chamber pressure, mixture ratio, chamber Mach number, and injector pattern design. A substantial amount of such information now exists,** although it is not complete, and considerable data scattering is present. Nevertheless, successful application to stability prediction and improvement has been demonstrated#.

* Crocco, L., Research on Combustion Instability in Liquid Propellant Rockets Twelfth Symposium (International) on Combustion, The Combustion Institute 1969.

** Reardon, F. H., Correlation of Sensitive-Time-Lag-Theory Combustion Parameters with Thrust Chamber Design and Operating Variables, Fifth ICRPG Combustion Conference, CPIA Publication No. 183, 1968.

Gemini Stability Improvement Program (GEMSIP), Final Report, Aerojet-General Corp., Report GEMSIP FR-1, 1965.

APPENDIX B

TEST PROGRAM FOR CONTRACT NAS 8-20672, PHASE II

Report 20672-P2D, Appendix B

CONTENTS

	<u>Page</u>
Purpose	249
Annular Injector Tests	249
Excitation Chamber Tests	251

TABLES

B-1	Transverse Excitation Chamber Stability and Performance Data	254
B-2	Extension of Test Remarks -- Excitation Chamber Tests	257

ILLUSTRATIONS

B-1	Triplet Injector before Firing	261
B-2	Triplet Injector after Firing in Annular Chamber	263
B-3	Annular Chamber after Firing	265
B-4	Transverse Excitation Chamber -- Disassembled	266
B-5	Transverse Excitation Chamber -- Installed on Test Stand	267
B-6	Injector Module Insert	268
B-7	Growth Rate/Decay Rate as Function of Frequency	270
B-8	Sensitive Time Lag Correlation	271

PURPOSE

The tests conducted during Phase I and Phase II of this program were intended to evaluate the characteristics of injectors using oxygen-hydrogen propellants with regard to combustion stability. Two injector elements were tested: an annular combustor using a coaxial injector which had been previously tested with cylindrical hardware and a triplet injector design of a type which was a primary candidate for use with the advanced cryogenic engine.

This discussion is concerned only with the triplet injector. Test results relating to the coaxial injector element were obtained during Contract NAS 8-11741 and are reported in Reference 1. Evaluations of the coaxial injector design with an annular combustor are reported in Reference 2.

ANNULAR INJECTOR TESTS

Testing of the triplet pattern with annular chambers during Phase II was limited to a single test of one injector. The test objective was to provide correlation with the results forthcoming from tests with the transverse excitation chamber as will be described later.

The triplet elements in the injector were designed to duplicate the elements that would be used in the excitation chamber. The arrangement is shown in Figure B-1. There were 192 triplets in all, arranged in 24 radial rows of 8 elements per row. The four middle triplets in each row were aligned at 60° to the row. The elements second from the end were oriented at 75° and the end elements at 90° to the row. The fuel streams were fed from a raised copper ridge and were directed parallel to the axis of the chamber, while the oxidizer streams impinged from either side, emerging from the stainless steel face of the injector. The lands on the injector face between the oxidizer orifices were flame-sprayed with a zirconium oxide

coating. The photographs (Figure B-1) show the injector prior to application of the coating. A central steel post held an ablative sleeve to form the centerbody for the annular combustor.

One test was conducted at nominal chamber pressure (1735 psia), 5.0 mixture ratio, and 66 lb/sec total weight flow. Seven high-frequency pressure transducers were installed at various locations in the chamber to aid in the identification of oscillatory modes. Three pulses of 20, 40, and 80 grain size were fired at 50-millisecond intervals during steady state operation. The 80-grain pulse initiated an instability of low amplitude (100 psi peak-to-peak), which was clearly identified on the test record. The total firing duration was 798 milliseconds.

The face of the injector was completely eroded as shown in Figure B-2. The erosion penetrated the oxidizer manifold, exposing the radial distribution channels and in some cases the oxidizer feed holes leading from the main manifold at the back of the injector, as can be seen in the photograph. The fuel manifold remained nearly intact. The fuel injection orifices appear in the photographs in the form of tubes of small diameter extending from the injector face. The test record indicated that the erosion had reached the oxidizer manifold at FS-1 +800 milliseconds.

The damage to the chamber was slight and occurred only in the vicinity of the injector. This is evident from the photograph (Figure B-3).

EXCITATION CHAMBER TESTS

A tool for the purpose of evaluating the combustion response of an injector element was developed and demonstrated during Phases I and II of this program. It is termed a transverse excitation chamber. It is a two-dimensional chamber, with walls converging at a constant angle to form the wider plane while the narrower plane is of constant height. Oscillations (combustion gain) are of greatest amplitude in the direction of flow and in the direction of approach to the converging walls. The chamber is most sensitive to modes of instability in the latter direction, that is transverse to the direction of flow. The chamber is provided with a removable lid and wedges, which when inserted, alter the wavelength of the fundamental mode, making it possible to test over a range of natural chamber frequencies while utilizing the same vehicle for testing. Two chambers were fabricated, one with a 30° included angle with range from 2000 Hz to 7000 Hz, and one with 25° included angle and a range from 2800 Hz to 7000 Hz. The length from the chamber to the nozzle was the same in both chambers and the nozzles were interchangeable. The chamber with the 36° included angle is shown disassembled in Figure B-4. Figure B-5 is a photograph of the chamber as installed on the test stand.

The injector consists of cylindrical modules which are installed in recesses at the end of the chamber opposite the nozzle and with the axes normal to the wider plane. Each module for this test program contained 11 triplet elements arranged similarly to the rows in the annular chamber discussed previously. Figure B-6 is a photograph of such a module and the method of installation is shown in Figure B-4. The modules are removable and the number used for a particular test is determined by the size of wedge used in the chamber.

Testing was conducted by bringing the combustor to steady state operation and observing the combustion response as influenced by the chamber acoustics.

During the test a pyrotechnic charge was fired in order to produce a pressure pulse of high amplitude in the chamber. When an instability developed spontaneously, its rate of growth to maximum amplitude (cycle limit) was measured from the high-frequency record. When an established, fully developed instability was subjected to a pulse, the effect was a momentary unorganization of the instability followed by a regrowth. If the operation was stable at the time of pulsing, the rate of decay of the induced oscillations was measured to determine the relative effect of system losses on the instability.

A total of 31 tests was conducted during Phase II. Table B-1 is a summary of the test data, taken at different times during most tests. Table B-2 is an extension of the Remarks of Table B-1 and includes additional observations pertinent to the testing. The testing was conducted at varied chamber pressure, mixture ratio and injection velocity ratio. In addition, Mach number was varied by altering the nozzle area between tests and the frequency of the fundamental mode was also varied by the use of the wedges to change the convergence angle of the chamber.

It was observed during the testing that combustion occurred from 1 to 2 in. away from the injector. There was erosion of the area adjacent to the last triplet at both ends of the injector modules which multiplied the number of times that the chamber had to be repaired as compared with the frequency of repairs required when operating with injectors having normal characteristics with regard to erosion.

The test data provide basic input for design criteria. (See Section 3 of the basic report for discussion of their use.) Figure B-7 is a plot of growth rate and of decay rate as functions of frequency. These data show that the sensitive frequency is in the vicinity of 2900 Hz.

A composite correlation equation was derived from the application of Sensitive Time Lag concepts to the test data. Figure B-8 was constructed by plotting the expression

$$\tau \propto \frac{(M_c)^{1/3}}{(d_{ox})^{1/2}}$$

against values of P_c/P_{crit} , where

τ = sensitive time lag, msec

M_c = Mach number

d_{ox} = oxidizer orifice diameter, in.

P_c = chamber pressure, psia, and

P_{crit} = critical pressure of the oxidizer

The correlation equations resulting are

$$\tau = 0.275 (d_{ox})^{1/2} M_c \frac{P_c}{P_{crit}}, \quad P_c < P_{crit},$$

and

$$\tau = 0.275 (d_{ox})^{1/2} (M_c)^{-1/2}, \quad P_c \geq P_{crit}.$$

It was concluded on the basis of the test results that:

- 1) The transverse excitation chamber is an effective tool for obtaining the sensitive frequency of an injector,
- 2) The sensitive frequency of the triplet injector that was tested is near 2900 Hz, and
- 3) Because of the erosion noted above that occurred during the testing, that the pattern of this injector is incompatible with the transverse excitation chamber.

Table B-1 -- Transverse Excitation Chamber Stability and Performance Data

Test No.	Time (msec)	No. Inerts	Freq (Hz)	P _o -P _k Amplitude (psi)	Geocath Rate (db/cycle)	MR	VR	P _o (psi)	T _{He} (°R)	W _h (#/sec)	ΔP _o (psi)	ΔP _{ex} (psi)	Sensitive Frequency (Hz)	Mach No.	Remarks
1	--	3	Invalid test, premature shutdown			4.84	4.24	1438	75	9.67	1045	1240	3280	0.047	Brief 4200 Hz oscillations occurred for 10 msec during start transient.
2	758	3	See remarks											0.047	Brief intermittent 4200 Hz oscillations seen throughout test essentially stable.
3	--	4	Invalid test												
4	565	4	3200 100		0.14	4.92	4.44	1353	84	15.39	1535	1366	3280	0.05	Rough combustion with intermittent periods of organized oscillations reaching 4 to 5% of P _o .
	656		3200 100		-0.125	5.20	4.22	1355	84	15.50	1450	1370	3200	0.05	
	750		3200 100		0.20	5.04	4.40	1256	94	14.90	1483	1351	3280	0.05	
	840		3200 125		0.56	5.30	4.34	1254	95	15.61	1448	1395	3280	0.05	
5	--	4	Invalid test												Helium bleed passage of pressure transducer restricted. Fundamental mode oscillations seen through amplitude distorted.
6	280	4	3200 140		0.375	Trans.	Trans.	1150	350 (Avg)		340	793	3280	0.05	Unstable throughout excellent growth rate data.
	570		3050 1100		0.164	5.67	7.24	1263	195	11.68	1435	959	3280	0.05	
	680		3050 100		0.164	5.60	7.98	1258	197	10.93	1360	960	3280	0.05	
7	650	3	See remarks			5.74	4.80	1517	114	9.22	802	1191	3280	0.05	Stable, no pulse; brief intermittent 4000 Hz oscillations.
8	652	7	2000		-1.0 (decay)	4.81	4.3	1500	73	22.14	760	1080	3280	0.043	Unstable after FS-2. Indication of fundamental mode oscillation during short pulse decay period.
	966		2000 150		0.28	4.93	4.4	1391	81	23.96	840	650	3280	0.043	
	1285		2000 250		1.00	0.75	25.4	277	69	9.2	1420	110	2380	0.043	
9	300	7	3450		0.16	Trans.	Trans.	1297	200		260	1160	3280	0.045	Harmonic mode occurred briefly during start transient, then test ran stable.
	653		2000		-2.00(decay)	5.36	4.3	1386	82	21.96	661	1138	3280	0.045	
	1003		2000 75		0.15	4.75	5.07	801	86	23.57	990	1160	3280	0.045	
	1200		2000 300		0.60	0.41	51.0	233	67	11.87	990	110	2240	0.045	
10	285	7	3500 350		0.186	Trans.	Trans.	7.60	350 (Avg)		160	1290	3280	0.047	Harmonic mode instability during entire test.
	500		3440 500		0.175	7.56	5.03	1426	180	20.23	1380	1150	3280	0.047	The oscillations have a tendency to grow, decay, then regrow in an aperiodic manner.
	620		3300 350		0.182	7.44	5.52	1397	189	21.00	1320	1180	3280	0.047	
	653		2000		-1.2 (decay)	7.41	0.96	1395	200	21.16	1280	1170	3280	0.047	
	663		3250 150		0.130	7.40	5.99	1395	202	21.20	1280	1190	3280	0.047	
11	262	7	See remarks			5.05	Trans.	658	350 (Avg)	22.0	30	1270	3160	0.046	Stable, no pulse; brief indications of 2000 Hz.
12	417	5	9200 100		0.122	11.20	4.62	221	124	19.47	734	832	3180	0.13	Undefined oscillation occurred briefly. Clear spontaneous fundamental mode. No pulse detected on test.
	520		2720 500		0.368	4.88	8.41	324	106	7.83	626	742	3510	0.13	
13	400	5	4300 300		0.326	10.12	5.81	226	219	19.50	1751	1048	3180	0.13	Spontaneous first harmonic mode which decayed during transient position of test. Spontaneous mode starts to grow during decay of harmonic mode.
	450		4300 450		0.116(decay)	6.87	8.10	433	201	13.96	1594	1104	3880	0.13	
	480		2620 450		0.610	8.53	6.67	401	206	17.06	1606	1296	3700	0.13	
	820		2470 300		0.190	4.17	3.77	545	200	13.85	1450	973	4180	0.13	
14	430	4	2900 150		0.172	5.25	6.78	399	132	14.43	1534	1297	4030	0.16	Spontaneous growth and decay. Indications of two modes (fundamental and first harmonic) occurring. 1T mode predominant after pulse.
	500		3000 700		0.467	3.26	9.31	393	113	9.83	1568	1050	4025	0.16	
	750		2900 150		Very Low	3.79	7.05	475	96	11.77	1440	1002	4260	0.16	

Table B-1 -- Transverse Excitation Chamber Stability and Performance
Data (cont.)

Test No.	Time (msec)	No. Inserts	Freq (Hz)	P _{Ex} Amplitude (psi)	Growth Rate (db/cycle)	MR	P ₀ (psi)	T _{1/2} (sec)	W _t (#/sec)	ΔP _r (psi)	ΔP _{ex} (psi)	Sensitive Frequency (Hz)	Mech No.	Remarks
15	550 765 950	4	2750 2850 2700	1475 200 100	0.29 0.105 0.167	6.06 6.07 5.65	7.23 6.61 4.42	145 129 120	10.80 11.69 -	1339 1228 1240	1228 1163 1292	4030 4160 4160	0.16 0.16 0.16	Clear spontaneous fundamental mode throughout test; relatively high amplitude briefly disturbed by pulse.
16	1445 225 650 1050	4	6700 2700 2750 2780	475 200 450 300	0.150 0.148 0.208 0.198	4.8 5.25 5.27 5.70	9.60 7.50 6.55 4.85	143 125 110 92	11.54 10.78 11.53 -	1232 1160 1100 1030	1260 1280 1223 1313	3690 3960 4030 4035	0.16 0.16 0.16 0.16	Undefined mode (only one transducer operating) Indications of two modes predominant.
17	--	3	No high frequency data recorded.											
18	520 695 745	3	3700 3500 3500	80 60	0.65 0.515 -2.0 (decay)	4.89 5.80 4.83	6.58 5.10 5.90	117 104 96	8.17 7.56 8.41	1273 1210 1186	1115 1012 1014	3860 3900 3900	0.13 0.13 0.13	Clear spontaneous fundamental mode grows and decays.
19	500 590 640 750+	3	3500 3400 3500 3450	30 40 50 50	0.257 0.41 - 0.59 0.63 -2.0 (decay)	6.12 5.32 5.94 6.37	7.84 8.44 7.44 6.86	184 174 170 163	7.69 7.99 8.24 8.56	1529 1573 1568 1514	1212 1124 1125 1106	3830 3960 4030 4060	0.13 0.13 0.13 0.13	Low level intermittent 3400 to 3500 Hz oscillation; essentially a stable test.
20	400 610 650 750	3	6800 3500 3500 3700	Reg. 50 285 240	-- 0.344 0.338 0.434	9.08 5.06 4.53 5.25	6.09 7.99 8.71 7.46	158 124 132 119	15.99 7.96 8.20 8.10	1144 918 944 940	1351 1121 1105 1069	2990 3840 3860 3920	0.13 0.13 0.13 0.13	Transient test. Clear, spontaneous oscillations.
21	700	3	--	--	--	1.24	37.85	274	3.71	710	142	2800	0.075	Test malfunction nominal flow data listed.
22	590 733	3	4100 4000	50	0.195 -2.0 (decay)	3.15 2.07	16.83 23.91	293 359	4.22 2.68	703 669	313 320	2830 3020	0.075 0.075	Brief low level oscillation lasting for only 30 msec. Remainder of the test was stable.
23	744	3	4000	--	-2.0 (decay)	3.18	22.38	406	3.19	1037	345	3160	0.075	Stable test.
24	447 630 680 760	3	3850 3900 3900 3900	60 50 50 80	0.36 0.690 0.372 0.436	3.51 3.55 3.55 3.79	10.87 8.45 8.18 7.39	160 122 118 1000	9.38 9.84 9.51 9.53	1324 1277 1265 1223	1137 1133 1109 1112	3840 3840 3840 3840	0.075 0.075 0.075 0.075	Spontaneous fundamental mode regrows - decays - and regrows. Mode returns after being temporarily disturbed by pulse disturbance.
25	744	3	4000	--	-2.0 (decay)	2.99	14.01	942	9.51	1755	1007	3840	0.075	Stable test.
26	500 640	5	5100 2900	225 620	0.40 0.534	6.97 4.39	11.52 15.71	423 411	8.08 5.93	549 551	553 446	3120 3100	0.070 0.070	Spontaneous first harmonic mode decays at 620 msec. Spontaneous fundamental mode sustains itself being only slightly affected by pulse disturbance.
27	460 800	5	2900 Combustion became stable	500	0.415	4.25	7.15	894	13.88	1187	862	3750	0.70	Spontaneous fundamental mode throughout test.
28	490 600 650 750	5	2800 2600 2500	225 300 250	0.785 0.460 0.200	4.51 5.14 4.89	18.29 14.24 15.75	489 542 565	6.94 8.00 8.62	1302 1232 1151	535 512 455	3280 3410 3480	0.070 0.070 0.070	Spontaneous fundamental mode grows and decays and regrows after being temporarily disturbed by pulse.
29	--	5	--	--	--	--	--	--	--	--	--	--	--	No high frequency data recorded.

Table B-1 -- Transverse Excitation Chamber Stability and Performance Data (cont.)

Test No.	Time (msec)	No. Inserts	Freq (Hz)	Pk-Pk Amplitude (psi)	Growth Rate (db/cycle)	MR	VR	Pc (psi)	Th2 (°C)	Wt (#/sec)	ΔPc (psi)	ΔPox (psi)	Sensitive Frequency (Hz)	Mach No.	Remarks
Contract 11741 Data*															
2	700	3	See remarks			8.49	9.40	1027	317	9.75	801	1188	3280	0.047	Stable; brief indications of 4500 Hz.
	1000		See remarks			17.20	3.27	940	203	9.84	1060	1285	3280	0.047	
5	520	4	3360	140	0.194	3.77	10.33	1361	200	11.4	1600	700	3280	0.048	
6	510	4	3300	210	0.182	3.76	15.04	1353	295	12.5	1582	842	3280	0.048	
	730		2900	190	0.114	3.85	7.92	1387	140	13.5	1480	793	3280	0.048	Unstable test; pulse briefly disturbs oscillation, allowing it to regrow at different rate.
Phase I Test Data**															
5	0.358	4			0.189			1250							Thermal ignition of 40 grain pulse.
	0.400		3450		0.189										
	0.520		3360		0.193	3.77	10.33	1361	200						
	0.560		3350		0.194	3.70	8.97	1374	160						
	0.595 (FS-2)		3300		0.197	3.57	8.35	1378	140						40 grain pulse temporarily knocks out instability.
	0.640		3300		0.197	3.89	6.84	1380	120						
6	0.304	4													
	0.490					3.70	15.88	1347	316						
	0.510		3300		0.182	3.76	15.04	1353	295						
	0.570		3260		0.184	3.59	13.53	1353	225						
	0.640		3150		0.190	3.61	10.35	1382	178						
	0.652					3.57	10.14	1387	167						
	0.669					3.51	9.78	1395	162						
	0.675					3.51	9.78	1395	160						
	0.730		3025		0.109	3.51	9.78	1387	140						
	0.900		2900		0.114	4.43	7.92	1378	128						

*Data taken from An Experimental Investigation of Combustion Stability Characteristics at High Chamber Pressure, Final Report Phase II, Aerojet-General Corporation Report No. 11741/SAG-F, Vol. I, 25 August 1966.
 **Data taken from Phase I Final Report for this Program, Aerojet-General Corporation Report No. 20672-PF1, 25 October 1968.

Table B-2 --- Extension of Test Remarks--Excitation Chamber Tests

<u>Test No.</u>	<u>Test Remarks</u>
1	The test was stable with low amplitude noise which appeared to be mostly transducer noise.
2	This test was similar to Test No. 1 in that low amplitude transducer noise could be seen throughout the test.
3	The helium bleed pressure transducer was plugged with particles of zirconium oxide and metal from the combustion chamber. A 3200 hz oscillation could be seen; however, the amplitude was distorted.
4	An intermittent growth of 3200 hz occurred during transient portions of the tests. However, the test was stable during the steady state operation.
5	Helium bleed pressure transducer was partially plugged with zirconium oxide coating as in Test No. 3; a 3200 hz oscillation was visible during the test; however, the amplitude was distorted.
6	This test was unstable and good growth rates were observed. The best data occurred at steady state conditions after the pulse had discharged.
7	This test was stable with some low amplitude noise present. No pulse was seen in this test.
8	This test was stable during the steady state portions of the test. A high rate of decay was recorded for this pulse in the fundamental mode at 2000 hz. The fundamental mode did occur during the shutdown portion of the test.
9	Results from this test were similar to Test No. 8 in that this test showed a high rate of decay of the pulse during the steady state portion of the test, and an instability occurred during the shutdown portion of the test.

Table B-2 -- Extension of Test Remarks--Excitation Chamber Tests (cont.)

Test No.	Test Remarks
10	The harmonic mode occurred during the entire test. The oscillations have a tendency to grow, decay, and regrow in an aperiodic manner. There was no indication of fundamental mode oscillations during the shutdown sequence.
11	This test was stable and no pulse was indicated. A low amplitude fundamental mode was indicated during the shutdown sequence.
12	Unstable test with an undefined mode at 9000 hz occurring during the transient part at the beginning of the test. The fundamental mode occurred spontaneously after the higher frequency mode decayed. No pulse was recorded during the test.
13	The instabilities of this test start with the harmonic mode during the initial part of the test, then a decay of the harmonic mode and growth of the fundamental mode. Decay rate of the harmonic mode was recorded at 450 msec after FSL.
14	An instability occurs early in this test at 3000 hz which shifts to 3250 hz during the test. The growth rate at 500 msec is indicative of a steady state growth.
15	The instability in this test starts at 450 msec and continues throughout the test. The pulse only briefly disturbed the oscillations.
16	During this test, two modes of instability occurred, a high frequency 6700 hz mode which occurred at the start of the test subsequently decayed, and the fundamental mode (2750 hz) started. The 6700 hz mode is not identifiable in that only one transducer was operating for this test.
17	No high frequency data was recorded during this test.

Table B-2 -- Extension of Test Remarks--Excitation Chamber Tests (cont.)

Test No.	Test Remarks
18	The fundamental mode grows and decays during the transient part of the test. The pulse discharged during a stable part of the test and clearly shows a high decay rate. The pulse decay occurs after the system is operating smoothly at steady state conditions; this point is considered the best of the data from this test.
19	This test was essentially stable. Low level intermittent growths and decays of the fundamental mode occurred barely above the noise level of combustion. A high rate of decay occurred at the pulse.
20	This test appears to be transient throughout. The fundamental mode however, grows and decays - regrows and is disturbed by the pulse and decays - later returns and regrows. The transient nature of the test appears to be the result of erratic valve travel.
21	This test was a malfunction due to a valve actuator problem.
22	This test was essentially stable with the exception of a low level (less than 10% P_c) instability during the transient portion of the test.
23	This test was stable throughout. A high decay rate occurred at the pulse.
24	This test is unstable and has good growth rate data between .36 - .44 d b/cycle. The pulse momentarily unorganized the instability which promptly regrew.
25	This test was stable throughout. A high decay rate occurred at the pulse.
26	This test was unstable with the first harmonic mode occurring first and was then followed by the growth of the fundamental mode which remained for the duration of the test and was only slightly disturbed by the pulse.

Table B-2 -- Extension of Test Remarks--Excitation Chamber Tests (cont.)

Test No.	Test Remarks
27	This test was unstable during most of the test and decays to the noise level of combustion just prior to FS2. A decay of the pulse is visible.
28	This test was unstable in the fundamental mode. The mode grows and decays during the transient portion of the test. The instability regrows after being temporarily disturbed by the pulse.
29	This test was invalid in that no high frequency data was recorded during the test.
30	This test was unstable throughout, and the instability regrew after the pulse. The growth rate after the pulse is probably most indicative of the sensitivity of the system.
31	This test was stable due to failure of the igniter to initiate combustion. The pulse initiated stable combustion. A brief period of fundamental mode oscillations occurred during the shutdown transient.

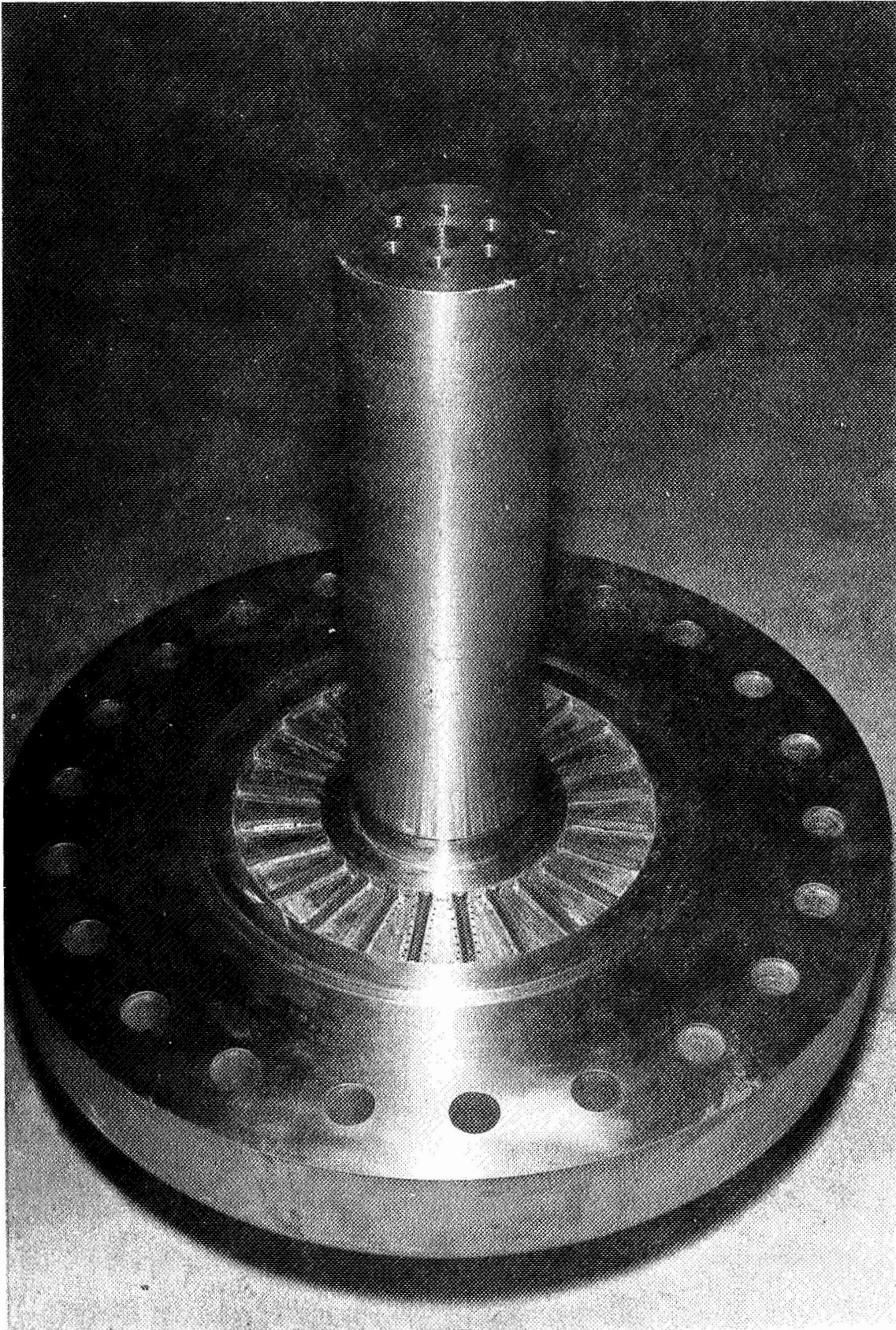


Figure B-1 --- Triplet Injector Before Firing, 1 of 2

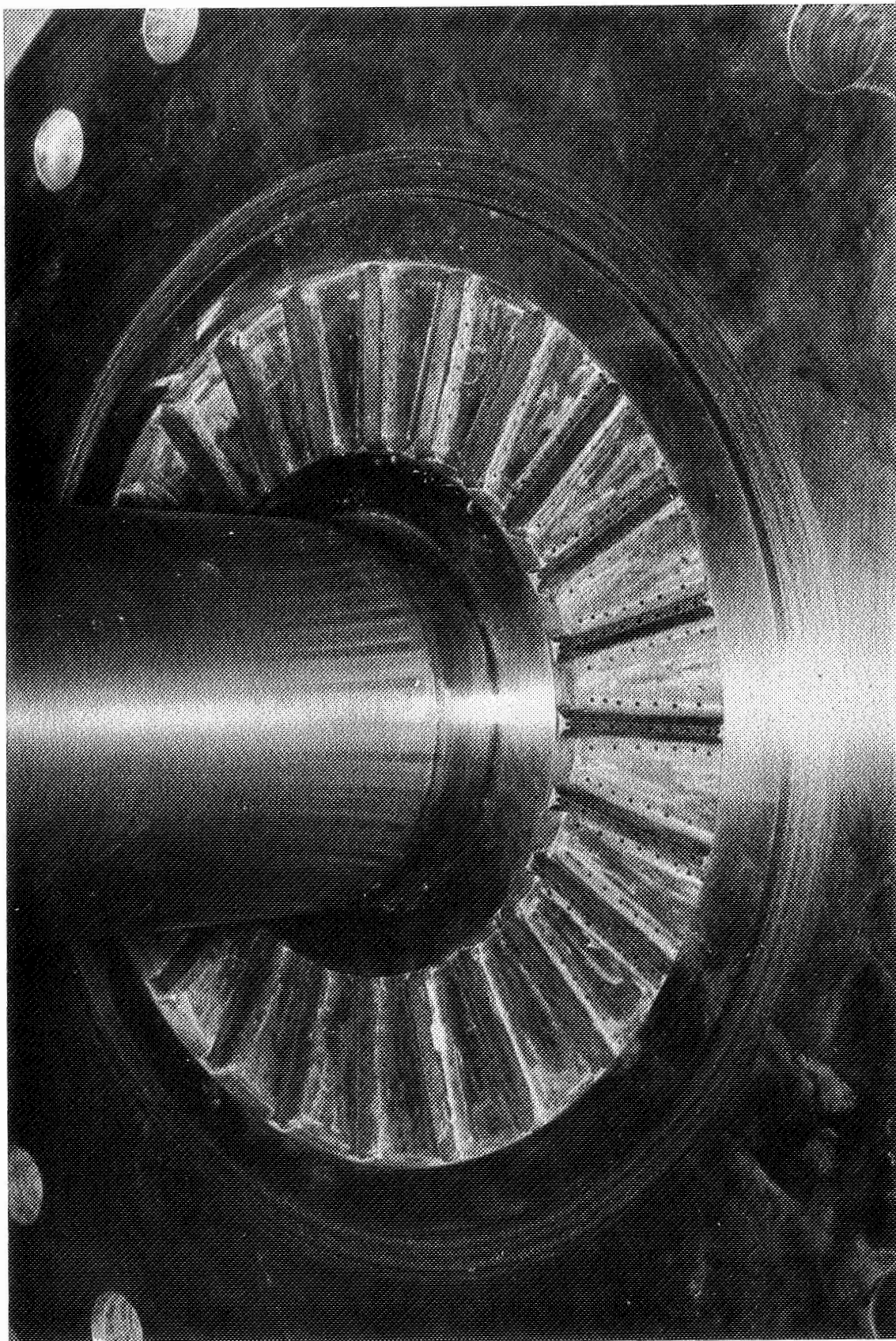


Figure B-1 -- Triplet Injector Before Firing, 2 of 2

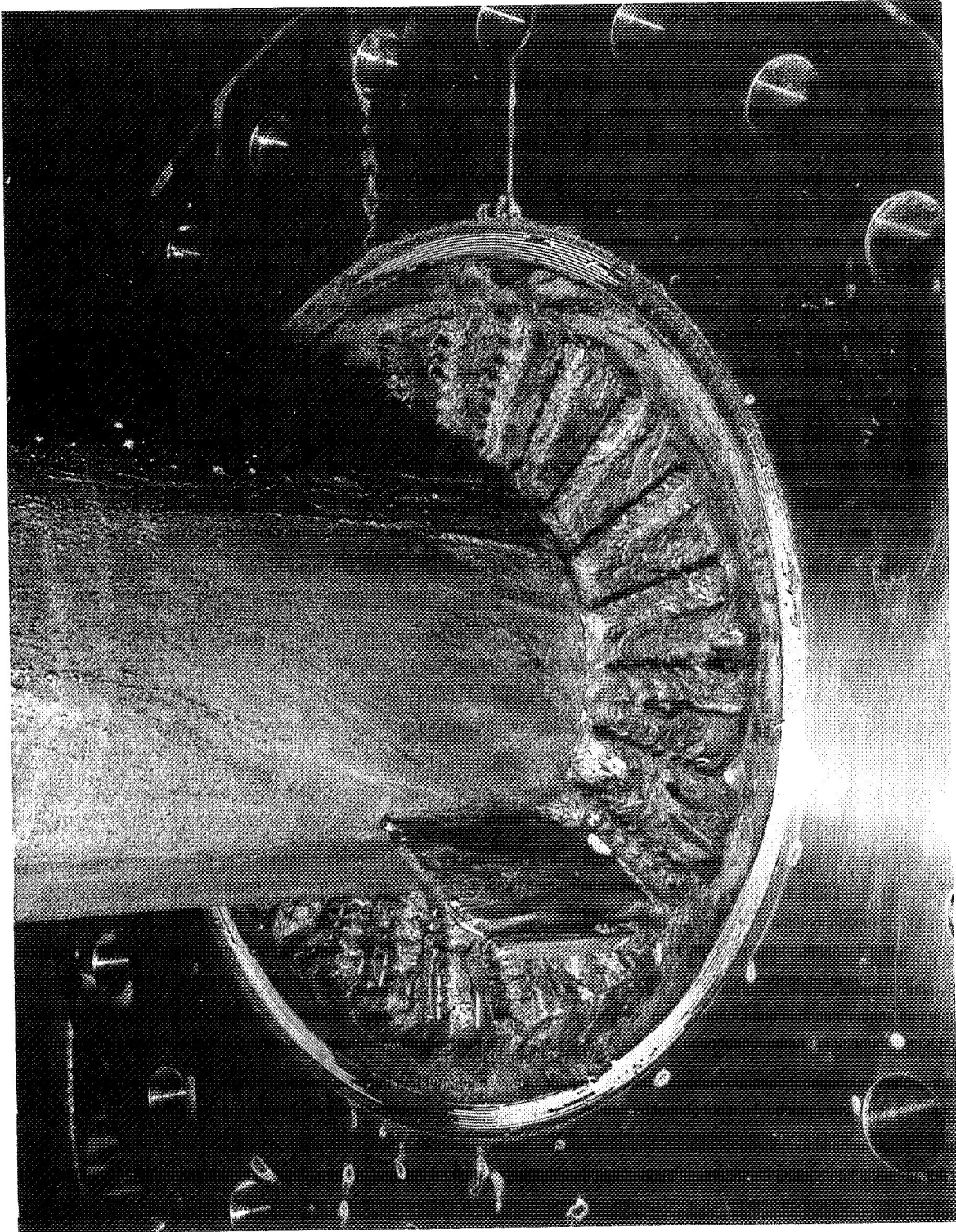


Figure B-2 --- Triplet Injector After Firing in Annular Chamber, 1 of 2

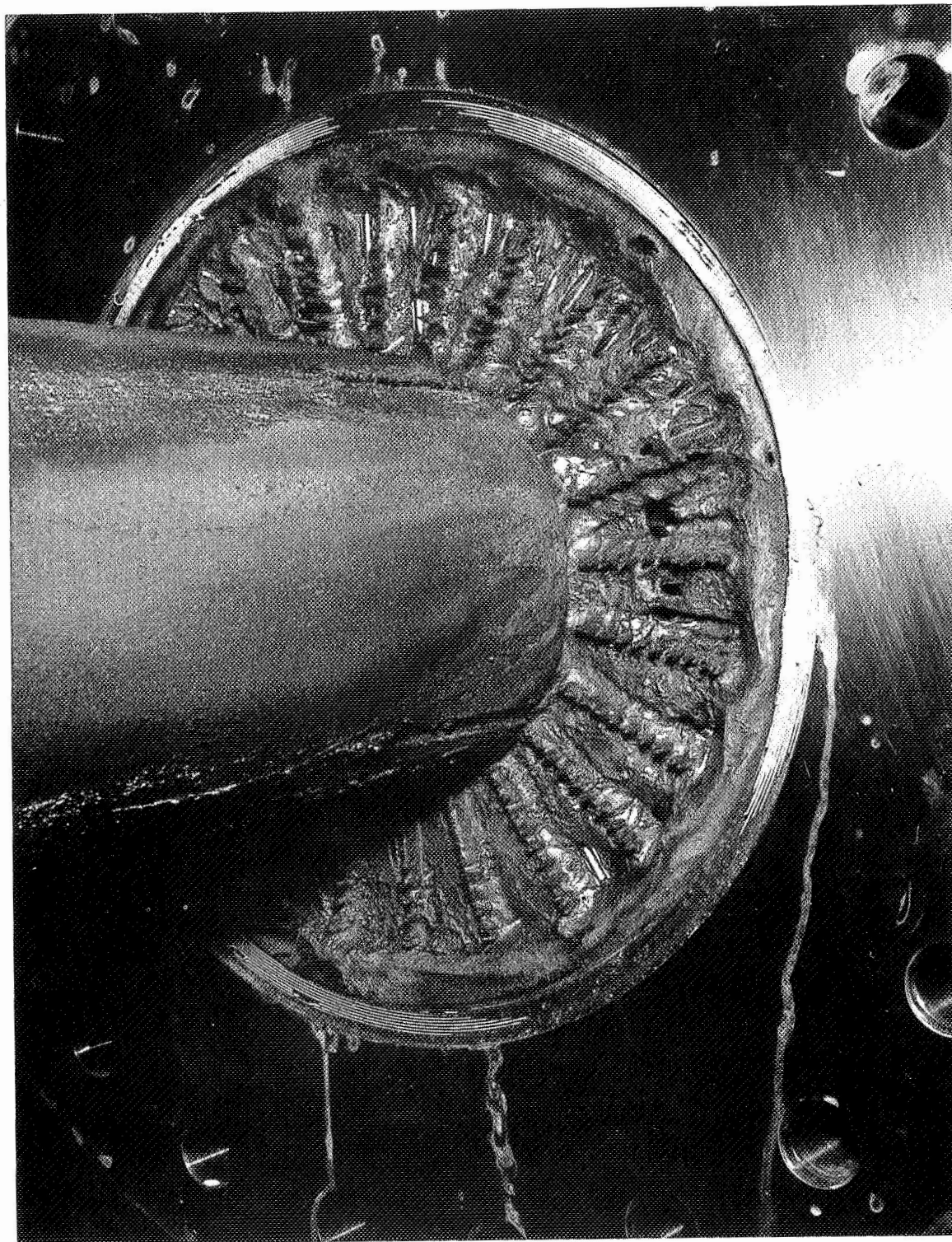


Figure B-2 -- Triplet Injector After Firing in Annular Chamber, 2 of 2

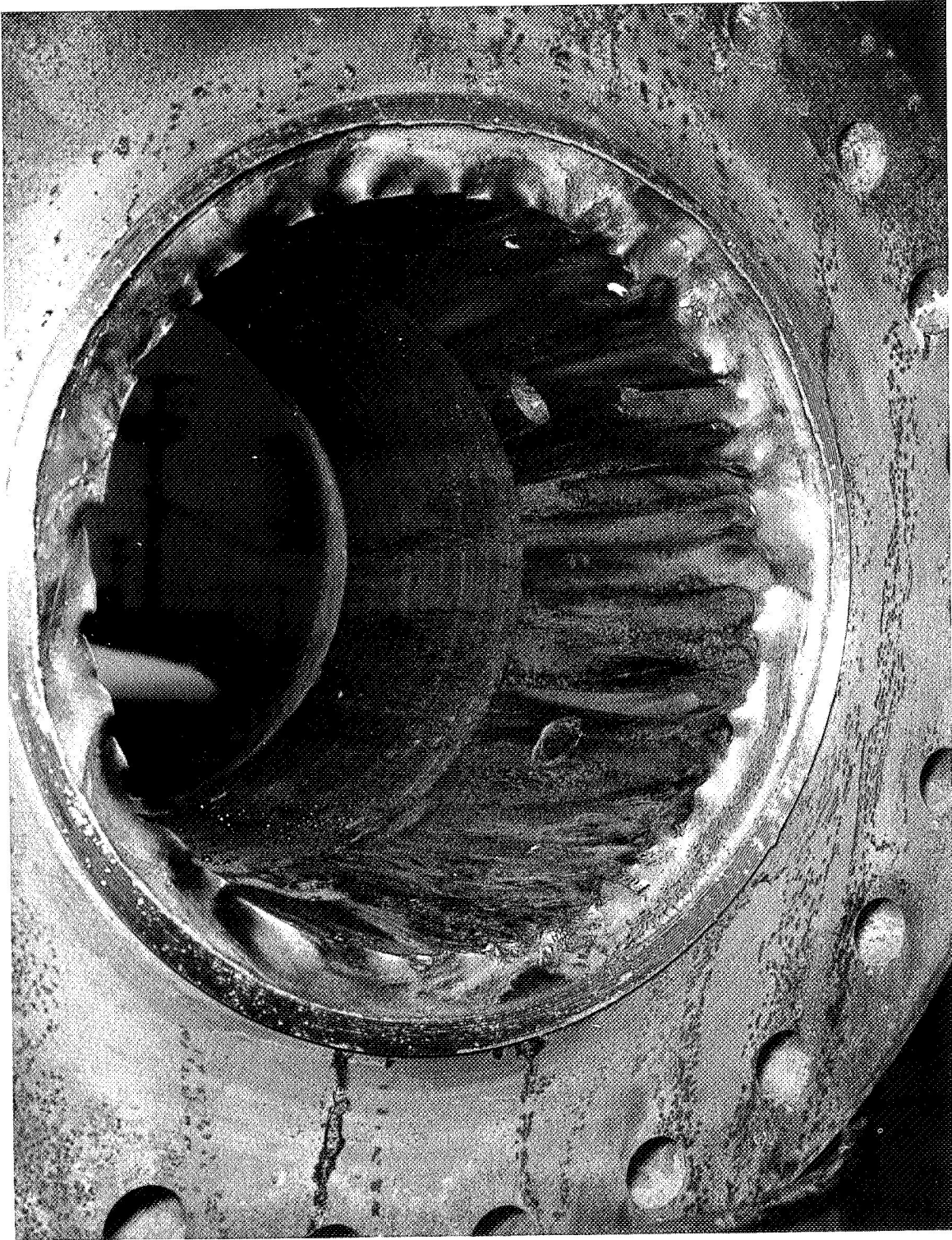


Figure B-3 -- Annular Chamber After Firing

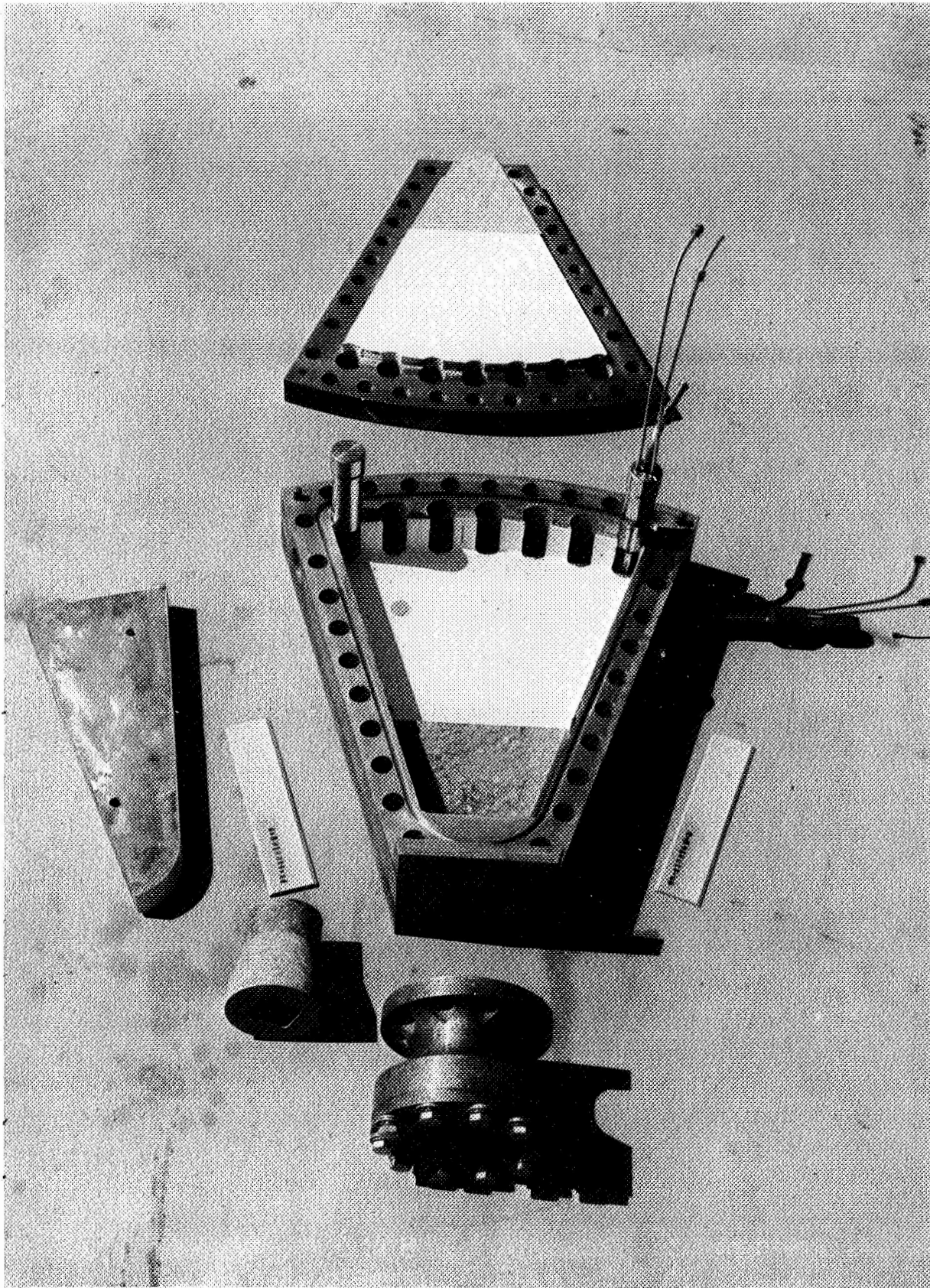


Figure B-4 -- Transverse Excitation Chamber - Disassembled

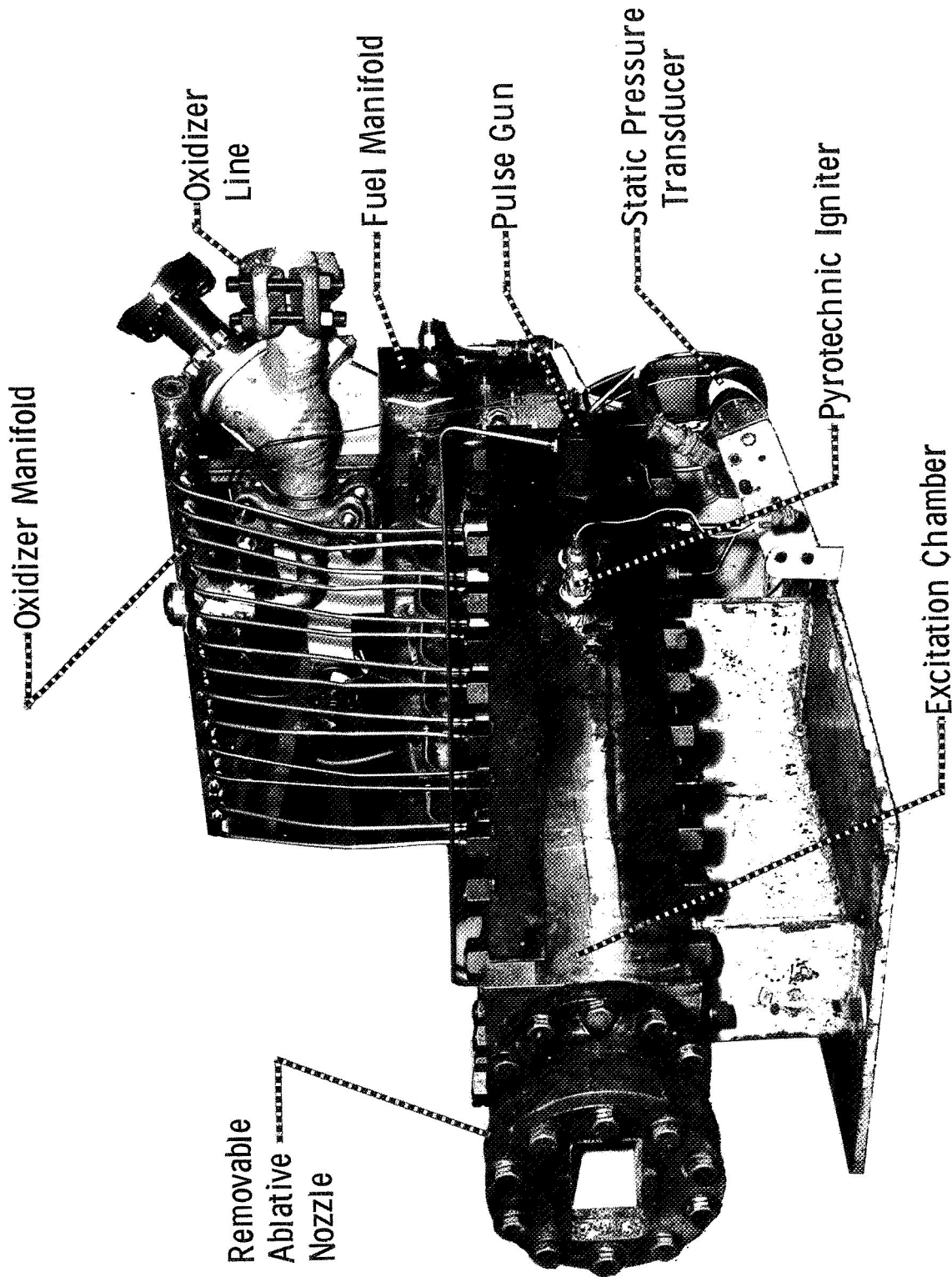


Figure B-5 -- Transverse Excitation Chamber -- Installed on Test Stand

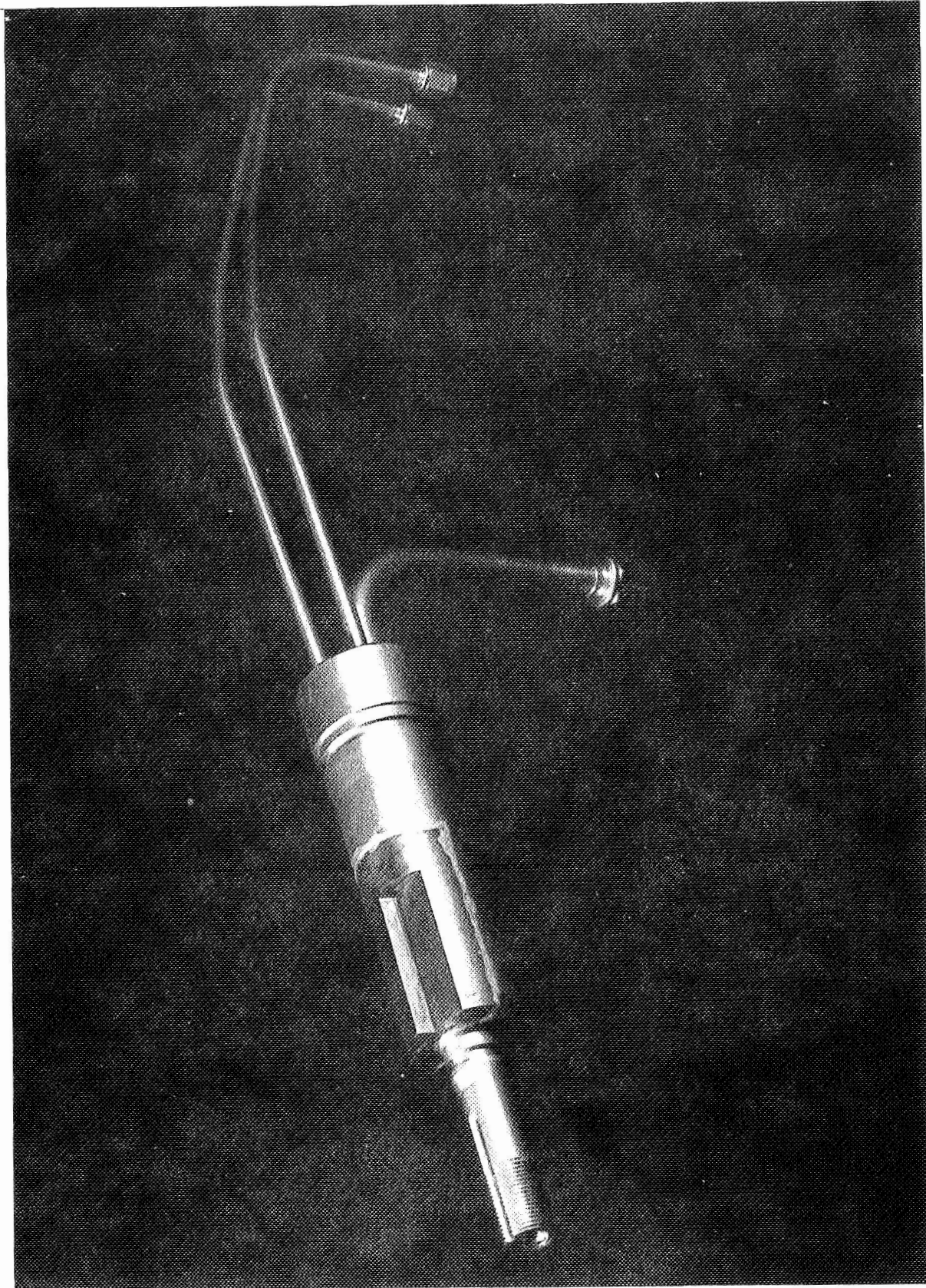


Figure B-6 -- Injector Module Insert, 1 of 2

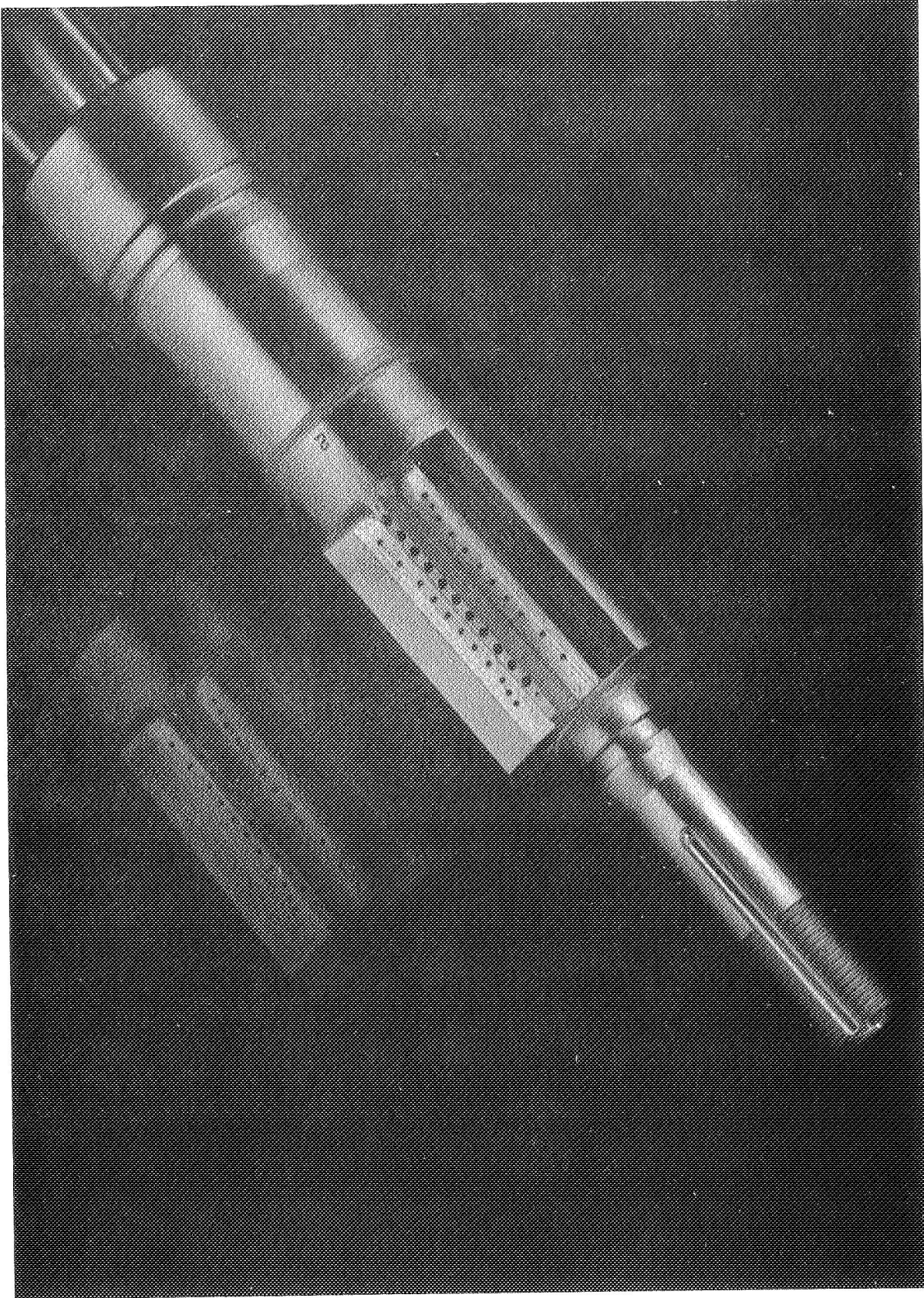


Figure B-6 --- Injector Module Insert, 2 of 2

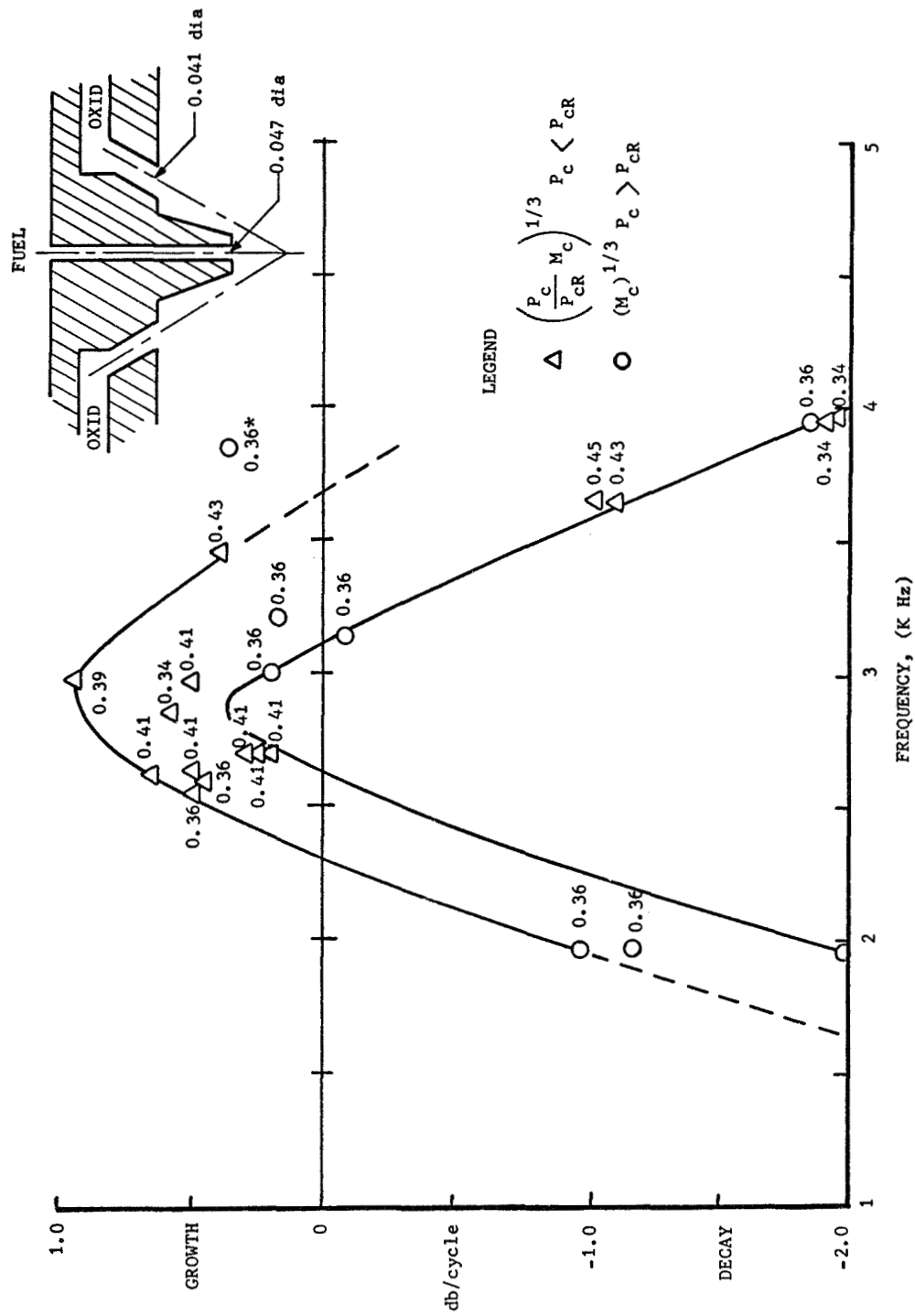


Figure B-7 -- Growth Rate/Decay Rate as Function of Frequency

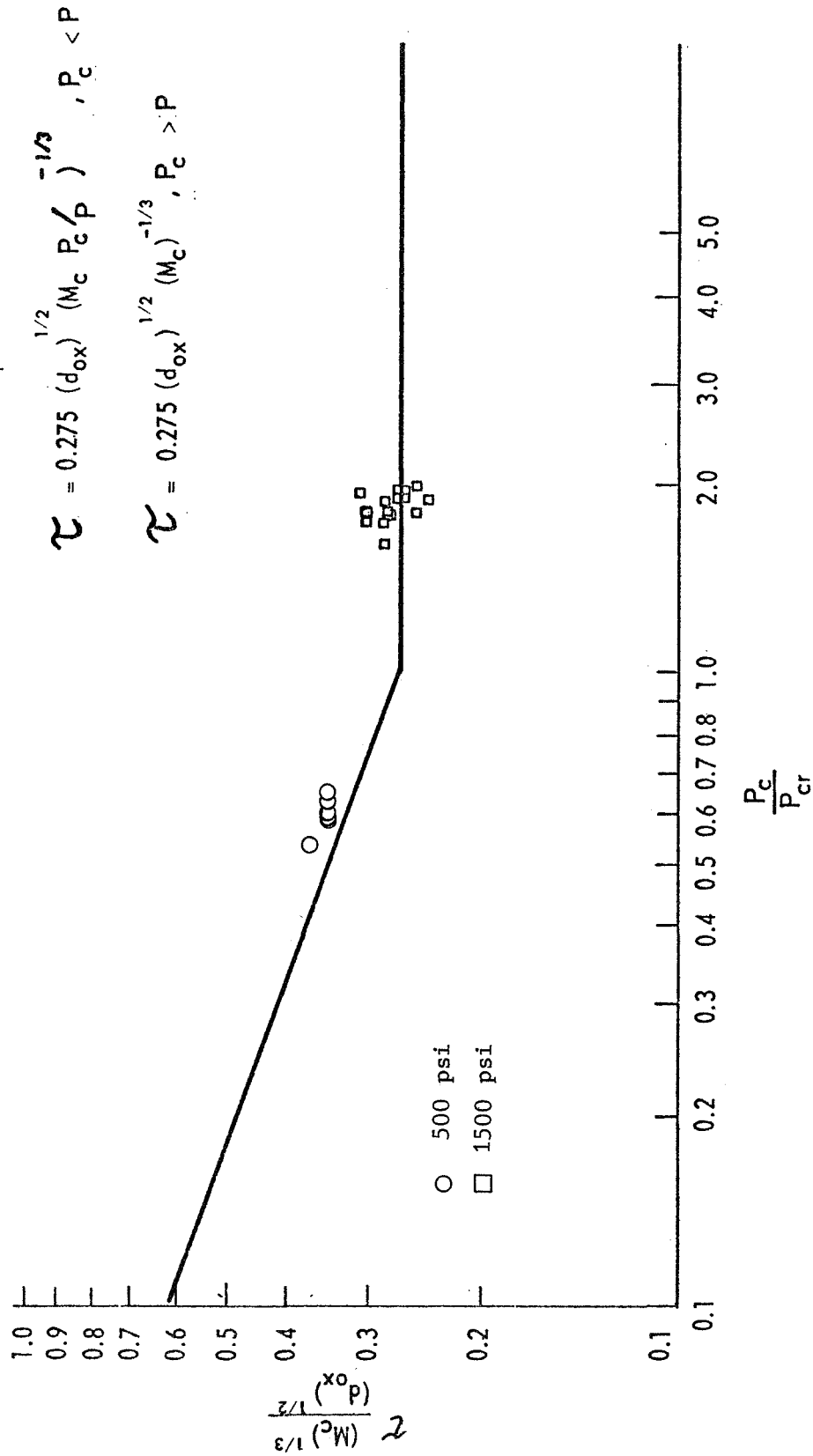


Figure B-8 -- Sensitive Time Lag Correlation

DISTRIBUTION

<u>Copies</u>	<u>Recipient</u>
	NASA Headquarters Washington, D. C., 20546
(2)	Attn: Chief, Liquid Propulsion Technology, RPL Office of Advanced Research and Technology
(1)	Attn: A. O. Tischler, RP
(1)	R. S. Levine, RP
(1)	Attn: Director, Launch Vehicles and Propulsion, SV Office of Space Sciences and Applications
(1)	Attn: Director, Technology Utilization
(1)	Attn: Director, Advanced Manned Missions, MT Office of the Manned Space Flight
	NASA Marshall Space Flight Center Huntsville, Alabama, 35812
(1)	Attn: Purchasing Office, A&TS-PR-MB
(1)	Attn: Office of Scientific and Technical Information, A&TS-MS-IP Attn: Technical Library, A&TS-MS-IL
(1)	Attn: Patent Office, A&TS-M-PAT
(1)	Attn: Technology Utilization Office, A&TS-MS-T
(2)	Attn: Robert Richmond, S&E-ASTN-PP
(1)	Attn: Rex Bailey, S&E-ASTN-PP
(1)	Attn: Dale Burrows, S&E-ASTN-P
	NASA Ames Research Center Moffett Field, California 94035
(1)	Attn: Mission Analysis Division
(1)	Attn: Hans M. Mark

DISTRIBUTION (cont.)CopiesRecipient

(1) NASA Goddard Space Flight Center
Greenbelt, Maryland 20771
Attn: Technical Librarian for Merland L. Moseson,
Code 620

(1) NASA Lewis Research Center
21000 Brookpark Road
Cleveland, Ohio 44135
Attn: Richard Priem

(1) Attn: E. W. Conrad, Ms500-204

(1) T. Male

(1) Technical Librarian for Abe Silverstein, Director

(1) NASA Jet Propulsion Laboratory
California Institute of Technology
4800 Oak Grove Drive
Pasadena, California 91103
Attn: Technical Librarian for Robert F. Rose,
Propulsion Division, 38

(1) Attn: Henry Burlage, Jr.

(1) Attn: Jack H. Rupe

(1) NASA Langley Research Center
Langley Station
Hampton, Virginia 23365
Attn: Technical Librarian for Edward Cortwright,
Director

(1) NASA Manned Spacecraft Center
Houston, Texas 77058
Attn: Technical Librarian for Robert R. Gilruth, Director

(1) Attn: J. G. Thibodaux, Propulsion & Power Division

(1) NASA John F. Kennedy Space Center
Cocoa Beach, Florida 32391
Attn: Technical Librarian for Kurt H. Debus, Director

DISTRIBUTION (cont.)

<u>Copies</u>	<u>Recipient</u>
(10)	Scientific and Technical Information Facility P. O. Box 33 College Park, Maryland 20740
(1)	Air Force Missile Development Center Holloman Air Force Base, New Mexico 88330 Attn: L. H. Ullian
(1)	Headquarters, U. S. Air Force Washington, D. C. 20546 Attn: Col. C. K. Stambaugh, AFRST
(1)	Advanced Research Projects Agency Washington 25, D. C. Attn: Technical Librarian for D. E. Mock
(1)	Defense Documentation Center Headquarters Cameron Station, Bldg. 5 5010 Duke Street Alexandria, Virginia 22314 Attn: Technical Librarian
(1)	Picatinny Arsenal Dover, New Jersey 07801 Attn: Technical Librarian for I. Forsten, Chief, Liquid Propulsion Laboratory, SMUPA-DL
(1)	Air Force Rocket Propulsion Laboratory Air Force Systems Command Edwards, California 93523 Attn: Technical Librarian for Commander
(1)	Attn: Tom Chew Attn: H. Main
(1)	U. S. Army Missile Command Redstone Arsenal, Alabama, 35808 Attn: Technical Librarian for Commander
(1)	Attn: Walter W. Wharton, AMSMI-RKL

DISTRIBUTION (cont.)

<u>Copies</u>	<u>Recipient</u>
	U. S. Naval Ordnance Test Station China Lake, California 93557
(1)	Attn: Technical Librarian for Chief, Mission Propulsion Division, Code 4562
(1)	Attn: T. Inouye, Code 4581
	Chemical Propulsion Information Agency Johns Hopkins University Applied Physics Laboratory 8621 Georgia Avenue Silver Spring, Maryland 20910
(1)	Attn: Tech. Librarian for Tom Reedy
(1)	Attn: T. W. Christian
	Air Force Systems Command Wright-Patterson AFB Dayton, Ohio 45433
(1)	Attn: K. Scheller
(1)	Attn: D. L. Schmidt, ASRCNC-2
	Space and Missile Systems Organization Air Force Unit Post Office Los Angeles, California 90045
(1)	Attn: Col. Clark, Technical Data Center
	Arnold Engineering Development Center Arnold Air Force Station Tullahoma, Tennessee 37388
(1)	Attn: H. K. Doetsch
	Bureau of Naval Weapons Department of the Navy Washington, D. C.
(1)	Attn: J. Kay, RTMS-41
	Headquarters Air Force Office of Scientific Research Propulsion Division 1400 Wilson Blvd. Arlington, Virginia 22209
(1)	Attn: R. Haffner

DISTRIBUTION (cont.)CopiesRecipient

(1)	Department of the Navy Office of Naval Research Washington, D. C. 20360 Attn: R. O. Jackel, 429
(1)	Aerojet-General Corporation P. O. Box 15847 Sacramento, California 95809 Attn: Technical Librarian for R. Stiff
(1)	Attn: J. M. McBride
(1)	Sacramento State College School of Engineering 6000 J. Street Sacramento, California 95819 Attn: Fred H. Reardon
(1)	Bellcomm 955 L'Enfant Plaza, S.W. Washington, D. C. Attn: H. S. London
(1)	Research Center Fairchild Hiller Corporation Germantown, Maryland Attn: R. Hall
(1)	Republic Aviation Corporation Farmingdale, Long Island, New York Attn: Technical Librarian
(1)	Avco Systems Division Wilmington, Massachusetts Attn: H. B. Winkler
(1)	Beech Aircraft Corporation Boulder Division P. O. Box 631 Boulder, Colorado Attn: J. H. Rodgers

DISTRIBUTION (cont.)CopiesRecipient

(1)	General Dynamics, Convair Division Library & Information Services (128-00) P. O. Box 1128 San Diego, California 92112 Attn: Frank Dore
(1)	Grumman Aircraft Engineering Corp. Bethpage, Long Island, New York Attn: Joseph Gavin
(1)	Hughes Aircraft Company Aerospace Group Centinela and Teale Streets Attn: E. H. Meier
(1)	Walter Kidde and Company, Inc. Aerospace Operations 567 Main Street Belleville, New Jersey Attn: R. J. Hanville
(1)	Ling-Temco-Vought Corporation P. O. Box 5907 Dallas, Texas 75222 Attn: Warren G. Trent
(1)	Aerospace Corporation P. O. Box 95085 Los Angeles, California 90045 Attn: Technical Librarian for J. C. Wilder
(1)	Attn: O. W. Dykema
(1)	Astropower Laboratory Douglas Aircraft Company 2121 Paularino Newport Beach, California 92663 Attn: Technical Librarian

DISTRIBUTION (cont.)CopiesRecipient

(1)	Astrosystems International, Inc. 1275 Bloomfield Avenue Fairfield, New Jersey 07007 Attn: Technical Librarian for A. Mendenhall
(1)	Atlantic Research Corporation Edsall Road and Shirley Highway Alexandria, Virginia 22314 Attn: Technical Librarian for R. Friedman
(1)	Arther D. Little, Inc. Acorn Park Cambridge, Massachusetts 02140 Attn: Technical Librarian
(1)	Bell Aerosystems Company P. O. Box 1 Buffalo, New York 14240 Attn: Technical Librarian for W. M. Smith
(1)	Attn: K. Berman
(1)	Attn: L. M. Wood
(1)	Boeing Company P. O. Box 3707 Seattle, Washington 98124 Attn: Technical Librarian for J. D. Alexander
(1)	Missile Division Chrysler Corporation P. O. Box 2628 Detroit, Michigan 48231 Attn: J. Gates
(1)	Curtiss-Wright Corporation Wright Aeronautical Division Wood-ridge, New Jersey 07075 Attn: Technical Librarian for G. Kelly
(1)	General Electric Company Cincinnati, Ohio 45125 Attn: Technical Librarian for D. Suichu
(1)	Lockheed Missiles and Space Company Technical Information Center P. O. Box 504 Sunnyvale, California 94008 Attn: Technical Librarian for J. Guill

DISTRIBUTION (cont.)

<u>Copies</u>	<u>Recipient</u>
(1)	The Marquardt Corporation 16555 Saticoy Street Van Nuys, California 91409 Attn: Technical Librarian for H. McForland
(1)	North American Rockwell, Inc. Space and Information Systems Division 12214 Lakewood Boulevard Downey, California 90241 Attn: Technical Librarian
(1)	TRW Incorporated One Space Park Redondo Beach, California 90278 Attn: G. W. Elverum
(1)	Stanford Research Institute 333 Ravenswood Avenue Menlo Park, California 94025 Attn: Technical Librarian for G. Marksman
(1)	McDonnell Douglas Aircraft Corporation P.O. Box 516 Municipal Airport St. Louis, Missouri 63166 Attn: R. A. Herzmark
(1)	TAPCO Division TRW, Incorporated 23555 Euclid Avenue Cleveland, Ohio 44117 Attn: Technical Librarian for P. T. Angell
(1)	Thiokol Chemical Corporation Redstone Division Huntsville, Alabama Attn: Technical Librarian for John Doodloe
(1)	United Aircraft Corporation Research Laboratories 400 Main Street East Hartford, Connecticut 06108 Attn: Technical Librarian for Erle Martin

DISTRIBUTION (cont.)CopiesRecipient

(1) United Technology Center
587 Mathilda Avenue
P.O. Box 358
Sunnyvale, California 94088
Attn: Technical Librarian for D. Altman

(1) Rocketdyne Division of North American Rockwell, Inc.
6633 Canoga Avenue
Canoga Park, California 91304
Attn: Technical Librarian for S. Hoffman

(1) Attn: J. Nestlerode

(1) Attn: R. Lawhead

(1) Attn: S. F. Iacobellis

(1) Martin Marietta Corporation
Baltimore Division
Baltimore, Maryland 21203
Attn: J. Calathes

(1) Northrop Space Laboratories
3401 West Broadway
Hawthorne, California
Attn: W. Howard

(1) Pratt and Whitney Aircraft
P.O. Box 2691
West Palm Beach, Florida 33402
Attn: Technical Librarian for R. J. Coar

(1) Attn: Gary Garrison

(1) Rocket Research Corporation
520 South Portland Street
Seattle, Washington 98108
Attn: Technical Librarian for Foy McCullough, Jr.

(1) Polytechnic Institute of Brooklyn
Graduate Center
Route 110
Farmingdale, New York 11735
Attn: V. D. Agosta

(1) Ohio State University
Department of Aeronautical & Astronautical Engineering
Columbus, Ohio 43210
Attn: R. Edse

DISTRIBUTION (cont.)

<u>Copies</u>	<u>Recipient</u>
(1)	Dynamics Science Corporation 1900 Walker Avenue Monrovia, California 91016 Attn: B. P. Breen
(1)	Tulane University 6823 St. Charles Avenue New Orleans, Louisiana Attn: J. C. O'Hare
(1)	Colorado State University Mechanical Engineering Department Fort Collins, Colorado 80521 Attn: C. E. Mitchell
(1)	University of California Mechanical Engineering Dept. Berkeley, California Attn: R. Sawyer
(1)	University of California Aerospace Engineering Dept. P.O. Box 109 La Jolla, California 92037 Attn: F. A. Williams
(1)	University of Illinois Aeronautic and Astronautic Engineering Dept. Transportation Bldg., Room 101 Urbana, Illinois 61801 Attn: R. A. Strehlow
(1)	The Pennsylvania State University Mechanical Engineering Dept. 207 Mechanical Engineering Blvd. University Park, Pennsylvania 16802 Attn: G. M. Faeth
(1)	Princeton University Forrestal Research Center Princeton, New Jersey Attn: D. T. Harrje 08540
(1)	Attn: I. Glassman

DISTRIBUTION (cont.)

<u>Copies</u>	<u>Recipient</u>
(1)	University of Wisconsin Dept. Mechanical Engineering 1513 University Avenue Madison, Wisconsin 53706 Attn: P. S. Myers
(1)	University of Michigan Dept. of Aerospace Engineering Ann Arbor, Michigan 48104 Attn: J. A. Nicholls
(1)	University of California Dept. of Chemical Engineering 6161 Etcheverry Hall Berkeley, California 94720 Attn: A. K. Oppenheim
(1)	Purdue University School of Mechanical Engineering Lafayette, Indiana 47407 Attn: J. R. Osborn
(1)	Attn: B. A. Reese
(1)	Attn: R. Goulard
(1)	Massachusetts Institute of Technology Department of Mechanical Engineering 77 Massachusetts Avenue Cambridge, Massachusetts 02139 Attn: T. Y. Toong
(1)	Illinois Institute of Technology Room 200 M.H. 3300 S. Federal Street Chicago, Illinois 60616 Attn: P. T. Torda
(1)	Georgia Institute of Technology Aerospace School Atlanta, Georgia 30332 Attn: B. T. Zinn